The Dissertation Committee for Kirk Alan Overhoff Certifies that this is the approved version of the following dissertation:

Improved Oral Bioavailability of Poorly Water Soluble Drugs Using Rapid Freezing Processes

Committee:

Robert O. Williams III, Supervisor

Keith P. Johnston

James W. McGinity

Robert L. Talbert

Nikolaos A. Peppas

Improved Oral Bioavailability of Poorly Water Soluble Drugs Using Rapid Freezing Processes

by

Kirk Alan Overhoff, B.S.

Dissertation

Presented to the Faculty of the Graduate School of

The University of Texas at Austin

in Partial Fulfillment

of the Requirements

for the Degree of

Doctor of Philosophy

The University of Texas at Austin

December, 2006

Dedication

To my loving and supportive parents, Mr. Dietrich K. Overhoff and Mrs. Courtnay C. Overhoff

Acknowledgements

First, and most importantly, I would like to thank, God, the Father, for blessing me with a loving family, teaching me humility and patience and allowing me the opportunity to develop into the person I am today. I would like to extend a heartfelt appreciation to my supervisor, Dr. Robert O. Williams III, for his leadership and direction during my graduate experience. His words have not only given me strength in times of weakness, but hope in times of despair. I would also like to thank Dr. Keith P. Johnston, for his valuable advice and wisdom. He has broadened my scientific foundation by teaching me to consider all possibilities and outcomes. I would like to thank Dr. James W. McGinity for his extensive knowledge in the area of drug delivery and pharmaceutical sciences. He, more than anyone, is responsible for preparing me for life outside of my graduate work by passing on his experiences and life lessons. I would also like to thank Dr. Robert L. Talbert for his valuable experience in the clinical and pharmacokinetic aspects of my research. I am extremely grateful and humbled to have a researcher like Dr. Nikolaos A. Peppas provide me with helpful tips, ideas and direction which have helped me craft a high quality dissertation.

I would like to show my appreciation to all of the faculty and staff of the College of Pharmacy, Department of Chemical Engineering and Department of Biomedical Engineering at the University of Texas at Austin, and the University of Texas Health

Improved Oral Bioavailability of Poorly Water Soluble Drugs Using Rapid Freezing Processes

Publication No._____

Kirk Alan Overhoff, Ph.D.

The University of Texas at Austin, 2006

Supervisor: Robert O. Williams III

A growing number of therapeutic compounds currently being developed by pharmaceutical companies are poorly water soluble leading to limited and/or erratic bioavailability. The rate limiting step for absorption of these compounds is dependent on the dissolution and apparent solubility. Nanoparticle formation has been exploited as a method to improve the bioavailability of these poorly water soluble active pharmaceutical ingredients (API) by increasing the dissolution rates and apparent solubilities.

The influence of hydrophilic stabilizers in powder compositions prepared by the spray freezing into liquid (SFL) process using either an emulsion feed dispersion or organic co-solvent feed solutions on enhancing the wetting and dissolution properties of nanostructured aggregates containing itraconazole (ITZ). Subsequently, an *in vivo* pharmacokinetic study was conducted comparing the SFL processed powder to commercial Sporanox®.

An ultra-rapid freezing (URF) technology has been developed to produce high surface area powders composed of solid solutions of an active pharmaceutical ingredient

(API) and a polymer stabilizer. Rapid freezing technologies are known to enhance the physico-chemical properties of APIs and thus increase bioavailability. However, the effect of the different freezing geometries and rates in the URF process are unknown. Therefore, this study investigated how solvent properties and thin film geometry of the droplet affect the freezing rate and thus the physico-chemical properties of micronized danazol powders.

Amorphous nanoparticles containing tacrolimus (TAC) in a solid dispersion were prepared using the Ultra-rapid Freezing (URF) process. The objective of this study was to assess the effects of combinations of polymeric stabilizers on the maximum degree and extent of supersaturation of TAC. An attempt to establish if an *in vitro-in vivo* correlation exists between supersaturation and improved pharmacokinetic parameters for orally dosed TAC was performed.

Enteric solid dispersions could overcome limitations of premature precipitation of supersaturated solutions by 1.) delaying dissolution until the compound enters the intestines where absorption is favored and 2.) increasing the apparent solubility at higher pH to increase the driving force for absorption. The objective of the study is to investigate the influence of composition parameters including drug:polymer ratio and polymer type, and particle structure of enteric solid dispersions on the release of ITZ.

Table of Contents

List of Tables

List of Figures

Chapter 1: Advances in Drug Delivery Technologies for Nanoparticulates

1.1 ABSTRACT

A growing number of therapeutic compounds currently being developed by pharmaceutical companies are poorly water soluble leading to limited and/or erratic bioavailability. Nanoparticle formation has been exploited as a method to improve the bioavailability of these poorly water soluble active pharmaceutical ingredients (API). Two strategies have been proposed for formation of nanoparticles, particle reduction and particle nucleation and stabilization. Particle reduction technologies include milling and homogenization, while nucleation and stabilization technologies include solvent evaporation, rapid freezing, and antisolvent technologies. Both strategies have the ability to enhance dissolution of the API leading to increased bioavailability. Examples of nanoparticle compositions have shown enhanced uptake across biological membranes due to their small size. Surface modification of nanoparticles has also proven beneficial by allowing for site specific targeting, increasing residence time, and protecting against degradation. Examples using these nanoparticle technologies introduced within this chapter focus on oral and pulmonary delivery of the API.

1.2 INTRODUCTION

Recent advances in synthesis and purification in the areas of medicinal and organic chemistry have brought about a number of new chemical entities (NCE) which hold promise in treating many of today's diseases and disorders. However, a large number of these NCEs display poor *in vivo* solubility (poorly water soluble) resulting in poor absorption and limited and/or erratic bioavailability. Therefore, many of these NCEs are never pursued by the pharmaceutical industry and subsequently developed into commercial products. Also, poorly water soluble active pharmaceutical ingredients (APIs) used to treat oncology patients may include solubilizing excipients which possess harmful side effects leading to patient non-compliance.[1, 2] It is desired that nanoparticulate systems reduce variability and increase bioavailability of poorly water soluble APIs through enhanced absorption due to improved wetting and dissolution.

Hydrophobic APIs are not the only compounds which benefit from delivery as nanoparticulate systems. Oral delivery of proteins, peptides, and nucleic acids has proven exceedingly difficult. While being water soluble, these compounds are susceptible to denaturation post-administration when exposed to low pH and gastric enzymes.[3] Most proteins have poor absorption across the intestinal barrier as well and therefore, micro- and nanoparticulate carrier systems could help increase absorption of these compounds.[4]

Nanotechnology has been employed in non-pharmaceutically related areas such as microchip manufacturing, and it is reported that products resulting from these technologies display enhanced properties such as ultradense integrated circuits and faster

processing speeds [5] compared to their larger counterparts. Only recently has the pharmaceutical industry applied nanotechnology as a viable method for improving drug delivery for NCEs and non-optimized drug products. Traditionally, nanoparticles have been defined as particles or structures no larger than 100 nm in diameter; however, it is common to see in the pharmaceutical literature the term 'nanoparticle' used to describe particles no greater than one micron in diameter.[6]

Within the fast evolving discipline of pharmaceutical drug delivery and formulation research, the use of nanoparticle technologies is still in its infancy but recent examples of nanotechnology have shown particular promise as a method to increase the bioavailability of poorly water soluble APIs. Development for these APIs in the form of nanoparticles, providing viable alternatives to more routine development strategies, including using a prodrug, salt form, or metastable drug form in order to increase bioavailability, has been made possible through advances in analytical characterization of nano-sized particles. Specifically, microscopic techniques including scanning electron microscopy (SEM), transmission electron microscopy (TEM), tunneling force microscopy, atomic force microscopy (AFM), and particle sizing techniques including dynamic and laser light scattering, have allowed scientists to have a greater understanding of the physico-chemical properties of nanoparticles. Z-contrast TEM or STEM dark-field imaging has enabled scientists to determine API domain locations within an excipient matrix by detecting differences in compositional changes and thicknesses within the sample.[7] Advances in AFM now permit scientists to understand differences in surface modification of nanoparticles at near atomic levels, while at the same time being able to view the surfaces of the particles in 3-dimension (3-D). Equally

3

important, researchers can now measure particle sizes down to 20 nm accurately using laser light scattering.[8] Even with the increased understanding of the physical properties of nanoparticles, the scientific community is only now beginning to understand how these nanoparticles are leading to improved bioavailability and efficacy of NCEs *in vivo*.

This chapter will review recently reported nanoparticle technologies and discuss important physical properties inherent to nanoparticles. We will discuss the relationship between these properties and *in vivo* performance, focusing on the influence of particle size on uptake as a function of various routes of administration. Finally, we will review the impact that surface modifications of nanoparticles have on absorption enhancement.

1.3 NANOPARTICLE TECHNOLOGIES

Nanoparticle formation can be described by two general strategies, particle reduction or particle nucleation and stabilization. For the particle reduction strategy, large API particles are fractured into smaller particles using a variety of processes and equipment. These nanoparticles are generally stabilized using various polymers and surfactants which can modify the surface charge of the particle preventing aggregation caused by electrostatic forces. Secondly, nanoparticles may also be formed by particle nucleation from solution in which the API, with or without stabilizing agents, is dissolved. Particle growth is arrested using stabilizing polymers or surfactants, and controlled by manipulating process parameters in order to obtain particles within a desired size range. This section will review recently reported strategies of nanoparticle formation.

4

1.3.1 Particle reduction

1.3.1.1 Milling processes

Dry powder milling processes such as ball milling or hammer milling are able to reduce particle sizes of powders down to about 1 micron in diameter through particle-substrate and particle-particle collisions. Further particle size reduction is restricted due to electrostatic forces generated during the milling process which can cause aggregation of the particles. Additional processing of the powder, such as blending, can become difficult if this occurs. In addition, the high energy required to break up the API particles generates excessive amounts of heat which can lead to thermal degradation of the API. To overcome these limitations, a wet milling process (Nanocrystal® technology) is reported to form uniform nanoparticles by milling the API particles in an aqueous polymer medium.[9] The milling takes place under controlled temperatures thereby reducing or eliminating thermal degradation due to friction. This technology is generally operated in a batch or recirculation mode and takes as little as 30-60 minutes to form crystalline nanoparticles measuring < 200 nm in diameter.[9]

1.3.1.2 Homogenization

High pressure homogenization is also a convenient process for reducing the particle size of API particles. Typically, API suspensions can be homogenized into the nanometer range using a piston-gap high pressure homogenizer (HPH). The homogenizer consists of a pumping mechanism which moves the fluid through a narrow gap consisting of a valve seat and an adjustable valve. Briefly, the API is pre-wetted as a

5

course suspension using a rotor/stator mixer before being transferred to the HPH. As the fluid is forced through the gap of the HPH, cavitation, high shear forces, and particle-particle collisions reduce the size of the particles with each pass through the gap. Particle size is controlled primarily by controlling the operating pressure (5,000-20,000 psi) and the number of passes (1-10 cycles) through the gap. Processed particle suspensions described as Disso Cubes® can undergo further processing by spray drying or lyophilization to form fine powders.[10]

1.3.2 Particle nucleation and stabilization

Precipitation technologies include methods in which particles are nucleated from a solution and particle growth is inhibited and controlled through the use of stabilizing polymers.[11-13]. Precipitation of API from a solution occurs when there is an increase in concentration above the solubility limit (e.g. supersaturation) or a decrease in solubility of the solute within the solvent. When the change in solvent strength is rapid, supersaturation can occur leading to an increase in homogeneous nucleation rate.[14] Changes in solvation strength can happen through solvent evaporation, rapid freezing, or addition of anti-solvents. Solvent evaporation is done through addition of heat or pressure reduction, while freezing is done using some type of cryogen. Anti-solvents have poor API solubility but must be miscible with the solvent in which the API is dissolved. Once precipitation has been initiated, particle growth proceeds by coagulation and/or condensation. Coagulation results when two particles collide forming one larger particle, while condensation takes place as dissolved solute adsorbs to a solid particle causing increased growth. The design of the particle engineering technology can have a

tremendous impact on nucleation and subsequent growth mechanisms leading to particle formation, which then influences the resulting physico-chemical properties of the powders. The following technologies have been generally described based on their mechanism of particle formation: solvent evaporation, rapid freezing, or anti-solvent precipitation.

1.3.2.1 Solvent evaporation

Solvent evaporation from solution

Spray-drying is one of the most common particle engineering processes due to its economic feasibility and scalability. The process comprises atomizing a solution (organic or aqueous) containing the API of choice and stabilizing polymers. The atomized cloud is then pulled downstream via vacuum into a heated zone. The high surface area droplets enhance evaporation of the solvent leaving dry particles. These dried particles are then collected using a cyclonic chamber. Particle size and distribution is primarily dependent on the droplet size exiting the atomizing nozzle. Therefore, nozzles which give a more uniform droplet size distribution, such as ultrasonic nozzles, will lead to particles with a narrow particle size distribution. Solvent choice, solids loading and drying rate also contribute to the resulting surface morphology of the particles.[15]

Aerosol flow reactors are similar to spray dryers and operate by atomizing an API solution via a collision-type air jet atomizer into an inert carrier gas which is passed through a heated tubular laminar flow chamber. Critical parameters include the spray

nozzle (e.g. type, diameter), spray rate, droplet size, temperature of the chamber zones, solvent, and solids loading.[16] Raula et al. reported that fast solvent removal rates lead to collapsed or hollow particles while poor solubility of the solute within the chosen solvent led to irregularly shaped particles. Smooth, spherical nanoparticles were formed with a uniform particle size of about 100 nm using solvents with good API solubility and high evaporation rates sprayed at moderate drying temperatures (less than 120°C).[17] Collapsed particles resulted from high solvent evaporation rates at the surface causing a solid crust to encapsulate the particle preventing further outward diffusion of the solvent. The remaining solvent within the particle most likely ruptured through a defect or hole in the solidified surface and rapidly evaporated, leaving a hollow particle. Solute/solids loading in the solvent also had an effect on the final surface morphology of the nanoparticles.[18] Low API amounts resulted in homogeneous particles having broad glass transition patterns indicating miscibility while higher API loadings above the solubility limits of the API in the solvent resulted in crystallization of the API.

Solvent evaporation processes such as evaporative precipitation into aqueous solution (EPAS) are designed to cause nucleation through the rapid removal of a solvent.[7, 19-24] In EPAS, the API is dissolved in a water immiscible organic solvent such as dichloromethane. Stabilizing polymers are then dissolved in the organic phase and/or aqueous phase. The organic solution is then sprayed under pressure into the heated aqueous phase. The pressure drop as the organic phase exits the nozzle causes atomization and the heat causes rapid evaporation of the organic solvent. Properties of the particles can be controlled by varying a number of parameters such as stabilizing polymer choice, concentration, and/or location, spraying rate, and pressure drop.

8

Solvent evaporation of emulsion systems

One of the simplest methods to manufacture solid nanoparticles is through emulsification, and this topic has been reviewed extensively [25, 26]. Common emulsification methods such as high shear mixing with a rotor-stator mixer, high pressure homogenization, or sonication are used to prepare either oil-in-water (o/w) or water-in-oil (w/o) emulsions. Emulsifying agents preferentially orient between the two phases at the interface of the droplet to prevent coalescence. Generally, oils or water-immiscible organic solvents (i.e. dichloromethane) and water are the typical solvents. The API is preferentially dissolved in the more soluble of the two phases (i.e. organic or oil phase for poorly water soluble APIs). Particles are formed during evaporation of the solvents either through increased heat and/or reduced pressure depositing the API within the core or adsorbed onto the surface. Mean particle size of the final particles is dependant on the droplet size of the internal phase and can range from nanoparticles to microparticles depending on the method of manufacture. Creating multiple emulsions such as oil-in-water-in-oil (o/w/o) or water-in-oil-in water (w/o/w) can lead to multiple layers allowing more flexibility and creativity in designing delivery systems according to the specific requirements of the clinical endpoint. Nanoparticles loaded with antitubercular drugs (rifampicin, isoniazid and pyrazinamide) and encapsulated with poly (DL-lactide-co-glycolide) (PLGA) were manufactured using a multiple emulsion system and administered via nebulization to guinea pigs.[27] Compositions were tested for aerodynamic performance, *in vivo* disposition, and chemotherapeutic efficacy. Pharmacokinetic analysis revealed a 6- to 19-fold increase in absolute bioavailability and

a 12- to 32-fold increase in relative bioavailability. For the chemotherapeutic efficacy studies, guinea pigs were inoculated with 1.5×105 viable bacilli of *M. tuberculosis* and allowed to incubate for 20 days. One treatment group received once a day oral dosing for 46 days while the other treatment group received every other day pulmonary dosing for 10 days. Control groups received no dosing or drug free PLG nanoparticles. Studies revealed no tuberculosis bacilli after 30 days post-inoculation for either the oral and nebulized API nanoparticles while the control groups had high *M. tuberculosis* counts within the lungs demonstrating the ability of nanoparticles to both improve bioavailability and decrease dosing regimens.

Fig. 1.1 shows a few of the many different carrier systems which have been developed using the emulsion evaporation technique to optimize drug delivery. The API of choice can exist within the particle as a molecular solution or as a solid dispersion characterized by discrete API domains within the matrix. In addition, the API can exist within the matrix core of the tablet or bead possibly encapsulated by a polymer coating. The API can also be adsorbed onto the surface of the core or within the polymer coating. Varying the design of the API carrier (API location, polymer choice, size, etc.) can result in immediate, delayed, or sustained release systems. Rosca et al. [28] studied the evaporation step of multiple emulsions to determine the effect on surface morphologies of the final microparticle encapsulation efficiency and release behavior. Results showed that lower encapsulation efficiency was attributed to fast solvent evaporation. SEM pictures also revealed nanoparticles adsorbed to the surface of the microparticles contributing to the burst effect in the release profile. Variations in double emulsion

composition can control the final microparticle morphology depending on the inner aqueous phase composition and the size of the emulsified droplet.

Emulsification allows for surface modification of the resulting particles which is useful for targeting to a specific site within the body, evading an immune response, or facilitating permeation through biological membranes. The polymer used for surface modification must be biocompatible and functional for the intended purpose. Examples of surface modified particles include PEGylated nanoparticles to evade immune responses, polyethyleneimine (PEI) and chitosan as gene carriers, and conjugated polyethylene glycol (PEG)-poly(lactide-co-glycolide) (PLGA) polymers for controlled API release.

Lipid based nanoparticle carriers use a mixture of lipids, waxes, and surface active stabilizers rather than hydrophilic polymers. Solid lipid nanoparticles (SLN), developed in the early 1990's [29], are well tolerated by the body [30] and have been developed for parenteral, oral, topical, and pulmonary delivery [31, 32]. Therefore, this technology is useful for many lipophilic APIs which have low aqueous solubility and may induce toxic side effects. The nanoparticles are prepared by either the hot homogenization technique or the cold homogenization technique [33]. In both techniques, the API is dissolved in the lipid which is heated just above its melting point. In the hot homogenization technique the lipid melt is dispersed into an aqueous surfactant solution heated to the same temperature, homogenized using a HPH and cooled to form the SLNs. In the cold homogenization technique the lipid melt is cooled into microparticles, dispersed into a cold surfactant solution and homogenized forming the

SLNs. Gasco [34] later developed a method for the preparation of SLNs by forming a microemulsion to further enhance absorption.

So called "stealth nanoparticles" are surface modified particles designed to escape clearance from the blood after intravenous injection.[35, 36] Nanoparticles injected directly in the bloodstream are vulnerable to clearance by the reticulo-endothelial system (RES), often within minutes after injection. Recognition of these particles by the RES is due in large part to the surface charge, hydrophobicity and size of the particles. Therefore, surface modification of these particles is critical to increase the circulation time of the particles. Typically, these particles have been covalently grafted with a hydrophilic non-ionic polymer through the double emulsion (w/o/w) technique described above. Examples of polymers include the polyethylene glycols (PEG), poloxamers, and polyvinylpyrrolidone (PVP).

1.3.2.2 Rapid freezing to induce nucleation

Freezing technologies such as Spray Freeze Drying (SFD) [37], Spray Freezing into Liquid (SFL) [38] and Ultra-rapid Freezing (URF) [39, 40] utilize a rapid freezing mechanism to form frozen nanoparticles which are then further processed to remove the frozen solvent yielding a dry powder. Briefly, the API and various stabilizing/surface active excipients are dissolved in a common solvent. This solution is then rapidly frozen either by spraying onto or directly into a cryogen. If the freezing rate is sufficiently fast, phase separation between the API and stabilizing agents is prevented creating frozen molecularly dispersed nanoparticles. Removal of the frozen solvent then follows, yielding high surface area nanoparticles of API in the matrix. In the SFL process, an

API/polymer feed solution is atomized through an insulating poly ether-ether ketone (PEEK) nozzle submerged directly into a cryogenic liquid (liquid N2). The fine droplets produced as the solution exits the nozzle ensures rapid freezing of the API in the amorphous state.[12, 41-48] The frozen particles are collected and lyophilized in a temperature controlled tray lyophilizer yielding highly porous nano-structured amorphous powders. High potency (> 90% API) compositions with sufficient stabilization are possible to further reduce possible excipient side effects.[49]

1.3.2.3 Anti-solvent precipitation

Anti-solvent precipitation using supercritical fluids

Precipitation technologies which utilize supercritical fluids to form micro- and nano-particles have existed commercially for over 30 years with the most common supercritical fluid being supercritical carbon dioxide (CO_2) due to its lack of toxicity, low critical temperature (31.1°C), and inexpensive cost.[50] Within these technologies, the supercritical fluid is used either as the solvent for the API and stabilizing polymers or as a non-solvent/anti-solvent. In processes such as Rapid Expansion of Supercritical Solutions (RESS), the API and excipients are dissolved in supercritical CO2, followed by rapid expansion of the solution through a nozzle.[51] The API becomes supersaturated resulting in homogeneous nucleation and particle formation. Physical processing parameters such as pressure and temperature of the precipitator and nozzle size can control the properties of the particles. However, solubility of the solutes within the supercritical fluids is the major limiting factor for this technology. On the other hand,

many technologies (i.e. Gas Antisolvent (GAS), Precipitation with Compressed Antisolvent (PCA)) have utilized the poor solvent capability of supercritical fluids as non-solvents or anti-solvents.[52, 53] In these processes, the API solution containing a solvent miscible with the supercritical fluid is sprayed via a nozzle into the supercritical fluid. Mass transfer of the supercritical fluid into the droplet causes precipitation and nucleation of the particles. Solution Enhanced Dispersion by Supercritical Fluids (SEDS) utilizes a coaxial nozzle design and mixing chamber. This design facilitates increased atomization (smaller droplets) and faster mass transfer rates resulting in faster precipitation rates of the particles and smaller particle sizes.   Surface coating and encapsulation has also been studied using these supercritical fluid technologies. Generally, particles are formed using the supercritical fluid processes as described above. The coating material or polymer is then sprayed into the particle dispersion using the same process and adsorbed to the surface of the newly formed particles.[54] Tsutsumi et al. [55] coated RESS processed powders using a fluidized bed coater but had limited success coating nanoparticles which tended to agglomerate during the coating process.

Anti-solvent precipitation using non-supercritical solvents

Anti-solvent technologies utilize organic or aqueous solvents as anti-solvents to initiate nucleation through a rapid decrease in solvent power. Generally, the API is dissolved in a water miscible organic solvent such as ethanol or acetone. The solution is then added rapidly to water causing nucleation. Stabilizing polymers can be dissolved in one or both phases. The organic solvent is then removed through evaporation leaving the nanoparticles dispersed in the aqueous phase. Dry powder can be made by further

removal of the water using lyophilization or spray drying. Rasenack and Müller developed an *in situ* micronization technique to form nanoparticles.[56] Briefly, the API is dissolved in a water-miscible organic solvent while the stabilizing agents are dissolved in water. The two phases are then mixed "batch-wise" forming a dispersion of nanoparticles. Subsequent studies have focused on pulmonary delivery of these enhanced powders [57, 58].using a dry powder inhaler (DPI).

The anti-solvent technology, Flash NanoPrecipitation was reported recently.[59-61] This process comprises mixing a solvent phase composed of the API and stabilizers (amphiphilic block copolymers) and an aqueous anti-solvent phase via a confined impinging jet (CIJ) mixer. The CIJ mixers result in rapid mixing of the two phases leading to supersaturation of the API inducing nucleation and minimizing particle growth.[62] Additionally, the concentration of the API and the copolymer type and loading profoundly impact nucleation and growth kinetics which affects the resulting particle size. If mixing times are sufficiently fast (Damköhler number, D_a, $\leq$ 1), homogenous kinetics occur where particle size is no longer a function of jet velocity allowing for a more robust operation and precise particle size distribution. Using β-carotene and polystyrene(10)-b-poly(ethyleneoxide)(68), Johnson was able to produce uniform nanoparticles measuring 83 nm in diameter.[63]

The controlled precipitation technology [64] reported by Rogers et al. is a process capable of forming crystalline nanoparticles of poorly water soluble APIs with enhanced dissolution rates. The process consists of dissolving the API and stabilizer(s) in a water-miscible organic solvent. The organic phase is then added to an aqueous mixing zone where a decrease in solvent power causes rapid precipitation of the API which is then

immediately stabilized by dissolved stabilizers. The remaining organic solvent is then evaporated leaving an aqueous slurry which can be dried further through conventional methods (e.g. lyophilization, spray drying, etc).

Microemulsions and mini-emulsions differ from coarse emulsions based on size and method of polymerization [65, 66], and are thermodynamically stable systems. Creation of a microemulsion requires that an emulsion (o/w) be formed in the presence of a co-surfactant. In the correct ratios as determined by a ternary phase diagram, a transparent, thermodynamically stable system is formed. Common co-surfactants include lecithin, bile salts, sodium lauryl sulfate, and waxy alcohols such as cetyl alcohol. Further addition of water under mild agitation causes spontaneous precipitation of API nanoparticles. The microemulsion template technology developed by Mumper et al. utilizes microemulsions as a template for the formation of nanoparticles. The particle size is dependent on the internal droplet size of the microemulsion and since formation of microemulsions leads to a uniform particle size distribution, the resulting nanoparticles are very uniform. Precipitation of the nanoparticles by this technology occurs by cooling rather than dilution to spontaneously form API loaded nanoparticles. Dilution to induce precipitation lowers the API concentration resulting in larger final volumes which then must subsequently be administered to the patient. Oyewumi et al. further developed the microemulsion template technology to form surface modified nanoparticles for delivery of APIs specifically across the blood brain barrier (BBB).[67, 68] Successful permeation across the BBB was found to be dependent on surface polymer selection and the accompanying surface charge [69]

1.4 DESIRABLE ATTRIBUTES OF NANOPARTICLES – *IN VITRO*

It is hypothesized that enhancing the *in vitro* properties of poorly water soluble APIs through the processes described above allows for more favorable absorption *in vivo*. Most important of these is the increase in API dissolution as a result of increased surface area (decreased particle size). Biopharmaceutical Classification System (BCS) Class II drugs are poorly water soluble but highly permeable across biological membranes.[70] Therefore, the rate limiting step to API absorption is hypothesized to be dissolution of the API. Increasing dissolution rates through decreasing particle size can have a profound effect on increasing the bioavailability of this class of APIs. Many nanoparticle engineering technologies also have the ability to design particles through surface modification which can render the particle 'invisible' to the bodies natural defenses. Modification of the surface can also enhance dissolution by creating hydrophilic surfaces which interact with water more easily.

Due to their small size, interactions between the nanoparticles and their surroundings are also different than those of larger particles. For example, nanoparticles are influenced much more by Brownian motion which can enhance stabilization of nanoparticle suspensions.

1.4.1 Dissolution enhancement

The dissolution rate of a particle is described by the Noyes-Whitney equation (Eq. 1), which mathematically describes the *in vitro* dissolution rate of an API, and reveals the

physical factors (e.g. surface area, boundary layer thickness) that can influence the dissolution rate:

$$\frac{dC}{dt} = \frac{AD(C_S - C)}{h}$$ (1)

Where dC/dt is the rate of dissolution, A is the surface area of the particle, D is the diffusion coefficient, C_s is the apparent solubility of the API in the dissolution medium, C is the solubility of the API at time t, and h is the diffusion boundary layer. *$(C_s$-$C)$* becomes the concentration driving force for dissolution and can be neglected if the dissolution occurs under sink conditions (e.g. volume of medium at least greater than three times that required to form a saturated solution of the API).[71] Therefore, the dissolution rate is directly proportional to the particle size or surface area of the API. Using conventional rotor/stator milling followed by HPH and spray drying, Hecq et al. [72] manufactured high potency nifedipine/hydroxypropyl methylcellulose nanoparticles with a mean particle size of 291 nm before spray drying. After spray drying the particles were 3.7 microns due to agglomeration during the process. As seen in Fig. 1.2 the spray dried particles have enhanced dissolution with 70% dissolved after 20 minutes and complete dissolution after 2 hours. Inclusion of mannitol in the composition helped prevent agglomeration during the spray drying process (339 nm after spray drying) and led to complete dissolution within 10 minutes. The physical mixture of the same composition had a mean particle size of 98.7 microns and after 2 hours less than 10% had dissolved.

Reducing the particle size can also increase the solubility of the API according to the Ostwald-Freundlich equation, which assumes spherical particles:

18

$$\ln \frac{S}{S_o} = \frac{2\upsilon\gamma}{rRT} = \frac{2M\gamma}{\rho rRT} \qquad (2)$$

Where r is the particle radius, υ is the molar volume, ρ is the density, γ is the interfacial tension, and S is the solubility at temperature T. S_o is the solubility on a flat, solid sheet, M is the molecular weight of the solid, and R is the ideal gas constant. However, increases in solubility due to particle size reduction are negligible until particle size is decreased to well below 200 nm as seen in the hypothetical model shown in Fig. 1.3 [73]. As the particle size is decreased below 200 nm, the solubility relative to the equilibrium solubility (i.e. the solubility ratio, S/S_o) increases exponentially. Therefore, increasing the intrinsic solubility allows for more API to dissolve leading to increased dissolution rates. This can have a profound affect on increasing absorption of APIs in which the rate limiting step is dissolution.

Many of the nanoparticle technologies have the ability to create amorphous API which also can facilitate dissolution by lowering the required energy needed for dissolution to occur.[74] Supersaturation of the API within the surrounding medium can also be achieved which can further enhance the driving force for absorption across biological membranes. However, stability of the amorphous API becomes a concern since crystalline APIs exhibit a lower thermodynamic energy state and are more stable. Amorphous materials exhibit a glass transition temperature (T_g) which when exposed to temperatures higher than the T_g, structural rearrangement into a more stable crystalline lattice begins. Therefore, careful attention to particle stability must be given when designing amorphous nanoparticles. In order to prevent recrystallization, high T_g polymers, such as PVP, cellulose polymers like hydroxypropyl methylcellulose (HPMC)

19

and ethylcellulose (EC), and carbomers, must be included in the composition, preferably intimately mixed within the amorphous composition such as a solid dispersion or solution. Doing so will increase the overall T_g of the composition increasing its physical stability when exposed to higher storage temperatures.

1.4.2 Physical stability of nanoparticles

Particles are constantly being acted upon by surrounding forces (e.g. gravitational forces, normal forces, electrostatic forces and particle-particle interactions). In the solid state, nanoparticles behave much like larger particles, however, when they are included in various delivery vehicles such as a suspension or aerosol, their size can influence both the physical stability of the system and the amount delivered in to the body

Nanoparticles in a surrounding liquid environment which can be formed by microemulsion processes discussed earlier are extremely stable because the diffusion rate (Brownian motion) is higher than the sedimentation (or creaming) rate caused by gravity.[75] These nanoparticlulate systems can be used to deliver spontaneously forming SLNs or other polymeric nanoparticles parenterally, orally, topically, or by inhalation.

Aggregation of micro- or nanoparticles can lead to suspension destabilization, and occurs due to electrostatic interactions between particles. As particles randomly approach each other, electrostatic forces will facilitate bonding or will repel the particles depending on the zeta potential or the surface charge of the particles compared to the dispersing medium. A high net charge difference either positive or negative will lead to repulsion of the two particles while the opposite will lead to aggregation. As the aggregate grows,

gravitational forces become more significant leading to creaming or settling of the suspension. Inclusion of cationic or anionic surfactants can help prevent aggregation by influencing the zeta potential in either a positive or negative direction, respectively.

Ostwald ripening, which occurs as a result of high polydispersity, is the primary mechanism for suspension destabilization (e.g. physical separation) of microemulsions.[76] In suspensions, there exists a certain amount of solubility of the API within the dispersing liquid. Fluctuations in temperature can increase the propensity for Ostwald ripening to occur. As the temperature of the system increases, solubility increases and the smaller particles, having a higher surface area-to-volume ratio dissolve first. When the temperature decreases, the dissolved substances will precipitate and preferentially adsorb onto the surface of larger particles causing particle growth over time. As temperatures continue to increase and decrease, particle growth will continue causing suspension destabilization.

1.5 BENEFITS OF USING NANOPARTICLES - *IN VIVO*

We have discussed the advantages that nanoparticles have *in vitro* focusing on dissolution enhancement of poorly water soluble APIs and an increase in solubility with a decrease in particle size. Improved physical stability occurs through addition of non-ionic surfactants to the surface of the particles in order to reduce electrostatic attraction while physical separation is minimized by Brownian motion in nanoparticle dispersions. However, those advantages have little consequence if there is little or no improvement to *in vivo* properties including increased API absorption and efficacy and reduced variability and toxicity. It is essential to understand the role of particle size and surface modification

21

in API absorption through a variety of biological membranes. Nanoparticles as carrier systems are more easily absorbed across biological membranes because of their smaller size. Likewise, permeation can be facilitated by modifying the surface properties which is of particular importance to APIs which display poor absorption characteristics like proteins and peptides. Targeting specific sites within the body to deliver treatment is possible using surface modified nanoparticles especially on the cellular level. Nanoparticles also have the ability to avoid clearance by the immune system or adhering onto mucous membranes thereby increasing the residence time allowing more time for treatment to occur. Encapsulated nanoparticles offer protection to APIs susceptible to degradation mechanisms.

1.5.1 Influence of size on uptake across biological membranes

Nanoparticles have the ability to facilitate transport across biological membranes through a number of different ways. As stated earlier, nanoparticles can enhance dissolution of poorly water soluble APIs which can then easily permeate biological membranes like the GI tract where the API is taken up into systemic circulation. Undissolved nanoparticles have also shown the ability to aid absorption across membranes through a number of different pathways. All mucous membranes are coated with a mucous gel layer of entangled glycoproteins.[77] Small nanoparticles have the ability to diffuse through this entangled polymer layer much more efficiently than larger sized particles (greater than one micron) of the same material as depicted in Fig. 1.4 Adsorption isotherms show a linear increase in adsorption sites for nanoparticles while a Langmuir type isotherm for micron size particles suggests that a monolayer of particles

forms before saturation occurs. Therefore, more adsorption sites exist for smaller particles leading to a faster diffusion rate across the gel layer. Once particles arrive at the surface of the gastrointestinal wall, different pathways are available for translocation across the gastrointestinal wall. Specifically for nanoparticles smaller than 200 nm endocytosis by the absorptive cells facilitates translocation.[77] For larger particles, transcellular uptake becomes much more difficult; however, addition of hydrophilic polymers can increase transcellular uptake. Paracellular uptake through tight junctions is unlikely with nanoparticles but is possible if the tight junctions are disrupted.[77] Nanoparticles are also preferentially taken up by the M cells of the Peyer's patches located in the follicle-associated epithelium of the gastrointestinal tract as shown by Pappo and Ermak [78]. However, uptake by the M cells is size specific with 34% of 50 nm particles absorbed, 10% of 300 nm particles absorbed, and less than 5% of 1 micron particles absorbed [79]. In a study reported by Loper [80, 81] to investigate the absorption of a poorly water soluble API, particles of varying mean particle size (0.1-5 micron) were manufactured using the wet milling technique previously described. When delivered orally to fasted dogs the bioavailability significantly improved as particle size was decreased as seen in Fig. 1.5 showing a direct correlation between nanoparticle size and increased absorption. Vaughn et al. [82] studied the increase in oral absorption of danazol using the EPAS and SFL technologies to produce nanoparticles. The enhanced danazol formulations from both processes form supersaturated solutions during *in vitro* dissolution studies. SFL processed powders displayed a concentration 33% greater than the apparent solubility of danazol for 90 minutes while EPAS processed powders showed a 27% higher concentration than the apparent solubility for up to 60 minutes. This

23

phenomenon was attributed to the small particle size of the processed powders which were found in a previous study using STEM [7] to be 30 nm for the SFL danazol domains and 100 nm EPAS danazol domains. When these powders were orally administered to mice, the SFL powders showed a two-fold increase in C_{max} and a 3.8-fold increase in AUC after 24 hours compared to the crystalline physical mixture. The EPAS powders also showed about a two-fold increase in Cmax while having a 2.2-fold increase in AUC. The enhanced pharmacokinetic parameters were a direct result of the ability of the amorphous danazol nanoparticles to supersaturate allowing more drug to be absorbed.

Delivering nanoparticles to their site of action can be particularly challenging when the dose delivered is dependent on particle size which is the case for pulmonary delivery. The lungs consist of a series of bifurcating tubes terminating in the alveolar sacs in the deep lung. Gas exchange occurs in the deep lungs which are the most favorable site for APIs to enter systemic circulation. Optimum delivery of APIs to the lungs requires particles to be in the range of 1-5 microns (mass median aerodynamic diameter, MMAD). Due to inertial forces, particles larger than 5 microns will impact on the back of the throat and subsequently swallowed by the patient. Particles smaller than one micron are eventually exhaled by the patient as a result of longer settling times.[83] However, a small fraction of these inhaled nanoparticles can settle into the deep lung through diffusional processes. Therefore, nanoparticles are generally delivered to the deep lung via inclusion within nebulized liquid droplets [84] or solid microparticles [85]. Nanoparticles have been dispersed within a non-chlorofluorocarbon (CFC) propellant and delivered to the deep lung via a pressurized metered dose inhaler (pMDI).[86] These inhaled nanoparticles can result in enhanced uptake of API across the epithelial

membrane making nanoparticle delivery to the lung an attractive strategy for increased drug delivery.[87] Sham et al. [85] created gelatin and polybutylcyanoacrylate (PBCA) nanoparticles through a two step desolvation method and emulsion polymerization process, respectively. The nanoparticles were then added to a dissolved lactose aqueous solution and spray dried to form nanoparticle loaded lactose microparticles within the respirable size range. Dailey et al. [84] investigated the properties of different nebulizers on the delivery of nanoparticles to the lungs. The biodegradable PLGA based nanoparticles were prepared using an anti-solvent mixing technique and nebulized using a jet, ultrasonic, or piezo-electric crystal nebulizer. Aggregation of the suspension during nebulization was examined by filtration separation (> 0.8 micron) pre- and post-nebulization including the remaining suspension within the nebulizer reservoir. Aggregation was determined to be a function of particle surface charge with hydrophobic particles exhibiting the greatest affinity for aggregation. Differences in nebulizer performance were also noted. Results revealed that both jet and ultrasonic nebulizers produced excellent respirable fractions while the piezo-electric crystal nebulizer emitted droplets with large MMADs and decreased API output.

McConville et al. [88] developed itraconazole (ITZ) compositions using the SFL and EPAS technologies and dosed the compositions to mice. Dosing of the mice consisted of administration of the nanoparticle suspension administered via an ultrasonic nebulizer to the mice contained within a restraint-free dosing chamber [88]. Characterization of the nebulized suspensions showed high respirable fractions between 71-85% and MMADs between 2.7-2.82 μm for all compositions tested. *In vivo* pharmacokinetic studies showed high ITZ within the lung for both EPAS (C_{max} = 16.8

μg/g, AUC = 99.7 μg*h/ml) and an SFL composition (C_{max} = 13.4 μg/g, AUC = 85.8 μg*h/ml). In a later study, Vaughn et al. [89] studied the effect of single and multiple dosing via ultrasonic nebulizer of SFL processed ITZ nanoparticles on both the lung and serum concentrations compared to the orally administered Sporonox® solution. The studies showed that administration of ITZ nanoparticles to the lungs is an effective treatment for invasive fungal infections. It was also estimated that ITZ absorption into systemic circulation after pulmonary dosing over 12 days achieved high enough steady state concentrations of ITZ to act as a prophylaxis against certain strains of fungi, namely *A. fumigatus*.

1.5.2 Effect of surface modification on delivery of nanoparticles

Along with particle size, the surface characteristics of particles play an important role in how particles are absorbed within the body. Nanoparticulate systems can be designed to facilitate transport across biological membranes, target specific tissues or sites within the body, avoid uptake by the immune system, increase residence time within the body, or protect against premature degradation or metabolic processes.

1.5.2.1 Transport across biological membranes

Delivery of APIs across the BBB can be extremely difficult due to the built in defenses of the body to protect the brain against foreign substances. The structure of the blood brain barrier is much like that of the GI tract; however, tight junctions between endothelial cells are sealed by claudins making paracellular transport virtually

impossible. While reducing particle size can help increase transport across the BBB, the addition of surface modification of the particles is critical to increasing transport across the BBB. The endothelial cells of the BBB also contain a host of different transporters, receptors, and enzymes which serve to remove substances back into the blood or metabolize the substance before it can gain access to the brain. Surface modification can limit the rate of basolateral to apical transport by disguising recognition of the API by the transporters. The template microemulsion produced nanoparticles with various surface bound polymers to examine their effect on permeation across the BBB. [69, 90, 91] Studies revealed that low concentrated anionic formulated nanoparticles showed improved uptake [69] while thiamine coated nanoparticles facilitated binding to BBB thiamine transporters resulting in increased permeation [91].

1.5.2.2 Site specific targeting

Nowhere is targeted nanoparticle drug delivery more valuable than in the area of cancer therapy.   Traditional chemotherapy consists of parenteral administration of chemotherapeutic agents. These agents, many of which cause severe side effects, destroy both tumor and healthy cells alike. Because many of these compounds are poorly water soluble, solubilizing agents and adjuvants are often included in the formulation. These excipients can also cause serious life threatening side effects themselves. One of the most commercially successful chemotherapeutic products, Taxol® (paclitaxel, PAC) includes the adjuvant Cremophor EL which is known to cause hypersensitivity, nephrotoxicity, neurotoxicity, and cardiotoxicity.[92] Therefore, there is a tremendous

need in this area for delivery systems which can both eliminate the use of toxic excipients and enhance absorption leading to decreased dose.

Nanoparticles composed of biodegradable materials have the ability to move through capillaries to target tumors and evade immune responses which can prematurely eliminate the API from the body.[93]   Tumor pore sizes within several tumor models range from 380-780 nm [94, 95] so nanoparticle delivery offers a tremendous advantage to deliver the therapeutic agent directly into the tumor. Tumors also contain many API resistant mechanisms including P-glycoprotein transport mechanisms and outward interstitial flow which prevent APIs from remaining within the tumor. Yoo et al. [96] investigated the *in vivo* application of controlled release doxorubicin (DOX) conjugated PLGA nanoparticles and found that a single injection of the nanoparticles had similar activity to daily injections of free DOX over 12 days. Chen et al. [97] developed a SLN formulation of PAC and found that the SLN compositions had increased half-lives (10.06 and 4.88 hr) compared to the commercial product containing Cremophor EL (1.36 hr). Likewise, Fundaro et al. (2000)[98] found increased circulation (24 hr) of DOX loaded stealth SLNs in rats compared to the commercially available solution formulation (4 hr).

Little success has been made to reduce the toxicity of new nanoparticle formulations with many of the compositions having similar cytotoxicity as the commercial product when delivered parenterally.[99]   It is hypothesized that localized delivery of the chemotherapeutic agent to the tumor site should increase efficacy thereby reducing the required amount needed for tumor size reduction. However, efflux mechanisms within the tumor continue to make success more difficult. One strategy is to develop "smart nanoparticles" which preferentially bind to tumors and deliver their

payload.   These strategies include targeting the tumor-specific cells, targeting the tumor vasculature, or targeting through vessel formation, and have been reviewed in detail.[100] Current therapies utilize antibodies [101, 102], transferrin [103], or oligonucleotides [104] to actively target tumor sites which have been shown to bind to specific tumor antigens .   At least four current cancer therapies utilize antibodies for targeting with Rituxan[®] being the most successful.

One strategy to specifically target microorganisms causing bacterial, viral, and fungal infections is to preferentially target macrophages of the immune system in which the microorganisms may reside.[105, 106] The hydrophobic surfaces attract more plasma protein markers to adsorb to the surface of the particles and undergo endocytosis by the macrophages. Makino et al. [107] investigated the effect of both particle size and surface charge on the rate of uptake of polystyrene nanoparticles by alveolar macrophages. They found that 200 nm particles had considerably higher uptake as seen in Fig. 1.6a Likewise, Fig. 1.6b shows the amount of uptake of particles with varying functional groups. Therefore, both size and surface properties have an affect on particle uptake by macrophages. From this information, one can design particles to either avoid or reside within the lymphatic system depending on the intended use of the API.

1.5.2.3 Increasing residence time

As mentioned earlier, surface modification plays an important role in increasing the residence time of an API within the body. For intravenously delivered nanoparticles, clearance from the bloodstream occurs rapidly and is a function of the physico-chemical properties of the particles, primarily size, surface charge, and surface hydrophobicity.

Addition of hydrophilic polymers such as PEG prevents recognition by various markers of the complement system within the blood avoiding uptake by the circulating macrophages. Bocca et al. [108] examined the phagocytic uptake of stealth SLNs versus non-stealth SLNs using cultured murine macrophages. The stealth SLNs included addition of PEG 2000 to the lipid nanoparticle. In all cases, the stealth SLNs showed less than 5% of the dose taken up by the macrophages while the non-stealth SLNs showed on average 35-40% of the dose taken up after 90 minutes. PEGylated nanoparticles have also been shown to have potential as carriers for proteins and peptides which have difficulty crossing biological membranes.

Mucoadhesive polymers have the ability to increase residence times of nanoparticle systems in non-parenteral delivery systems. Some mucoadhesive polymers include chitosan, cellulose based polymers such as HPMC, carbomers, and sodium alginate. Many routes of administration have been employed mucoadhesive polymers to increase residence time including oral, nasal, transdermal, ocular, and vaginal drug delivery. The mechanism of polymer attachment is not well understood, however, it is believed that physical entanglement between the mucoadhesive polymer and mucin, a glucosylated glycoprotein found in abundance in mucus membranes, is responsible. It is also possible that electrostatic, hydrophobic, H-bonding or van der Waals' forces could contribute to further bonding interactions [109].

1.5.2.4 *Protection against enzymatic and chemical degradation*

Surface modified nanoparticles have also been used as protective carriers for delivery of APIs susceptible to enzymatic or chemical degradation, the most common

example being oral delivery of proteins, peptides, and nucleic acids. While water soluble compounds lie outside the scope of this review, it is worth briefly mentioning the use of nanoparticulate carriers that are able to increase absorption of these compounds by providing protection against degradation while facilitating permeation across biological membranes. Traditionally, the protein is loaded into the core of the nanoparticles and encapsulated in a protective shell through emulsification or phase separation methods.[110] The polymeric shell consists of polymers which can facilitate absorption across the GI tract as well as provide protection against degradation. Takeuchi et al. [111] recently designed chitosan-coated liposomes for delivery of calcitonin. *In vivo* studies showed the chitosan-coated liposomes had a prolonged pharmacological effect compared to the non-coated liposomes. The authors concluded that the prolonged pharmacological effect was due to the retentive properties of chitosan as well as its ability to avoid uptake by enterocytes.

1.6 CONCLUSION

Recently, nanoparticle research directed to pharmaceutical applications has resulted in many effective delivery systems which have improved the absorption and bioavailability of many poorly water soluble APIs. The *in vitro* properties inherent to nanoparticles are becoming more fully understood through the development of more accurate analytical techniques and equipment such as the TEM and AFM. At the same time, new particle engineering technologies are being developed to control the physico-chemical properties of nanoparticles to develop systems with superior *in vitro* properties. These technologies include those designed to reduce the particle size of existing particles

such as milling, as well as technologies designed to nucleate and stabilize nanoparticles. Significant research in formation and delivery of nanoparticles has been accomplished particularly in the areas of enhancing the properties of poorly water soluble APIs. This includes the effect of size on dissolution rate enhancement as well as addition of surface modifiers for dissolution enhancement, stabilization, and drug targeting. Only now are researchers beginning to understand how these nanoparticles, with their enhanced physico-chemical properties in combination with human physiology, are able to enhance absorption and bioavailability of these particles. Currently, work is being conducted to develop nanoparticles which have the ability to target specific sites within the body which can lead to increased efficacy, decreased dose requirements and decreased side effects. Research is also focusing on increasing the residence time within the body to allow for more API release. Nanoparticles are being designed to avoid unwanted metabolism and clearance through the use of surface modification (i.e. stealth and mucoadhesive particles).

1.7 REFERENCES

[1]   Terwogt, J.M.M., B. Nuijen, W.W.T. Huinink, and J.H. Beijnen, Alternative
        formulations of paclitaxel. Cancer Treat. Rev., **1997**, *23*(2): p. 87-95.

[2]   Cross, L.J., J. Bagg, and T.C. Aitchison, Efficacy of the cyclodextrin liquid
        preparation of itraconazole in treatment of denture stomatitis: Comparison with
        itraconazole capsules. Antimicrob. Agents Chemother., **2000**, *44*(2): p. 425-427.

[3]   Lee, V.H.L., Enzymatic Barriers to Peptide and Protein-Absorption. Critical Rev.
        in Therapeut. Drug Carrier Sys., **1988**, *5*(2): p. 69-97.

[4]   Delie, F. and M.J. Blanco-Prieto, Polymeric particulates to improve oral
        bioavailability of peptide drugs. Molecules, **2005**, *10*(1): p. 65-80.

[5]   Fu, L., L.C. Cao, Y.Q. Liu, and D.B. Zhu, Molecular and nanoscale materials and
        devices in electronics. Adv. Colloid Interface Sci., **2004**, *111*(3): p. 133-157.

[6]   Soppimath, K.S., T.M. Aminabhavi, A.R. Kulkarni, and W.E. Rudzinski,
        Biodegradable polymeric nanoparticles as drug delivery devices. J. Control.
        Release, **2001**, *70*(1-2): p. 1-20.

[7]   Vaughn, J.M., X.X. Gao, M.J. Yacaman, K.P. Johnston, and R.O. Williams,
        Comparison of powder produced by evaporative precipitation into aqueous
        solution (EPAS) and spray freezing into liquid (SFL) technologies using novel Z-
        contrast STEM and complimentary techniques. Eur. J. Pharm. Biopharm., **2005**,
        60(1): p. 81-89.

[8]   Dalgleish, D.G. and F.R. Hallett, Dynamic Light-Scattering - Applications to
        Food Systems. Food Res. Int., **1995**, *28*(3): p. 181-193.

[9]   Liversidge, G.G. and K.C. Cundy, Particle-Size Reduction for Improvement of
        Oral Bioavailability of Hydrophobic Drugs .1. Absolute Oral Bioavailability of
        Nanocrystalline Danazol in Beagle Dogs. Int. J. Pharm., **1995**, *125*(1): p. 91-97.

[10]   Muller, R.H., C. Jacobs, and O. Kayser, Nanosuspensions as particulate drug
        formulations in therapy Rationale for development and what we can expect for the
        future. Adv. Drug Deliv. Rev., **2001**, *47*(1): p. 3-19.

[11]   Rogers, T.L., K.P. Johnston, and R.O. Williams, Solution-based particle
        formation of pharmaceutical powders by supercritical or compressed fluid CO_2

and cryogenic spray-freezing technologies. Drug Dev. Ind. Pharm., **2001**, *27*(10): p. 1003-1015.

[12]   Hu, J.H., K.P. Johnston, and R.O. Williams, Nanoparticle engineering processes for enhancing the dissolution rates of poorly water soluble drugs - a review. Drug Dev. Ind. Pharm., **2004**, *30*(3): p. 247-258.

[13]   Hutchenson, K.W. and N.R. Foster, *Innovations in supercritical fluid science and technology*, in *Innovations in Supercritical Fluids*. 1995, ACS Press: Washington. p. 1-31.

[14]   Weber, M., L.M. Russell, and P.G. Debenedetti, Mathematical modeling of nucleation and growth of particles formed by the rapid expansion of a supercritical solution under subsonic conditions. J. Supercrit. Fluids, **2002**, *23*(1): p. 65-80.

[15]   Gander, B., P. Johansen, H. NamTran, and H.P. Merkle, Thermodynamic approach to protein microencapsulation into poly(D,L-lactide) by spray drying. Int. J. Pharm., **1996**, *129*(1-2): p. 51-61.

[16]   Raula, J., H. Eerikainen, and E.I. Kauppinen, Influence of the solvent composition on the aerosol synthesis of pharmaceutical polymer nanoparticles. Int. J. Pharm., **2004**, *284*(1-2): p. 13-21.

[17]   Eerikainen, H., W. Watanabe, E.I. Kauppinen, and P.P. Ahonen, Aerosol flow reactor method for synthesis of drug nanoparticles. Eur. J. Pharm. Biopharm., **2003**, *55*(3): p. 357-360.

[18]   Eerikainen, H., E.I. Kauppinen, and J. Kansikas, Polymeric drug nanoparticles prepared by an aerosol flow reactor method. Pharm. Res., **2004**, *21*(1): p. 136-143.

[19]   Vaughn, J.M., J.T. McConville, R.O. Williams III, and K.P. Johnston, Supersaturation Produces High Bioavailability of Amorphous Danazol Particles Formed by Evaporative Precipitation into Aqueous Solution (EPAS) and Spray Freezing into Liquid(SFL) Technologies. Drug Dev. Ind. Pharm., **2005**, *In Press*.

[20]   Sinswat, P., X. Gao, M.J. Yacaman, R.O. Williams III, and K.P. Johnston, Stabilizer choice for rapid dissolving high potency itraconazole particles formed by evaporative precipitation into aqueous solution. Int. J. Pharm., **2005**, *302*(1-2): p. 113-124.

[21]   Chen, X., J.M. Vaughn, M.J. Yacaman, R.O. Williams III, and K.P. Johnston, Rapid dissolution of high-potency danazol particles produced by evaporative precipitation into aqueous solution. J. Pharm. Sci., **2004**, *93*(7): p. 1867-1878.

[22]   Chen, X., Z. Benhayoune, R.O. Williams III, and K.P. Johnston, Rapid dissolution of high potency itraconazole particles produced by evaporative precipitation into aqueous solution. J. Drug Deliv. Sci. Technol., **2004**, *14*(4): p. 299-304.

[23]   Chen, X., T.J. Young, M. Sarkari, R.O. Williams III, and K.P. Johnston, Preparation of cyclosporine A nanoparticles by evaporative precipitation into aqueous solution. Int. J. Pharm., **2002**, *242*(1-2): p. 3-14.

[24]   Sarkari, M., J. Brown, X. Chen, S. Swinnea, R.O. Williams III, and K.P.

Johnston, Enhanced drug dissolution using evaporative precipitation into aqueous

solution. Int. J. Pharm., **2002**, *243*(1-2): p. 17-31.

[25]   Kawasaki, E.S. and A. Player, Nanotechnology, nanomedicine, and the

development of new, effective therapies for cancer. Nanomedicine, **2005**, *1*(2): p.

101-109.

[26]   Agnihotri, S.A., N.N. Mallikarjuna, and T.M. Aminabhavi, Recent advances on

chitosan-based micro- and nanoparticles in drug delivery. J. Control. Release,

2004, *100*(1): p. 5-28.

[27]   Pandey, R., A. Sharma, A. Zahoor, S. Sharma, G.K. Khuller, and B. Prasad, Poly

(DL-lactide-co-glycolide) nanoparticle-based inhalable sustained drug delivery

system for experimental tuberculosis. J. Antimicrob. Chemother., **2003**, *52*(6): p.

981-986.

[28]   Rosca, I.D., F. Watari, and M. Uo, Microparticle formation and its mechanism in

single and double emulsion solvent evaporation. J. Control. Release, **2004**, *99*(2):

p. 271-280.

[29]   Schwarz, C., W. Mehnert, J.S. Lucks, and R.H. Muller, Solid Lipid Nanoparticles

(Sln) for Controlled Drug-Delivery .1. Production, Characterization and

Sterilization. J. Control. Release, **1994**, *30*(1): p. 83-96.

[30]   Muller, R.H., S. Maassen, C. Schwarz, and W. Mehnert, Solid lipid nanoparticles

(SLN) as potential carrier for human use: Interaction with human granulocytes. J.

Control. Release, **1997**, *47*(3): p. 261-269.

[31]   Wissing, S.A., O. Kayser, and R.H. Muller, Solid lipid nanoparticles for parenteral drug delivery. Adv. Drug Deliv. Rev., **2004**, *56*(9): p. 1257-1272.

[32]   Muller, R.H., K. Mader, and S. Gohla, Solid lipid nanoparticles (SLN) for controlled drug delivery - a review of the state of the art. Eur. J. Pharm. Biopharm., **2000**, *50*(1): p. 161-177.

[33]   Mehnert, W. and K. Mader, Solid lipid nanoparticles - Production, characterization and applications. Adv. Drug Deliv. Rev., **2001**, *47*(2-3): p. 165-196.

[34]   Gasco, M.R., Method for producing solid lipid microspheres having a narrow size distribution, US Patent #5,250,236. 1993

[35]   Moghimi, S.M. and J. Szebeni, Stealth liposomes and long circulating nanoparticles: critical issues in pharmacokinetics, opsonization and protein-binding properties. Prog. Lipid Res., **2003**, *42*(6): p. 463-478.

[36]   Gref, R., M. Luck, P. Quellec, M. Marchand, E. Dellacherie, S. Harnisch, T. Blunk, and R.H. Muller, 'Stealth' corona-core nanoparticles surface modified by polyethylene glycol (PEG): influences of the corona (PEG chain length and surface density) and of the core composition on phagocytic uptake and plasma protein adsorption. Colloid Surf. B-Biointerfaces, **2000**, *18*(3-4): p. 301-313.

[37]   Oyler, J., Liquid substances freeze-drying systems and methods, US Patent #5,208,998. 1993

[38]   Williams, R.O., K.P. Johnston, T.L. Rogers, M.K. Barron, T.J. Young, Z. Yu, and J. Hu, Process for production of nanoparticles and microparticles by spray freezing into liquid, US Patent #6,862,890. 2003

[39]   Overhoff, K., B. Scherzer, E. Elder, K.P. Johnston, and R.O. Williams III. *Ultra-rapid Freezing to Micronize Water Insoluble Drugs - A Comparison to Spray Freezing into Liquid*. in The Proceedings of the American Association of Pharmaceutical Sciences. 2004. Salt lake city, UT.

[40]   Purvis, T., R.O. Williams III, and K.P. Johnston. *Rapid Dissolving Repaglinide Powders Produced by Ultra-Rapid Freezing Process*. in The Proceedings of the American Association of Pharmaceutical Scientists. 2005. Memphis, TN.

[41]   Hu, J.H., K.P. Johnston, and R.O. Williams, Stable amorphous danazol nanostructured powders with rapid dissolution rates produced by spray freezing into liquid. Drug Dev. Ind. Pharm., **2004**, *30*(7): p. 695-704.

[42]   Rogers, T.L., K.P. Johnston, and R.O. Williams, Physical stability of micronized powders produced by spray-freezing into liquid (SFL) to enhance the dissolution of an insoluble drug. Pharm. Dev. Technol., **2003**, *8*(2): p. 187-197.

[43]   Rogers, T.L., K.A. Overhoff, P. Shah, P. Santiago, M.J. Yacaman, K.P. Johnston, and R.O. Williams, Micronized powders of a poorly water soluble drug produced by a spray-freezing into liquid-emulsion process. Eur. J. Pharm. Biopharm., **2003**, *55*(2): p. 161-172.

[44]   Hu, J., K.P. Johnston, and R.O. Williams III, Spray freezing into liquid (SFL) particle engineering technology to enhance dissolution of poorly water soluble drugs: organic solvent versus organic/aqueous co-solvent systems. Eur. J. Pharm. Sci., **2003**, *20*(3): p. 295-303.

[45]   Hu, J.H., T.L. Rogers, J. Brown, T. Young, K.P. Johnston, and R.O. Williams III, Improvement of dissolution rates of poorly water soluble APIs using novel spray freezing into liquid technology. Pharm. Res., **2002**, *19*(9): p. 1278-1284.

[46]   Yu, Z.S., K.P. Johnston, and R.O. Williams, Spray freezing into liquid versus spray-freeze drying: Influence of atomization on protein aggregation and biological activity. Eur. J. Pharm. Sci., **2006**, *27*(1): p. 9-18.

[47]   Rogers, T.L., A.C. Nelsen, M. Sarkari, T.J. Young, K.P. Johnston, and R.O. Williams III, Enhanced aqueous dissolution of a poorly water soluble drug by novel particle engineering technology: Spray-freezing into liquid with atmospheric freeze-drying. Pharm. Res., **2003**, *20*(3): p. 485-493.

[48]   Rogers, T.L., A.C. Nelsen, J. Hu, J.N. Brown, M. Sarkari, T.J. Young, K.P. Johnston, and R.O. Williams III, A novel particle engineering technology to enhance dissolution of poorly water soluble drugs: spray-freezing into liquid. Eur. J. Pharm. Biopharm., **2002**, *54*(3): p. 271-280.

[49]   Hu, J., K.P. Johnston, and R.O. Williams III, Rapid dissolving high potency danazol powders produced by spray freezing into liquid process. Int. J. Pharm., **2004**, *271*(1-2): p. 145-154.

[50]   York, P., Strategies for particle design using supercritical fluid technologies. Pharm. Sci. Tech. Today, **1999**, *2*(11): p. 430-440.

[51]   Debenedetti, P.G., J.W. Tom, X. Kwauk, and S.D. Yeo, Rapid Expansion of Supercritical Solutions (Ress) - Fundamentals and Applications. Fluid Phase Equilib., **1993**, *82*: p. 311-321.

[52]   Dixon, D.J., G. Lunabarcenas, and K.P. Johnston, Microcellular Microspheres and Microballoons by Precipitation with a Vapor-Liquid Compressed Fluid Antisolvent. Polymer, **1994**, *35*(18): p. 3998-4005.

[53]   Yeo, S.D., G.B. Lim, P.G. Debenedetti, and H. Bernstein, Formation of Microparticulate Protein Powders Using a Supercritical Fluid Antisolvent. Biotechnol. Bioeng., **1993**, *41*(3): p. 341-346.

[54]   Wang, Y.L., R.N. Dave, and R. Pfeffer, Polymer coating/encapsulation of nanoparticles using a supercritical anti-solvent process. J. Supercrit. Fluids, **2004**, *28*(1): p. 85-99.

[55]   Tsutsumi, A., S. Nakamoto, T. Mineo, and K. Yoshida, A Novel Fluidized-Bed Coating of Fine Particles by Rapid Expansion of Supercritical-Fluid Solutions. Powder Technol., **1995**, *85*(3): p. 275-278.

[56]   Rasenack, N. and B.W. Muller, Dissolution rate enhancement by in situ micronization of poorly water-soluble drugs. Pharm. Res., **2002**, *19*(12): p. 1894-1900.

[57]   Steckel, H., N. Rasenack, P. Villax, and B.W. Muller, In vitro characterization of jet-milled and in-situ-micronized fluticasone-17-propionate. Int. J. Pharm., **2003**, *258*(1-2): p. 65-75.

[58]   Steckel, H., N. Rasenack, and B.W. Muller, In-situ-micronization of disodium cromoglycate for pulmonary delivery. Eur. J. Pharm. Biopharm., **2003**, *55*(2): p. 173-180.

[59] Crooks, R., M. Joanicot, R.K. Prud'Homme;, and J. Coret, Aqueous suspension of nanoparticles comprising an agrochemical active ingredient, US Patent #6,638,994. 2003

[60] Johnson, B.K. and R.K. Prud'homme, Flash NanoPrecipitation of organic actives and block copolymers using a confined impinging jets mixer. Aust. J. Chem., **2003**, *56*(10): p. 1021-1024.

[61] Johnson, B.K. and R.K. Prud'homme, Mechanism for rapid self-assembly of block copolymer nanoparticles. Phys. Rev. Lett., **2003**, *91*(11).

[62] Johnson, B.K. and R.K. Prud'homme, Chemical processing and micromixing in confined impinging jets. Aiche J., **2003**, *49*(9): p. 2264-2282.

[63] Johnson, B.K., *Flash NanoPrecipitation of Organic Actives via Confined Micromixing and Block Copolymer Stabilization*, in *Chemical Engineering*. 2003, Princeton University: Princeton, NJ. p. 363.

[64] Rogers, T.L., I.B. Gillespie, J.E. Hitt, K.L. Fransen, C.A. Crowl, C.J. Tucker, G.B. Kupperblatt, J.N. Becker, D.L. Wilson, C. Todd, and E.J. Elder, Development and characterization of a scalable controlled precipitation process to enhance the dissolution of poorly water-soluble drugs. Pharm. Res., **2004**, *21*(11): p. 2048-2057.

[65] Schork, F.J., G.W. Poehlein, S. Wang, J. Reimers, J. Rodrigues, and C. Samer, Miniemulsion polymerization. Colloid Surf. A-Physicochem. Eng. Asp., **1999**, *153*(1-3): p. 39-45.

[66] Antonietti, M. and K. Landfester, Polyreactions in miniemulsions. Prog. Poly. Sci., **2002**, *27*(4): p. 689-757.

[67]   Oyewumi, M.O. and R.J. Mumper, Engineering tumor-targeted gadolinium hexanedione nanoparticles for potential application in neutron capture therapy. Bioconjugate Chem., **2002**, *13*(6): p. 1328-1335.

[68]   Oyewumi, M.O. and R.J. Mumper, Gadolinium-loaded nanoparticles engineered from microemulsion templates. Drug Dev. Ind. Pharm., **2002**, *28*(3): p. 317-328.

[69]   Lockman, P.R., J.M. Koziara, R.J. Mumper, and D.D. Allen, Nanoparticle surface charges alter blood-brain barrier integrity and permeability. J. Drug Target., **2004**, *12*(9-10): p. 635-641.

[70]   Amidon, G.L., H. Lennernas, V.P. Shah, and J.R. Crison, A Theoretical Basis for a Biopharmaceutic Drug Classification - the Correlation of in-Vitro Drug Product Dissolution and in-Vivo Bioavailability. Pharm. Res., **1995**, *12*(3): p. 413-420.

[71]   Brown, C.K., *Dissolution Method Development: An Industry Perspective*, in *Pharmaceutical Dissolution Testing*, J.B. Dressman and J. Kramer, Editors. 2005, Taylor & Francis: Boca Raton, FL. p. 351-372.

[72]   Hecq, J., M. Deleers, D. Fanara, H. Vranckx, and K. Amighi, Preparation and characterization of nanocrystals for solubility and dissolution rate enhancement of nifedipine. Int. J. Pharm., **2005**, *299*(1-2): p. 167-177.

[73]   Kipp, J.E., The role of solid nanoparticle technology in the parenteral delivery of poorly water-soluble drugs. Int. J. Pharm., **2004**, *284*(1-2): p. 109-122.

[74]   Yoshihashi, Y., H. Kitano, E. Yonemochi, and K. Terada, Quantitative correlation between initial dissolution rate and heat of fusion of drug substance. Int. J. Pharm., **2000**, *204*(1-2): p. 1-6.

[75]   Solans, C., P. Izquierdo, J. Nolla, N. Azemar, and M.J. Garcia-Celma, Nano-emulsions. Curr. Opin. Colloid In., **2005**, *10*(3-4): p. 102-110.

[76]   Tadros, T., R. Izquierdo, J. Esquena, and C. Solans, Formation and stability of nano-emulsions. Adv. Colloid Interface Sci., **2004**, *108-09*: p. 303-318.

[77]   Ponchel, G. and J.M. Irache, Specific and non-specific bioadhesive particulate systems for oral delivery to the gastrointestinal tract. Adv. Drug Deliv. Rev., **1998**, *34*(2-3): p. 191-219.

[78]   Pappo, J. and T.H. Ermak, Uptake and Translocation of Fluorescent Latex-Particles by Rabbit Peyers Patch Follicle Epithelium - a Quantitative Model for M Cell Uptake. Clin. Exp. Immunol., **1989**, *76*(1): p. 144-148.

[79]   Jani, P., G.W. Halbert, J. Langridge, and A.T. Florence, The Uptake and Translocation of Latex Nanospheres and Microspheres after Oral-Administration to Rats. J. Pharm. Pharmacol., **1989**, *41*(12): p. 809-&.

[80]   Loper, A. *Poorly soluble compounds: vehicle selection and solubilization*. in Land O'Lakes Conference: Drug Metabolism and Pharmacokinetics. 1999.

[81]   Merisko-Liversidge, E., G.G. Liversidge, and E.R. Cooper, Nanosizing: a formulation approach for poorly-water-soluble compounds. Eur. J. Pharm. Sci., **2003**, *18*(2): p. 113-120.

[82]   Vaughn, J.M., J.T. McConville, R.O. Williams, and K.P. Johnston, Supersaturation Produces High Bioavailability of Amorphous Danazol Particles Formed by Evaporative Precipitation into Aqueous Solution (EPAS) and Spray Freezing into Liquid(SFL) Technologies. Drug Dev. Ind. Pharm., **2005**, *In Press*.

[83]   Hickey, A.J., *Delivery of Drugs by the Pulmonary Route*, in *Modern Pharmaceutics*, G.S. Banker and C.T. Rhodes, Editors. 2002, Marcel Dekker, Inc.: New York, NY. p. 479-500.

[84]   Dailey, L.A., T. Schmehl, T. Gessler, M. Wittmar, F. Grimminger, W. Seeger, and T. Kissel, Nebulization of biodegradable nanoparticles: impact of nebulizer technology and nanoparticle characteristics on aerosol features. J. Control. Release, **2003**, *86*(1): p. 131-144.

[85]   Sham, J.O.H., Y. Zhang, W.H. Finlay, W.H. Roa, and R. Lobenberg, Formulation and characterization of spray-dried powders containing nanoparticles for aerosol delivery to the lung. Int. J. Pharm., **2004**, *269*(2): p. 457-467.

[86]   Dickinson, P.A., S.W. Howells, and I.W. Kellaway, Novel nanoparticles for pulmonary drug administration. J. Drug. Target., **2001**, *9*(4): p. 295-302.

[87]   Borm, P.J.A. and W. Kreyling, Toxicological hazards of inhaled nanoparticles - Potential implications for drug delivery. J. Nanosci. Nanotechnol., **2004**, *4*(5): p. 521-531.

[88]   McConville, J.T., R.O. Williams, T.C. Carvalho, A.N. Iberg, K.P. Johnston, R.L. Talbert, D. Burgess, and J.I. Peters, Design and evaluation of a restraint-free small animal inhalation dosing chamber. Drug Dev. Ind. Pharm., **2005**, *31*(1): p. 35-42.

[89]   Vaughn, J.M., J.T. McConville, D. Burgess, R.L. Talbert, J.I. Peters, R.O. Williams III, and K.P. Johnston, Single Dose and Multiple Dose studies of Aerosolized Itraconazole Nanoparticles. Eur. J. Pharm. Biopharm., **2005**, *63*(2): p. 95-102.

[90]   Koziara, J.M., P.R. Lockman, D.D. Allen, and R.J. Mumper, In situ blood-brain barrier transport of nanoparticles. Pharm. Res., **2003**, *20*(11): p. 1772-1778.

[91]   Lockman, P.R., M.O. Oyewumi, J.M. Koziara, K.E. Roder, R.J. Mumper, and D.D. Allen, Brain uptake of thiamine-coated nanoparticles. J. Control. Release, **2003**, *93*(3): p. 271-282.

[92]   Weiss, R.B., R.C. Donehower, P.H. Wiernik, T. Ohnuma, R.J. Gralla, D.L. Trump, J.R. Baker, D.A. Vanecho, D.D. Vonhoff, and B. Leylandjones, Hypersensitivity Reactions from Taxol. J. Clin. Oncol., **1990**, *8*(7): p. 1263-1268.

[93]   Evora, C., I. Soriano, R.A. Rogers, K.M. Shakesheff, J. Hanes, and R. Langer, Relating the phagocytosis of microparticles by alveolar macrophages to surface chemistry: the effect of 1,2-dipalmitoylphosphatidylcholine. J. Control. Release, **1998**, *51*(2-3): p. 143-152.

[94]   Hobbs, S.K., W.L. Monsky, F. Yuan, W.G. Roberts, L. Griffith, V.P. Torchilin, and R.K. Jain, Regulation of transport pathways in tumor vessels: Role of tumor type and microenvironment. Proc. Natl. Acad. Sci. U. S. A., **1998**, *95*(8): p. 4607-4612.

[95]   Yuan, F., M. Dellian, D. Fukumura, M. Leunig, D.A. Berk, V.P. Torchilin, and R.K. Jain, Vascular-Permeability in a Human Tumor Xenograft - Molecular-Size Dependence and Cutoff Size. Cancer Res., **1995**, *55*(17): p. 3752-3756.

[96]   Yoo, H.S., K.H. Lee, J.E. Oh, and T.G. Park, In vitro and in vivo anti-tumor activities of nanoparticles based on doxorubicin-PLGA conjugates. J. Control. Release, **2000**, *68*(3): p. 419-431.

[97]   Chen, D.B., T.Z. Yang, W.L. Lu, and Q. Zhang, In vitro and in vivo study of two types of long-circulating solid lipid nanoparticles containing paclitaxel. Chem. Pharm. Bull., **2001**, *49*(11): p. 1444-1447.

[98]   Fundaro, A., R. Cavalli, A. Bargoni, D. Vighetto, G.P. Zara, and M.R. Gasco, Non-stealth and stealth solid lipid nanoparticles (SLN) carrying doxorubicin: Pharmacokinetics and tissue distribution after i.v. administration to rats. Pharmacol. Res., **2000**, *42*(4): p. 337-343.

[99]   Feng, S.S. and S. Chien, Chemotherapeutic engineering: Application and further development of chemical engineering principles for chemotherapy of cancer and other diseases. Chem. Eng. Sci., **2003**, *58*(18): p. 4087-4114.

[100]   Brannon-Peppas, L. and J.O. Blanchette, Nanoparticle and targeted systems for cancer therapy. Adv. Drug Deliv. Rev., **2004**, *56*(11): p. 1649-1659.

[101]   Kohler, G. and C. Milstein, Continuous Cultures of Fused Cells Secreting Antibody of Predefined Specificity. Nature, **1975**, *256*(5517): p. 495-497.

[102]   Cortez-Retamozo, V., N. Backmann, P.D. Senter, U. Wernery, P. De Baetselier, S. Muyldermans, and H. Revets, Efficient cancer therapy with a nanobody-based conjugate. Cancer Res., **2004**, *64*(8): p. 2853-2857.

[103]   Xu, Z.H., W.W. Gu, J. Huang, H. Sui, Z.H. Zhou, Y.X. Yang, Z. Yan, and Y.P. Li, In vitro and in vivo evaluation of actively targetable nanoparticles for paclitaxel delivery. Int. J. Pharm., **2005**, *288*(2): p. 361-368.

[104]   Schiffelers, R.M., A. Ansari, J. Xu, Q. Zhou, Q.Q. Tang, G. Storm, G. Molema, P.Y. Lu, P.V. Scaria, and M.C. Woodle, Cancer siRNA therapy by tumor

selective delivery with ligand-targeted sterically stabilized nanoparticle. Nucleic Acids Res., **2004**, *32*(19).

[105]   Chellat, F., Y. Merhi, A. Moreau, and L. Yahia, Therapeutic potential of nanoparticulate systems for macrophage targeting. Biomaterials, **2005**, *26*(35): p. 7260-7275.

[106]   Pinto-Alphandary, H., A. Andremont, and P. Couvreur, Targeted delivery of antibiotics using liposomes and nanoparticles: research and applications. Int. J. Antimicrob. Agents, **2000**, *13*(3): p. 155-168.

[107]   Makino, K., N. Yamamoto, K. Higuchi, N. Harada, H. Ohshima, and H. Terada, Phagocytic uptake of polystyrene microspheres by alveolar macrophages: effects of the size and surface properties of the microspheres. Colloid Surf. B-Biointerfaces, **2003**, *27*(1): p. 33-39.

[108]   Bocca, C., O. Caputo, R.B. Cavalli, L. Gabriel, A. Miglietta, and M.R. Gasco, Phagocytic uptake of fluorescent stealth and non-stealth solid lipid nanoparticles. Int. J. Pharm., **1998**, *175*(2): p. 185-193.

[109]   Salamat-Miller, N., M. Chittchang, and T.P. Johnston, The use of mucoadhesive polymers in buccal drug delivery. Adv. Drug Deliv. Rev., **2005**, *57*(11): p. 1666-1691.

[110]   Takeuchi, H., H. Yamamoto, and Y. Kawashima, Mucoadhesive nanoparticulate systems for peptide drug delivery. Adv. Drug Deliv. Rev., **2001**, *47*(1): p. 39-54.

[111]   Takeuchi, H., Y. Matsui, H. Sugihara, H. Yamamoto, and Y. Kawashima, Effectiveness of submicron-sized, chitosan-coated liposomes in oral administration of peptide drugs. Int. J. Pharm., **2005**, *303*(1-2): p. 160-170.

[112]   Ponchel, G., M.J. Montisci, A. Dembri, C. Durrer, and D. Duchene,

Mucoadhesion of colloidal particulate systems in the gastro-intestinal tract. Eur. J.

Pharm. Biopharm., **1997**, *44*(1): p. 25-31.

1.8 DISSERTATION OBJECTIVES AND OUTLINE

Many new chemical entities (NCE) being developed today display poor water solubility and as a result suffer from poor oral bioavailability. Therefore, a need exists to modify the physical properties of these NCEs allowing the body to more easily absorb the chemicals and acquire the desired therapeutic effect. In chapter 1, several techniques for improving the bioavailability of these poorly water soluble compounds through nanoparticle formation and nanoparticle delivery systems are introduced. In addition, the desirable *in vitro* and *in vivo* properties of these systems are described in great detail to assess the importance of size reduction and surface modification on the improvement of these compounds. The overall objective of this dissertation was to formulate, characterize, and evaluate nanoparticle delivery systems developed from rapid freezing processes through *in vitro* and *in vivo* analysis. Active pharmaceutical ingredients (API) were selected based on a need within the pharmaceutical industry for bioavailability improvement. Formulations were produced using the rapid freezing technologies spray freezing into liquid (SFL) or ultra-rapid freezing (URF). *In vivo* studies were performed using well established animal models to assess the improvement of the processed powders compared to the bulk material or the current commercial product containing the API.

The aim of chapter 2 was to investigate the influence of hydrophilic stabilizers in powder compositions prepared by the spray freezing into liquid (SFL) process using either an emulsion feed dispersion or an organic co-solvent feed solution on enhancing the wetting and dissolution properties of nanostructured aggregates containing itraconazole. The particles were evaluated based on degree of crystallinity, dissolution

rate and morphology to determine the optimum stabilizer combination for testing in an animal model. The *in vivo* performance of the optimum micronized powder was compared to the itraconazole commercial product in a study performed in collaboration with the University of Texas Health Science Center in San Antonio highlighting the importance of these studies to validate these technologies for clinical use.

Up to this point, a majority of the particle engineering utilizing rapid freezing was performed with the SFL process. A novel freezing technology was introduced to facilitate process scale up under commercial manufacturing conditions. The URF process entails freezing an API/excipient solution drop-wise onto the surface of a solid cryogen. The hypothesis is that the URF process can produce powders with enhanced physico-chemical properties leading to improvements in bioavailability of poorly water soluble compounds. In order to determine if the freezing rates were sufficient to manufacture powders with the desired physico-chemical properties, a study was conducted to model the freezing rates and to determine any limiting factors that may exist. The study described in chapter 3 provides an detailed explanation of how the solvent's physical properties and thin film geometry influence the freezing rate and consequently the final physicochemical properties of URF processed powders. Sound engineering concepts of heat transfer were applied to model the freezing droplet and assess the advantages of using this method of rapid freezing. In addition, a novel approach to measuring the heat transfer between the droplet and the cryogenic substrate was performed using a high speed infra-red camera. Lastly, particle performance was evaluated using *in vitro* tests to validate the URF process.

In subsequent studies (chapters 4 and 5), the URF process was utilized to manufacture enhanced compositions for immediate release of tacrolimus and modified release of itraconazole, respectively. The objective of chapter 4 was to investigate the

50

effects of combinations of polymeric stabilizers on the maximum degree and extent of supersaturation of tacrolimus and to establish if an *in vitro-in vivo* correlation exists between supersaturation and improved pharmacokinetic parameters for orally administered tacrolimus. It was hypothesized that the production of supersaturated solutions could enhance the transport of tacrolimus across biological membranes thereby enhancing the bioavailability of tacrolimus. Differences were observed in supersaturated dissolution profiles of the tacrolimus compositions which correlated to differences in the pharmacokinetic profiles for each of the compositions. In addition, it was found that the URF micronized powders showed enhanced absorption over the commercial tacrolimus product as a result of the improved physico-chemical properties.

Because of the enhanced physico-chemical properties such as rapid dissolution rates are associated with rapid freezing processes, these processes have traditionally been utilized to develop immediate release systems. However, increased bioavailabilities can also be achieved through the utilization of modified drug release by controlling the release of the drug thereby preventing premature precipitation and recrystallization which can decrease drug absorption. Amorphous solid dispersions containing enteric polymers could overcome these limitations by 1.) delaying dissolution until the compound enters the small intestines and preventing premature precipitation of the ITZ and 2.) increasing the apparent solubility at higher pH to increase the driving force for absorption. The objective of the final study was to investigate the influence of composition parameters including drug:polymer ratio and polymer type, and particle structure of enteric solid dispersions on the release of ITZ under sink and supersaturated dissolution conditions. Particles were characterized by thermal methods, to determine the miscibility limits of itraconazole in the polymers. Once miscibility limits were established, the dissolution performance of the particles under both sink and supersaturated conditions was evaluated

51

to elucidate how the release kinetics were influenced by the miscibility of ITZ within the polymer.

Chapter 2: The Influence of Hydrophilic Stabilizer on Dissolution Enhancement and Oral Bioavailability of Itraconazole Nanoparticles Prepared by Spray Freezing into Liquid

2.1 ABSTRACT

The aim of this study is to investigate the influence of hydrophilic stabilizers in powder compositions prepared by the spray freezing into liquid (SFL) process using either an emulsion feed dispersion or organic co-solvent feed solutions on enhancing the wetting and dissolution properties of nanostructured aggregates containing itraconazole (ITZ). Subsequently, an *in vivo* pharmacokinetic study was conducted comparing powder from the emulsion feed dispersion, commercially available cyclodextrin-based Sporanox® oral solution, and micronized crystalline ITZ. SFL A was manufactured from an emulsion feed dispersion consisting of ITZ, sorbitan monooleate (S80), poloxamer 188 (P188), and polyethylene glycol 8000 (PEG) (1:1:2:1) in a 33:67 dichloromethane:water emulsion. SFL B and C were manufactured from an organic co-solvent feed solution and consisted of ITZ, poloxamer 407 (P407) and polysorbate 80 (T80) (1:0.75:0.75) or ITZ, polysorbate 20 (T20) and polyvinylpyrrolidone K15 (PVPK15) (10:1:2), respectively. Examination by scanning electron microscopy of particles produced by the SFL process revealed porous aggregated structures, compared to dense aggregates with crystalline habits for the bulk micronized ITZ. Both SFL A and SFL C produced powders containing nanoparticle domains containing ITZ. BET analysis showed high surface areas of 15.5-20.3 m^2/g for the SFL powders while x-ray diffraction

studies revealed a lack of crystallinity in any of the SFL processed samples. According to the *in vitro* characterization, the SFL process created high surface area particles containing amorphous ITZ allowing for rapid dissolution enhancement. The pharmacokinetic profiles obtained for SFL A and Sporanox[®] oral solution showed similarities between both the absorption profiles and the estimated pharmacokinetic parameters. Analysis of the $AUC_{(0-24)}$ revealed that the SFL formulation was 84% of the commercially available Sporanox[®], further demonstrating the similarity of performance of SFL A compared to the cyclodextrin-based Sporanox *in vivo*. Serum levels for the micronized crystalline ITZ powder were not detected. In conclusion, the SFL powder from an emulsion feed dispersion produced surface stabilized amorphous nanoparticle domains which enhanced the physico-chemical properties (wetting, surface area, particle size) leading to enhanced dissolution rate and *in vivo* oral bioavailability.

2.2 INTRODUCTION

Diagnosis of systemic fungal infections has increased dramatically over the last 20 years, in part due to the increasing number of immunosuppressed or immunocompromised patients such as those receiving chemotherapy treatment, transplant recipients, HIV/AIDS patients, and the elderly.[1] *Aspergillus spp.* continues to be one of the most common and deadly invasive fungal infection responsible for 62% of cases. However, first line treatment using amphotericin B deoxycholate or liposomal amphotericin has failed to improve mortality rates which can reach as high as 90% in central nervous system (CNS) patients.[2] Likewise, case fatality rates were 99%, 86%, and 66% for cerebral, pulmonary, and sinus aspergillosis, respectively.[3, 4] While amphotericin B has failed to show improvements in mortality rates of patients with aspergillosis, itraconazole (ITZ) treatment has lowered the mortality rates of patients more than 15% compared to amphotericin treatments.[3]

Itraconazole, a broad-spectrum triazole anti-fungal agent developed in the early 1980s by Janssen Research Foundation [5] is a Biopharmaceutical Classification System (BCS) class II drug. Because of the solubility and dissolution rate limitations of class II drugs, ITZ has shown poor bioavailability in vivo. Likewise, ITZ is a weak base (pK_a=3.7), and has a higher water solubility at low pH, 4 µg/ml in pH = 1.0 compared to ~1 ng/ml in de-ionized water.[6]

In the SFL process, a poorly water soluble drug and stabilizing agent(s) are dissolved in a suitable solvent to create a liquid feed (solution or emulsion), atomized

under high pressure through a nozzle which is submerged below the surface of liquid nitrogen, and subsequently freeze-dried to remove any frozen solvent. Rogers et al. demonstrated that an emulsion feed dispersion could be used to manufacture powders with high danazol:polymer ratios and high solids loadings (using less organic solvents) while maintaining enhanced physico-chemical properties traditionally seen in co-solvent feeds.[7] The focus of the Rogers et al. study was to investigate high potency danazol compositions surface stabilized by poloxamer 407 (P407), polyvinyl alcohol (PVA) and polyvinylpyrrolidone (PVP), while this study investigates the effect of different stabilizers to enhance the dissolution of an extremely hydrophobic API, ITZ.

The objective of this study is to investigate the influence of hydrophilic stabilizers in powder compositions prepared by the SFL process using either an emulsion feed dispersion or organic co-solvent feed solutions on enhancing the wetting and dissolution properties of nanostructured aggregates containing itraconazole. Feeds included a composition (SFL A) manufactured from an emulsion in which the drug, ITZ, is primarily localized within the organic phase of the o/w emulsion having stabilizing excipients on the surface. Two other compositions were manufactured from an organic co-solvent feed solution. SFL B, composed of highly wettable surfactants, poloxamer 407 (P407) and polysorbate 80 (T80), should lead to rapid dissolution rates while SFL C, was a high potency composition containing a wetting agent (polysorbate 20; T20) and a stabilizing polymer polyvinylpyrrolidone (PVPK15). The various excipients were investigated to determine their contribution to the dissolution process such as enhancement of wetting properties and their effect on surface characteristics such as morphology and surface area. The study also investigates the *in vivo* release of an

amorphous ITZ composition prepared using SFL compared with the commercially available liquid Sporanox® solution and micronized crystalline ITZ.

2.3 MATERIALS AND METHODS

2.3.1 Materials

Itraconazole (ITZ) was purchased from Hawkins Chemical (Minneapolis, MN, USA). Poloxamer 407 (P407) and 188 (P188), polyethylene glycol 8000 (PEG), polysorbate 20 (T20) and 80 (T80) sodium lauryl sulfate (SLS), polyvinylpyrrolidone K15 (PVPK15), and sorbitan monooleate (S80) were purchased from Spectrum Chemicals (Gardena, CA, USA). Diethanolamine and hydrochloric acid (HCl) were purchased from VWR International (West Chester, PA, USA). Acetonitrile (ACN), dichloromethane (DCM) and methanol were purchased from EM Industries Inc. (Gibbstown, NJ, USA). Methoxyflurane (Metofane®) was purchased from Pittman-Moore Inc. (Mundelein, IL, USA).

2.3.2 Preparation of SFL Powders

SFL powders were prepared from either an emulsion feed dispersion or organic co-solvent feed solution. For the SFL powder prepared from an emulsion feed dispersion, the organic phase was prepared by adding ITZ (0.7g) and S80 (0.7g) to DCM. P188 (1.4g) and PEG (0.7g) was added to purified water to make the aqueous phase of

the 33:67 DCM:water emulsion. The organic phase was slowly added to the aqueous phase and blended using a rotor-and-stator homogenizer (Polytron 10/35 with TS 10 mm Generator; VWR Scientific Corporation, West Chester, PA, USA) for 90 seconds. The resultant course emulsion was added to an Emulsiflex C-5 high-pressure homogenizer (Avestin, Inc., Ottawa, ON, Canada) and homogenized at a pressure of 18,000 PSI for ten cycles. For SFL powders prepared from an organic co-solvent feed solution, ITZ and the surfactants in their appropriate ratios according to Table 2.1 were dissolved first in a small amount of DCM. ACN was slowly added to volume under constant stirring.

During the SFL process the feed was pumped at 50 mL/min via a piston using an ISCO model 100DX syringe pump (ISCO, Inc., Lincoln, NE, USA) and atomized through 127 μm ID polyether-ether ketone (PEEK) (Upchurch Scientific, Oak Harbor, WA, USA) tubing below the surface of liquid nitrogen. The atomized droplets were instantly frozen to produce a suspension of fine frozen particles. The particles were transferred to a non-insulated container and lyophilized using a VirTis Advantage Benchtop Tray Lyophilizer (VirTis Corp., Gardiner, NY, USA) equipped with a liquid nitrogen trap to condense sublimed organic solvents. The primary drying phase was performed at -60°C for 10 hours and -40°C 14 hours. The shelf temperature was then ramped up at a rate of 0.9° per minute to 25°C where the secondary drying phase was conducted for a minimum of 12 hours. A vacuum of 200 mTorr was maintained for the primary drying phase and increased to 100 mTorr for the remainder of the freeze-drying cycle.

2.3.3 Scanning Electron Microscopy (SEM)

The powder samples were sputter coated using a model K575 sputter coater (Emitech Products, Inc., Houston, TX, USA) with gold-palladium for 35 seconds and viewed using a Hitachi S-4500 field emission scanning electron microscope (Hitachi High-Technologies Corp., Tokyo, Japan). An accelerating voltage of 5-10 kV was used to view the images. All SEMs pictured were representative of the entire sample.

2.3.4 Contact Angle Measurements

Tablets were pressed from the SFL powder samples (50mg) using a Model M Carver Laboratory Press (Fred S. Carver, Inc., Menomonee Falls, WI, USA) and a compression force of 300 kg. A droplet of dissolution media, 0.1N HCl 0.5%w/w SLS, (3μL) was placed on the flat face of the tablet and the contact angle was measured using a Model 100-00-115 goniometer (Ramè-Hart Inc., Mountain Lakes, NJ, USA). Each sample was measured in triplicate.

2.3.5 Dissolution Testing

Dissolution testing was performed on the SFL powder samples using a USP 24 Type II paddle apparatus model VK7000 (Varian Inc., Cary, NC, USA). An equivalent of 7 mg ITZ was added to 900 ml of 0.1N HCl 0.5%w/w SLS (pH 1.2) dissolution media and stirred at 50 rpm. The dissolution media was maintained at $37.0 \pm 0.2°C$.

Samples (5ml) were withdrawn at 2, 5, 10, 20, 30 and 60 minute time points, filtered using a 0.45μm GHP Acrodisc filter and analyzed using a Shimadzu LC-10 liquid

chromatograph (Shimadzu Corporation, Kyoto, Japan) equipped with an Alltech ODS-2 5 μm C_{18} column (Alltech Associates, Inc., Deerfield, IL, USA). A mobile phase of ACN:water:diethanolamine (70:30:0.05) at 1ml/min eluted the ITZ peak at 5.5 min and absorbance was measured at $\lambda = 263$ nm.

2.3.6 X-Ray Diffraction (XRD)

The x-ray diffraction pattern of the SFL powders were analyzed using a model 1710 x-ray diffractometer (Philips Electronic Instruments, Inc., Mahwah, NJ, USA). Data were collected using primary monochromated radiation (CuKα1, $\lambda = 1.54056$ Å), a 2θ step size of 0.05 and a dwell time of 1.0 second per step.

2.3.7 BET Specific Surface Area Analysis

Specific surface area was measured using a Nova 2000 v.6.11 instrument (Quantachrome Instruments, Boynton Beach, FL, USA). Weighed powder was added to a 12 mm quantachrome bulb sample cell and degassed for a minimum of three hours. The sample was then analyzed by the NOVA Enhanced Data Reduction Software v. 2.13 using the BET theory of surface area.

2.3.8 Particle and Droplet Size Analysis

Low angle laser light scattering using a Mastersizer S (Malvern Instruments Limited, Malvern, UK) was used to determine (i) droplet size of the emulsion feed dispersion prior to SFL processing, and (ii) the particle size distribution of aggregated

nanoparticles following lyophilization. The Mastersizer S was equipped with a large volume flow through cell and a 300RF lens (0.1-1000μm).

The emulsion feed dispersion was diluted by dropping into purified water in a large volume flow through cell to reach a laser obscuration between 10 and 25%.

Approximately 5 mg of lyophilized SFL powder was pre-dispersed in a saturated water/itraconazole solution and sonicated for 30 seconds. The pre-dispersed solution was added drop wise to a saturated itraconazole solution in the large volume cell to achieve a laser obscuration between 10 and 25%. Median particle/droplet sizes were determined along with span indices. Span indices were calculated according to the following equation:

$$\frac{\left(D_{90} - D_{10}\right)}{D_{50}} \tag{1}$$

where D_{90}, D_{50} and D_{10} are the cumulative particle sizes less than 90%, 50% and 10%, respectively.

2.3.9 Pharmacokinetic analysis

The *in vivo* study was conducted with approval from the Institutional Animal Care and Use Committee (IACUC) at the University of Texas Health Science Center at San Antonio. Forty-two (42) seven week old male ICR/Swiss mice, disease and pathogen free (Harlan-Sprague-Dawley, Indianapolis, IN) weighing 32 g were used. Animals were housed 4 per cage and allowed water *ad libitum*. The mice were subdivided into 3 groups

61

of 14 to be dosed with the SFL product, the liquid Sporanox® or bulk micronized ITZ suspension.

A suspension of the SFL product (2.4 mg/ml; dose equivalent of 30 mg/kg of itraconazole) was used for each of 14 mice (0.96 mg total). This dose was selected as it had previously been reported to be the highest concentration administered orally prior to the onset of diarrhea. The itraconazole formulation was delivered orally in 0.4 ml suspension using a curved gavage tube in a single dose. Liquid oral Sporanox® was also delivered to 14 mice at the same dose equivalent of 30 mg/kg. In addition, a suspension of the bulk crystalline ITZ was made with 0.01% T80 (as a wetting agent), this was administered at the same dose equivalent of 30 mg/kg to the mice.

Blood samples (0.5-1 ml) were taken via cardiac puncture of anaesthetized mice (using methoxyflurane) at time points of 0.5, 1, 2, 4, 6, 10, 24 hrs. Mice were then euthanized by cervical dislocation; two mice were allocated for each time point. Blood samples were placed in Monoject Samplette® capillary serum separator tubes (Kendall Healthcare, Mansfield, MA) and held at room temperature for 30 minutes before centrifugation at 2,500 rpm for 3 minutes. The supernatant (serum sample) from each sample time point was collected and stored at -20°C prior to analysis.

ITZ concentration was determined by HPLC analysis. The HPLC system (Waters Inc., Miliford, MA, USA) consisted of a UV-detector (W486), pump (W510), autosampler (W717) and column heater, and an Altima® (Alltech Associates, Deerfield, IL, USA) reversed phase column (C-18 base-deactivated, 5 µm, 250 x 4.6 mm) protected by a guard column (C-18, 5 µm, 7.5 x 4.6 mm). Calibration and pharmacokinetic

samples were analyzed using a method in which the mobile phase comprised ACN, deionized water and methanol (55:35:10 v/v) (flow-rate 1.0 ml/min, λ = 263 nm).

Serum samples (250 µL) were pipetted into 0.3 N barium hydroxide / 0.4 N zinc sulfate heptahydrate solution (50 µL) and vortex mixed (30 seconds). Acetonitrile (1 mL) was added before a further vortex mixing (1 min), followed by centrifugation at 2,500 rpm (15 min). The supernatant was transferred to flat bottom tubes and immersed in a water bath (50°C) under a stream of nitrogen to dryness. Samples were then reconstituted with 250 µL mobile phase and vortex mixed (1 min) before transferring to a micro centrifuge tubes and centrifuging at 12,500 rpm (10 min). The supernatant was then transferred into HPLC injection vials with low volume inserts (250 µL).

Pharmacokinetic parameters were analyzed using non-compartmental pharmacokinetic analysis: Area under curve (AUC) between 0-24 hours was calculated using the trapezoidal rule; C_{max} and T_{max} were determined from the concentration-time profiles; $T_{1/2}$ was calculated by using the elimination rate constant (K_d); K_d was obtained from the natural log of the concentration-time profile.

2.4 RESULTS

2.4.1 *In vitro* Characterization of SFL Processed Powders

Various compositions containing ITZ were prepared using the SFL process. These compositions, summarized in Table 2.1, were characterized and evaluated based on their *in vitro* attributes. Table 2.2 summarizes the average particle size, available surface

area, and contact angle measurements of each of the SFL powders. For the SFL A composition which was prepared from an emulsion feed dispersion, the droplet size distribution of the emulsion feed dispersion was determined. The results show that the SFL A emulsion feed dispersion was composed of stabilized submicron droplets of DCM within an aqueous polymer solution. Interestingly, the distribution of submicron droplets (760 nm) was found to be very narrow, as indicated by a span index of 1.39. A slightly larger average particle size was determined on dried powder prepared from the emulsion feed dispersion after rapidly freezing and lyophilization. SFL powders B and C, which were made from organic co-solvent feed solutions revealed larger average particle sizes of 5.82 and 6.21 μm, respectively. In addition, the surface area of the SFL powder was significantly greater than that of micronized ITZ. Surface areas for the SFL powders range from 15.58 to 20.25 m^2/g while the micronized ITZ has a surface area of 4.22 m^2/g. The wettability of the powders was assessed by measuring the contact angle of an aqueous droplet on the flat surface of a compressed tablet of the powder. As the contact angle of the droplet decreases, it is assumed that the droplet is able to more completely wet the powder surface and therefore will have a lower surface energy between the water and the solid powder. As seen in Table 2.2, all SFL powders have lower contact angles compared to the bulk ITZ. Bulk ITZ is a hydrophobic compound and therefore has a high contact angle measuring 57.9° ± 2.4° while the SFL powders have measured contact angles between 7.5 and 46.5°. A direct correlation exists between the contact angle and the potency of the composition with higher potency compositions having higher contact angles due to the hydrophobicity of ITZ . SFL A is composed of 60% hydrophilic material, including P188 and PEG and therefore has the lowest contact angle of all the

samples. However, SFL C, which has the highest potency, has a significantly lower contact angle compared to the micronized ITZ indicating that intimate mixing between hydrophobic ITZ and the hydrophilic polymer PVP occurred.

The scanning electron micrographs in Fig. 2.1 confirm the particle size and surface area results presented in Table 2.2. The SFL powders A-C (Fig. 2.1a-c) all show highly porous aggregates containing nanostructures. Close inspection of the micrograph of SFL A (Fig. 2.1a) reveals many small particles about one to two microns in diameter appearing mostly circular in diameter. SFL B (Fig. 2.1b), on the other hand, appears to contain particles with smoothed edges which have agglomerated or fused together. This is most likely a result of the high level of T80 in the composition. T80, a liquid at room temperature, could cause an increase in mobility of the particles causing them to fuse together forming the agglomerated particles. SFL C (Fig. 2.1c) is composed of nanoparticles with very high surface area particles. Lastly, the micronized ITZ appears to have smooth flat particle surfaces while the particles themselves appear to have a plate shape. Close inspection of each of the SFL powders (Fig. 2.2a-c) reveals differences between the compositions. SFL A (Fig. 2.2a) displays many individual spherical nanoparticles embedded within a surrounding polymer matrix. SFL B shows agglomerated nanoparticles with smoothed edges as a result of the high levels of the liquid surfactant. SFL C (Fig. 2.2c) reveals particles composed of aggregated nanoparticles (<200 nm) surrounding an inner polymer matrix most likely created from the small amount of liquid T20 in the composition.

The crystallinity of the powders was measured using x-ray powder diffraction and the XRD patterns are shown in Fig. 2.2. Analysis of the bulk micronized ITZ reveals the

many peaks associated with crystallinity however the characteristic ITZ peaks (most intense) used for determining crystallinity of the SFL processed samples are located at 17.45 and 17.95 (doublet), 20.30, and 23.45 two theta degrees. The x-ray diffraction pattern for SFL A reveals two crystalline peaks associated with poloxamer 407 and PEG (19.65 and 23.80), however, there are no peaks associated with crystalline ITZ. The XRD pattern of each pure excipient revealed similar patterns with both excipients producing peaks around 19.6 and 23.8 two theta degrees. Similarly, SFL B displays the crystalline peaks resulting from poloxamer but appears to lack the characteristic ITZ peaks indicating an amorphous sample. Lastly, SFL C lacks any crystalline peaks but displays one broad low intensity (> 50 counts) halo and is characteristic of amorphous particles.

Investigation of the dissolution properties of the SFL processed powders was performed under sink conditions as shown in Fig. 2.3. Bulk ITZ had the slowest dissolution of all samples investigated with 20% dissolved after 10 minutes, increasing up to about 45% after 30 minutes and 60% after 60 minutes. Interestingly, bulk ITZ showed a nearly constant dissolution rate over 60 minutes. The dissolution rate for Sporanox® solution was also determined as a control for the SFL processed powders. As expected, the dissolution of ITZ from the composition into the media was instantaneous, occurring within the first two minutes of the experiment. Rapid dissolution was observed by all SFL processed powders showing greater than 90% dissolution within 20 minutes. However, differences were seen within the first 20 minutes between the three SFL processed powders. SFL A appeared to dissolve instantaneously on contact with the surface of the dissolution media and shows the fastest dissolution of all SFL processed

powders. From the dissolution profile, the SFL A powder is 80% dissolved within the first two minutes and completely dissolved within the first five minutes. SFL B also wetted very well in the dissolution medium and exhibited rapid dissolution with 75% dissolved after five minutes and nearly completely dissolved after 10 minutes. SFL C, on the other hand, did not wet well and therefore displayed the slowest dissolution rate of all the SFL processed powders. Upon addition to the aqueous dissolution media, the SFL C powder remained on the surface and required agitation of the paddles for complete wetting. As a result, a slower dissolution rate was observed for SFL C within the first 10 minutes (40% dissolved in 5 minutes and 65% dissolved in 10 minutes). Therefore, the dissolution rate rank order for the SFL processed powders was SFL A > SFL B > SFL C.

2.4.2 *In vivo* Characterization

After evaluation of the *in vitro* performance of each SFL composition, SFL A was selected for testing in a mouse model. Mice were dosed via an oral gavage of an SFL A aqueous suspension and the pharmacokinetic parameters were determined for a single dose over 24 hours. Results were compared with the commercial product, Sporanox® oral solution.

Due to the number of samples per time point (pooling of samples) and model selection in previous studies examining oral delivery of ITZ solid dispersions [8-10], non- compartmental analysis was utilized to analyze the pharmacokinetic parameters of the ITZ oral dosing. ITZ serum concentration vs. time is shown in Fig. 2.5 [11]. Absorption profiles were similar for both the SFL A and Sporanox® compositions; however, greater variation was seen with the SFL A composition. From Fig. 2.5 and

Table 2.3 the pharmacokinetic parameters are displayed. Pharmacokinetic parameters are reported for both the SFL A composition and the Sporanox® oral solution. The ITZ serum levels of the micronized crystalline ITZ were below the limit of quantitation and therefore the pharmacokinetic parameters are not reported. The C_{max}, T_{max}, elimination rate constant K_d, $T_{1/2}$, and AUC (0-24 hr) for the Sporonox oral liquid and SFL A are 1.59 and 1.28 µg/mL, 1.0 and 2.0 hr, 0.36 and 0.51 hr^{-1}, 5.42 and 4.56 mg*hr/mL, respectively.

2.5 DISCUSSION

Because ITZ is a BCS class II compound, absorption is dissolution rate limited and therefore, enhancing the dissolution should lead to overall enhanced absorption and improved oral bioavailability. ITZ has extremely low solubility in neutral or alkaline media such as that of the upper small intestines, and it was hypothesized that complete dissolution and absorption of ITZ within the stomach is desirable for delivery of ITZ. Immediate dissolution would allow maximum time for absorption within the stomach before the dose is emptied into the upper small intestine, resulting in a pH shift that may cause precipitation of ITZ out of solution and subsequent recrystallization. Excipients used in SFL A, which was produced from an emulsion feed dispersion, were chosen for two reasons: their ability to stabilize the emulsion feed dispersion for a sufficient period of time necessary to allow processing and increase the wettability and dissolution properties of the powder. S80 is a sorbitan fatty acid ester with a low hydrophilic-lipophilic balance (HLB) value of 4.3 used as the primary emulsifying agent allowing for

stable droplet sizes of 760 nm in diameter. Surfactant/stabilizers P188 and PEG were added to the aqueous phase increase wetting of the amorphous ITZ domains after lyophilization as well as aid in stabilization at the droplet interface. Excipients used in SFL B were chosen also to enhance the wetting of ITZ. P407 is a block copolymer with an HLB value greater than 20 and was used as a wetting/stabilizing agent while T80 has an HLB value of 16.7. Because the powders were developed from an organic co-solvent feed solution, the ITZ should be either dissolved within the polymers (i.e. solid solution) or exist as nanostructured domains within the polymer matrix. PVPK15 was used as a stabilizer to prevent recrystallization of the ITZ. However, binary mixtures of ITZ and PVP showed poor wetting during dissolution and therefore, T20 was added in order to overcome dissolution limitations associated with poor wetting.

All three SFL processed powders were amorphous as a results of the rapid freezing process, regardless of the excipient composition used. Amorphous materials are known to dissolve faster than their crystalline counterparts due to their lower heat of solution and energy required for dissolution to occur.[12] Equally important is that an API in its amorphous state temporarily has a higher apparent solubility in a given solvent compared to its crystalline counterpart. This leads to a higher concentration driving force $(C_s\text{-}C)$ allowing for dissolution rate enhancement.[13] Although not tested in this study, Vaughn et al. investigated the relationship between danazol supersaturation *in vitro* and bioavailability enhancement, and concluded that there was a direct correlation.[14] It is estimated that the SFL process using liquid nitrogen as a cryogen can achieve freezing rates on the order of 10^4 K/sec.[15] This freezing rate is sufficient to arrest the

recrystallization process inherent in slower freezing processes regardless of the liquid feed composition.

However, the choice of feed composition is critical in controlling the particle's structural characteristics. The emulsion feed dispersion allowed for the preferential distribution of the stabilizer to the surface of the ITZ while the organic co-solvent feed solutions led to co-precipitation of the ITZ and the stabilizers. This localization of the stabilizer to the particle surface leads to more efficient use of the hydrophilic stabilizers. Sinswat et al. further showed adsorption of the stabilizer onto the surface of the particle is largely dependent on the HLB value and the hydrophobicity of ITZ.[16] Since P407 and PEG, which are both very hydrophilic, are less likely to adsorb to the hydrophobic regions of ITZ, S80, a nonionic surfactant, was added to the organic phase to reduce the hydrophobicity of the droplet allowing for greater adsorption of the stabilizers. This led to greater physical stabilization of the emulsion as well as providing for enhanced wetting capabilities of the lyophilized powder. Based on this and other high potency studies,[7, 16, 17] it is estimated that the potency of this composition could be increased without sacrificing the desired wetting and dissolution characteristics of the powder.

SFL B was produced from an organic co-solvent feed solution which is a homogeneous mixture of ITZ and the hydrophilic stabilizers. As freezing occurs, solubility differences from temperature change result in rapid nucleation of both the ITZ and the stabilizers. If freezing rates are sufficiently fast spontaneous and simultaneous nucleation should result in a solid solution containing both ITZ and the stabilizers. However, because of the intimate mixing between the ITZ molecules and the stabilizers, the stabilizers can exert a greater influence on the final powder characteristics. For

example, Hu et al. found dramatic differences in surface areas between danazol:P407 and danazol:PVP compositions at equal ratios. The surface area for the danazol:PVP was over 45-times greater than the surface area for the danazol:P407 composition, although dissolution rates were comparable.[18]

SFL C was a high potency composition which displayed remarkable dissolution rate enhancement despite having higher regions of hydrophobicity compared to the other two compositions as indicated by contact angle studies. Previous studies using technologies such as spray-drying, solvent evaporation, and melt-extrusion [19-21] to increase ITZ potencies in solid dispersions have, in some instances, seen a dramatic decrease in dissolution rate as potency is increased. Verreck et al. found that dissolution rates of ITZ:HPMC solid dispersions were a function of polymer content and rates decreased tremendously as HPMC content decreased from 60% to 33%.

SFL A was further investigated to determine its *in vivo* performance in a mouse model compared to a commercially available ITZ product and micronized crystalline ITZ because the composition displayed the best physico-chemical properties of all the SFL processed powders investigated. The SFL A powder was composed high surface area aggregates containing nanoparticle amorphous API domains surface stabilized with hydrophilic polymers. The powder also displayed the fastest dissolution rate as a result of its lower potency (increased wetting agent) and enhanced physico-chemical properties. The improved pharmacokinetic parameters for SFL A validate the enhanced physico-chemical properties of the composition. Absorption of ITZ occurred rapidly most likely due to the enhanced wetting of the composition while the high serum levels were attributed to the increased absorption from improved dissolution. The extent of ITZ

absorption, as indicated by the AUC, was comparable to the Sporanox® oral solution having about 85% relative bioavailability. The lack of an absorption profile for the micronized crystalline ITZ is the result of poor wetting of the ITZ preventing dissolution *in vivo* and solubility limitations resulting from the crystalline structure of the ITZ. The Sporanox® oral liquid contains hydroxypropyl-β-cyclodextrin which has formed a complex with ITZ thereby enhancing the solubility of ITZ in both and acidic and higher pH (intestinal) environment. Because Sporanox® exists as a solution, dissolution within the stomach is not necessary and absorption can begin immediately. Likewise, within the cyclodextrin complex, ITZ should remain in solution upon entering the upper intestinal tract and absorption should continue. Despite these advantages of the oral solution, the ITZ absorption profiles for SFL A and the Sporanox® oral liquid were similar although statistical analysis could not be performed due to the number of samples per time point (n=2). Therefore, these studies have shown that the SFL process can create highly wettable high surface solid dispersions of amorphous API leading to enhanced absorption of poorly water soluble APIs.

2.6 Conclusion

Three compositions were manufactured using the SFL process to investigate the influence of hydrophilic stabilizer on the enhancing the wetting and dissolution rate. SFL A, sprayed from an emulsion feed dispersion, resulted in a solid dispersion of amorphous nanoparticle API domains stabilized by adsorption of stabilizing polymers on the surface. SFL B and SFL C were sprayed from organic co-solvent feed solutions and resulted in

porous structures thought to contain nanodomains of ITZ. SFL B contained lower melting point stabilizers which resulted in agglomeration of the nanoparticles lowering the surface area. SFL C, although having a high potency, still maintained a rapid dissolution rate due in part to its high surface area and amorphous nanoparticle domains. Studies revealed that the *in vitro* properties were enhanced first through the rapid freezing process to create amorphous ITZ. Secondary to the process, properties were further enhanced by addition of the stabilizers to the surface of the amorphous ITZ using an emulsion feed dispersion. This surface adsorption allowed for better wetting of the particles leading to enhanced dissolution. The effect of the polymer on particle characteristics was much more pronounced and led to particle agglomeration in SFL B. Likewise, a high potency composition had a decreased dissolution rate compared to SFL A and SFL B and was attributed to the increased hydrophobicity of the particle from the ITZ. An *in vivo* study proved increased efficacy of the SFL A micronized powder compared to the commercially available Sporanox® oral solution and micronized crystalline ITZ. In conclusion, the SFL powder prepared from the emulsion feed dispersion produced surface stabilized amorphous ITZ nanostructured aggregates which enhanced the physico-chemical properties (wetting, surface area, particle size) leading to enhanced dissolution rate and *in vivo* absorption with high and rapid onset of C_{max} and a relative bioavailability of 85% that of Sporanox® oral solution. .

2.7 ACKNOWLEDGEMENTS

Education (AFPE) Fellow from 2004 to 2006 and a 2005-2006 University Continuing

Fellowship recipient.

2.8 REFERENCES

[1]   Maertens, J. and M. Boogaerts, The place for itraconazole in treatment. J.

Antimicrob. Chemother., **2005**, *56*: p. 33-38.

[2]   Chiller, T.M. and D.A. Stevens, Treatment strategies for Aspergillus infections.

Drug Resist. Update, **2000**, *3*(2): p. 89-97.

[3]   Lin, S.J., J. Schranz, and S.M. Teutsch, Aspergillosis case - Fatality rate:

Systematic review of the literature. Clin. Infect. Dis., **2001**, *32*(3): p. 358-366.

[4]   Denning, D.W., Therapeutic outcome in invasive aspergillosis. Clin. Infect. Dis.,

1996, *23*(3): p. 608-615.

[5]   Heeres, J. and L.J.J. Backx, Heterocyclic derivatives of (4-phenylpiperazin-1-yl-

aryloxymethyl-1,3-dioxolan-2-yl)methyl-1H-imidaz oles and 1H-1,2,4-triazoles,

US Patent #U.S. Patent 4,267,179. **1981**

[6]   Peeters, J., N. P., J.P. Tollenaere, P.V. Remoortere, and M.E. Brewster,

Characterization of the Interaction of 2-Hydroxypropyl-bcyclodextrin with

Itraconazole at pH 2, 4, and 7. J. Pharm. Sci., **2002**, *91*(6): p. 1414-1422.

[7]   Rogers, T.L., K.A. Overhoff, P. Shah, P. Santiago, M.J. Yacaman, K.P. Johnston,

and R.O. Williams, Micronized powders of a poorly water soluble drug produced

by a spray-freezing into liquid-emulsion process. Eur. J. Pharm. Biopharm., **2003**, *55*(2): p. 161-172.

[8]   Vaughn, J.M., J.T. McConville, D. Burgess, R.L. Talbert, J.I. Peters, R.O. Williams III, and K.P. Johnston, Single Dose and Multiple Dose studies of Aerosolized Itraconazole Nanoparticles. Eur. J. Pharm. Biopharm., **2005**, *63*(2): p. 95-102.

[9]   Yoo, S.D., E. Kang, B.S. Shin, H. Jun, S.H. Lee, K.C. Lee, and K.H. Lee, Interspecies comparison of the oral absorption of itraconazole in laboratory animals. Arch. Pharm. Res., **2002**, *25*(3): p. 387-391.

[10]   Yoo, S.D., S.H. Lee, E.H. Kang, H. Jun, J.Y. Jung, J.W. Park, and K.H. Lee, Bioavailability of itraconazole in rats and rabbits after administration of tablets containing solid dispersion particles. Drug Dev. Ind. Pharm., **1999**, *26*(1): p. 27-34.

[11]   Frei, B.L., *Investigation of pulmonary and oral delivery of itraconazole produced by evaporative precipitiation into aqueous solution (EPAS) and spray freezing into liquid (SFL) technology in a murine model*,The University of Texas at Austin, **2003**.

[12]   Terada, K., H. Kitano, Y. Yoshihashi, and E. Yonemochi, Quantitative correlation between initial dissolution rate and heat of solution of drug. Pharm. Res., **2000**, *17*(8): p. 920-924.

[13]   Hancock, B.C. and M. Parks, What is the true solubility advantage for amorphous pharmaceuticals? Pharm. Res., **2000**, *17*(4): p. 397-404.

[14]   Vaughn, J.M., J.T. McConville, M.T. Crisp, R.O. Williams III, and K.P. Johnston, Supersaturation Produces High Bioavailability of Amorphous Danazol Particles Formed by Evaporative Precipitation into Aqueous Solution (EPAS) and Spray Freezing into Liquid(SFL) Technologies. Drug Dev. Ind. Pharm., **2006**, *32*(5): p. 559-567.

[15]   Engstrom, J., D. Simpson, E. Lai, R.O. Williams, and K.P. Johnston, Morphology of Protein Particles Produced by Spray Freezing of Concentrated Solutions. Eur. J. Pharm. Biopharm., **2006**, *In Press*.

[16]   Sinswat, P., X. Gao, M.J. Yacaman, R.O. Williams III, and K.P. Johnston, Stabilizer choice for rapid dissolving high potency itraconazole particles formed by evaporative precipitation into aqueous solution. Int. J. Pharm., **2005**, *302*(1-2): p. 113-124.

[17]   Chen, X., Z. Benhayoune, R.O. Williams III, and K.P. Johnston, Rapid dissolution of high potency itraconazole particles produced by evaporative precipitation into aqueous solution. J. Drug Deliv. Sci. Technol., **2004**, *14*(4): p. 299-304.

[18]   Hu, J.H., K.P. Johnston, and R.O. Williams, Stable amorphous danazol nanostructured powders with rapid dissolution rates produced by spray freezing into liquid. Drug Dev. Ind. Pharm., **2004**, *30*(7): p. 695-704.

[19]   Jung, J.-Y., S.D. Yoo, S.-H. Lee, K.-H. Kim, D.-S. Yoon, and K.-H. Lee, Enhanced solubility and dissolution rate of itraconazole by a solid dispersion technique. **1999**, *187*: p. 209-218.

[20]   Kapsi, S.G. and J.W. Ayres, Processing factors in development of solid solution

formulation of itraconazole for enhancement of drug dissolution and

bioavailability. Int. J. Pharm., **2001**, *229*(1-2): p. 193-203.

[21]   Verreck, G., K. Six, G. Van den Mooter, L. Baert, J. Peeters, and M.E. Brewster,

Characterization of solid dispersions of itraconazole and

hydroxypropylmethylcellulose prepared by melt extrusion--part I. **2003**, *251*(1-2):

p. 165-174.

Chapter 3: Novel Ultra-rapid Freezing Particle Engineering Process for Enhancement of Dissolution Rates of Poorly Water Soluble Drugs

3.1 ABSTRACT

An ultra-rapid freezing (URF) technology has been developed to produce high surface area powders composed of solid solutions of an active pharmaceutical ingredient (API) and a polymer stabilizer. A solution of API and polymer excipient(s) is spread on a cold solid surface to form a thin film that freezes in 50 ms to 1s. This study provides an understanding of how the solvent's physical properties and the thin film geometry influence the freezing rate and consequently the final physicochemical properties of URF processed powders. Theoretical calculations of heat transfer rates are shown to be in agreement with infrared images with 10 ms resolution. Danazol (DAN)/polyvinylpyrrolidone (PVP) powders, produced from both acetonitrile (ACN) and tert-butanol (T-BUT) as the solvent, were amorphous with high surface areas (~28-30 m^2/g) and enhanced dissolution rates. However, differences in surface morphology were observed and attributed to the cooling rate (film thickness) as predicted by the model. Relative to spray freezing processes that use liquid nitrogen, URF also offers fast heat transfer rates as a result of the intimate contact between the solution and cold solid surface, but without the complexity of cryogen evaporation (Leidenfrost effect). The ability to produce amorphous high surface area powders with submicron primary particles with a simple ultra rapid freezing process is of practical interest in particle engineering to increase dissolution rates, and ultimately bioavailability.

3.2 INTRODUCTION

A significant number of active pharmaceutical ingredients (API) being discovered display desirable therapeutic properties, but have undesirable physicochemical properties (e.g. solubility) making formulation into an effective drug product challenging. The Biopharmaceutical Classification System (BCS) class II APIs, which have been reported to account for as many as 40% of new chemical entities[1], present particular challenges in creating successful drug products. For example, BCS class II compounds do not readily dissolve in the biological media of the digestive tract and thus exhibit poor or variable bioavailability. Consequently, the major obstacle in formulating these compounds into successful commercialized products is the difficulty in enhancing the dissolution rate.

A number of strategies and processes have been reported to facilitate the dissolution of these poorly water soluble APIs. These include particle reduction/milling, solution based precipitation techniques, and emulsification/precipitation, etc., as described extensively in reviews.[2-6]   Cryogenic technologies, in particular, have been shown to enhance the dissolution rates of poorly water soluble APIs by creating highly porous nano-structured particles[7-10] The processes Spray Freezing into Liquid (SFL) and Spray Freeze Drying (SFD) use cryogens, particularly N_2, to form a solid dispersion or solid solution[11] composed of nanoparticle domains of API within a polymer matrix. The particles are produced by rapidly freezing a feed solution in a cryogenic liquid and removing the solvent(s) through lyophilization. Micronized powders containing nanoparticles of API have been successfully manufactured with the SFL technology

using a variety of different types of solvents.[12, 13] Early work utilized aqueous co-solvent systems such as tetrahydrofuran (THF):water which has the ability to dissolve both a poorly water soluble API as well as hydrophilic excipients. Subsequently, organic solvents such as acetonitrile (ACN) which have the unique ability to dissolve both an API and a hydrophilic excipient were used to increase API loading and reduce the risk of liquid-liquid phase separation. However, Hu et al.[14] found that increasing API loading has a profound effect on the surface morphology of the processed powders. Later, Rogers et al.[13] developed an oil-in-water (o/w) emulsion system in which the API and emulsifiers were dissolved in dichloromethane while hydrophilic stabilizers were dissolved in the aqueous phase. High pressure homogenization was used to reduce the mean diameter of the oil droplets to less than 1 μm before freezing the sample via the SFL process.

Ultra-rapid freezing (URF) was recently developed as a particle engineering technology designed to enhance the dissolution rates and bioavailability of poorly water soluble APIs.[15] Briefly, the process involves freezing an API contained in a polymer solution onto the surface of a cryogenic substrate with a thermal conductivity k between 10-20 W/(m*K), collecting the frozen particles and removing the solvent. Because of rapid conductive heat transfer, resulting in high supersaturation and nucleation rates, the URF technology has the potential to create powders with superior physico-chemical properties, similar to those produced by other rapid freezing technologies. As in other freezing technologies, the rapid freezing of the API/polymer composition is critical in preventing phase separation during freezing, allowing for the active to be molecularly dispersed with the polymer. Recrystallization of the active is avoided by the inclusion of

high glass transition temperature (T_g) polymers such as polyvinylpyrrolidone (PVP) or hypromellose (HPMC).

Previously, criteria for selection of the solvent(s) suitable for the SFL process included sufficient solubility of the solids and the ability to remove the solvent without re-crystallizing the API. These solvents generally have freezing points between 208K and 273K which are ideal for tray lyophilization. Solvents with freezing points below 208K melt during lyophilization while solvents with freezing points higher than 273K may freeze prematurely within the atomizing nozzle. Because the URF technology applies the droplets directly onto the cryogenic substrate, premature freezing is not a concern and high freezing point solvents may be used. These solvents could prove beneficial by reducing the lyophilization time [16] or eliminating the solvent removal process altogether as some of these solvents sublime at ambient conditions or higher[17].

The objectives of this study are to introduce the URF technology as a novel method to manufacture pharmaceutical powders and to investigate how solvent properties and thin film geometry of the droplet affect the freezing rate and thus the physico-chemical properties of the final micronized powders. To determine the effect of the solvent properties, powders were manufactured from solutions from two solvents, tert-butanol (T-BUT) and ACN. T-BUT was selected for its higher freezing point and good lyophilization characteristics while ACN was selected for its good heat transfer properties. Heat transfer calculations of freezing rates are compared with those measured by infrared imaging. The model and results from imaging with a focal plane array infrared camera are complementary and are utilized to demonstrate differences in freezing rates between the two solvent systems. The physico-chemical properties of the

processed powders were compared to the unprocessed bulk API, and co-ground physical mixtures to assess the potential benefit of the URF technology. The powders were evaluated based on degree of crystallinity, surface area, surface morphologies, wettability and dissolution rate. It is hypothesized that the URF technology can produce powders with enhanced physico-chemical properties, for example low crystallinity and high surface area, leading to faster dissolution rates which could potentially enhance *in vivo* absorption for the BCS class II compounds.

3.3 MATERIALS AND METHODS

3.3.1 Materials

Micronized danazol (DAN), sodium lauryl sulfate (SLS), and polyvinylpyrrolidone (PVP) K-15 were purchased from Spectrum Chemicals (Gardena, CA, USA). High performance liquid chromatography (HPLC) grade acetonitrile (ACN) was obtained from EM Science (Gibbstown, NJ, USA), and tert-butanol (T-BUT) was purchased from Fisher Scientific (Fair Lawn, NJ, USA).

3.3.2 Preparation of the URF Micronized Powders

The compositions were prepared by dissolving DAN and PVP K15 at a 1:2 ratio and 0.55% total solids in either T-BUT heated to 313K or ACN at room temperature. The DAN/PVP feed solutions were processed using the URF apparatus (process schematic shown in Fig. 3.1). The feed solutions were applied to a cryogenic solid

substrate cooled to a temperature range of 193 K to 243K, collected, and lyophilized using a VirTis Advantage benchtop tray lyophilizer (The VirTis Company, Inc. Gardiner, NY, USA).

3.3.3 Preparation of Control Powders

The bulk API was used as received while the co-ground physical mixtures were prepared by adding the API and excipients to a glass mortar and pestle and mixed/triturated using the geometric dilution technique until a uniform powder was achieved.

3.3.4 Infrared Imaging of Freezing Droplets

A single droplet of ACN or T-BUT was released from a pipette with a 2 mm diameter tip 10 cm above a cryogenically cooled surface and allowed to impinge on the surface of the cryogenic substrate. An InSb focal plane array (FPA) camera (Phoenix digital acquisition system (DAS) camera, Indigo Systems, Santa Barbara, CA, USA) was positioned to acquire infrared images from above the freezing droplet on the substrate. The FPA camera detected 3–5 μm radiation, and the images were acquired at 100 frames per second (10 ms/image). The dimensions of each frame were 256 pixels by 256 pixels (15 mm X 15 mm). The image spatial resolution was approximately 40 μm per pixel. Average intensity values were calculated using MATLAB® version 6 (20 x 20 pixel square within the center of the droplet) and plotted versus time to determine the time for the center of the droplet to reach thermal equilibrium with the substrate.

3.3.5 Scanning Electron Microscopy (SEM*)*

The powder samples were sputter coated using a model K575 sputter coater (Emitech Products, Inc., Houston, TX, USA) with gold-palladium for 35 seconds and viewed using a Hitachi S-4500 field emission scanning electron microscope (Hitachi High-Technologies Corp., Tokyo, Japan). An accelerating voltage of 5-15 kV was used to view the images. All SEMs pictured were representative of the entire sample.

3.3.6 Dissolution Testing

Dissolution testing was performed on all powder samples using a United States Pharmacopeia (USP) 24 Type 2 apparatus (VanKel VK6010 Dissolution Tester with a Vanderkamp VK650A heater/circulator, Cary, NC, USA).   The dissolution medium consisted of 0.3% SLS dissolved in de-ionized water and maintained at 37.0 ± 0.2°C throughout the study. Five ml samples were withdrawn at 2, 5, 10, 20, 30 and 60 minute time points, filtered using a 0.45μm GHP Acrodisc filter and analyzed using a Shimadzu LC-10 liquid chromatograph (Shimadzu Corporation, Kyoto, Japan) equipped with an Alltech ODS-2, 5 μm C_{18} column (Alltech Associates, Inc., Deerfield, IL, USA). A 70:30 ACN:water mobile phase at 1 ml/min eluted the DAN peak at 5 min[11]. The maximum absorbance was measured at λ=288 nm. System suitability requirements were met ($R^2 \geq 0.999$, precision $\leq 2.0\%$ RSD).

3.3.7 X-Ray Powder Diffraction (XRD)

84

The x-ray diffraction patterns of all powder samples were analyzed using a Philips 1710 x-ray diffractometer with a copper target and nickel filter (Philips Electronic Instruments, Inc., Mahwah, NJ, USA). The leveled powder was measured from 5 to 45 2θ degrees using a step size of 0.05 2θ degrees and a dwell time of one second.

3.3.8 Surface Area Analysis

Specific surface area was measured using a Nova 2000 v.6.11 instrument (Quantachrome Instruments, Boynton Beach, FL, USA). A known weight of powder was added to a 12 mm Quantachrome bulb sample cell and degassed for a minimum of three hours. The sample was then analyzed (n=3) by the NOVA Enhanced Data Reduction Software v. 2.13 via the Brunauer, Emmett, and Teller theory of surface area[18].

3.3.9 Contact Angle Measurement

A 50 mg aliquot of sample powder was compacted with a Model M Carver laboratory press (Fred S. Carver, Inc., Menomonee Falls, WI, USA) using a compaction force of 500 kg to form a smooth surfaced tablet. A 3 µl drop of purified water was added to the surface of the tablet and the contact angle was quantitated using a goniometer (Ramè-Hart Inc., Mountain Lakes, NJ, USA) by measuring the tangent to the curve of the droplet on the surface of the tablet.

3.3.10 Statistical analysis

One-way analysis of variance (ANOVA) was used to determine statistically significant differences between results. Results with P values < 0.05 were considered statistically significant. Post-hoc comparisons using Tukey's test were made to determine differences between the URF compositions and the controls.

3.4 RESULTS

3.4.1 Infrared Measurements of Cooling Droplets on Cryogenic Plate

An infrared (IR) camera was used to quantitate the amount of IR energy radiated from the spread droplet over time on a cryogenic plate. The IR camera outputs intensity values assigned on a grayscale with white having a high intensity and black having a low intensity in relation to the amount of radiant energy emitted from the droplet. A thermal equilibrium was established when the intensity value was constant over time, indicating that the rate of heat transfer approached zero. It is estimated that at thermal equilibrium, the temperature of the droplet is near the temperature of the cryogenic substrate and confirmed via direct thermocouple measurement using a surface measuring probe. As the droplets enter the field of view, they appear white for both ACN and T-BUT. Figures 3.2 and 3.3 contain time lapse IR photographs for ACN and T-BUT, respectively. For ACN, complete spreading of the droplet occurred within the first 10 ms interval indicating that the time of droplet spreading, $t_{spreading}$, was much less than the freezing time, $t_{freeze.}$. Therefore, t=0 was defined as the first frame in which impingement was observed. When dropped from a height of 10 cm, the diameter for the spread ACN droplet as measured by a ruler and confirmed by IR camera was 1.9 cm. At t=20 ms, the droplet began to

visually darken evenly throughout the entire droplet. Since IR radiation between 3 and 5 microns is not readily absorbed by either ACN or T-BUT, it is believed that the initial darkening is a result of the cooling of the solvent near the droplet-surface interface. Between 20 and 70 ms, a cooling front is observed moving radially inward as the remaining droplet freezes. After 70 ms a slight fluctuation in intensity is observed before thermal equilibrium around 2280 intensity units is established. Figure 3.4a is a plot of the average intensity at the center of the ACN droplet as a function of time. After a rapid decrease in intensity is initially observed in which the bottom of the solvent immediately freezes, the rate begins to slow slightly until a minimum intensity value of 2280 is reached at 70 ms.

With a melting point near room temperature (296-298 K), the T-BUT samples were heated to 313 K to prevent premature freezing before spreading of the droplet on the cryogenic surface. As in the case of the ACN droplet, impingement and complete spreading of the T-BUT droplet also occurred within the first 10 ms interval. When dropped from a height of 10 cm, the spread diameter for the frozen T-BUT droplet measured 0.8 cm, less than half that of the ACN droplet. At 150 ms, the appearance of a black ring around the edge of the droplet appears indicating that the cooling rate is faster near the edge of the droplet (Fig 3.3b). As cooling continues, the cooling front proceeds radially inward towards the center of the droplet and has much greater contrast than observed with the ACN droplet. At 400 ms, IR intensity throughout the droplet was decreased (Fig. 3.3c) and at 1000 ms thermal equilibrium was established (Fig. 3.3d). Similar to the case for the ACN droplet, the first few frames indicate a sharp decrease in intensity as the liquid in contact with the cryogenic surface immediately cools (Fig. 3.4b).

After the initial drop in intensity where the droplet freezes instantaneously at the solid liquid interface, the rate of intensity decrease begins to slow and becomes much slower than for the ACN droplet. Since solidification occurs in the axial direction according to this model, the resulting solid solvent and solid API/polymer particles act as an insulating layer[19] decreasing the rate of heat transfer. Ultimately, the droplet thermally equilibrates around 2030 at around 1000 ms.

3.4.2 Physico-chemical Properties and Dissolution Rates of URF Processed Powders

DAN powders were produced using the URF technology, and the physico-chemical properties were compared to the bulk API and the physical mixture. The characteristic crystalline peaks for DAN were found at 15.90 and 19.15 2θ degrees with a doublet peak around 17.30 2θ degrees, as seen in the bulk DAN and physical mixture samples in Fig. 3.5. The physical mixture sample showed a reduction in crystalline intensity due to the dilution of PVP in the sample. Both URF processed powders lacked the characteristic crystalline peaks and therefore were considered to contain amorphous DAN. This is attributed to the rapid freezing occurring during the URF process and the ability of PVP to inhibit crystal growth.

As seen in Table 3.1, high specific surface areas (SSA) were reported for both the URF processed powder from T-BUT, with values of 29.3 and 25.9 m^2/g, respectively. The SSA was 50-60X greater than that of the micronized bulk DAN and about 40X greater than that of the physical mixture.

Differences between the two URF processed powders are evident in the surface morphology. The URF processed powder from ACN showed compacted aggregates of

88

uniform nanoparticles with diameters of about 100 nm or smaller (Fig. 3.6a) in all areas of the sample. The surface morphology of the 1:2 DAN:PVP composition dissolved in T-BUT and processed by URF indicated regions of nanoparticles with similar particle sizes (Fig. 3.6b); however, particle sizes were not as uniform as those present from powders produced from ACN. Likewise, other areas of the powder exhibited very thin plate-like domains.

Dissolution rates for the processed powders are compared in Fig. 3.7 with those of the bulk DAN and the physical mixture. Samples processed from URF revealed rapid dissolution with at least 85% API dissolved within 10 minutes and showed statistically greater release than the bulk DAN and the physical mixture ($p<0.05$). The URF processed powders produced from both T-BUT and ACN had nearly identical dissolution profiles ($p>0.05$). The similar profiles may be rationalized by the observation that both compositions were amorphous and had similar and very high surface areas. These factors produced very rapid dissolution rates. Inclusion of PVP in the physical mixture increased the dissolution only slightly, relative to pure danazol indicating that the low surface area and crystallinity of DAN limited the dissolution rate.

ANOVA statistical analysis revealed that significant differences in contact angle existed between the four sample groups ($F > F_{crit}$). Contact angle measurements for both the processed powders and the physical mixture of 1:2 DAN:PVPK15 showed a statistically significant ($p < 0.05$) decrease in contact angle (30.5°-39.5°) compared to the bulk DAN (64.0°) indicating better wettability of the powders as seen in Table 3.1. There were no significant differences between the two URF processed powders (e.g.

$\overline{X}_{T-BUT} - \overline{X}_{ACN} = 2.5 < 3.85$) but there were differences between the URF processed powders and the physical mixture. This is most likely due to the intimate mixing of PVP and DAN during the process allowing for a more homogenous distribution of the PVP throughout the powder.

3.5 DISCUSSION

3.5.1 Theoretical Modeling

The phenomena of droplet spreading and solidifying/freezing for an impinging droplet on a solid substrate have been studied extensively by many research groups.[19-32] The fluid dynamics and heat transfer can be coupled requiring a numerical solution. However, in our IR imaging studies the heat transfer was much slower than the droplet spreading. Thus the model can be solved analytically to describe the cooling rate in URF.[33] The validity of the model will be evaluated by comparison to the experimental IR data for ACN and T-BUT.

In the model it is first assumed that droplet spreading after impact occurs on a much shorter time scale than heat transfer. Consequently, significant heat transfer does not occur until spreading is complete. The second assumption is that the droplet spreads to form a thin cylindrical disk. Because of the small height of the disk relative to the diameter, the third assumption is that only one-dimensional heat transfer is present in the z direction. Conduction in the radial direction through the thin disk parallel to the surface may be neglected. The final assumption is that the thermal diffusivity α is constant over

90

the entire temperature range and remains unchanged during the phase change of freezing. Given the above assumptions the transient heat transfer equation through the cylindrical disk simplifies to

$$\frac{\partial T}{\partial t} = \alpha \frac{\partial^2 T}{\partial x^2}$$

(1)

where the temperature T is a function of time t and x is the distance into the disk from the top surface of the thin film exposed to air. The thermal diffusivity of the spread droplet is defined as $\alpha = k / \rho * C_p$, where k is the thermal conductivity, ρ is the density, and C_p is the heat capacity.

The first boundary condition for Equation 1 assumes that heat transfer through the top surface of the disk exposed to the air is negligible. Therefore, the air is assumed to act as an insulator. The second boundary condition assumes the cryogenic plate temperature, T_{plate}, remains constant during the cooling process with negligible heat transfer resistance between the plate and spread droplet. These boundary conditions are

$$\left. \frac{\partial T}{\partial x} \right|_{x=0} = 0$$

(2)

$$T(L,t) = T_{plate}$$

(3)

91

Here x = L is the bottom surface of the disk in contact with the plate. The initial condition assumes that the droplet temperature is uniform before impact and is defined as:

$$T(x,0) = T_i \qquad (4)$$

where T_i is the initial solvent temperature. Equation 1 is then solved analytically for a finite disk thickness [33] to give

$$T(x,t) = T_{plate} + \frac{2}{L}\sum_{n=0}^{\infty} e^{-\alpha(2n+1)^2 \pi^2 t / 4L^2} \cos\frac{(2n+1)\pi x}{2L}\left\{\frac{2L(-1)^{n+1} T_{plate}}{(2n+1)\pi} + \int_0^L T_i \frac{\cos(2n+1)\pi x'}{2L} dx'\right\} \qquad (5)$$

where L is the disk thickness. Cooling times are then determined by calculating the time, t, it takes for the surface of the solvent film at x = 0 with thickness L to reach a given temperature T using the software MATHCAD® version 11.

The spread droplet thickness was easily determined with the assumption that the droplet impacting on the cold substrate deformed into a cylinder with an equivalent volume to the original droplet volume before impact. Droplet volume was determined by dropping 100 droplets into a graduated cylinder and measuring the total volume. Frozen spread droplet diameters were measured with a ruler across two directions and averaged for 10 droplets. Droplet thicknesses were then calculated from the known volume of the falling droplet and the diameter of the frozen spread droplet and were 109±10 μm and

92

403±32 μm for ACN and T-BUT, respectively. Modeling the frozen spread droplet as a thin cylindrical disk has been used in many previous models [20-22, 25, 34] and has been experimentally justified when the Weber number, $We = \rho V^2 D / \gamma$ (inertial to interfacial forces), of the impacting droplet is >>1 [26] where V is the impact velocity, D is the droplet diameter, and γ is the droplet interfacial tension. The impact velocity, V was calculated from the free-fall equation in a gravitational field, $V = (2gH)^{1/2}$ [34] where the falling height, H, of the droplet was 10 cm resulting in an impact velocity of 1.4 m/s. The densities and interfacial tensions for each solvent were determined using the DIPPR database (Brigham Young University, Provo, UT) at the initial temperatures of 298 K and 313 K for ACN and T-BUT, respectively. The resulting We numbers were 207 and 274 for the ACN and the T-BUT droplets, respectively, which supports the assumption that the impinging droplets deform into thin cylindrical disks.[26] The thermal diffusivity, α, used for each solvent in this model was determined by first taking the average of each property in the definition of α evaluated between the initial droplet temperature to the freezing temperature of each solvent.(Table 3.2). The α for each solid solvent was not determined since thermal conductivity values were not available for each solvent in solid form.

The calculation of cooling times for each solvent was based on the time it takes for the top of the spread droplet at x = 0 to reach a given temperature, T. The cooling time to reach the freezing point of each solvent was calculated first. Fig. 3.8a is the calculated temperature profile for an ACN spread droplet. After 72 ms the top of the spread droplet defined at x = 0 reaches the freezing point of ACN, 230 K. For T-BUT

(Fig. 3.8b) the cooling time to reach the freezing temperature of 299 K was 483 ms. Since the freezing points of each solvent are greater than the surface temperature of the solid substrate, 213 K, the spread droplet will continue to cool below the freezing point until an equilibrium temperature is reached. Therefore, a cooling time was calculated for the droplet to reach an arbitrary temperature of 225 K, which is approximately 5% greater than the cryogenic substrate temperature. These times were 86 and 3037 ms for ACN and T-BUT, respectively.

3.5.2 Comparison of ACN IR data to calculated cooling times

To evaluate the accuracy of the predictions of the proposed model, the calculated cooling times were compared to the IR images. The initial intensity of 2783 for time t = 0 ms correlated to the initial ACN temperature of 25ºC (Fig. 3.4a). Due to the small thickness of the spread droplet it is reasonable to assume that the equilibrium intensity of 2280 at the top surface of the spread droplet is close to the temperature of the cryogenic substrate (213 K). The calculated cooling times to reach the freezing point, 230 K, and 225 K were 72 and 86 ms, respectively. The similarity in these times is consistent with the small difference in temperature between the freezing temperature and 225 K. The calculated cooling time is located at the bottom of the initial steep descent for the experimental curve in Fig. 3.4a. The calculated equilibrium cooling time occurs shortly thereafter at the beginning of the flat part of the intensity curve. The abrupt change in slope of the intensity curve near 70 ms may be an indication of ACN changing from the liquid to solid phase. The discontinuity in the slope of the intensity curve was confirmed when the experiment was repeated a second time. The good agreement between the

calculated cooling times and the shape of the intensity curve supports the assumption that the heat transfer time is considerably slower, and essentially uncoupled, from the rapid spreading of the droplet on impact. Frame by frame analysis of the impinging ACN droplet showed that complete spreading occurred in less than 10 ms. Furthermore, the spreading diameter on the cryogenic substrate was similar to that on the same substrate at room temperature, indicating that cooling and freezing of the droplet did not inhibit spreading. Although the model calculates cooling times that are consistent with experimental IR data, it does not account for the radial cooling front observed during the latter stages of cooling of the spread ACN droplet. In spite of the radial cooling front observed during cooling, the calculated cooling times do not vary significantly from the experimental cooling times.

3.5.3 Comparison of T-BUT IR data to calculated cooling times

The cooling behavior was substantially different for T-BUT compared to ACN. As shown in Fig. 3.3, cooling along the radial direction of the spread T-BUT droplet appeared to be significant. Also, after the T-BUT droplet impacted the cryogenic substrate the final spread droplet diameter was only 0.8 cm which was significantly smaller compared to the 1.9 cm formed on the same substrate at room temperature. The smaller spread diameter corresponds to a frozen spread droplet thickness 4X greater than ACN. The calculated cooling time to freezing (299 K) for T-BUT was 483 ms starting from an initial droplet temperature of 313 K. In (Fig. 3.4b) the approximate intensity value at t = 483 ms was 2185 which was slightly above the asymptotic equilibrium intensity (~213 K) of 2016, but well below the initial intensity of 3227 correlated to 313

K. The intensity curve reaches equilibrium at approximately t = 1000 ms which is assumed to correlate to an approximate spread droplet surface temperature of 213 K. The calculated time for the top droplet surface to reach the defined equilibrium temperature of 225 K was 3037 ms which is about 3 fold the experimental value of 1000 ms. However, the model correctly predicted that the experimental observation that the cooling was much slower than for ACN.

Various factors may contribute to the faster cooling in the experiments versus the model. The difference cannot be explained by cooling of the droplet during free fall. The free fall cooling effect on droplets, initially at 313 K, according to the model of Bennett and Poulikakos,[34] would produce an insignificant change of less than 1K. The more rapid cooling for the experimental measurements may be the result of radial cooling as the droplet spread, and even after spreading. The movement of the radial cooling front was about 30X slower for T-BUT than for ACN. Thus radial cooling appeared to play a greater role for T-BUT, which is consistent with the thicker disk for T-BUT, which corresponds to a greater cross-sectional surface area for radial conduction, and a smaller surface area for axial conduction.

The effect of radial cooling was shown for molten metal droplets impinging on a cold substrate by other research groups.[19, 32] It was determined that significant heat transfer can occur during spreading of the droplet after impact.[19, 32] Zhao et al. described that the radial cooling front occurs because during impaction high temperature solvent is continuously supplied to the center region of impact while the spreading front cools at a faster rate by contacting the low temperature surface of the substrate.[32] Fukai et al. determined that the spreading diameter of droplets can be arrested on a cold

substrate as the edges freeze.[19] It is likely that the spreading diameter was reduced for T-BUT by freezing of the droplet edge, since the temperature difference from the initial droplet temperature (313 K) to freezing point (299 K) is only 14 K versus 68 K for ACN. The effect of radial cooling and partial cooling before complete spreading led to an overestimation by the model; however, it gave a reasonable result that was instructive for explaining the slower cooling for T-BUT versus ACN.

3.5.4 Influence of solvent system on powder properties

Even though there are substantial differences in the freezing characteristics of each solvent, both solvents produced powders comprising DAN and PVP with similar physico-chemical properties indicating sufficient cooling rates in both solvents. The URF technology was used to manufacture micronized powders containing DAN and PVPK15 in a 1:2 ratio using both ACN and T-BUT as the solvent system.

The rapid freezing of the URF technology produced powders with amorphous characteristics which can enhance dissolution rates through increasing the solubility driving force[35] and lowering the heat of solution of the API[36]. According to the contact angle measurements, wetting of the DAN was improved through the use of the hydrophilic polymer PVP which also acts as a stabilizer to prevent recrystallization of DAN. Statistical differences was seen between the contact angles for the processed powders and the physical mixtures at the current ratios, while even higher potency powders produced from URF (not published) or SFL[11, 14] have also shown significant differences in wetting compared to their physical mixture counterparts. Despite the similar surface areas for both URF micronized powders, the particle morphologies were

97

very different. Both processed powder SEMs revealed discrete nanoparticle domains containing DAN. However, flat plate-like regions were also observed throughout the powder sample in Fig. 3.6b for T-BUT. This is attributed to a difference in cooling rates between the two solvents.[28, 29] The temperature decrease over time at the top of the droplet (x=0) is much slower for the T-BUT droplet which drops 17 degrees Kelvin in 600 ms compared to the ACN which drops 75 degrees Kelvin within 70 ms. The slower cooling for T-BUT provided time for growth to occur, forming the plate-like regions. The growth may have been non-uniform, as more time for growth was available closest to the air surface where the temperature was the highest. However, the freezing rates appeared to be sufficiently fast in both solvents to produce high surface area powders with low crystallinity. Differences in surface morphology could also be attributed to possible differences in solubility within the solvent based on the temperature-composition phase diagram of the API/polymer solution.[37, 38] However, these diagrams were not determined and therefore, the extent of this phenomenon on the particle morphology is not known at this time.

3.6 CONCLUSIONS

Sample powders were prepared by URF technology from two different solvents with different thermal and physical properties, T-BUT and ACN. The differences in the thermal properties of the solvent and droplet dimensions had a dramatic effect on the cooling rate of the droplets as evidenced by the heat transfer model and IR studies. An axial heat transfer model for the spread droplets indicated ACN droplets cooled in 72 ms while T-BUT droplets required a much greater time of 483 ms. The much longer cooling

time for T-BUT was also observed by IR imaging. However, it was found that the rate of cooling was sufficiently rapid in both solvents to produce amorphous powders with high surface areas on the order of 25.9-29.3 m^2/g and high wettability. Relative to physical mixtures, the URF processed powders had much more rapid dissolution profiles, which were attributed to nano-structured amorphous API domains, and the improved surface areas and wettability. The surface morphology of the powders was different for the two processing solvents, despite the similar surface areas.   The primary particles in powders produced from ACN were spherical and uniform in size as a result of the more rapid and uniform cooling of the droplet relative to T-BUT. The use of ACN as a solvent allows for high heat transfer rates, which is beneficial for producing small rapidly dissolving particles, however, its low melting point can cause loss in particle surface area prior to solvent removal. T-BUT, on the other hand, has a lower (but sufficient) heat transfer rate compared to ACN, but is less susceptible to melting at ambient conditions prior to solvent removal.. As a result of fast cooling rates and thus high supersaturation, the URF technology is a viable and robust process for producing high surface area nano-structured powders of poorly water soluble APIs with rapid dissolution rates, which will likely lead to enhanced bioavailability *in vivo*.

3.7 ACKNOWLEDGEMENTS

is a continuing American Fellowship for Pharmaceutical Education (AFPE) Fellow from 2004 to 2006 and a 2005-2006 University Continuing Fellowship recipient.

3.8 REFERENCES

[1]   Lipinski, C., Poor aqueous solubility - an industry wide problem in drug discovery. Am. Pharm. Rev., **2002**, *5*: p. 82-85.

[2]   Date, A.A. and V.B. Patravale, Current strategies for engineering drug nanoparticles. Curr. Opin. Colloid Interface Sci., **2004**, *9*(3-4): p. 222-235.

[3]   Muller, R.H., K. Mader, and S. Gohla, Solid lipid nanoparticles (SLN) for controlled drug delivery - a review of the state of the art. Eur. J. Pharm. Biopharm., **2000**, *50*(1): p. 161-177.

[4]   Soppimath, K.S., T.M. Aminabhavi, A.R. Kulkarni, and W.E. Rudzinski, Biodegradable polymeric nanoparticles as drug delivery devices. J. Control. Release, **2001**, *70*(1-2): p. 1-20.

[5]   Vaughn, J.M. and R.O. Williams, *Nanoparticle Engineering*, in *Encyclopedia of Pharmaceutical Technology*, J. Swarbrick, Editor. In Press, Dekker.

[6]   Rasenack, N. and B.W. Muller, Micron-size drug particles: Common and novel micronization techniques. Pharm. Dev. Technol., **2004**, *9*(1): p. 1-13.

[7]   Hu, J.H., K.P. Johnston, and R.O. Williams III, Nanoparticle engineering processes for enhancing the dissolution rates of poorly water soluble drugs - a review. Drug Dev. Ind. Pharm., **2004**, *30*(3): p. 247-258.

[8]   Leuenberger, H., Spray freeze-drying - the process of choice for low water soluble drugs? J. Nanopart. Res., **2002**, *4*(1-2): p. 111-119.

[9]   Maa, Y.F., P.A. Nguyen, T. Sweeney, S.J. Shire, and C.C. Hsu, Protein inhalation powders: Spray drying vs spray freeze drying. Pharm. Res., **1999**, *16*(2): p. 249-254.

[10]   Rogers, T.L., K.P. Johnston, and R.O. Williams, Solution-based particle formation of pharmaceutical powders by supercritical or compressed fluid CO2 and cryogenic spray-freezing technologies. Drug Dev. Ind. Pharm., **2001**, *27*(10): p. 1003-1015.

[11]   Vaughn, J.M., X.X. Gao, M.J. Yacaman, K.P. Johnston, and R.O. Williams, Comparison of powder produced by evaporative precipitation into aqueous solution (EPAS) and spray freezing into liquid (SFL) technologies using novel Z-contrast STEM and complimentary techniques. Eur. J. Pharm. Biopharm., **2005**, *60*(1): p. 81-89.

[12]   Hu, J., K.P. Johnston, and R.O. Williams III, Spray freezing into liquid (SFL) particle engineering technology to enhance dissolution of poorly water soluble drugs: organic solvent versus organic/aqueous co-solvent systems. Eur. J. Pharm. Sci., **2003**, *20*(3): p. 295-303.

[13]   Rogers, T.L., K.A. Overhoff, P. Shah, P. Santiago, M.J. Yacaman, K.P. Johnston, and R.O. Williams, Micronized powders of a poorly water soluble drug produced by a spray-freezing into liquid-emulsion process. Eur. J. Pharm. Biopharm., **2003**, *55*(2): p. 161-172.

[14]   Hu, J., K.P. Johnston, and R.O. Williams III, Rapid dissolving high potency danazol powders produced by spray freezing into liquid process. Int. J. Pharm., **2004**, *271*(1-2): p. 145-154.

[15]   Evans, J.C., B.D. Scherzer, C.D. Tocco, G.B. Kupperblatt, J.N. Becker, D.L. Wilson, S.A. Saghir, and E.J. Elder, *Preparation of Nanostructured Particles of Poorly Water Soluble Drugs via a Novel Ultra-Rapid Freezing Technology*, in *Polymeric Drug Delivery Volume II - Polymeric Matrices and Drug Particle Engineering*, S. Svenson, Editor. ACS Symposium Series 924, American Chemical Society: Washington D.C., **2006**, p. 30-328.

[16]   Ni, N., M. Tesconi, E.S. Tabibi, S. Gupta, and S.H. Yalkowsky, Use of pure t-butanol as a solvent for freeze-drying: a case study. Int. J. Pharm., **2001**, *226*(1-2): p. 39-46.

[17]   Tesconi, M.S., K. Sepassi, and S.H. Yalkowsky, Freeze-drying above room temperature. J. Pharm. Sci., **1999**, *88*(5): p. 501-506.

[18]   Brunauer, S., P.H. Emmett, and E. Teller, Adsorption of gases in multimolecular layers. J. Am. Chem. Soc., **1938**, *60*: p. 309-319.

[19]   Fukai, J., T. Ozaki, H. Asami, and O. Miyatake, Numerical simulation of liquid droplet solidification on substrates. J. Chem. Eng. Jpn., **2000**, *33*(4): p. 630-637.

[20]   Bennett, T. and D. Poulikakos, Splat-Quench Solidification - Estimating the Maximum Spreading of a Droplet Impacting a Solid-Surface. J. Mater. Sci., **1993**, *28*(4): p. 963-970.

[21]   Kang, B., Z. Zhao, and D. Poulikakos, Solidification of Liquid-Metal Droplets Impacting Sequentially on a Solid-Surface. J. Heat Transf.-Trans. ASME, **1994**, *116*(2): p. 436-445.

[22]   Madejski, J., Solidification of Droplets on a Cold Surface. Int. J. Heat Mass Transf., **1976**, *19*(9): p. 1009-1013.

[23]   Pasandideh-Fard, M., R. Bhola, S. Chandra, and J. Mostaghimi, Deposition of tin droplets on a steel plate : simulations and experiments. Int. J. Heat Mass Transfer, **1998**, *41*: p. 2929-2945.

[24]   Pasandideh-Fard, M., S. Chandra, and J. Mostaghimi, A three-dimensional model of droplet impact and solidification. Int. J. Heat Mass Transfer, **2002**, *45*: p. 2229-2242.

[25]   Sanmarchi, C., H. Liu, E.J. Lavernia, R.H. Rangel, A. Sickinger, and E. Muehlberger, Numerical-Analysis of the Deformation and Solidification of a Single Droplet Impinging onto a Flat Substrate. J. Mater. Sci., **1993**, *28*(12): p. 3313-3321.

[26]   Sivakumar, D. and H. Nishiyama, Numerical analysis on the impact behavior of molten metal droplets using a modified splat-quench solidification model. J. Heat Transf.-Trans. ASME, **2004**, *126*(6): p. 1014-1022.

[27]   Trapaga, G. and J. Szekely, Mathematical-Modeling of the Isothermal Impingement of Liquid Droplets in Spraying Processes. Metall. Trans. B, **1991**, *22*(6): p. 901-914.

[28]   Wang, G.X. and E.F. Matthys, Modeling of Heat-Transfer and Solidification During Splat Cooling - Effect of Splat Thickness and Splat Substrate Thermal Contact. Int. J. Rapid Solidif., **1991**, *6*(2): p. 141-174.

[29]   Wang, G.X. and E.F. Matthys, Numerical Modeling of Phase-Change and Heat-Transfer During Rapid Solidification Processes - Use of Control Volume Integrals with Element Subdivision. Int. J. Heat Mass Transf., **1992**, *35*(1): p. 141-153.

[30]   Zhang, H., X.Y. Wang, L.L. Zheng, and X.Y. Jiang, Studies of splat morphology and rapid solidification during thermal spraying. Int. J. Heat Mass Transf., **2001**, *44*(24): p. 4579-4592.

[31]   Zhao, Z., D. Poulikakos, and J. Fukai, Heat transfer and fluid dynamics during the collision of a liquid droplet on a substrate .2. Experiments. Int. J. Heat Mass Transf., **1996**, *39*(13): p. 2791-2802.

[32]   Zhao, Z., D. Poulikakos, and J. Fukai, Heat transfer and fluid dynamics during the collision of a liquid droplet on a substrate .1. Modeling. Int. J. Heat Mass Transf., **1996**, *39*(13): p. 2771-2789.

[33]   Carslaw, H.S. and J.C. Jaeger, *Conduction of Heat in Solids*. 1959, Oxford University Press: London.

[34]   Bennett, T. and D. Poulikakos, Heat-Transfer Aspects of Splat-Quench Solidification - Modeling and Experiment. J. Mater. Sci., **1994**, *29*(8): p. 2025-2039.

[35]   Hancock, B.C. and M. Parks, What is the true solubility advantage for amorphous pharmaceuticals? Pharm. Res., **2000**, *17*(4): p. 397-404.

[36]   Terada, K., H. Kitano, Y. Yoshihashi, and E. Yonemochi, Quantitative correlation between initial dissolution rate and heat of solution of drug. Pharm. Res., **2000**, *17*(8): p. 920-924.

[37]   Gao, C.Y., A. Li, L.X. Feng, X.S. Yi, and J.C. Shen, Factors controlling surface morphology of porous polystyrene membranes prepared by thermally induced phase separation. Polym. Int., **2000**, *49*(4): p. 323-328.

[38]   Nam, Y.S. and T.G. Park, Porous biodegradable polymeric scaffolds prepared by thermally induced phase separation. J. Biomed. Mater. Res., **1999**, *47*(1): p. 8-17.

Chapter 4: Effect of Stabilizer on the Maximum Degree and Extent of Supersaturation and Oral Absorption of Tacrolimus Made By Ultra-Rapid Freezing

4.1 ABSTRACT

Supersaturated solutions are known to enhance transport across biological membranes by increasing the concentration driving force. Amorphous nanoparticles containing tacrolimus (TAC) in a solid dispersion with the ability to form supersaturated solutions in aqueous media were prepared using the Ultra-rapid Freezing (URF) process. Maximum supersaturation levels (C/Ceq_{max}), defined as the ratio of the highest instantaneous TAC concentration C to the equilibrium solubility of crystalline TAC (Ceq), and extent of supersaturation, as measured by the area under the supersaturation curve (AUC), were used to assess the performance of the URF compositions. The stabilizers included poly(vinyl alcohol) (PVA), poloxamer 407 (P407), and sodium dodecyl sulfate (SDS).. The correlation between *in vitro* supersaturation and *in vivo* absorption enhancement in rats was investigated for various URF compositions of TAC. Dissolution studies were conducted at supersaturated conditions in both acidic media (0.2% NaCl in 0.1N HCl) for 24 hours and at delayed release conditions (USP 25 enteric test method A; with acid to base pH change) to better simulate intestinal transit. The rank order of C/Ceq_{max} in the dissolution studies at acidic conditions was URF-P407 (TAC:P407) > URF-SDS (TAC:SDS) > Prograf[®] (PRO) > URF-PVA:P407 (TAC:PVA:P407). For C/Ceq_{max} under delayed release (enteric) conditions, the order

was URF-SDS > PRO > URF–PVA:P407 > URF-P407, and for the extent of supersaturation (AUC) in acidic and pH shift conditions it was URF-SDS > PRO > URF-PVA:P407 > URF-P407. However, analysis of the pharmacokinetic data suggests URF-P407 had the greatest absorption having statistically higher C_{max} and a 1.5-fold increase in AUC ($p > 0.05$) compared to PRO. All URF compositions had a significantly shorter T_{max} ($p < 0.05$) compared to PRO, as well.   High standard deviations in the pharmacokinetic data (e.g. C_{max}, AUC_{0-24}) are attributed to various biological interferences such as enzymatic degradation or P-glycoprotein efflux associated with oral absorption of TAC, making *in vitro-in vivo* correlations difficult. The nanostructured powders containing various stabilizing polymers formed by the URF process offer enhanced supersaturation characteristics leading to increasing oral absorption of TAC.

4.2 INTRODUCTION

Tacrolimus (TAC) is a hydrophobic macrolide antibiotic (MW 822.1 kDa) that has shown promise as a potent immunosuppressive agent.[1] Clinical and pharmacokinetic studies revealed that TAC may have superior immunosuppressive properties compared to cyclosporine A (CsA), but similar erratic absorption properties have limited its potential.[2-4] Mean oral bioavailability is reported to be 25% and ranges from 4-93%.[5, 6] Various strategies have been employed to increase the bioavailability of TAC including compounding TAC as an oral liquid [7], solid dispersions [8], complexation with cyclodextrins [9, 10], and incorporation into liposomes for oral [11, 12] and pulmonary [13] delivery.

The formation of a supersaturated state with solid dispersions and solid solutions may increase oral bioavailability of active pharmaceutical ingredients (APIs) which suffer from poor/erratic bioavailability. In fact, it was proposed that increasing the solubility greater than two-fold through polymorphism can have a significant increase in biopharmaceutical activity.[14-16] Mechanistically speaking, APIs in a polymorph with a higher thermodynamic activity form a supersaturated solution with a apparent solubility above the equilibrium solubility and therefore have an increased driving force for transport across biological membranes such as the epithelial membrane within the GI tract.[17] Another challenge, however, is to maintain the supersaturated state and prevent precipitation of the API out of solution. Stabilizing polymers such as hydroxypropylmethyl cellulose (HPMC), which are known to form hydrogen bonds with the API preventing precipitation [18, 19], can be incorporated into the composition.

HPMC and polyvinylpyrrolidone (PVP) have been shown to be two of the best polymers for maintaining supersaturation of poorly water soluble APIs by preventing precipitation of the API into solution. However, the ability of other polymers/surfactants to stabilize supersaturated solutions and prevent precipitation is largely unknown.

Rapid freezing processes such as the Spray Freezing into Liquid (SFL) [20-22] and Ultra-rapid Freezing (URF) [23, 24] have been shown to produce particles with enhanced dissolution rates for biopharmaceutical classification system (BCS) class II active pharmaceutical ingredients (API). Recently, *in vivo* studies have shown that nanostructured danazol particles produced from SFL have increased oral absorption in mice [21] and nanostructured itraconazole particles from SFL have improved both oral and pulmonary absorption in mice compared to the commercial product[25]. The URF process utilizes a cryogenic surface to rapidly freeze the API/polymer solution to produce nanostructured powders characterized by their high surface area, increased wettability, amorphous API structure, and rapid dissolution rates. Briefly, the process involves freezing an API/polymer solution directly onto the surface of a cryogenic substrate with a thermal conductivity k between 10-20 W/(m*K), collecting the frozen particles and removing the solvent via lyophilization.

However, determining an *in vivo-in vitro* correlation with amorphous particles can be problematic as supersaturation levels in the GI tract may not correlate with levels in the dissolution vessel. Premature precipitation of the active following oral administration can decrease the overall absorption of the API by decreasing the driving force for transport across the biological membrane and limiting the time available for absorption. Although the mechanism for inhibition of recrystallization in supersaturated

109

solutions has not been established [26], it is believed that adsorption of polymer onto the hydrophobic surface of crystals inhibit growth of embryo that nucleate from metastable solutions [27] and suspensions [28]. Recently, Raghaven et al. have proposed hydrogen-bonding as a mechanism to inhibit or retard crystal growth of hydrocortisone acetate in supersaturated solutions containing HPMC.[18, 29] Therefore, inclusion of polymers such as HPMC and PVP which have a number of hydrogen-bonding acceptor and donor sites have been shown to maintain supersaturation of TAC, hydrocortisone acetate, and an experimental poorly water soluble compound RS-8359 for up to 24 hours.[8, 19, 30] However, the effectiveness of the polymer stabilizer is API dependent as illustrated for HPMC, which is known to maintain a supersaturated solution of hydrocortisone acetate for up to 72 hours. However the supersaturation of an oestradiol solution decreased 60% after only six hours [26].

The objective of this study was to assess the effects of combinations of polymeric stabilizers on the maximum degree and extent of supersaturation of TAC, and attempt to establish if an *in vitro-in vivo* correlation exists between supersaturation and improved pharmacokinetic parameters for orally dosed TAC. The selected polymers were partially hydrolyzed polyvinyl(alcohol) (PVA) which has been shown to increase drug concentration *in vitro* [31] and poloxamer 407 (P407) which has been shown to alter surface properties of crystals [32]. Sodium dodecyl sulfate (SDS), a non-polymeric anionic surfactant, may be expected to facilitate wetting and dissolution rates, but supersaturation of pharmaceuticals with SDS has not been reported below the critical micelle concentration. TAC/stabilizer particles were manufactured using the Ultra-rapid Freezing Process (URF) and the physico-chemical properties were compared with those

of the bulk API, as well as the commercially available amorphous solid dispersion of TAC and HPMC.[33] The maximum degree and extent of supersaturation *in vitro* was established for each TAC/excipient composition in both acidic media (for 24 hours) and under shifting pH conditions according to United States Pharmacopoeia (USP). Pharmacokinetic analysis of orally administered TAC compositions in a single dose study design was conducted to determine the performance of the compositions.

4.3 MATERIALS AND METHODS

4.3.1 Materials

Bulk tacrolimus (TAC) and Prograf® (PRO) capsules (5 mg and 1 mg, Fujisawa) were generously donated by the Dow Chemical Company (Midland, MI, USA). Poly(vinyl) alcohol (PVA, Mw 13,000-23,000, 87-89% hydrolyzed) and sodium dodecyl sulfate (SDS) were purchased from Sigma-Aldrich (St. Louis, MO, USA). Poloxamer 407 (P407), Mw 9,800-14,600) was purchased from Spectrum Chemicals (Gardena, CA, USA). Sodium phosphate tribasic (Na_3PO_4) was purchased from Fisher Scientific chemicals (Fair Lawn, NJ, USA). High performance liquid chromatography (HPLC) grade acetonitrile (ACN) was obtained from EM Science (Gibbstown, NJ, USA).

4.3.2 Preparation of the URF Micronized Powders

The URF compositions investigated in this study are described in Table 4.1. The compositions were prepared by dissolving TAC and hydrophilic excipients at a 1:1

API/excipient ratio and 1.0% solids in a 60/40 mixture of ACN and water. The

TAC/excipient feed solutions were processed using the URF apparatus. The feed

solutions were applied to a cryogenic substrate cooled to a temperature of -150°C,

collected, and lyophilized using a VirTis Advantage benchtop tray lyophilizer (The

VirTis Company, Inc. Gardiner, NY, USA). Micronized powders were stored at room

temperature and under desiccant until characterized.

4.3.3 Scanning Electron Microscopy (SEM*)*

The powder samples were sputter coated using a K575 sputter coater (Emitech

Products, Inc., Houston, TX, USA) with gold-palladium for 35 seconds and viewed using

a Hitachi S-4500 field emission scanning electron microscope (Hitachi High

Technologies Corp., Tokyo, Japan). An accelerating voltage of 5-10 kV was used to

view the images. All SEM fields of view were representative of the entire sample.

4.3.4 Supersaturated Dissolution Testing Under Acidic Conditions

Supersaturated dissolution testing was carried out on PRO and all URF

micronized powder samples using a small volume dissolution apparatus equipped with a

paddle stirring mechanism (VanKel VK6010 Dissolution Tester with a Vanderkamp

VK650A heater/circulator, Varian Inc., Cary, NC, USA). The small volume vessels were

filled with 100 mL of deaerated (via He sparge) 0.2% NaCl in 0.1N HCl (Japanese

Pharmacopeia XIX, JP first media) and heated and maintained at 37.0 ± 0.2°C throughout

the dissolution study. Amounts of drug compositions were weighed out corresponding to

28X the aqueous solubility of TAC (7 mg TAC/vessel) and added to the vessels. The

paddle speed was set to 200 RPM and a 3 mL aliquot of sample was taken manually at 10, 20, 30, 60, 120, 240, and 1440 minutes, with no medium replacement. This aliquot was filtered first through a 0.45 μm GHP Acrodisc syringe filter (Pall, East Hills, NY, USA) and then through a 0.02 μm Whatman Anotop 25 membrane filter (Maidstone, UK). A 0.75 mL portion of the filtered solution was transferred to a 1.5 mL HPLC vial and diluted with 0.75 mL ethanol, vortexed and analyzed using a modified method developed by Nishikawa et al [34]. A Shimadzu LC-10 liquid chromatograph (Shimadzu Corporation, Kyoto, Japan) equipped with an Alltech Inertsil ODS-2 5 μm C_{18} column (Alltech Associates, Inc., Deerfield, IL, USA) maintained at 60°C was used to quantitate the TAC. A 70:30 ACN:water mobile phase at 0.9 mL/min eluted the TAC peak at 8.5 min. The maximum absorbance was measured at wavelength λ=214 nm. System suitability requirements were met ($R^2 \geq 0.999$, precision $\leq 2.0\%$ RSD).

4.3.5 Supersaturated Dissolution Testing Under pH Shift Conditions

All dissolution conditions were maintained as described in section 4.3.4 except that the dissolution medium was changed during the dissolution test. Using the USP enteric test (method A) conditions as a guide, 75 mL of 0.1N HCl was added to the small volume dissolution vessels and heated to 37.0 ± 0.2°C. All dissolution media was deaerated via He sparge. Sample powders were added to the vessels stirred at 200 RPM. After 2 hours, 21 mL of 0.2 M Na_3PO_4 (1:3 v/v buffer:acid ratio observed) was added to increase the pH to 6.8 for the remainder of the study. Samples were taken at the

113

following time points: 15, 30, 60, 120, 135, 150, 240, and 1440 minutes; then filtered, diluted, and analyzed by HPLC as stated above.

4.3.6 X-Ray Powder Diffraction (XRD)

The x-ray diffraction pattern of all powder samples were analyzed using a Philips 1710 x-ray diffractometer with a copper target and nickel filter (Philips Electronic Instruments, Inc., Mahwah, NJ, USA). The leveled powder was measured from 5 to 45 2θ degrees using a step size of 0.05 2θ degrees and a dwell time of one second.

4.3.7 Surface Area Analysis

Specific surface area was measured using a Nova 2000 v.6.11 instrument (Quantachrome Instruments, Boynton Beach, FL, USA). Weighed powder was added to a 12mm Quantachrome bulb sample cell and degassed for a minimum of three hours. The sample was then analyzed (n=3) by the NOVA Enhanced Data Reduction Software v. 2.13 via the Brunauer, Emmett, and Teller theory of surface area [35].

4.3.8 *In Vivo* Oral Absorption Studies

An animal study was designed and approved by the University of Texas at Austin Institute of Animal Care and Use Committee (IACUC). Four groups of six pre-catheterized male Sprague-Dawley rats (300 g) were dosed with 5 mg/kg tacrolimus in size 9 gelatin capsules (Torpac Inc., Fairfield, NJ, USA) followed by administration of 0.4 mL water via oral gavage. An aliquot of 300 µl of blood was withdrawn at 0.5, 1,

114

1.5, 2, 3, 4, 6, and 24 hours and replaced with 6 units/µl heparinized normal saline solution. Fifty µl of the whole blood sample was analyzed by the PRO-Trac[TM] II FK-506 ELISA assay (Diasorin Inc., Stillwater, MN) to quantitate amount of tacrolimus.[36] Whole blood samples were diluted when necessary with the calibrator 0 provided with the PRO-Trac[TM] kit in order to fit within the specified standard curve range (0.3-30 ng/mL). Pharmacokinetic parameters were determined using a non-compartmental analysis in WinNonlin Professional version 2.1 (Pharsight Corporation, Mountain View, CA, USA).

4.3.9 Statistical Analysis

One-way analysis of variance (ANOVA, $\alpha = 0.05$) was used to determine statistically significant differences between results. Results with p-values<0.05 were considered statistically significant. Post- hoc analysis using Tukey's honestly significant difference (HSD) test was performed after analysis to determine individual differences between compositions. Mean differences greater than the HSD were deemed statistically significant.

4.4 RESULTS

4.4.1 *In vitro* Characterization of URF Micronized Powders

The micronized powders were analyzed using SEM to observe the surface morphology. Bulk TAC in Fig. 4.1a displays a plate-like shape with particle sizes ranging from a few microns to over 20 microns in diameter. The particle surfaces appear to be smooth with few pores. In contrast, the URF micronized powders (Fig. 4.1b-d), are a highly porous network of nanostructured aggregates. URF-SDS powder (Fig. 4.1b) is composed of discrete nanoparticles measuring less than 200 nm in diameter. URF-PVA:P407 powder (Fig. 4.1c) appears to be a combination of agglomerated or fused nanoparticles with smoothed edges. The size of the fused particles appears to be larger than those in Fig. 4.1a but still appear to be less than one micron in diameter. Lastly, URF-P407, (Fig. 4.1d) appears to have few submicron domains. A magnified view reveals large agglomerated nanoparticles which have fused to create a porous macrostructure.

Figure 4.2 shows the XRD results for bulk TAC which has a characteristic doublet peak at 19.10 and 19.95 2θ degrees and a secondary crystalline peak at 23.45 2θ degrees. All compositions of the URF micronized powders lack any characteristic crystalline peaks of TAC. URF-P407 contains two crystalline peaks at 19.4 and 23.6 2θ degrees and is associated with the P407 in the composition, which is partially crystalline after lyophilization as has been observed in rapidly frozen or melt compositions[20, 37, 38]. Likewise, these two peaks are seen to a lesser degree in the URF-PVA:P407 composition due to a decrease in P407 in the composition.

In vitro supersaturation dissolution studies were conducted in acidic media for 24 hours for each of the URF micronized powders, as well as the control, the PRO powder, as shown in Fig. 4.3 and summarized in Table 4.3. Sample powders were added to the

dissolution media at approximately 28-times the equilibrium solubility of TAC in the media as measured by HPLC. The degree of supersaturation is defined as the concentration (C) of TAC in the media divided by the equilibrium solubility (Ceq) of crystalline TAC within the medium, C/C_{eq}. All URF micronized powders had rapid dissolution rates reaching their maximum supersaturation within 2 hours. URF-SDS displayed a high C/Ceq_{max} with an extended supersaturation that produced the highest AUC of all compositions investigated. URF-PVA:P407 displayed the lowest C/Ceq_{max} at 14.5-times equilibrium solubility, and precipitated out to 3.5-times equilibrium solubility after 24 hours. URF-P407 had the fastest dissolution rate and the highest maximum supersaturation of all powders examined with a C/C_{eq} of 22.8-times equilibrium solubility at 1 hr. However, URF-P407 rapidly precipitates to 6.3-times equilibrium solubility at 6 hours and was the only one of the three URF processed powders investigated to reach equilibrium solubility at 24 hrs. PRO powder, which is composed of equal ratios of amorphous TAC and HPMC[33], showed a slower dissolution rate reaching its maximum supersaturation level (17-times) after 6 hours. However, for PRO TAC, a supersaturation at 11-times equilibrium solubility was still present after 24 hours.

Because the powders were to be administered orally, supersaturated dissolution was also investigated using an enteric dissolution test method to more accurately represent the pH conditions encountered during transit from the acidic environment in the stomach to the basic environment in the upper small intestine (Fig. 4.4; parameter summary in Table 4.3). TAC is known to have pH independent solubility over the pH range 1-9 [39] and therefore has the same solubility in acidic media as in the pH 6.8 buffer (2.2 μg/mL) [8]. Upon a pH shift from pH 1.2 to 6.8 at 2 hours, URF-SDS was the

only composition with an increase in supersaturation level reaching its C/Ceq_{max} 15 minutes after the pH shift occurred. After 15 minutes, TAC precipitated out from solution and after 24 hours had 2-times equilibrium solubility in the basic dissolution media. Both URF-PVA:P407 and URF-P407 had similar supersaturation profiles reaching their maximum supersaturation before precipitation occurred. PRO, however, began to precipitate out of solution immediately after the pH shift occurred. As a result of the pH shift, PRO was not able to achieve the level of supersaturation observed in the acidic media. After the pH shift occurred, a high level of supersaturation was not maintained. PRO precipitated to only 2.5-times equilibrium solubility after 24 hours, unlike the case in acid conditions where supersaturation was extended at high levels.

Both URF-SDS and URF-P407 had significantly higher ($p<0.05$) maximum supersaturation ratios (C/Ceq_{max}) in acidic medium while only URF-SDS had a significantly higher ($p<0.05$) C/Ceq_{max} when tested with the pH shift dissolution conditions compared to PRO. The URF micronized powders reached their C/Ceq_{max} within one to two hours in acidic media while PRO reached its C/Ceq_{max} at 6 hours. All URF compositions reached their C/Ceq_{max} before PRO under acidic conditions indicating the rapid wetting that occurs with URF micronized powders. .However, both URF-PVA:P407 and URF-P407 had lower extents of supersaturation (AUC) compared to PRO, while URF-SDS had better AUC than PRO under acidic and pH shift conditions, respectively.

4.4.2 *In Vivo* Characterization of URF Micronized Powders

Whole blood samples were analyzed using a commercially available immuno-assay kit and the TAC whole blood concentrations vs. time are plotted in Fig. 4.5. The absorption profiles for the URF compositions indicate faster absorption and higher TAC blood levels during the absorption phase. From these profiles, non-compartmental analysis, as discussed by Arima et al.[10], was performed to determine the appropriate pharmacokinetic parameters for each of the compositions tested and are summarized in Table 4.4. One-way ANOVA revealed that there were significant differences ($p<0.05$) between the four compositions in regards to C_{max} and T_{max} while there were no statistical differences ($p>0.05$) regarding the tacrolimus half-life ($T_{1/2}$), the elimination rate constant (K_{el}), or the AUC. All URF micronized powders had higher C_{max} values ranging from 65.2-138 ng/mL as compared to the PRO powder which had a C_{max} of 51.5 ng/mL. However, only URF-P407 powder had a significantly higher C_{max} compared to PRO while URF-SDS and PVA:P407 powders were not statistically different$_{ly}$ ($p>0.05$). The measured T_{max} for each URF micronized powder was between 0.5 and 0.67 hr while the PRO powder had a measured T_{max} of 1.3 hours. All powders had similar K_{el} while PRO had the lowest at 0.094 hr^{-1} and URF C had the highest K_{el} at 0.106 hr^{-1}. Consequently, URF-P407 had the fastest clearance of TAC and therefore had the fastest half-life at $T_{1/2}$=6.9 hrs. Lastly, URF-P407 had the highest AUC$_{(0-24)}$ at 450.6 ng*hr/mL. Despite having a 1.5 fold increase in AUC compared to PRO, this was not statistically significant ($p>0.05$). URF-PVA:P407 had the next highest AUC at 319.8 ng*hr/mL followed by PRO at 298.8 ng*hr/mL. URF-SDS had the lowest AUC at 223.6 ng*hr/mL. Therefore, the pharmacokinetic parameters assessed in the study were enhanced by the URF compositions (C_{max}, T_{max}, $T_{1/2}$, and AUC) as compared to PRO. The average relative

bioavailability for URF-SDS, URF-PVA:P407, and URF-P407 are 77.1%, 105.6%, 144.2%, respectively.

4.5 DISCUSSION

In the present study, nanostructured aggregate powders containing TAC and excipients, manufactured by the URF process were characterized in order to better understand the mechanism of supersaturation stabilization. Furthermore, an attempt is made to identify the effect of supersaturation on increasing the bioavailability of TAC.

In vitro characterization of the URF micronized powders revealed that they were composed of nanoparticle domains containing amorphous TAC. URF-P407 displayed the lowest surface area at 7.73 m^2/g. Similar results were reported by Hu et al. [20] who produced binary mixtures containing danazol and a hydrophilic polymer by another rapid freezing process, spray freezing into liquid. The surface area of danazol:P407 was 5.5 m^2/g, while danazol:PEG and danazol:PVP powders had surface areas of 12.0 and 89.8 m^2/g, respectively. In a similar study by McConville et al., low surface areas were attributed to incorporation of high levels (>30%) of a liquid surfactant, polysorbate 20.[38] In that study, it was hypothesized that surface area reduction occurred during the lyophilization process. During lyophilization, compositions containing excipients, which exist in a liquid state at ambient conditions, have more molecular mobility than those containing solid excipients with high glass transition temperatures (e.g. PVP). With the greater mobility, the particles may coalesce to reduce the surface area, as has been observed for polysorbate 20. However, all polymers used in this study are solids at room temperature and should provide greater rigidity compared to liquid surfactants during

lyophilization and gave much higher surface areas than polysorbate 20. The modestly lower surface area for P407, relative to the other formulations in Table 4.2, may reflect its much lower T_g.

Specifically regarding TAC supersaturation studies, Yamashita et al. investigated the performance of HPMC, PVP, and polyethylene glycol (PEG) on maintaining the supersaturation of TAC.[8] While all samples had reached the same C/Ceq_{max}, only HPMC was able to maintain at least 95% of the maximum supersaturation over 24 hours in acidic medium. To date, the mechanism by which they maintain supersaturation of dissolved drug has not been delineated.

Apart from their particle formation properties, polymers also play an important role in enhancing dissolution rates through wettability, and at supersaturated conditions, maintaining API supersaturation. Both SDS and P407 are known to increase wetting due to their high hydrophilic-lipophilic balance (HLB) values, while PVA is used as a stabilizing agent and has been reported to enhance supersaturation.[31] Suzuki and Sunada report that although PVA maintained supersaturation to a lesser degree than HPMC or PVP, dissolution supersaturation was enhanced by more than 20-times compared to the crystalline API. The present supersaturation studies indicate that P407 is not able to maintain supersaturation for extended periods of time of up to 24 hours, but the enhanced wetting properties of the polymer allow for high supersaturation levels at short times. Inclusion of PVA into the composition decreases the level of supersaturation but allows for slightly slower precipitation rates in the acidic media after six hours. SDS, although not a polymer, was able to maintain supersaturation of TAC at a similar level to HPMC under both supersaturated dissolution conditions tested. It is important to note

that the concentrations of SDS present in the medium reached only 10% of the critical micelle concentration in aqueous media (conc. $SDS_{disso} = 2.5 \times 10^{-4}$ M and $SDS_{CMC} = 2.8 \times 10^{-3}$ M) containing a salt as calculated by Dutkiewicz and Jakubowska.[40]   SDS dissociates in the electrolyte medium to produce a hydrogen-bonding acceptor site.   In addition, the interaction between the hydrophobic tail of a surfactant molecule and the hydrophobic surface of the API molecule, and a second complimentary interaction between the sulfate group of the surfactant molecule with an adjacent hydrogen bonding donor site on the API may facilitate solvation of the drug in water.   The same type of mechanism may take place for the polymeric stabilizers with hydrophobic moieties and hydrogen bonding sites.   Furthermore, it is likely that, other SDS molecules will adsorb with tails oriented onto the surface of embryo crystals of TAC with the head groups extending into water. The anionic sulfate groups on the adsorbed surfactant will provide electrostatic repulsion inhibiting particle growth from coagulation.

In solution, the polymers may adsorb onto the surface of small embryo particles and inhibit crystal growth by blocking active surface and providing steric stabilization. In addition, hydrogen bonding between TAC and the stabilizers may complement hydrophobic interactions between these species to help maintain supersaturation. Structurally, HPMC has many hydroxyl groups which are both hydrogen bond donors and acceptors for the TAC.   Investigation of the TAC structure (Fig. 4.6) reveals four possible H-bond acceptor sites indicated by circles along with three possible donor sites indicated by triangles. PVA has one H-bond donor and acceptor per monomer unit while P407, on the other hand, has one donor site per polymer unit.

PRO maintained supersaturation under acidic conditions to a similar extent as SDS, as shown in Table 4.3. The less effective stabilization by PVA and P407 may reflect weaker adsorption on the surfaces of the embryo particles and thus less steric stabilization against particle growth. In addition P407 with only one H-bonding donor sight per chain may not have interacted strongly enough with hydrogen bond acceptor sites on TAC to inhibit crystallization. PVA:P407 was slightly better than P407 alone, perhaps indicating that the addition of hydrogen bond donor sites in PVA provided beneficial interactions with TAC.

The shift in media pH at 2 hours during the supersaturation dissolution studies dramatically affected the physical stability of the supersaturated solutions even though the solubility of the API in aqueous media without stabilizers is independent of pH. While URF-PVA:P407 and URF-P407 began precipitating before the pH shift occurred the PRO composition immediately began precipitating after the pH was increased. This precipitation may produce a loss in bioavailability as a result of decreased absorption in the small intestine. Interestingly, the degree of supersaturation for URF-SDS increased for at least 15 minutes after the pH shift occurred before it then decreased. However, the rate of precipitation out of solution over the next 21 hours was much more pronounced than under acidic conditions in Figure 4.3 indicated by the supersaturation level at 24 hours. This trend was seen for all compositions investigated at pH 6.8 compared to the acidic media and could be the result of bonding strength changes from the presence of inorganic salts.[41] Khutoryanskiy et al. suggests that the presence of inorganic salts such as Na_3PO_4 (in particular, the divalent and trivalent phosphates) in the dissolution media can alter the ionic strength or thermodynamic properties of the solution and salt

out the API. Introduction of inorganic salts can cause collapse of the polymer chains on the surface of embryo API particles. This collapse will weaken steric stabilization and may lead to precipitation of the API out of solution, particularly with P407 in the presence of NaCl and Na_3PO_4.[42]

Both the acidic and enteric *in vitro* supersaturation test condition studies reveal that the URF micronized powders rapidly wet and dissolve resulting in solutions with high C/Ceq_{max}. The *in vivo* absorption profiles also indicate rapid wetting and dissolution as evidenced by the rapid T_{max} for all URF compositions leading to rapid absorption times. This rapid dissolution could be a combination of both the polymer characteristics (i.e. wetting enhancement) as well as the rapid freezing process which create amorphous nanoparticle domains of API. Because the powders were dosed within a size #9 hard gelatin capsule by oral gavage, the powders were not pre-wetted by aqueous solution containing a surfactant. Therefore, the powders must rely on the gastric fluid and on the enhanced powder wetting properties (i.e. polymer/surfactant wettability, and available surface area) to wet, disintegrate, and dissolve the particles. It is clear from both the *in vitro* and *in vivo* data that the URF micronized powders are wetted more effectively than PRO leading to enhanced absorption profiles early in the absorption phase. While numerous studies have reported increases in bioavailability as a result of API being in a supersaturated state, rapid dissolution and supersaturation could prove counter productive, especially for examples in which the API can precipitate during transit when the pH increases from the stomach to upper small intestine. Absorption of the API can be compromised in instances when all of the powder is dissolved in the stomach but not fully absorbed through the stomach lining. As the API moves into the upper small

intestine, the solution begins to precipitate arresting absorption. While it is true that the measured pharmacokinetic parameters for the URF micronized powders were superior to those of PRO, premature precipitation while in transit could have prevented the powders from achieving their full potential. This is evidenced by URF-P407 which showed a high C/Ceq_{max} *in vitro* under acidic conditions and also had the highest C_{max} *in vivo*. In this case, URF-P407 probably completely dissolved into a supersaturated solution leading to excellent absorption initially but rapid precipitation limited further absorption.

Absorption of TAC within the small intestine is also affected by a number of biological processes making further *in vitro-in vivo* correlations difficult. TAC is reported as a substrate for p-glycoprotein (P-gp), a plasma protein involved with efflux pumps and responsible for multi-drug resistance.[43] In addition, TAC is known to degrade enzymatically within the GI lining from CYP3A metabolic enzymes further lowering its absorption potential. However, recent studies have suggested that within the rat and mouse small intestine, the CYP3A enzymes play a larger role in limiting TAC absorption rather than P-gp as previously thought.[44-46] Saitoh et al. showed via an *in situ* intestinal loop technique that when TAC was administered with a specific CYP3A inhibitor (clotrimazole) the TAC AUC increased seven fold.[47] Food effects can also cause changes in TAC absorption. Kagayama et al. showed that rats receiving TAC in a fasted state can have twice the AUC of rats who received the same dose of TAC in a fed state.[48] Regardless, these barriers to TAC absorption are well documented in rats [48] and because there is a fair correlation between mammal species regarding intestinal absorption [49], this animal model is valid for preliminary pharmacokinetic analysis of the URF micronized compositions containing TAC.

4.6 Conclusion

The relationship between supersaturation behavior, measured during dissolution, and *in vivo* absorption enhancement was investigated for various compositions of TAC prepared by the URF process. The ability of two polymers, PVA and P407, and one low molecular weight surfactant, SDS, to provide sufficient supersaturation levels (C/Ceq_{max}) and to maintain supersaturation under acidic and pH shifted conditions was determined. The supersaturation for URF-SDS was equal to or better than PRO under acidic and pH shift conditions, respectively, even though the levels of SDS were well below the CMC in the medium. It is hypothesized that SDS was able to maintain supersaturation of TAC through adsorption onto the surface of tiny embryo particles to inhibit growth and precipitation. For URF-PVA:P407 and URF-P407, maintenance of supersaturation *in vitro* was poorer than for PRO. URF-P407 was the only composition where the concentration decayed to the equilibrium value after 24 hours in acidic medium. URF-PVA:P407 and URF-P407 both began to precipitate while still in acid, while PRO began to precipitate immediately after the shift. Although TAC solubility and chemical stability are independent of pH, the rate of precipitation was more extensive at pH 6.8 than in acidic media possibly as the result of changes caused by the presence of inorganic salts in the buffer. *In vivo* results in a rat model reveal enhanced C_{max} and T_{max} for all URF micronized compositions and higher AUC in URF-PVA:P407 and URF-P407 resulting from enhanced dissolution properties (e.g. rapid onset of supersaturation) of the processed powders. Based on the pharmacokinetic parameters and supporting *in vitro*

126

supersaturation data, it is concluded that the enhanced physico-chemical properties of URF micronized powders led to enhanced *in vivo* absorption enhancement over PRO.

4.7 ACKNOWLEDGEMENTS

4.8 REFERENCES

[1]   Peters, D.H., A. Fitton, G.L. Plosker, and D. Faulds, Tacrolimus - a Review of Its Pharmacology, and Therapeutic Potential in Hepatic and Renal-Transplantation. Drugs, **1993**, *46*(4): p. 746-794.

[2]   Jusko, W.J., W. Piekoszewski, G.B. Klintmalm, M.S. Shaefer, M.F. Hebert, A.A. Piergies, C.C. Lee, P. Schechter, and Q.A. Mekki, Pharmacokinetics of Tacrolimus in Liver-Transplant Patients. Clin. Pharmacol. Ther., **1995**, *57*(3): p. 281-290.

[3]   Lampen, A., U. Christians, F.P. Guengerich, P.B. Watkins, J.C. Kolars, A. Bader, A.K. Gonschior, H. Dralle, I. Hackbarth, and K.F. Sewing, Metabolism of the immunosuppressant tacrolimus in the small intestine: Cytochrome P450, drug interactions, and interindividual variability. Drug Metab. Dispos., **1995**, *23*(12): p. 1315-1324.

127

[4]   Mancinelli, L.M., L. Frassetto, L.C. Floren, D. Dressler, S. Carrier, I. Bekersky, L.Z. Benet, and U. Christians, The pharmacokinetics and metabolic disposition of tacrolimus: A comparison across ethnic groups. Clin. Pharmacol. Ther., **2001**, *69*(1): p. 24-31.

[5]   Wallemacq, P.E. and R.K. Verbeeck, Comparative clinical pharmacokinetics of tacrolimus in paediatric and adult patients. Clin. Pharmacokinet., **2001**, *40*(4): p. 283-295.

[6]   Venkataramanan, R., A. Swaminathan, T. Prasad, A. Jain, S. Zuckerman, V. Warty, J. McMichael, J. Lever, G. Burckart, and T. Starzl, Clinical pharmacokinetics of tacrolimus. Clin. Pharmacokinet., **1995**, *29*(6): p. 404-430.

[7]   Jacobson, P.A., C.E. Johnson, N.J. West, and J.A. Foster, Stability of tacrolimus in an extemporaneously compounded oral liquid. Am. J. Health-Syst. Pharm., **1997**, *54*(2): p. 178-180.

[8]   Yamashita, K., T. Nakate, K. Okimoto, A. Ohike, Y. Tokunaga, R. Ibuki, K. Higaki, and T. Kimura, Establishment of new preparation method for solid dispersion formulation of tacrolimus. Int. J. Pharm., **2003**, *267*(1-2): p. 79-91.

[9]   Arima, H., K. Yunomae, F. Hirayama, and K. Uekama, Contribution of P-glycoprotein to the enhancing effects of dimethyl-beta-cyclodextrin on oral bioavailability of tacrolimus. J. Pharmacol. Exp. Ther., **2001**, *297*(2): p. 547-555.

[10]   Arima, H., K. Yunomae, K. Miyake, T. Irie, F. Hirayama, and K. Uekama, Comparative studies of the enhancing effects of cyclodextrins on the solubility and oral bioavailability of tacrolimus in rats. J. Pharm. Sci., **2001**, *90*(6): p. 690-701.

[11]   Lee, M.J., R.M. Straubinger, and W.J. Jusko, Physicochemical, Pharmacokinetic and Pharmacodynamic Evaluation of Liposomal Tacrolimus (Fk-506) in Rats. Pharm. Res., **1995**, *12*(7): p. 1055-1059.

[12]   Moffatt, S.D., V. McAlister, R.Y. Calne, and S.M. Metcalfe, Potential for improved therapeutic index of FK506 in liposomal formulation demonstrated in a mouse cardiac allograft model. Transplantation, **1999**, *67*(9): p. 1205-1208.

[13]   Canadas, O., R. Guerrero, R. Garcia-Canero, G. Orellana, M. Menendez, and C. Casals, Characterization of liposomal tacrolimus in lung surfactant-like phospholipids and evaluation of its immunosuppressive activity. Biochemistry, **2004**, *43*(30): p. 9926-9938.

[14]   Egawa, H., S. Maeda, E. Yonemochi, T. Oguchi, K. Yamamoto, and Y. Nakai, Solubility Parameter and Dissolution Behavior of Cefalexin Powders with Different Crystallinity. Chem. Pharm. Bull., **1992**, *40*(3): p. 819-820.

[15]   Sato, T., A. Okada, K. Sekiguchi, and Y. Tsuda, Difference in Physico-Pharmaceutical Properties between Crystalline and Noncrystalline 9,3"-Diacetylmidecamycin. Chem. Pharm. Bull., **1981**, *29*(9): p. 2675-2682.

[16]   Imaizumi, H., N. Nambu, and T. Nagai, Pharmaceutical Interaction in Dosage Forms and Processing .18. Stability and Several Physical-Properties of Amorphous and Crystalline Forms of Indomethacin. Chem. Pharm. Bull., **1980**, *28*(9): p. 2565-2569.

[17]   Gao, P., M.E. Guyton, T.H. Huang, J.M. Bauer, K.J. Stefanski, and Q. Lu, Enhanced oral bioavailability of a poorly water soluble drug PNU-91325 by supersaturatable formulations. Drug Dev. Ind. Pharm., **2004**, *30*(2): p. 221-229.

129

[18]   Raghavan, S.L., B. Kiepfer, A.F. Davis, S.G. Kazarian, and J. Hadgraft, Membrane transport of hydrocortisone acetate from supersaturated solutions; the role of polymers. Int. J. Pharm., **2001**, *221*(1-2): p. 95-105.

[19]   Raghavan, S.L., A. Trividic, A.F. Davis, and J. Hadgraft, Effect of cellulose polymers on supersaturation and in vitro membrane transport of hydrocortisone acetate. Int. J. Pharm., **2000**, *193*(2): p. 231-237.

[20]   Hu, J.H., K.P. Johnston, and R.O. Williams, Stable amorphous danazol nanostructured powders with rapid dissolution rates produced by spray freezing into liquid. Drug Dev. Ind. Pharm., **2004**, *30*(7): p. 695-704.

[21]   Vaughn, J.M., J.T. McConville, M.T. Crisp, R.O. Williams III, and K.P. Johnston, Supersaturation Produces High Bioavailability of Amorphous Danazol Particles Formed by Evaporative Precipitation into Aqueous Solution (EPAS) and Spray Freezing into Liquid(SFL) Technologies. Drug Dev. Ind. Pharm., **2006**, *32*(5): p. 559-567.

[22]   Overhoff, K.A., K.P. Johnston, and R.O. Williams, *Improvement of Dissolution Rate of Poorly Water Soluble Drugs Using a New Particle Engineering Process: Spray Freezing into Liquid*, in *Polymeric Drug Delivery II: Polymeric Matrices and Drug Particle Engineering*, S. Svenson, Editor. 2006, American Chemical Society: Washington D.C. p. 305-319.

[23]   Overhoff, K.A., J. Engstrom, B. Chen, B. Scherzer, T.E. Milner, K.P. Johnston, and R.O. Williams, Novel Ultra-rapid Freezing Particle Engineering Process for Enhancement of Dissolution Rates of Poorly Water Soluble Drugs. Eur. J. Pharm. Biopharm., **2006**, *In Press*.

[24]   Rogers, T.L., J.H. Hu, Z.S. Yu, K.P. Johnston, and R.O. Williams III, A novel particle engineering technology: spray-freezing into liquid. Int. J. Pharm., **2002**, *242*(1-2): p. 93-100.

[25]   Vaughn, J.M., J.T. McConville, D. Burgess, R.L. Talbert, J.I. Peters, R.O. Williams III, and K.P. Johnston, Single Dose and Multiple Dose studies of Aerosolized Itraconazole Nanoparticles. Eur. J. Pharm. Biopharm., **2005**, *63*(2): p. 95-102.

[26]   Megrab, N.A., A.C. Williams, and B.W. Barry, Estradiol Permeation through Human Skin and Silastic Membrane - Effects of Propylene-Glycol and Supersaturation. J. Control. Release, **1995**, *36*(3): p. 277-294.

[27]   Sung, M.H., J.S. Kim, W.S. Kim, and I. Hirasawa, Modification of crystal growth mechanism of yttrium oxalate in metastable solution. J. Cryst. Growth, **2002**, *235*(1-4): p. 529-540.

[28]   Law, S.L. and J.B. Kayes, Adsorption of Non-Ionic Water-Soluble Cellulose Polymers at the Solid Water Interface and Their Effect on Suspension Stability. Int. J. Pharm., **1983**, *15*(3): p. 251-260.

[29]   Raghavan, S.L., A. Trividic, A.F. Davis, and J. Hadgraft, Crystallization of hydrocortisone acetate: influence of polymers. Int. J. Pharm., **2001**, *212*(2): p. 213-221.

[30]   Usui, F., K. Maeda, A. Kusai, K. Nishimura, and K. Yamamoto, Inhibitory effects of water-soluble polymers on precipitation of RS-8359. Int. J. Pharm., **1997**, *154*(1): p. 59-66.

[31]   Suzuki, H. and H. Sunada, Influence of water-soluble polymers on the dissolution of nifedipine solid dispersions with combined carriers. Chem. Pharm. Bull., **1998**, *46*(3): p. 482-487.

[32]   Mackellar, A.J., G. Buckton, J.M. Newton, and C.A. Orr, The Controlled Crystallization of a Model Powder .2. Investigation into the Mechanism of Action of Poloxamers in Changing Crystal Properties. Int. J. Pharm., **1994**, *112*(1): p. 79-85.

[33]   Ueda, K., K. Shimojo, T. Shimazaki, I. Kado, and K. Honbo, Solid Dispersion of FR-900506 substance, US Patent #US4,916,138. 1990

[34]   Nishikawa, T., H. Hasumi, S. Suzuki, H. Kubo, and H. Ohtani, Kinetic-Analysis of Molecular Interconversion of Immunosuppressant Fk506 by High-Performance Liquid-Chromatography. Pharm. Res., **1993**, *10*(12): p. 1785-1789.

[35]   Brunauer, S., P.H. Emmett, and E. Teller, Adsorption of gases in multimolecular layers. J. Am. Chem. Soc., **1938**, *60*: p. 309-319.

[36]   Dietemann, J., P. Berthoux, J.P. Gay-Montchamp, M. Batie, and F. Berthoux, Comparison of ELISA method versus MEIA method for daily practice in the therapeutic monitoring of tacrolimus. Nephrol. Dial. Transplant., **2001**, *16*(11): p. 2246-2249.

[37]   Chutimaworapan, S., G.C. Ritthidej, E. Yonemochi, T. Oguchi, and K. Yamamoto, Effect of water-soluble carriers on dissolution characteristics of nifedipine solid dispersions. Drug Dev. Ind. Pharm., **2000**, *26*(11): p. 1141-1150.

[38]   McConville, J.T., K.A. Overhoff, P. Sinswat, J.M. Vaughn, B.L. Frei, D.S. Burgess, R.L. Talbert, J.I. Peters, K.P. Johnston, and R.O. Williams, Targeted

high lung concentrations of itraconazole using nebulized dispersions in a murine model. Pharm. Res., **2006**, *23*(5): p. 901-911.

[39]   Tamura, S., A. Ohike, R. Ibuki, G.L. Amidon, and S. Yamashita, Tacrolimus is a class II low-solubility high-permeability drug: The effect of P-glycoprotein efflux on regional permeability of tacrolimus in rats. J. Pharm. Sci., **2002**, *91*(3): p. 719-729.

[40]   Dutkiewicz, E. and A. Jakubowska, Effect of electrolytes on the physicochemical behaviour of sodium dodecyl sulphate micelles. Colloid Polym. Sci., **2002**, *280*(11): p. 1009-1014.

[41]   Khutoryanskiy, V.V., G.A. Mun, Z.S. Nurkeeva, and A.V. Dubolazov, pH and salt effects on interpolymer complexation via hydrogen bonding in aqueous solutions. Polym. Int., **2004**, *53*(9): p. 1382-1387.

[42]   Pandit, N., T. Trygstad, S. Croy, M. Bohorquez, and C. Koch, Effect of Salts on the Micellization, Clouding, and Solubilization Behavior of Pluronic F127 Solutions. J. Colloid Interface. Sci., **2000**, *222*(2): p. 213-220.

[43]   Benet, L.Z., T. Izumi, Y.C. Zhang, J.A. Silverman, and V.J. Wacher, Intestinal MDR transport proteins and P-450 enzymes as barriers to oral drug delivery. J. Control. Release, **1999**, *62*(1-2): p. 25-31.

[44]   Hashimoto, Y., H. Sasa, M. Shimomura, and K. Inui, Effects of intestinal and hepatic metabolism on the bioavailability of tacrolimus in rats. Pharm. Res., **1998**, *15*(10): p. 1609-1613.

[45]   Yokogawa, K., M. Takahashi, I. Tamai, H. Konishi, M. Nomura, S. Moritani, K. Miyamoto, and A. Tsuji, P-glycoprotein-dependent disposition kinetics of

tacrolimus: Studies in mdr1a knockout mice. Pharm. Res., **1999**, *16*(8): p. 1213-1218.

[46]   Chiou, W.L., S.M. Chung, and T.C. Wu, Apparent lack of effect of P-glycoprotein on the gastrointestinal absorption of a substrate, tacrolimus, in normal mice. Pharm. Res., **2000**, *17*(2): p. 205-208.

[47]   Saitoh, H., Y. Saikachi, M. Kobayashi, M. Yamaguchi, M. Oda, Y. Yuhki, K. Achiwa, K. Tadano, Y. Takahashi, and B.J. Aungst, Limited interaction between tacrolimus and P-glycoprotein in the rat small intestine. Eur. J. Pharm. Sci., **2006**, *28*(1-2): p. 34-42.

[48]   Kagayama, A., S. Tanimoto, J. Fujisaki, A. Kaibara, K. Ohara, K. Iwasaki, Y. Hirano, and T. Hata, Oral Absorption of Fk506 in Rats. **1993**, *10*(10): p. 1446-1450.

[49]   Lin, J.H., Species Similarities and Differences in Pharmacokinetics. Drug Metab. Dispos., **1995**, *23*(10): p. 1008-1021.

Chapter 5: Solid Dispersions of Itraconazole and Enteric Polymers Made by Ultra-Rapid Freezing

5.1 ABSTRACT

The primary objective of the study is to investigate the influence of degree of miscibility of a dispersion of ITZ and an enteric polymer, either hydroxypropylmethyl cellulose phthalate (HP-55) or Eudragit® L100-55 (L100-55), prepared by Ultra-rapid Freezing (URF), on enhanced dissolution of ITZ in pH 6.8 dissolution media. Bioavailability can be increased for drugs that form supersaturated solutions in the small intestine allowing for maximum area for absorption. Delayed release until the drug reaches the upper small intestine prevents premature precipitation and subsequent recrystallization for compounds which display higher solubility in acidic conditions such as itraconazole (ITZ). Furthermore the effect of composition parameters (e.g. ITZ potency, enteric polymer type, and total solids loading) on dissolution rates at both sink and supersaturated conditions was studied. Modulated differential scanning calorimetry (MDSC) was utilized to define the level of ITZ miscibility with each polymer. The compositions were completely miscible at 60% ITZ for both polymers and as high as 70% in HP-55. High potency composition glass transition temperatures (T_g) correlated with predicted T_g's from the Gordon-Taylor equation, however, recrystallization exotherms revealed pure amorphous regions indicating that phase separation occurred during particle formation. Furthermore, *in vitro* studies including x-ray powder diffraction (XRD), scanning electron microscopy (SEM), surface area analysis (BET),

and dissolution were performed to determine differences between low potency (completely miscible) and high potency (partially miscible) compositions. Dissolution studies on low potency ITZ compositions revealed that miscibility plays an active role in ITZ release under sink conditions, and $t^{1/2}$ diffusion through the enteric polymer is observed. In dissolution studies at supersaturated conditions, high potency compositions had maximum saturation levels (C/Ceq_{max}) between 10.6 and 8-times (X) equilibrium solubility, but with higher cumulative extents of supersaturation, compared to low potency compositions which had C/Ceq_{max} values between 15-19.6X. However, these low potency compositions tended to rapidly precipitate leading to significantly lower AUCs ($p<0.05$). The change in the miscibility of the solid dispersion had a pronounced effect of drug release (sink) while differences in potency influenced supersaturated dissolution profiles.

5.2 INTRODUCTION

Itraconazole (ITZ) is a broad spectrum triazole antifungal with pH dependent solubility. It is a weak base (pKa_1 = 3.7) and is more soluble in the gastric environment of the stomach compared to the more neutral pH of the other parts of the small intestine.[1] Intuitively, it may appear that the likely site of absorption would be in the acidic environment of the stomach. However, variable gastric emptying times can lead to variable absorption rates, while food effects can alter the pH leading to further variability. Likewise the surface area (SA) of the stomach available for absorption is small relative to other absorption sites in the GI tract. In fact, investigation of the stomach lining reveals epithelial layers which continually shed cells limiting absorption.[2] However, the intestinal surface is composed of microscopic finger-like projections known as villi and microvilli which increase the absorptive surface area of the small intestine 600-fold (> 170 m^2)[3] making it an excellent site for absorption. However, as ITZ enters the small intestines, the change in pH has the potential to precipitate ITZ that was dissolved in the stomach, slowing the absorption process and decreasing bioavailability. In addition, any undissolved particles would remain insoluble with a pH above the pKa. Amorphous solid dispersions containing enteric polymers could overcome these limitations by 1.) delaying dissolution until the compound enters the intestines preventing premature precipitation of the ITZ and 2.) increasing the apparent solubility at higher pH to increase the driving force for absorption. Amorphous drugs can achieve a supersaturated state due to their low heat of fusion.[4] Hancock and Parks have shown that amorphous indomethacin has a 2.5X increase in apparent solubility compared to its crystalline counterpart [5] while up

137

to a 25X increase in solubility has been reported for tacrolimus and diacetylmidecamycin.[6, 7]   However, these supersaturated solutions are thermodynamically unstable and will precipitate and return to the equilibrium state over time. Therefore, a stabilizing polymer must be included to extend the time the compound remains supersaturated. These polymers are able to prevent recrystallization or particle growth in solution through hydrogen-bonding [8, 9] or adsorbing on the surface of solid particles blocking the addition of other solute onto the surface[10-12].

Modified release systems including delayed release systems are used to target delivery of the API within a specific section of the GI tract or when gastric degradation can severely limit the effectiveness of the API. One common approach is to coat the surface of the delivery system (microspheres, tablets, beads/pellets, etc.) with a gastro-resistant polymer, which often displays pH dependent solubility. These polymers typically contain functional groups which ionize at specific pH values, allowing for targeted delivery of the API to certain sections of the GI tract and are often referred to as enteric polymers. Hasagawa et al. were the first to develop solid dispersions comprising a binary mixture of a poorly water soluble API, nifedipine, and an enteric polymer.[13] A variety of technologies have been employed to develop these enteric solid dispersions such as traditional melt dispersion [14], hot melt extrusion/spheronization[15, 16], anti-solvent precipitation[17], solvent evaporation[18, 19], and spray drying[20]. A novel technique based on the aerosol flow reactor has also been used to produce solid dispersions [21]. Oral absorption of poorly-water soluble compounds has been achieved using these enteric solid dispersions [18, 22] particularly since they can delay dissolution and supersaturation until the API reaches the upper small intestine[19]. To date, high

potency compositions with desirable delayed release properties have not been achieved as a result of miscibility limitations between the API and the enteric polymer.

The objective of the study is to investigate the influence of composition parameters including drug:polymer ratio and polymer type, and particle structure of enteric solid dispersions on the release of ITZ under sink and supersaturated dissolution conditions. Solid dispersions containing ITZ and an enteric polymer were produced using the Ultra-rapid freezing (URF) process. The URF process is shown to create amorphous API allowing for supersaturation, while the enteric polymer protects the ITZ from premature dissolution in the acidic environment and prevents particle growth in higher pH environments. Since drug release for modified release systems is dependent on the polymer release characteristics, the degree of miscibility may be expected to play a key role on dissolution. To define the level of ITZ miscibility with the enteric polymers, MDSC was performed on varying ITZ potency URF micronized powders. Once ITZ miscibility limits were established, the effects of ITZ potency, enteric polymer type, and % total solids in the feed on *in vitro* dissolution were assessed.

5.3 MATERIALS AND METHODS

5.3.1 Materials

Itraconazole (ITZ) was purchased from Hawkins Chemical (Minneapolis, MN, USA). The enteric polymers hydroxypropylmethyl cellulose phthalate NF (HP55) and Eudragit L100-55 (L100-55) were purchased from Shin Etsu Chemical (Tokyo, Japan)

and Röhm GmbH (Darmstadt, Germany), respectively. Histological grade 1,4-dioxane, 99%+, was purchased from Sigma-Aldrich (St. Louis, MO, USA). HPLC grade Acetonitrile (ACN) was purchased from EMD chemicals (Gibbstown, NJ, USA). Diethanolamine, hydrochloric acid and tribasic sodium phosphate was purchased from Fisher chemicals (Fair Lawn, NJ, USA). Polysorbate 20 was purchased from Spectrum Chemical (Gardena, CA, USA).

5.3.2 Preparation of URF Powders

ITZ and the pH-dependent polymer were dissolved in an appropriate amount of 1,4-dioxane and rapidly frozen using the URF apparatus. The API/polymer solutions were applied to a cryogenic solid substrate cooled to -60°C, collected, and lyophilized using a VirTis Advantage benchtop tray lyophilizer (The VirTis Company, Inc. Gardiner, NY, USA).

5.3.3 Modulated Differential Scanning Calorimetry (MDSC)

Samples in the range of 8-10 mg of processed and bulk powders were added to crimp sealed aluminum pans and measured on a TA Instruments model 2920 MDSC (New Castle, DE, USA). Samples were heated at a rate of 2°C/min from $30 - 200$°C at a modulating oscillatory frequency of 0.21°C/min. Samples were purged with nitrogen gas at 150 mL/min. Glass transition temperatures were measured at the midpoint of the step transition. The MDSC was calibrated using an indium standard.

5.3.4 True Density measurements

True density was measured using the true density of the pure amorphous ITZ and enteric polymer was determined using helium pycnometry (Micrometrics AccuPyc 1330 pycnometer; Norcross, GA). URF processed pure components were immediately tested after removal from the lyophilizer to limit water adsorption and placed in a sample cup and purged twenty times at 19.85 psi followed by six analytical runs at 19.85 psi. The equilibration rate was 0.0050 psi/minute. Measurements were performed in triplicate.

5.3.5 Scanning Electron Microscopy (SEM)

The powder samples were sputter coated using a model K575 sputter coater (Emitech Products, Inc., Houston, TX, USA) with gold-palladium for 35 seconds and viewed using a Hitachi S-4500 field emission scanning electron microscope (Hitachi High-Technologies Corp., Tokyo, Japan). An accelerating voltage of 5 kV was used to view the images. All SEMs pictured were representative of the entire sample.

5.3.6 Sink Dissolution Testing

Dissolution testing was performed on the URF powder samples using a USP 25 Type II paddle apparatus model VK7000 (Varian Inc., Cary, NC, USA). An equivalent of 1 mg ITZ was pre-wetted with 0.075% Polysorbate 20 in de-ionized water and added to 900 mL of 0.1N HCl (pH 1.2) dissolution media.   The dissolution media was maintained at 37.0 ± 0.2°C and the paddle speed was maintained at 100 rpm throughout the testing period.

141

Samples (5 mL) were withdrawn at 15, 30, 45, 60, 90 and 120 minute time points, filtered using a 0.20μm Whatman nylon filter (Clifton, NJ, USA), diluted with HPLC grade ACN, and analyzed using a Shimadzu LC-10 liquid chromatograph (Shimadzu Corporation, Kyoto, Japan) equipped with an Alltech ODS-2 5 μm C_{18} column (Alltech Associates, Inc., Deerfield, IL, USA). A mobile phase of ACN:water:diethanolamine (70:30:0.05) at 1 mL/min eluted the ITZ peak at 5.5 min and absorbance was measured at wavelength $\lambda = 263$ nm.

5.3.7 Supersaturation Dissolution Testing

Dissolution testing was performed on the URF powder samples using a USP 25 dissolution apparatus model VK7000 (Varian Inc., Cary, NC, USA). Dissolution was conducted according to USP enteric test method A for delayed release dosage forms using 100 mL glass dissolution vessels and stirred with appropriate small paddles. An equivalent of 8.8 mg ITZ (20X ITZ equilibrium solubility) was pre-wetted with 5 mL 0.008% Polysorbate 20 in 0.1N HCl and added to 70 mL 0.1N HCl (75 mL total). The dissolution media was maintained at 37.0 ± 0.2°C and the paddle speed was maintained at 50 rpm throughout the testing period. After 2 hours, 0.2M tribasic sodium phosphate (Na_3PO_4) containing 0.28% sodium dodecyl sulfate was equilibrated to 37.0 ± 0.2°C and added to the dissolution vessels. Therefore, the final SDS concentration was 0.07% which was determined to give equal equilibrium solubilities of ITZ in both pH environments. For each time point, 3 mL of medium was withdrawn and filtered using a

0.20μm nylon filter, diluted with HPLC grade ACN, and analyzed according to the HPLC method outlined above.

5.3.8 X-Ray Diffraction (XRD)

The x-ray diffraction pattern of the SFL powders were analyzed using a model 1710 x-ray diffractometer (Philips Electronic Instruments, Inc., Mahwah, NJ, USA). Data were collected using primary monochromated radiation (CuKα1, λ = 1.54056 Å), a 2θ step size of 0.05 and a dwell time of 1.0 second per step.

5.3.9 BET Specific Surface Area Analysis

Specific surface area was measured using a Nova 2000 v.6.11 instrument (Quantachrome Instruments, Boynton Beach, FL, USA). Weighed powder was added to a 12 mm Quantachrome bulb sample cell and degassed for a minimum of three hours. The sample was then analyzed by the NOVA Enhanced Data Reduction Software v. 2.13 using the BET theory of surface area.

5.3.10 Statistical Analysis

One-way analysis of variance (ANOVA, α = 0.05) was used to determine statistically significant differences between results. Results with p-values<0.05 were considered statistically significant. Post- hoc analysis using Tukey's honestly significant difference (HSD) test was performed after analysis to determine individual differences

between compositions. Mean differences greater than the HSD were deemed statistically significant.

5.4 RESULTS

5.4.1 ITZ miscibility in URF Micronized Powders

MDSC was used to determine the level of ITZ which could be added to the mixture before reaching phase separation and partial miscibility. Fig. 5.1a shows the MDSC profiles for increasing levels of ITZ in HP-55 (every 10% up to 80% ITZ) prepared via the URF process from a feed solution of 2.0%. Pure amorphous ITZ manufactured by the URF process was also included as a reference. To investigate if the nucleation process during rapid freezing and particle formation can enhance the miscibility of ITZ and HP-55, MDSC was also performed on the ITZ:HP-55 URF powders from 0.2% total solids loading. Profiles for the 0.2% loading were identical to those presented in Fig. 5.1b, however, the data is not shown. For samples with ITZ lower than 60% ITZ, no melting endotherms were detected and only a single glass transition (T_g) was detected while the T_g decreased with increasing ITZ potency. Upon increasing the ITZ potency to 70%, a slight melting endotherm was detected, while increasing the ITZ potency to 80% caused a large melting endotherm for both feed concentrations. Interestingly, only one single T_g was detected at 70% ITZ and two T_g's were detected at 80% ITZ (2% only). The melting point for the 70% and 80% ITZ compositions were measured at 158.4°C and 162.7°C, respectively, which are lower than the melting point of micronized crystalline ITZ (166.8°C) which was measured separately (data not

shown). The slight melting point depression is thought to occur from the polymer HP-55, which is estimated to melt at 150°C. Figure 5.1b shows the MDSC profiles for the ITZ:L100-55 binary mixtures manufactured from the URF process. Increasing levels of ITZ in L100-55 (every 10%) were analyzed to determine if phase separation occurs. Just as in the previous figures, a melting endotherm was detected for ITZ potencies greater than or equal to 70%. In addition, only a single T_g was detected for all potencies and decreased with increasing levels of ITZ.

Compositions containing 70% ITZ or greater displayed a recrystallization exotherm when analyzing total heat flow MDSC profiles. Examples of these recrystallization exotherms can be seen in Fig. 5.2. Compositions containing 70% ITZ in HP-55 showed a slight melting endotherm, but did not produce the recrystallization exotherm associated with pure amorphous ITZ. The recrystallization endotherm is present when the potency is increased to 80%. For the ITZ:L100-55, a small recrystallization endotherm appears at 70% ITZ and increases as potency increases. Likewise, as the recrystallization endotherm increases, the melting endotherm increases as a result of the melting amorphous ITZ.

The Gordon-Taylor equation is used to predict the T_g's for binary mixtures (T_{g12}) of polymers and has also been applied to estimate the T_g for API (small molecule) and polymer mixtures. Briefly, the Gordon-Taylor equation is as follows:

$$T_{g12} = \frac{w_1 T_{g1} + K w_2 T_{g2}}{w_1 + K w_2} \tag{1}$$

where T_{g1} and T_{g2} are the glass transition temperatures of the pure amorphous components and K is a constant determined by the Simha-Boyer rule:

$$K \cong \frac{\rho_1 T_{g1}}{\rho_2 T_{g2}} \quad\quad\quad (2)$$

where ρ_1 and ρ_2 are the true densities of the pure amorphous components. The measured T_g's for the increasing potencies of ITZ were plotted against the estimated T_g's from the Gordon-Taylor equation for each of the ITZ:polymer binary mixtures as depicted in Fig. 5.3a and 5.3b. The predicted T_g's values were constructed by first measuring the T_g's and true density of the pure amorphous components using MDSC and helium pycnometry, respectively. The measured T_g's for amorphous ITZ, HP-55, and L100-55 are 59°C, 147°C, and 128°C, respectively. The true densities were measured at 1.37, 1.75, and 1.32 g/cm^3, respectively, and agree closely with literature values.[23] Fig. 5.3a plots the T_g's for the ITZ:HP-55 binary mixtures from both the 2.0% and 0.2% total solids feed solutions. Interestingly, all potencies revealed a very close correlation with the predicted T_g. At 80% ITZ, two T_g's exist for the 2.0% total solids loading (as stated above) and the measured values are 74.7°C and 60.5°C, the latter in good agreement with pure amorphous ITZ at 59°C. Measured T_g values for the powders produced from a 0.2% feed solution also closely agreed with the predicted values at all potencies. In Fig. 5.3b, the measured T_g's for the ITZ:L100-55 binary mixtures are shown. Again, measured T_g's for all potencies up to 90% ITZ were very close to T_g's predicted by the Gordon-Taylor equation.

5.4.2 *In Vitro* Analysis of Low and High Potency URF micronized Binary Mixtures

In order to determine the effect of ITZ potency on the *in vitro* performance of the powders, low (1:4 ITZ:polymer ratio) and high potency ITZ (4:1 ITZ:polymer ratio)

146

compositions were manufactured via the URF process. For compositions containing HP-55, two total solids feed solution concentrations (0.2% and 2.0%) were examined. Compositions containing L100-55 were manufactured from 0.2% total solids feed solutions due to solubility limitations of this polymer in the feed solvent. For convenience, the compositions will be referred to by the ITZ:polymer ratio (1:4 or 4:1), followed by the polymer type (HP55 or L100-55) and concluding with the % total solids in the feed (2% or 0.2%)

The crystallinities of URF processed powders were examined using XRD and the profiles are depicted in Fig. 5.4. From the diffraction profile, the characteristic ITZ peaks (most intense) used for determining crystallinity of the URF processed samples are located at 17.45 and 17.95 (doublet), 20.30, and 23.45 two theta degrees. XRD profiles for the all URF micronized powders lacked the diffraction peaks associated with crystalline ITZ implying the samples contained amorphous ITZ.

Scanning electron micrographs were taken to determine the surface morphology of each of the URF micronized compositions at 30,000x magnification (Fig. 5.5a-f). Both 4:1HP55(2%) and 1:4HP55(2%) (Fig. 5.a-b) are composed of a porous matrix while 4:1HP55(0.2%) and 1:4HP55(0.2%) (Fig. 5.c-f) are composed of aggregated nanoparticles. For compositions containing HP-55, dramatic differences in surface morphology were observed when comparing the solids loadings with 2% solids loadings forming a porous matrix while 0.2% loadings forming disrete nanoparticle domains. ITZ potency also had a dramatic effect on the surface morphologies of compositions containing HP-55. The morphology of 4:1HP55(2%) in Fig. 5.5a is a porous matrix composed of both macropores on the order of 800 nm and embedded micropores (> 50

147

nm) making the surface appear rough. 1:4HP55(2%) (Fig. 5.5b) is composed of pores ranging from 50-200 nm in diameter; however, the matrix surface appears smooth and flat. Likewise, 4:1HP55(0.2%) which contains a high level of ITZ (80%) appears different from 1:4HP55(0.2%) which contains low levels of ITZ (20%). 4:1HP55(0.2%) appears to display smooth thread-like structures over a majority of the particle surface, while spherical nanoparticles filled in the rest of the areas. A few of these nanoparticle regions can be seen on the left side and bottom region of the SEM. 1:4HP55(0.2%) revealed regions of clearly defined nanoparticles (~100 nm in diameter) but also displayed larger particles (> 600 nm) with smooth surfaces. Finally, both 4:1L100-55(0.2%) and 1:4L100-55(0.2%) which were composed of ITZ and L100-55 both displayed nanoparticles which appear to be > 100 nm in diameter. From these SEM it appears that the % total solids in the feed had a substantial effect on particle formation dictating whether nanoparticles or a porous matrix would result.

The specific surface areas of the URF micronized powders (Table 5.1) were very high and ranged from 19.12-122 m^2/g. 4:1HP55(2%) which was composed of a highly porous matrix with both macro- and micro-sized pores had a measured surface area of 54.2 m^2/g while its lower potency counterpart 1:4HP55(2%) had a measured surface area of 19.1 m^2/g. While this value was lower than those of all other compositions, it still represents a 4.5-fold increase in surface area over micronized ITZ. The compositions which displayed nanoparticles in the SEM also had high surface areas of greater than 57.3 m^2/g with 1:4L100-55(0.2%) having the highest measured surface area of 122 m^2/g. Interestingly, both compositions containing L100-55 had larger surface areas compared to the compositions containing HP-55 (4:1HP55(0.2%) and 1:4HP55(0.2%)).

Sink dissolution studies in 0.1N HCl were performed to investigate the effect of potency on drug release. All URF micronized powders were compared to crystalline micronized ITZ which was 65% dissolved after 2 hours. The dissolution profiles in Fig. 5.6a-c show that as potency increases, the rate and cumulative release increases, with 4:1HP55(2%) having the most ITZ (68.8%) released after two hours. In the first 30-45 minutes the slope is particularly large for the high potency samples. Here localized regions of pure amorphous ITZ could exist and be exposed to the dissolution medium creating a burst effect. After 45 minutes the ITZ release reaches an asymptote. Although all URF micronized powders lacked any crystalline ITZ according to XRD, the total amount of ITZ released was never higher statistically than for crystalline ITZ, despite the amorphous morphology and considerably higher surface areas. Low ITZ potency compositions released very little ITZ into solution ranging from 12.9 to 27.5% dissolved ITZ after two hours. The dissolution data were modeled using the simplified Higuchi model to describe diffusional drug release kinetics. Figure 5.7a and 5.7b show the Higuchi plots for the low potency and high potency compositions, respectively. Q_t is the amount of ITZ dissolved per unit area based on the surface area of the powders. In addition, the correlation coefficients (R^2), Higuchi dissolution constants (K_h), and the diffusion coefficients (D) for the low potency compositions are listed in Table 5.2.

Dissolution studies were also performed under supersaturated conditions (20-times the crystalline ITZ equilibrium solubility) to determine the maximum concentrations, and the cumulative supersaturation, which depends both upon dissolution of the powder and the ability of the enteric polymers to inhibit precipitation of ITZ. The dissolution studies were conducted according to the USP XXV enteric test method A, and

the results are given in Table 5.3. After two hours in acidic media, aliquots were removed and the ITZ concentrations were determined. Table 5.3 also lists the percentage of total ITZ added which dissolved within the first two hours. All values were lower than those which were calculated under sink conditions with 4:1HP55(2%) having the highest release (23.8%; 6.6-times) and 1:4L100-55(0.2%) having the lowest % release (5.3%; 1.4-times). Upon addition of the buffer an increase in supersaturation was observed for all compositions as the enteric polymer dissolved and released the amorphous ITZ within the polymer. It was also observed that the degree of supersaturation increase was strongly dependent on the level of polymer in the composition. After the buffer was added, the enteric polymer immediately dissolved leading to the maximum extent of supersaturation (C/Ceq_{max}) for all URF compositions. Low potency ITZ compositions had the highest C/Ceq_{max} 15 minutes after the buffer was added with 1:4HP55(2%) having the highest measured C/Ceq_{max} value of 19.7X. For high potency ITZ compositions, the supersaturation increased after addition of the buffer, with 4:1HP55(2%) having the highest measured C/Ceq_{max} value at 10.7-times equilibrium solubility. However, the supersaturation levels were not as high as those of the low potency compositions.

The supersaturation profiles also indicate that the compositions which achieved a high C/Ceq_{max} were also subject to greater subsequent losses in supersaturation, regardless of the stabilizing polymer. In addition, for compositions with a smaller C/Ceq_{max}, smaller amounts of subsequent precipitation were observed. To place the results in further perspective, the cumulative extent of supersaturation (AUC) was calculated as the area-under-the-supersaturation-curve, as listed in Table 5.3. High

150

potency URF compositions had significantly higher ($p<0.05$) AUCs ranging from 33.1 to 38.0 mg*min/mL compared to the low potency URF compositions which had AUCs ranging from 17.6 to 22.9 mg*min/mL. Further analysis revealed that there were also significant differences in AUC versus the total solids loading for both high and low potencies. The 1:4L100-55(0.2%) sample has a significantly higher ($p<0.05$) AUC than 1:4HP55(0.2%) indicating that L100-55 is able to maintain supersaturation of ITZ longer than HP-55.

5.5 DISCUSSION

5.5.1 ITZ Miscibility in pH Dependent Polymer Binary Mixtures

For immediate release systems, Craig et al. described the mechanism for API release from solid dispersions containing water-soluble polymers [24]. They concluded that when the API was dispersed within the polymer on a molecular level (i.e. solid solution) API release was carrier mediated. However, if localized regions of pure API existed (i.e. solid dispersion) and were sufficiently large, dissolution of the API may also be API mediated. In addition, Six et al. investigated the effect of ITZ miscibility within water-soluble polymers to determine the effect of miscibility on dissolution rate.[25, 26] The results suggest that for immediate release systems, ITZ miscibility within a polymer carrier is not critical to achieve rapid dissolution rates. In fact, both the carrier, in this case, Eudragit® E100, and the physical state of the ITZ contribute to the dissolution rate. In other words, the E100 dissolves immediately into solution (within the media) while aiding wetting of any immiscible ITZ domains. Additionally, having the ITZ in an

amorphous state contributes to the dissolution process by largely removing the crystalline heat of fusion and raising the solubility. However, a carrier is needed along with the amorphous API in order to achieve delayed release, sustained release or extended release. Consequently, if an API is only partially miscible in an enteric solid dispersion, localized regions of API near the particle surface could dissolve rendering the delayed release preference unfavorable. Therefore, it is critical to determine the effect of API miscibility on these modified release systems.

MDSC analysis for the URF micronized powders revealed T_g's which correlated very closely to predicted Tg's estimated from the Gordon-Taylor equation for all ITZ potency levels, solids loadings, and polymer type. Thus the API domains are too small to produce a separate T_g peak. The API may be molecularly dispersed with the polymer or the domains may be smaller than about 50 nm. Rapid freezing technologies can produce powders with nanoparticle domains as small as 20 nm in diameter.[27] The rapid freezing arrested particle growth and inhibited phase separation.

A variety of methods exist to assess miscibility limits within polymers [21, 28, 29]. For nanoparticles produced using the aerosol flow reactor method, Eerikäinen et al. determined the level at which a crystalline melting endotherm was observed for the APIs ketoprofen and naproxen. The endotherm indicates that the API solubility limit within the polymer was exceeded.[21, 30] Because this process involved heat to evaporate solvent, evaporation rates could be sufficiently slow to allow crystallization of the API during phase separation. Since no melting endotherms were observed for samples with 60% ITZ potency or lower, ITZ miscibility within both HP-55 and L100-55 is at least 60%. The experimental miscibility limit of ITZ in L100-55 was unexpected since ITZ

miscibility levels with a structurally similar polymethacrylate polymer, Eudragit$^®$ E100, was measured at 13%.[25] In addition, Six et al. investigated the miscibility of ITZ with the hydrophilic polymer Eudragit$^®$ E100 and found that "cold crystallization", a recrystallization exotherm at about 133°C was indicative of regions of pure amorphous ITZ. Investigation of total heat flow profiles for the URF powders greater than 60% ITZ revealed recrystallization exotherms indicating cold crystallization into pure itraconazole for compositions 80% ITZ and greater.   Therefore it is determined that for URF micronized powders containing ITZ and either HP-55 or L100-55, the partial miscibility of the ITZ occurs between 60-80%, more likely occurring between 70-80% ITZ.

Six et al. investigated phase separation as a function of T_g by comparing the measured T_g of the solid dispersion to that of the predicted Gordon-Taylor equation. Deviations from the predicted value indicate possible partial miscibility. Also, multiple T_g's indicate phase separation or partial miscibility is occurring. For instance, the composition 4:1HP55(2%) showed a slight transition at 60.3°C (T_g near pure ITZ) and a larger transition at 74.7°C providing further evidence of partial miscibility at 80% ITZ potency.

5.5.2 Modeling kinetics of compositions under sink and supersaturated conditions

In acidic media, the enteric polymer is insoluble and ITZ release can only occur via diffusion through the polymer, assuming the system is completely miscible and no cracks or pores within the polymer exist. Therefore, the dissolution release kinetics were modeled using the simplified Higuchi model which describes drug release as a diffusion process based on Fick's law resulting in $t^{1/2}$ dependence.[31] It was assumed that the

system was planar and the matrix was homogeneous, since ITZ was completely miscible with the polymer at low concentrations. The release is described by [32]:

$$Q_t = \sqrt{Dt(2A - C_s)C_s}$$ (3)

where Q_t is the amount of ITZ released in time t per unit area, D is the diffusion coefficient, A is the total amount of drug present in the matrix per unit volume, and C_s is the solubility of the drug in the matrix substance. Eq. 3 can be expressed as the simplified Higuchi equation:

$$Q_t = K_h t^{1/2}$$ (4)

where K_h is the Higuchi diffusion-related parameter. The linear fit of the data suggested that the mechanism of diffusion through the polymer matrix is consistent with the data. Other kinetic models such as zero-order release and first order release gave poor fits of the data. Only the Higuchi square root model for diffusion through the matrix offered acceptable correlation coefficients ($R^2 > 0.99$) for ITZ release under acidic conditions. Eerikäinen et al. was able to accurately predict diffusional drug release of ketoprofen from an enteric solid dispersion using the Higuchi square root model. Total ketoprofen release was estimated based on calculating the diffusion penetration depth in a 100 nm particle and the concentration of ketoprofen from within the nanoparticle.[21]

The plots based on the Higuchi square root model in Fig. 5.7b reveal much less accurate fits for the high potency compositions ($R^2 < 0.94$) indicating a release mechanism other than diffusion through the matrix occurs during the initial phase of dissolution. Based on the MDSC data it is predicted that the ITZ within the high potency compositions existed in a partially miscible state having domains rich in ITZ, and also a

significant amount of ITZ at the miscibility limit dissolved within the polymer. The MDSC data confirmed the possibility of ITZ rich regions by revealing recrystallization exotherms. Amorphous ITZ rich domains could readily dissolve within the acidic media because of their lower heat of solution and higher apparent solubility resulting in higher drug release rates during the initial phase of dissolution. The dissolution of the ITZ rich domains could also create pores and channels for additional dissolution of ITZ rich domains within the core of the particle leading to higher percentages of ITZ dissolved. This possibility is supported by the dissolution profiles since they showed faster release rates in the first 45 minutes compared to the final hour and 15 minutes. After dissolution of the ITZ rich domains, diffusion of ITZ from the polymer could continue to cause drug release, but at a slower rate as observed.

5.6 CONCLUSION

Particles composed of ITZ and enteric polymer were manufactured using the ultra rapid freezing process to determine the importance of composition parameters such as ITZ:polymer ratio, enteric polymer type, and particle structure on modified drug release systems. MDSC data revealed the ITZ solubility/miscibility limit within the enteric polymers HP-55 and L100-55 and were between 60-70% ITZ. Completely miscible low potency (20% ITZ) and partially miscible high potency (80% ITZ) high surface area powders, prepared using the URF process, were found to be amorphous. Compositions from 2% solids loading appeared to be a highly porous matrix structure while 0.2% solids loading created nanostructured domains. For dissolution studies conducted at sink conditions in acid (i.e. non-eroding polymer condition), the matrix diffusion of ITZ in

completely miscible low potency powders showed Higuchi square root kinetics, while partially miscible high potency powders exhibited additional diffusional mechanisms. Supersaturation dissolution studies, following USP guidelines for enteric release, were highly complimentary to the sink dissolution studies. All low potency compositions produced very high C/Ceq_{max} ranging from 15-times to 19-times the equilibrium value, but the high saturation driving force produced rapid precipitation. Relative to these compositions, the lower C/Ceq_{max} levels for all high potency compositions produced less precipitation, as shown in the greater cumulative supersaturation over time. The behavior of the dissolution, under both sink and supersaturated conditions for these enteric solid dispersions is strongly influenced by the ITZ:polymer ratio, and to a lesser extent, the degree of polymer -API miscibility.

5.7 ACKNOWLEDGEMENTS

5.8 REFERENCES

[1]   Peeters, J., P. Neeskens, J.P. Tollenaere, P.V. Remoortere, and M.E. Brewster, Characterization of the Interaction of 2-Hydroxypropyl-bcyclodextrin with Itraconazole at pH 2, 4, and 7. J. Pharm. Sci., **2002**, *91*(6): p. 1414-1422.

[2]   Mayersohn, M., *Principles of Drug Absorption*, in *Modern Pharmaceutics*, G.S. Banker and C.T. Rhodes, Editors. **2002**, Marcel Dekker, Inc.: New York, NY. p. 23-66.

[3]   Sherwood, L., *Human Physiology: From Cells to Systems*. Fifth ed. **2004**, Belmont, CA: Thomson Learning

[4]   Yoshihashi, Y., H. Kitano, E. Yonemochi, and K. Terada, Quantitative correlation between initial dissolution rate and heat of fusion of drug substance. Int. J. Pharm., **2000**, *204*(1-2): p. 1-6.

[5]   Hancock, B.C. and M. Parks, What is the true solubility advantage for amorphous pharmaceuticals? Pharm. Res., **2000**, *17*(4): p. 397-404.

[6]   Yamashita, K., T. Nakate, K. Okimoto, A. Ohike, Y. Tokunaga, R. Ibuki, K. Higaki, and T. Kimura, Establishment of new preparation method for solid dispersion formulation of tacrolimus. Int. J. Pharm., **2003**, *267*(1-2): p. 79-91.

[7]   Sato, T., A. Okada, K. Sekiguchi, and Y. Tsuda, Difference in Physico-Pharmaceutical Properties between Crystalline and Noncrystalline 9,3"-Diacetylmidecamycin. Chem. Pharm. Bull., **1981**, *29*(9): p. 2675-2682.

[8]   Raghavan, S.L., B. Kiepfer, A.F. Davis, S.G. Kazarian, and J. Hadgraft, Membrane transport of hydrocortisone acetate from supersaturated solutions; the role of polymers. Int. J. Pharm., **2001**, *221*(1-2): p. 95-105.

[9]   Raghavan, S.L., A. Trividic, A.F. Davis, and J. Hadgraft, Crystallization of hydrocortisone acetate: influence of polymers. Int. J. Pharm., **2001**, *212*(2): p. 213-221.

[10]   Sung, M.H., J.S. Kim, W.S. Kim, and I. Hirasawa, Modification of crystal growth mechanism of yttrium oxalate in metastable solution. J. Cryst. Growth, **2002**, *235*(1-4): p. 529-540.

[11]   Mackellar, A.J., G. Buckton, J.M. Newton, and C.A. Orr, The Controlled Crystallization of a Model Powder .2. Investigation into the Mechanism of Action of Poloxamers in Changing Crystal Properties. Int. J. Pharm., **1994**, *112*(1): p. 79-85.

[12]   Suzuki, H. and H. Sunada, Influence of water-soluble polymers on the dissolution of nifedipine solid dispersions with combined carriers. Chem. Pharm. Bull., **1998**, *46*(3): p. 482-487.

[13]   Hasegawa, A., H. Nakagawa, and I. Sugimoto, Solid Dispersion Obtained from Nifedipine and Enteric Coating Agent .1. Dissolution Behavior. Yakugaku Zasshi-J. Pharm. Soc. Jpn., **1984**, *104*(5): p. 485-489.

[14]   Hasegawa, A., M. Taguchi, R. Suzuki, T. Miyata, H. Nakagawa, and I. Sugimoto, Supersaturation Mechanism of Drugs from Solid Dispersions with Enteric Coating Agents. Chem. Pharm. Bull., **1988**, *36*(12): p. 4941-4950.

[15]   Varshosaz, J., R.A. Kennedy, and E.M. Gipps, Use of enteric polymers for production of microspheres by extrusion-spheronization. **1997**, *72*(3): p. 145-152.

[16]   Nakamichi, K., T. Nakano, H. Yasuura, S. Izumi, and Y. Kawashima, The role of the kneading paddle and the effects of screw revolution speed and water content on the preparation of solid dispersions using a twin-screw extruder. Int. J. Pharm., **2002**, *241*(2): p. 203-211.

[17]   Sertsou, G., J. Butler, J. Hempenstall, and T. Rades, Physical stability and

enthalpy relaxation of drug-hydroxypropyl methylcellulose phthalate solvent

change co-precipitates. J. Pharm. Pharmacol., **2003**, *55*(1): p. 35-41.

[18]   Kohri, N., Y. Yamayoshi, H. Xin, K. Iseki, N. Sato, S. Todo, and K. Miyazaki,

Improving the oral bioavailability of albendazole in rabbits by the solid dispersion

technique. J. Pharm. Pharmacol., **1999**, *51*(2): p. 159-164.

[19]   Kondo, N., T. Iwao, K. Hirai, M. Fukuda, K. Yamanouchi, K. Yokoyama, M.

Miyaji, Y. Ishihara, K. Kon, Y. Ogawa, and T. Mayumi, Improved Oral

Absorption of Enteric Coprecipitates of a Poorly Soluble Drug. J. Pharm. Sci.,

1994, *83*(4): p. 566-570.

[20]   Takeuchi, H., T. Handa, and Y. Kawashima, Spherical Solid Dispersion

Containing Amorphous Tolbutamide Embedded in Enteric Coating Polymers or

Colloidal Silica Prepared by Spray-Drying Technique. Chem. Pharm. Bull., **1987**,

35(9): p. 3800-3806.

[21]   Eerikainen, H., L. Peltonen, J. Raula, J. Hirvonen, and E.I. Kauppinen,

Nanoparticles containing ketoprofen and acrylic polymers prepared by an aerosol

flow reactor method. AAPS PharmSciTech, **2004**, *5*(4).

[22]   Kai, T., Y. Akiyama, S. Nomura, and M. Sato, Oral absorption improvement of

poorly soluble drug using solid dispersion technique. Chem. Pharm. Bull., **1996**,

44(3): p. 568-571.

[23]   Rowe, R.C., P.J. Sheskey, and P.J. Weller, eds. *Handbook of pharmaceutical

excipients*. 4th ed. **2003**, Pharmaceutical Press: London.

[24]   Craig, D.Q.M., The mechanisms of drug release from solid dispersions in water-soluble polymers. Int. J. Pharm., **2002**, *231*(2): p. 131-144.

[25]   Six, K., C. Leuner, J. Dressman, G. Verreck, J. Peeters, N. Blaton, P. Augustijns, R. Kinget, and G. Van den Mooter, Thermal properties of hot-stage extrudates of itraconazole and eudragit E100 - Phase separation and polymorphism. J. Therm. Anal., **2002**, *68*(2): p. 591-601.

[26]   Six, K., G. Verreck, J. Peeters, M. Brewster, and G. Van den Mooter, Increased physical stability and improved dissolution properties of itraconazole, a class II drug, by solid dispersions that combine fast- and slow-dissolving polymers. J. Pharm. Sci., **2004**, *93*(1): p. 124-131.

[27]   Rogers, T.L., K.A. Overhoff, P. Shah, P. Santiago, M.J. Yacaman, K.P. Johnston, and R.O. Williams, Micronized powders of a poorly water soluble drug produced by a spray-freezing into liquid-emulsion process. Eur. J. Pharm. Biopharm., **2003**, *55*(2): p. 161-172.

[28]   Six, K., J. Murphy, I. Weuts, D.Q.M. Craig, G. Verreck, J. Peeters, M. Brewster, and G. Van den Mooter, Identification of phase separation in solid dispersions of itraconazole and Eudragit (R) E100 using microthermal analysis. Pharm. Res., **2003**, *20*(1): p. 135-138.

[29]   Van den Mooter, G., M. Wuyts, N. Blaton, R. Busson, P. Grobet, P. Augustijns, and R. Kinget, Physical stabilisation of amorphous ketoconazole in solid dispersions with polyvinylpyrrolidone K25. Eur. J. Pharm. Sci., **2001**, *12*(3): p. 261-269.

[30]   Eerikainen, H., E.I. Kauppinen, and J. Kansikas, Polymeric drug nanoparticles prepared by an aerosol flow reactor method. Pharm. Res., **2004**, *21*(1): p. 136-143.

[31]   Costa, P., J. Manuel, and S. Lobo, Modeling and comparison of dissolution profiles. Eur. J. Pharm. Sci., **2001**, *13*(2): p. 123-133.

[32]   Higuchi, T., Mechanism of Sustained-Action Medication. J. Pharm. Sci., **1963**, *52*(12): p. 1145-1149.

Tables

Table 2.1: Summary of compositions and feed systems used to manufacture SFL

processed powders

Composition	API (A)	Exipient(s) (E)	A:E ratio (A:E1:E2:E3)	Feed System	API Potency	% Total Solids (w/w)
SFL A	ITZ	S80:P407:PEG	1:1:2:1	Emulsion (33:67 DCM:H2O)	20%	4.0%
SFL B	ITZ	P407:T80	1:0.75:0.75	Organic co-solvent (0.5% DCM in ACN)	40%	0.9%
SFL C	ITZ	T20:PVPK15	10:1:2	Organic co-solvent (0.5% DCM in ACN)	77%	0.7%

Table 2.2: Mean particle size, specific surface area, and contact angle measurements for

SFL processed compositions compared to micronized crystalline ITZ

Composition	$D_{(0.5)}$ (μm)	Span Index	BET Surface Area (m^2/g)	Contact Angle (°)
SFL A Feed Emulsion	0.76[*]	1.39	---	---
SFL A Powder	0.94	3.54	20.25	7.5 ± 0.5
SFL B Powder	5.82	2.92	15.58	25.5 ± 2.5
SFL C Powder	6.21	2.64	18.76	46.5 ± 3.5
Micronized crystalline ITZ	4.22	2.16	4.22	57.9 ± 2.4

[*] Indicates average droplet size of feed emulsion

Table 2.3: Pharmacokinetic parameters for Sporanox® and SFL A powder

Composition	C_{max} (μg/ml) (±S.E.)	T_{max} (hrs)	K_d (hrs^{-1})	$T_{1/2}$ (hrs)	AUC (μg*h/ml)
Sporanox® oral solution	1.59(0.03)	1.0	0.36	1.94	5.42
SFL A	1.28(0.35)	2.0	0.51	1.36	4.56

Table 3.1: Surface area and contact angles of the URF compositions investigated

Composition	Surface Area (m²/g)	Contact Angle (°)
URF 1:2 DAN:PVPK15 (in ACN)	25.93	30.5 ± 0.5
URF 1:2 DAN:PVPK15 (in T-BUT)	29.33	32.5 ± 0.5
Phys. Mix. 1:2 DAN:PVPK15	0.69	$39.5 \pm 4.5^{*,\dagger}$
Bulk DAN	0.52	$64.0 \pm 3.0^{*,\dagger}$

Using Tukey's HSD test, HSD = $q\sqrt{\dfrac{s^2}{N}} = 3.85$

[*]=statistically different from URF 1:2 DAN:PVPK15 in ACN
[†]=statistically different from URF 1:2 DAN:PVPK15 in T-BUT

Table 3.2: Thermal and physical properties used to calculate t_{freeze} for ACN and T-BUT.

Property	ACN[a]	T-BUT[b]
k (W/m-K)	0.218	0.121
ρ (g/cm^3)	0.811	0.774
C_p (J/g-K)	2.182	3.057
α (cm^2/s)	0.0012	0.00051
Estimated t_{freeze} (ms)	61	483
Measured t_{equil} (ms)	70	1000

[a] For ACN, the average values calculated at T_{freeze}=229K and T_i =298K.
[b] For T-BUT, the average values calculated at T_{freeze}=298K and T_i=313K

Table 4.1: Tacrolimus compositions produced using the URF process

URF Composition	Active (A)	Excipient (E1:E2)	Ratio (A:E1:E2)	% Total Solids
URF-SDS	TAC	SDS	1:1	1.00
URF-PVA:P407	TAC	PVA:P407	1:0.5:0.5	1.00
URF-P407	TAC	P407	1:1	1.00

Table 4.2: Specific surface area of URF micronized compositions

Composition	Surface Area (m^2/g)
URF-SDS	54.96
URF-PVA:P407	43.68
URF-P407	7.73
Bulk TAC	0.53

Table 4.3: Maximum supersaturation and AUC ratios of URF micronized compositions compared to PRO for *in vitro* dissolution in acid media and dissolution according to USPXXV enteric test method A involving 0.1N HCl for two hours followed by addition of buffer to increase pH to 6.8

Composition	C/Ceq_{max} (Acid)	T_{max} (Acid) (min)	Area Ratio to Prograf[®] (Acid)	C/Ceq_{max} (enteric)	T_{max} (enteric) (min)	Area Ratio to Prograf[®] (enteric)
URF-SDS	20.9 ± 0.3	120	1.04	21.8 ± 2.7	135	1.18
URF-PVA:P407	14.5 ± 3.3	60	0.45	12.0 ± 0.8	60	0.34
URF-P407	22.8 ± 0.3	60	0.38	11.0 ± 1.2	60	0.32
Prograf[®]	17.0 ± 1.7	240	1.00	13.8 ± 0.6	120	1.00

Table 4.4: Pharmacokinetic parameters for URF micronized compositions and the commercially available tacrolimus product

Composition	C_{max} (ng/mL)	T_{max} (hr)	$T_{1/2}$ (hr)	K_{el} (hr^{-1})	AUC (0-24) (ng*hr/mL)	AUC (inf) (ng*hr/ml)	Avg. Relative Bioavailability (%F)
URF-SDS	65.2 ± 43.4	0.67 ± 0.4	7.5 ± 1.8	0.096 ± 0.0	223.6 ± 102.7	254.8 ± 113.3	77.1
URF-PVA:P407	67.9 ± 11.7	0.5 ± 0.0	7.5 ± 1.4	0.095 ± 0.0	319.8 ± 138.2	348.6 ± 141.4	105.6
URF-P407	138.5 ± 69.1	0.6 ± 0.2	6.9 ± 2.3	0.106 ± 0.0	450.6 ± 188.1	476.1 ± 187.1	144.2
Prograf®	51.5 ± 19.8	1.3 ± 0.4	7.7 ± 1.8	0.094 ± 0.0	298.8 ± 83.2	330.2 ± 84.9	-

AUC = area under the curve

Table 5.1: Specific surface area for URF micronized powders containing ITZ and an

enteric polymer, HP-55 or L100-55

Composition	Surface Area (m^2/g)
1:4HP55(2%)	19.1
1:4HP55(0.2%)	61.8
1:4L100-55(0.2%)	122
4:1HP55(2%)	54.2
4:1HP55(0.2%)	57.4
4:1L100-55(0.2%)	79.9
Bulk ITZ	4.22

Table 5.2: Diffusion modeling correlation and diffusion coefficients for dissolution of

       URF micronized powders

Composition	Higuchi Corr. Coeff. (R^2)	Higuchi Dissolution Constant (K_h)	Calculated Diffusion Coeff. (D_m) from Simplified Higuchi model (1×10^{-13} cm^2/min)
1:4HP55(2%)	0.982	0.118	1.88
1:4HP55(0.2%)	0.991	0.045	0.273
1:4L100-55(0.2%)	0.990	0.011	0.017
4:1HP55(2%)	0.939	-	-
4:1HP55(0.2%)	0.922	-	-
4:1L100-55(0.2%)	0.837	-	-

Corr. Coeff. = Correlation Coefficient

Table 5.3: Supersaturation data for URF micronized powders containing ITZ and enteric

polymer

Composition	% Dissolved After 2 Hours in Acidic Media[a]	C/Ceq$_{max}$	AUC$_{ss}$ (mg*min/mL)[b]
1:4HP55(2%)	14.62 ± 0.63	19.67	17.58 ± 1.31
1:4HP55(0.2%)	14.14 ± 1.63	17.45	22.41 ± 1.21
1:4L100-55(0.2%)	5.26 ± 0.62	15.20	22.93 ± 3.21
4:1HP55(2%)	23.85 ± 0.99	10.68	33.11 ± 2.02
4:1HP55(0.2%)	14.49 ± 1.09	8.44	37.97 ± 1.08
4:1L100-55(0.2%)	14.94 ± 1.14	9.27	35.45 ± 2.50

[a] - Percent of total ITZ dissolved in gastric medium after two hours under supersaturated conditions (based on weight added)
[b] – Area under curve at supersaturated conditions calculated via trapezoidal rule

Table A.1: Compositions of URF feed solutions

Active [A]	Excipient 1 [E1]	Excipient 2 [E2]	Ratio [A:E1:E2]	% Total Solids	Solvent(s)
DAN	P407	PVPK30	4:3:3	0.5, 2.00	T-BUT
DAN	P407	PVPK30	6:2:2	0.5, 2.00	T-BUT
DAN	P407	PVPK30	9:0.5:0.5	2.00	T-BUT

Table A.2: Surface area of the URF compositions investigated

Composition	URF (m^2/g)	Physical Mixture (m^2/g)
4:3:3 DAN:P407:PVPK30	23.69	1.24
6:2:2 DAN:P407:PVPK30	30.87	1.34
9:0.5:0.5 DAN:P407:PVPK30	27.59	1.53
Bulk DAN	-	0.52

Table A.3: Contact angle of the URF compositions investigated

Composition	Contact Angle Processed Powder (°)	Contact Angle Physical Mixture (°)
4:3:3 DAN:P407:PVPK30	24.0 ± 1.0	26 ± 1.0
6:2:2 DAN:P407:PVPK30	24.0 ± 1.0	26.5 ± 0.5
9:0.5:0.5 DAN:P407:PVPK30	27.0 ± 0.75	39.5 ± 2.5
Bulk DAN	-	64.0 ± 3.0

Table B.1: Analysis of extraction solvent in lyophilization/evaporation step using of

spiked sample at a concentration of 2.2 µg/ml in JP1 medium (n=3)

Reconstitution Solvent	Average Total TAC Recovered
Acetone	83.38% ± 0.85%
75/25 (v/v) ACN/water	89.20% ± 2.64%
50/50 EtOH/DCM	92.67% ± 3.26%
Chloroform	83.06% ± 5.35%

Table B.2: Analysis of extraction mixing method during lyophilization/evaporation step

using spiked sample at a concentration of 2.2 µg/ml in JP1 medium

extracted with EtOH/DCM (n=3)

Extraction mixing method	Average Total TAC Recovered
1 washing aliquot	79.94% ± 7.11%
3 washing aliquots	94.00% ± 1.08%
Vortex 1 min	97.18% ± 5.81%
Sonicate 5 min	98.04% ± 2.65%

Table B.3: Effect of SPE cartridge packing and amount of recovery of TAC spiked

       sample at 2.2 µg/ml (n=3)

SPE Cartridge	% Total Recovered in 1st mL	Average Total TAC Recovered
DSC-18 (100 mg, C18)	95.14%	98.14% ± 7.58%
JT-18 (100 mg, C18)	91.81%	95.28% ± 6.29%
JT-8 (500 mg, C8)	81.15%	93.38% ± 3.09%

Table B.4: Total recovery of high and low concentration spiked samples using DSC-18

SPE cartridge (n=3)

Spiked Concentration	Average Total TAC Recovered
2.2 µg/ml	100.66% ± 12.27%
1.1 µg/ml	114.40% ± 1.68%
0.22 µg/ml	71.18% ± 18.22%

Table C.1: Tacrolimus screen compositions manufactured for dissolution studies conducted at non-supersaturated conditions

Composition	Active	Polymer(s)	Drug/polymer Ratio	Potency (%)	% Total Solids	Solvent(s)	Aqueous Work Up
1	Tacrolimus	HPMC E5	1:1	50.00%	2.00%	ACN:water (60/40)	N
2	Tacrolimus	HPMC E5:SDS	1:0.5:0.5	50.00%	2.00%	ACN:water (60/40)	N
3	Tacrolimus	HPMC E5:SDS	1:0.8:0.2	50.00%	2.00%	ACN:water (60/40)	N
4	Tacrolimus	HPMC E5:Polox 407	1:05:0.5	50.00%	2.00%	ACN:water (60/40)	N
5	Tacrolimus	PVPK30:Polox 407	1:0.75:0.75	40.00%	2.00%	ACN:water (60/40)	N
6	Tacrolimus	Lactose:SDS	1:05:0.5	50.00%	1.50%	ACN:water (60/40)	N
7	Tacrolimus	Mannitol SDS	1:05:0.5	50.00%	1.50%	ACN:water (60/40)	N
12	Tacrolimus	PVA	1:1	50.00%	1.00%	ACN	Y; PVA
13	Tacrolimus	PVA:SDS	1:0.5:0.5	50.00%	1.00%	ACN	Y; PVA
14	Tacrolimus	PVA:Polox407	1:0.5:0.5	50.00%	1.00%	ACN	Y; PVA
15	Tacrolimus	NaCMC:Polox407	1:0.5:0.5	50.00%	1.00%	ACN	Y; NaCMC
16	Tacrolimus	HPMC E5:SDS	1:0.5:0.5	50.00%	1.00%	ACN	Y, HPMC E5
17	Tacrolimus	Docusate Na	1:1	50.00%	2.00%	Acetone	Y
18	Tacrolimus	Docusate Na:Polox 407	1:0.5:0.5	50.00%	2.00%	Acetone	Y; Polox 407
19	Tacrolimus	HPMC E5:Docusate Na	1:0.5:0.5	50.00%	2.00%	Acetone:water (50/50)	Y
20	Tacrolimus	HPMC E5:Docusate Na	1:0.5:0.5	50.00%	2.00%	Acetone:water (50/50)	Y;HPMCE5
21	Tacrolimus	NaCMC:Docusate Na	1:0.5:0.5	50.00%	2.00%	Acetone:water (50/50)	Y; NaCMC
22	Tacrolimus	NaCMC:SDS	1:0.5:0.5	50.00%	2.00%	ACN:water (60/40)	Y; NaCMC
23	Tacrolimus	NaCMC:PVPK30	1:0.5:0.5	50.00%	2.00%	ACN:water (60/40)	Y; NaCMC
24	Tacrolimus	PVA	1:1	50.00%	1.00%	ACN:water (40/60)	N
25	Tacrolimus	PVA:Polox 407	1:0.5:0.5	50.00%	1.00%	ACN:water (40/60)	N
26	Tacrolimus	PVPK30:Polox407	1:0.75:0.75	40.00%	2.00%	ACN:water (60/40)	N
27	Tacrolimus	PVPK30:PVA	1:0.5:0.25	57.14%	1.00%	ACN:water (40/60)	N
28	Tacrolimus	PVPK30:Polox407:PVA	1:0.25:0.25:0.25	57.14%	1.00%	ACN:water (40/60)	N
29	Tacrolimus	Lactose:SDS:PVA	1:0.25:0.25:0.5	50.00%	1.00%	ACN:water (40/60)	N
30	Tacrolimus	SDS:PVA	1:0.1:0.4	66.67%	1.00%	ACN:water (40/60)	N
31	Tacrolimus	Polox407:SDS	1:0.5:0.5	50.00%	2.00%	ACN:water (60/40)	N

Table C.2: Advantages and disadvantages of polymers/stabilizers considered for use in URF

micronized powders containing tacrolimus

Polymer/Stabilizer	Advantages	Disadvantages
HPMC E5 LV	• Proven supersaturation • High Tg • Hydrophilic polymer	• Slow dissolver, swelling • Patent protected
PVP K30	• Proven supersaturation • High Tg • Hydrophilic polymer, good wetting	• Hydroscopic (stability) • Patented in dependent claim
Poloxamer 407	• Excellent wetting agent/surfactant	• Low Tg
SDS	• Excellent wetting agent/surfactant • High Tm and Tg	• Dissolved too quickly for comparable formulation
Docusate Na	• Excellent wetting agent/surfactant • High Tm and Tg	• Dissolved too quickly for comparable formulation • Only soluble in acetone and water
PVA (MW 13-23,000)	• Good stabilizer, High Tg • Can slow down dissolution rate • No mention in patents	• Unknown supersaturation
Na CMC	• Good stabilizer, High Tg • Can slow down dissolution rate	• Soluble only in water (aqu-workup only) • Cellulose derivative (patent protected?)
Lactose, Mannitol	• Hydrophilic, rapid dissolution • Pore forming agent • High Tm	• Wets too well • Patented in dependent claim

Figures

Nanoparticles   Nanocapsules

Solid
Dispersion

Solid
Solution
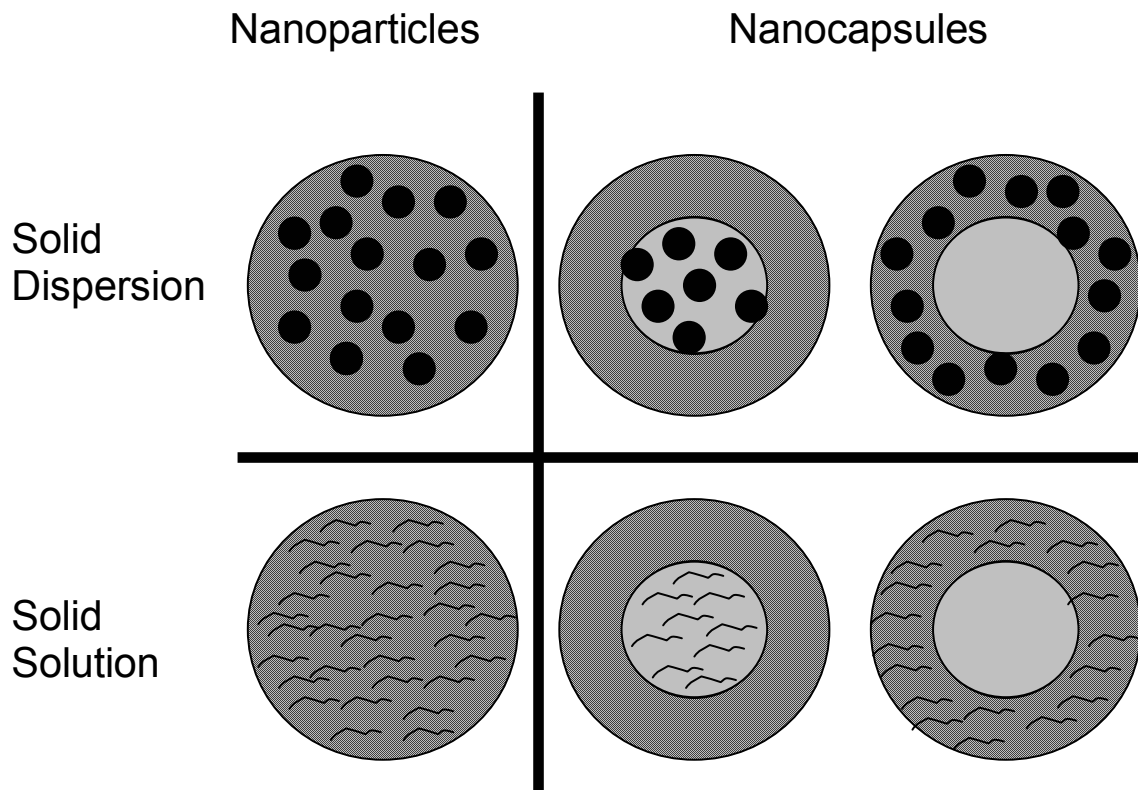
Figure 1.1: Nanoparticulate delivery systems for drugs within a core matrix

(nanoparticles) or encapsulated (nanocapsules)
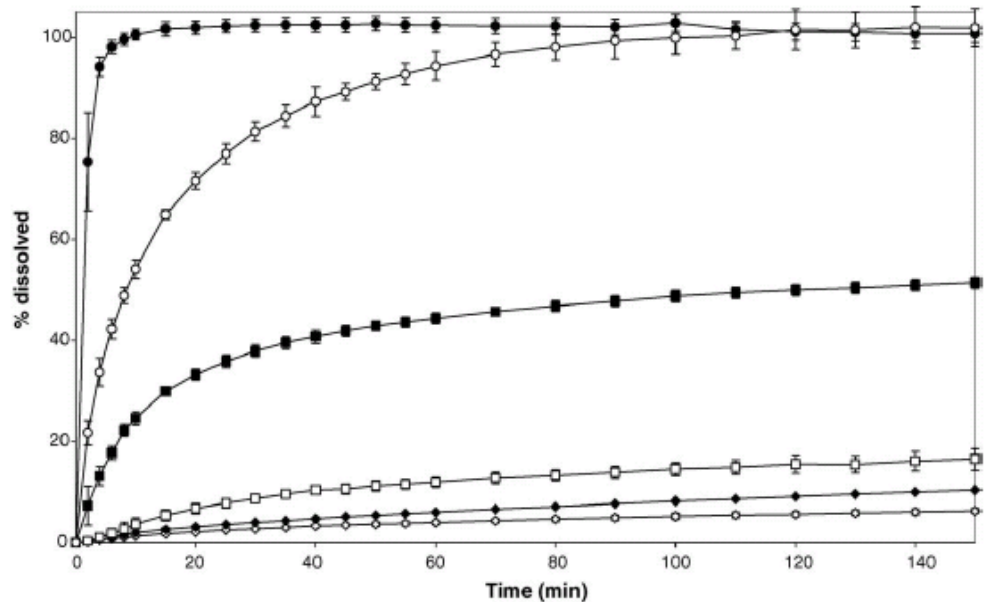
Figure 1.2: Dissolution profiles for: (◊) un-milled commercial NIF; (♦) NIF/HPMC, 10:1

(w/w) physical mixture (mortar); (□) spray-dried formulation A (no

milling); (■) spray-dried formulation A (Turrax® milling); (○) spray-dried

formulation A (HPH milling); (●) Spray-dried formulation B (HPH milling).

With permission from (Hecq et al., 2005)
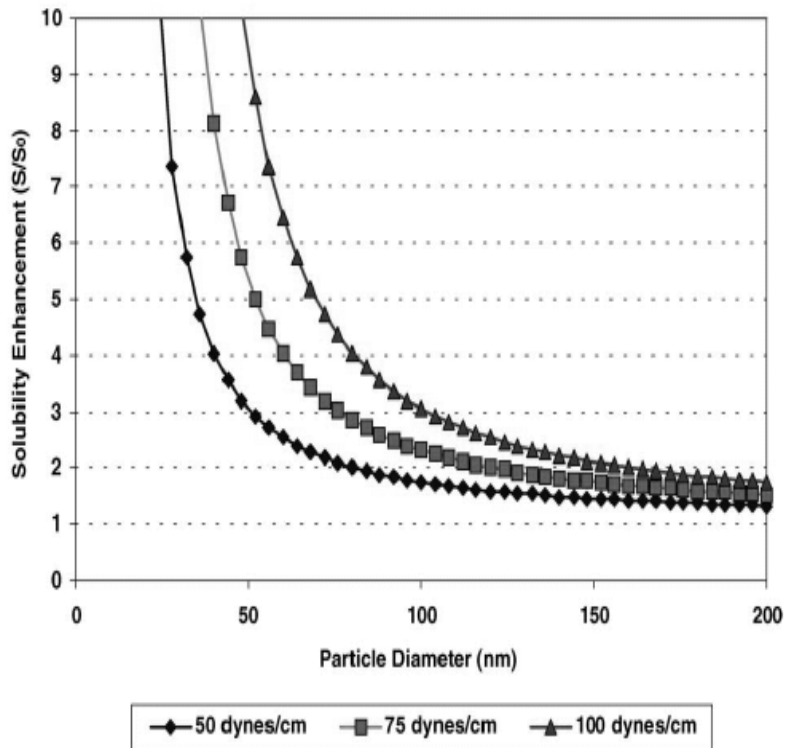
Figure 1.3: Effect of solid particle diameter on solubility for hypothetical examples (S: solubility at the surface of the particle; S_0: intrinsic solubility). With permission from (Kipp, 2004)
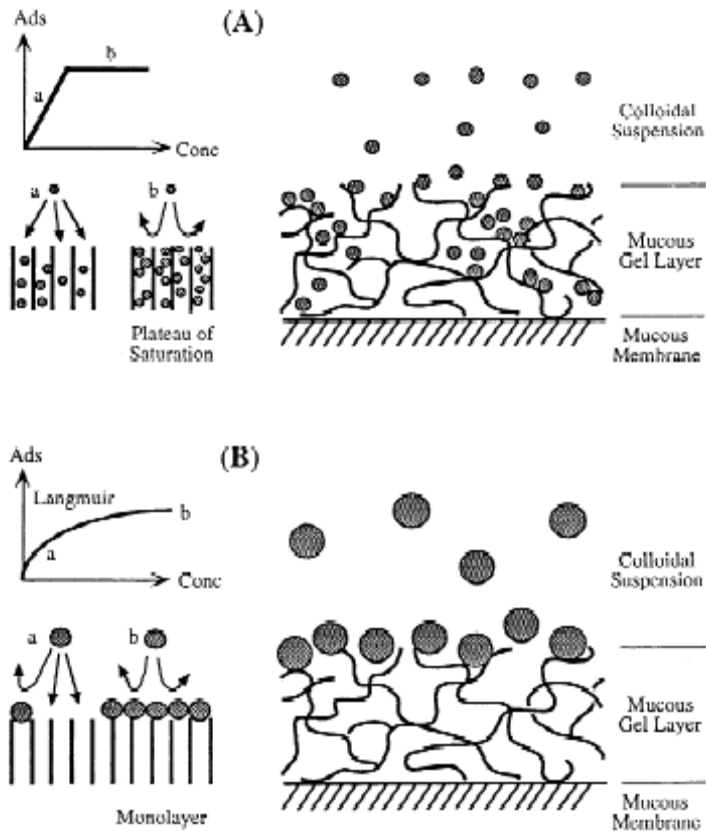
Figure 1.4: Differences between nanoparticle (A) and microparticle (B) adsorption

isotherms with corresponding adsorption models. With permission from

(Ponchel et al., 1997)
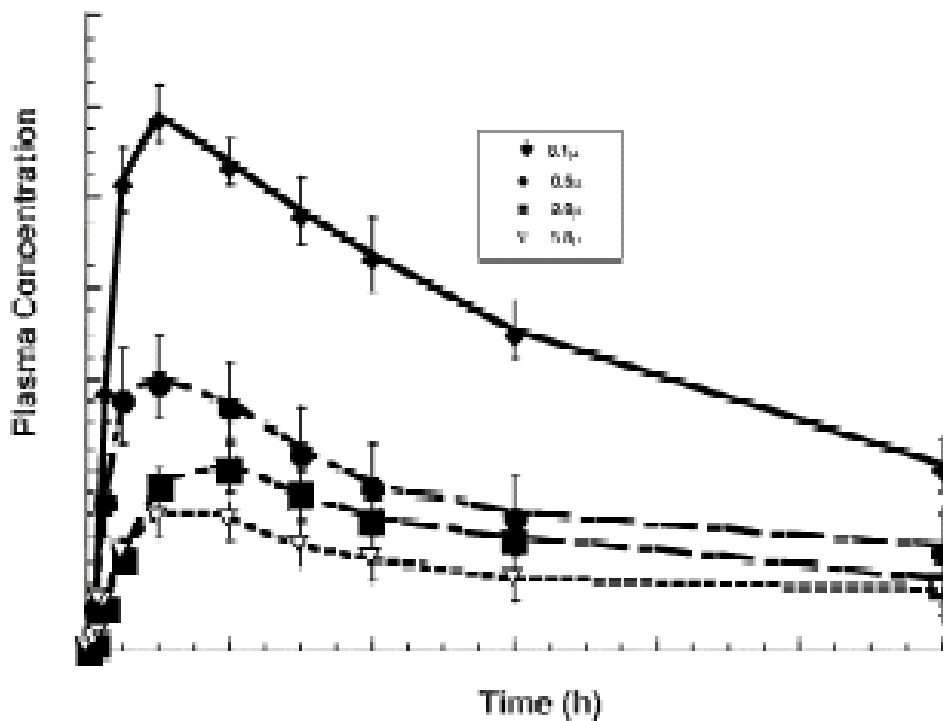
Figure 1.5: For poorly-water-soluble compounds, the particle size of the drug crystals
can affect bioavailabity. The graph shows the plasma concentration time
curve of a poorly-water-soluble discovery compound. The compound was
administered orally at an identical dose to fasted dogs as nanoparticles or as
cruder dispersions. The only variable was the mean particle size of each
dispersion: 100 nm (♦); 500 nm (●); 2 microns (■); and 5 microns (∇).
With permission from (Merisko-Liversidge et al., 2003)
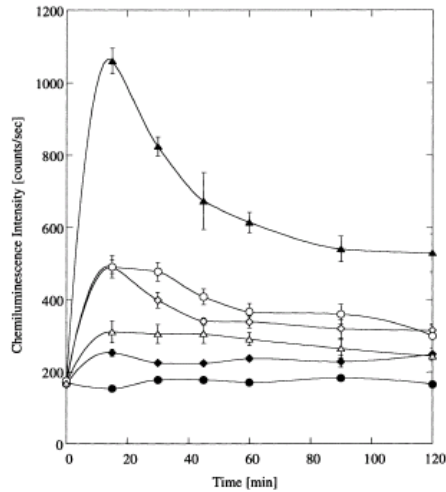
a.)
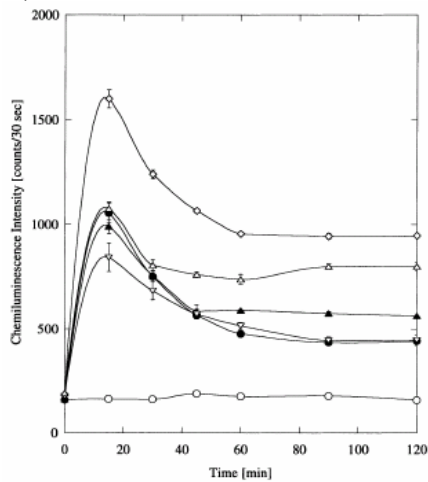
b.)

Figure 1.6: a) Effects of sizes of polystyrene microspheres on the superoxide release

from alveolar macrophages. Polystyrene microspheres with diameters of ♦,

0.2; ◊, 0.5; ▲, 1.0; ○, 6.0; Δ, 10.0 μm and ●, PBS⁻ (control) were added to

macrophages. b) Effects of functional groups existing on the polystyrene

microsphere surfaces on the superoxide release from alveolar macrophages.

Polystyrene microspheres having ◊, primary amine; ▽, sulfate; ▲, hydroxyl;

Δ, carboxyl groups on their surfaces; ●, unmodified polystyrene

microspheres, and ○, PBS⁻ (control) were added to macrophages. With

permission from (Makino et al., 2003)

188
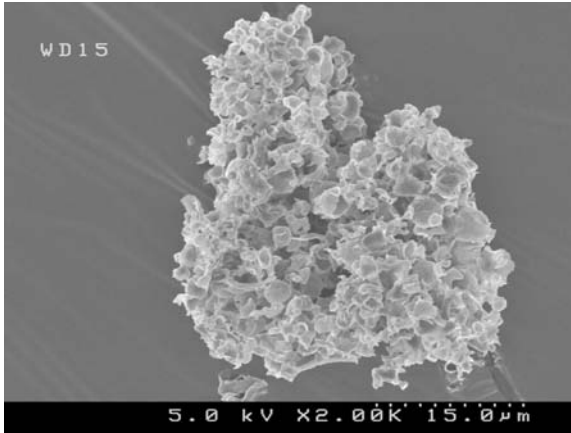
a.)
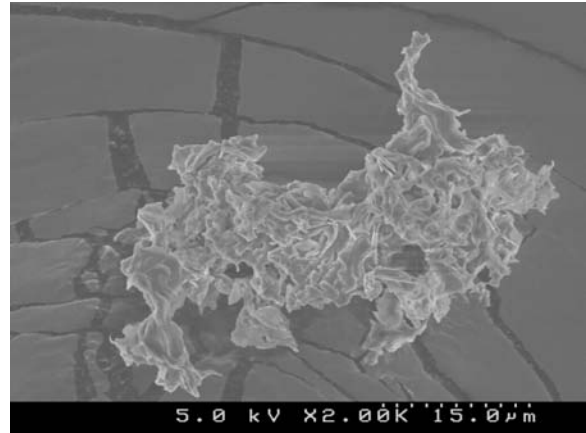
b.)
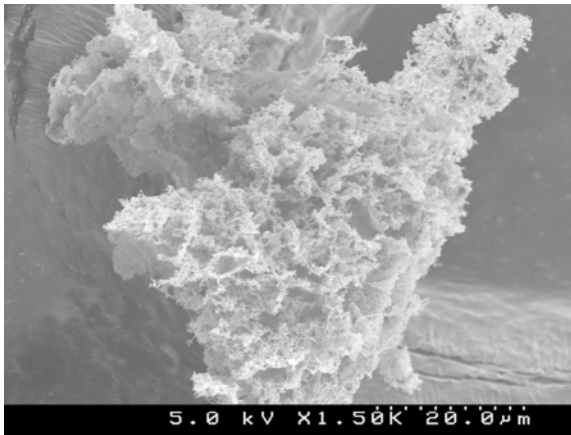
c.)
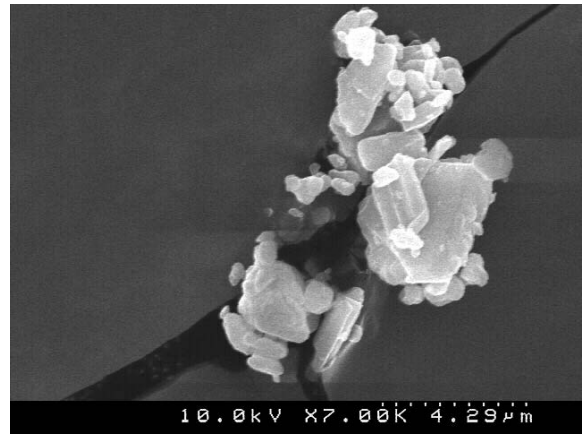
d.)

Figure 2.1: Electron micrograph of SFL A (a), SFL B (b), SFL C (c), micronized

crystalline ITZ
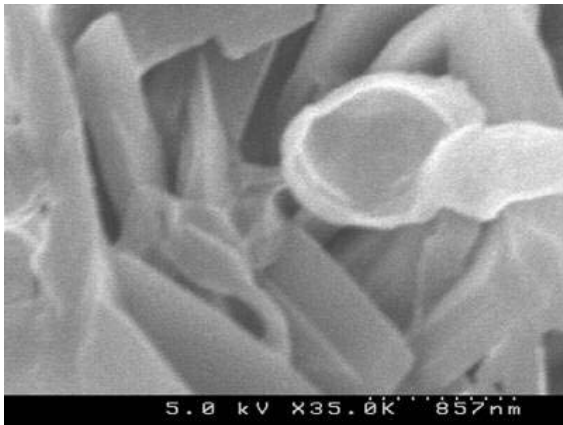
a.)
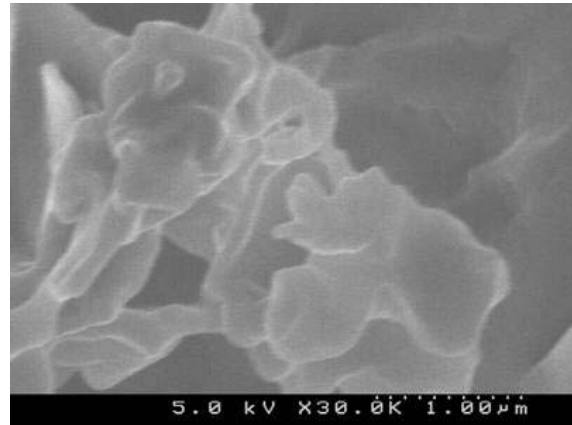
b.)
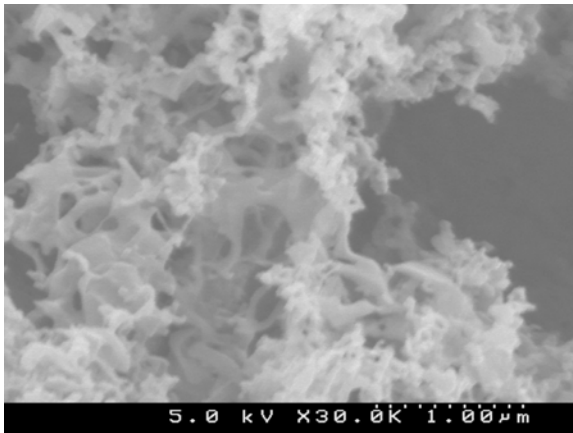
c.)

Figure 2.2: Electron micrograph of SFL A (a), SFL B (b), SFL C (c)
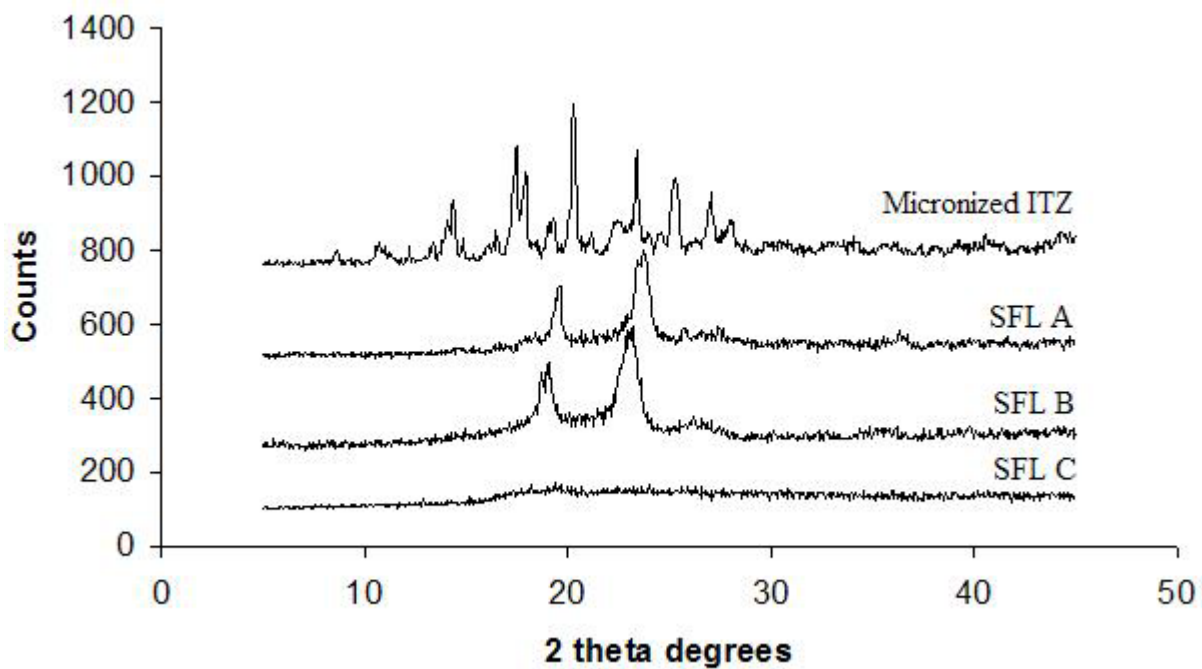
Figure 2.3: X-ray diffraction patterns of SFL processed powders compared to micronized
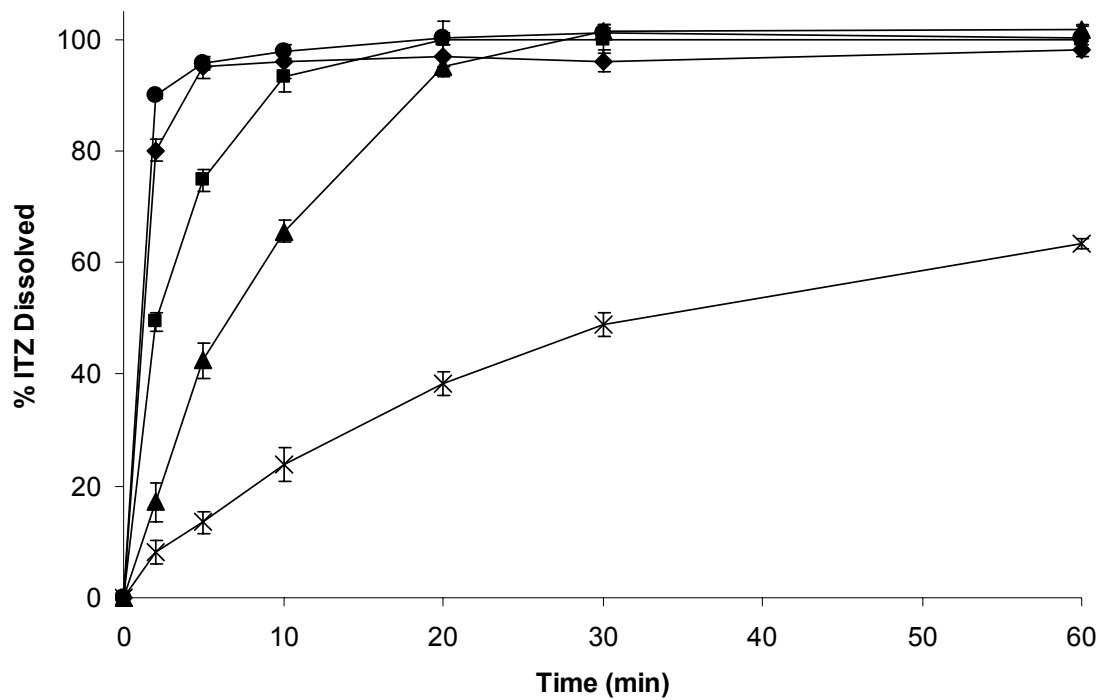
crystalline ITZ

Figure 2.4: Dissolution of amorphous itraconazole prepared using the SFL process:

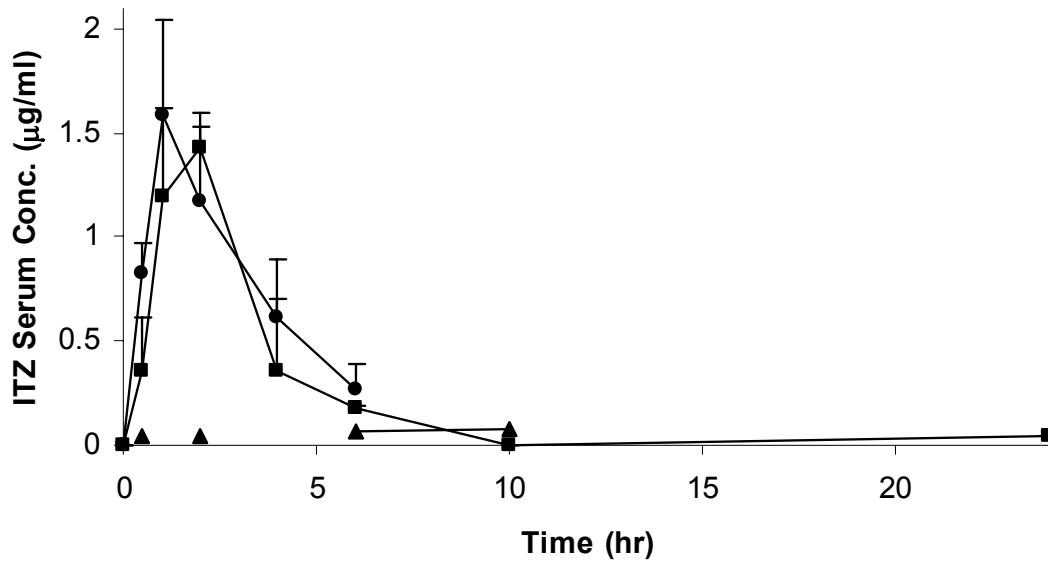Sporanox[®] oral solution (●), SFL A (♦), SFL B (■) SFL C (▲), micronized

crystalline ITZ (x)

Figure 2.5: Pharmacokinetic profiles of Sporanox[®] oral solution (●), SFL A (■), micronized crystalline ITZ wetted with 0.01% polysorbate 80 (▲)
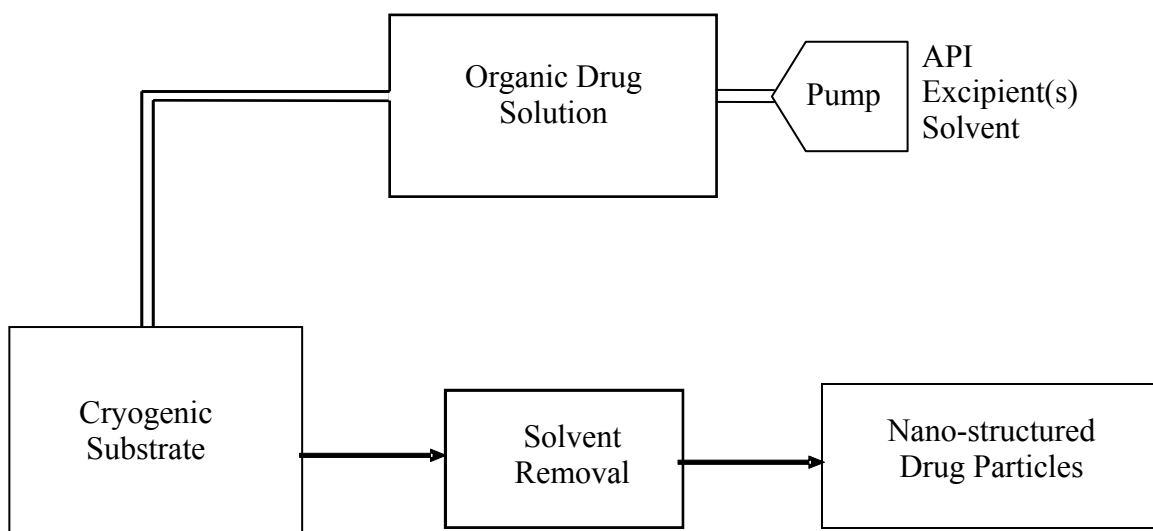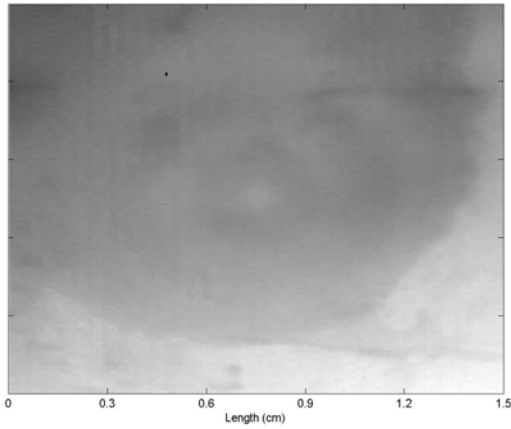
Figure 3.1: Schematic of URF process
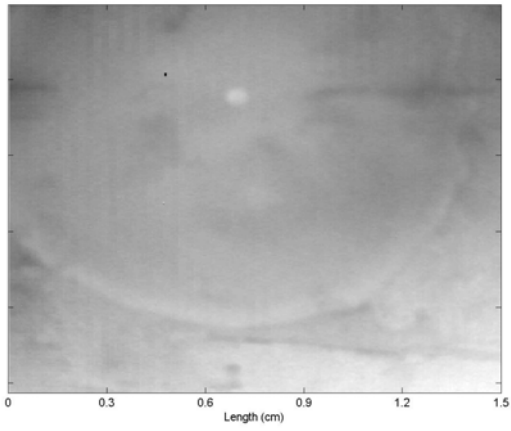
a.)
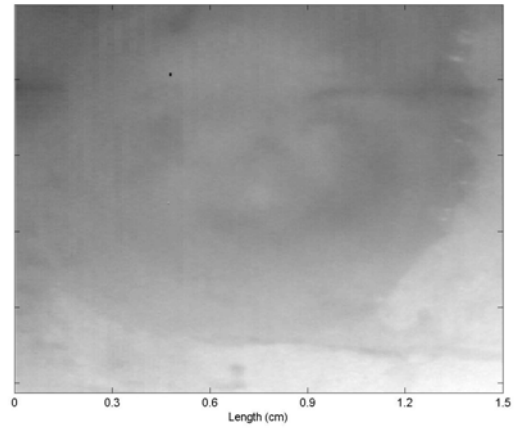
b.)

c.)

Figure 3.2: IR photographs of ACN droplet impinging and freezing on -60°C surface at

t=0 ms (a), t=20 ms (b), t=70 ms (c)
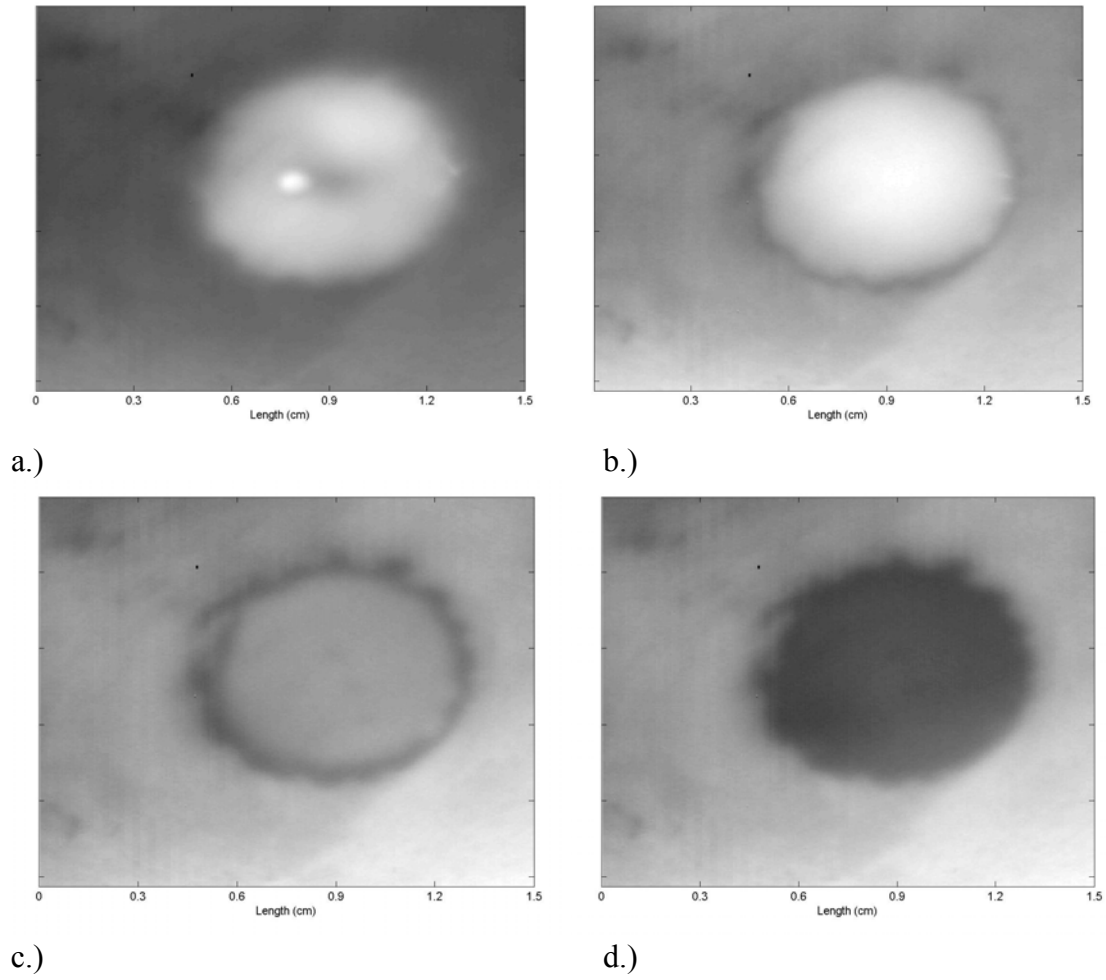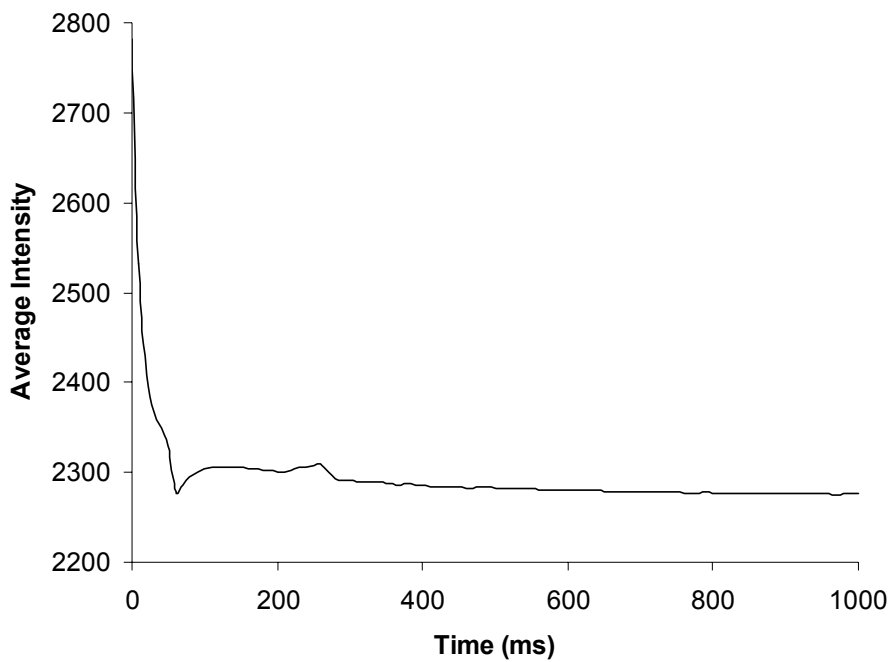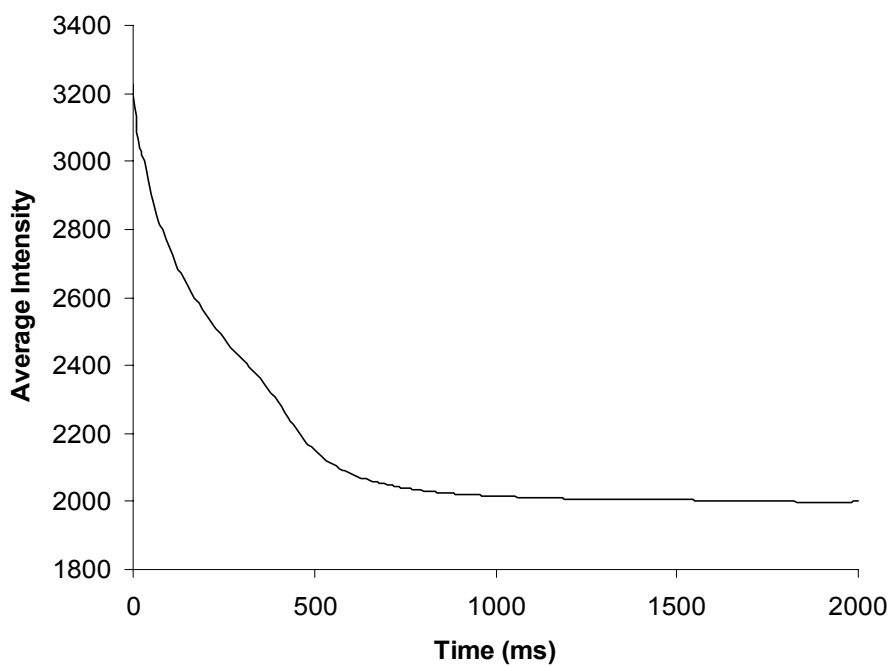
a.)

b.)

c.)

d.)

Figure 3.3: IR photographs of T-BUT droplet impinging and freezing on -60°C surface

at t=0 ms (a), t=150 ms (b), t=400 ms (c), t= 1000 ms (d)

a.)

b.)

Figure 3.4: IR droplet intensity vs. time for ACN (a) and T-BUT (b)

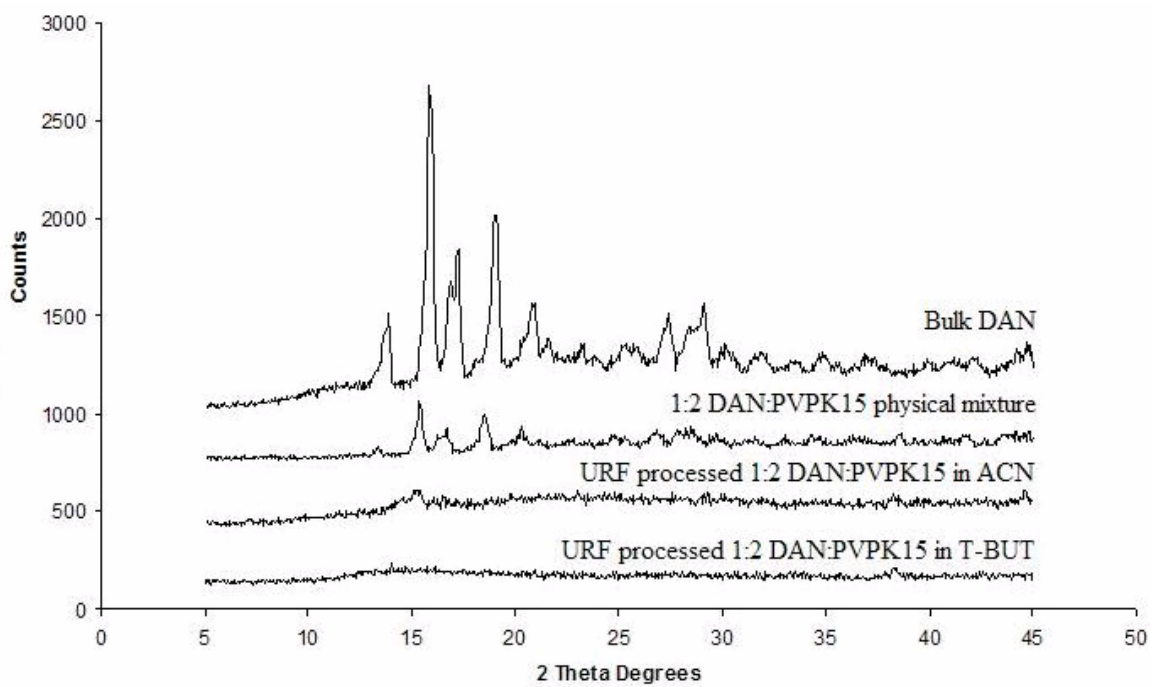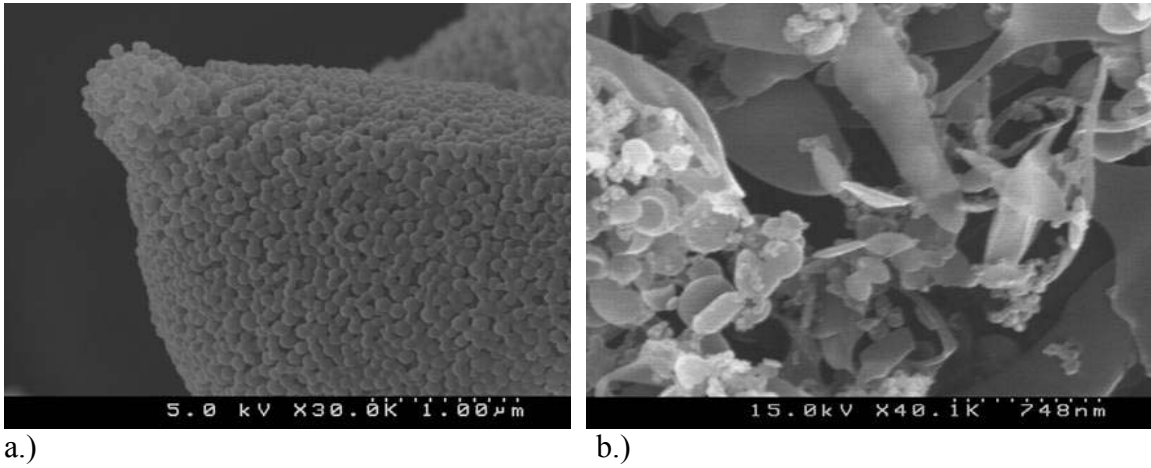Figure 3.5: X-ray diffraction patterns of URF processed DAN:PVP compositions

compared to bulk DAN

a.)   b.)

Figure 3.6: SEM micrographs of URF processed 1:2 DAN:PVPK15 in ACN (a), URF processed 1:2 DAN:PVPK15 in T-BUT (b)
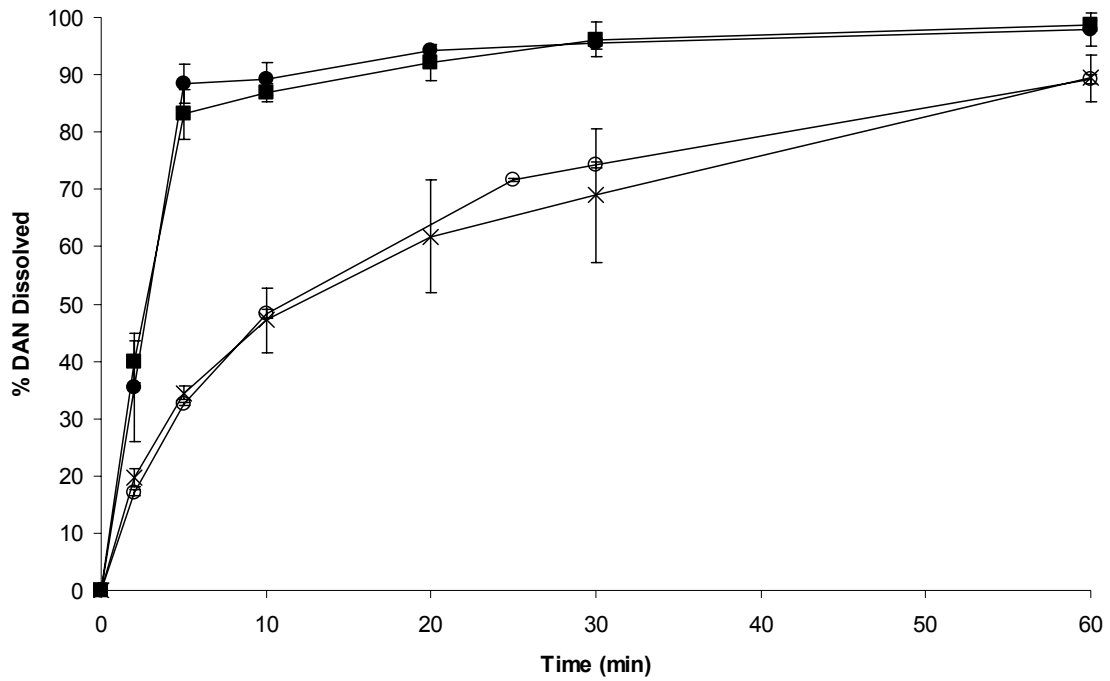
Figure 3.7: Dissolution profile for URF processed 1:2 DAN:PVPK15 in ACN (●), URF

processed 1:2 DAN:PVPK15 in T-BUT (■), 1:2 DAN:PVPK15 Physical

mixture (○), Bulk DAN (X)
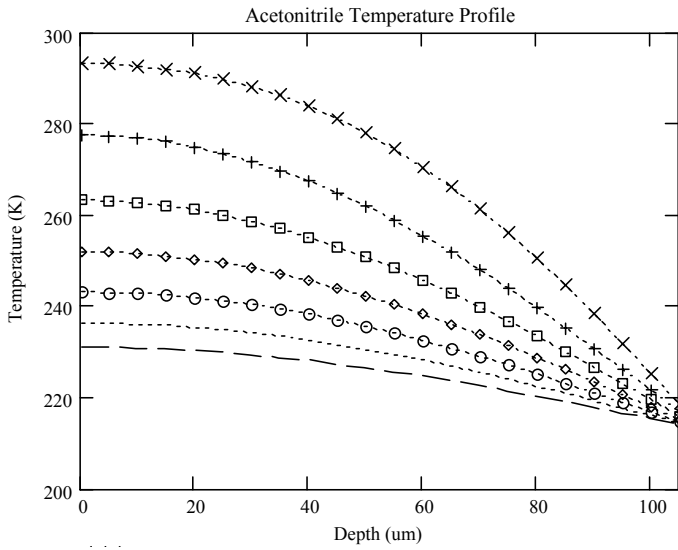
a.)
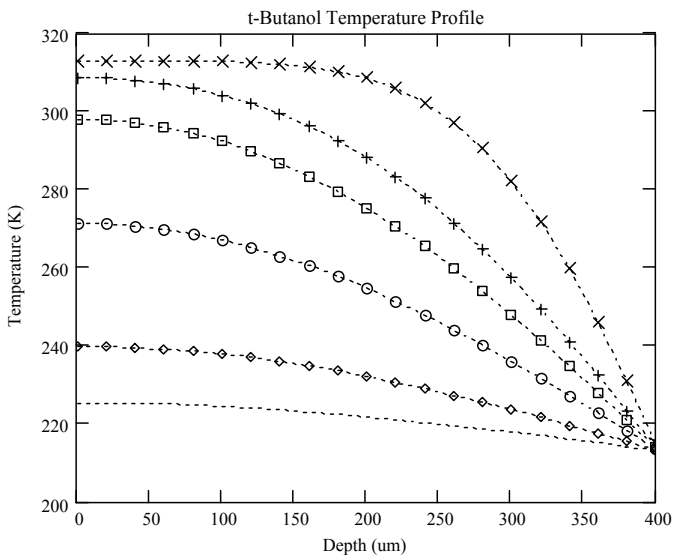
b.)

Figure 3.8: Theoretical temperature profile of ACN droplet (a) on a cryogenic surface at

10 ms (x), 20 ms (+), 30 ms (□), 40 ms (◊), 50 ms (○), 60 ms (···), 70 ms (–).

Theoretical temperature profile of T-BUT droplet (b) on a cryogenic surface

at 100 ms (x), 300 ms (+), 500 ms (□), 1000 ms (○), 2000 ms (◊), 3000 ms

(···)

201

a)

b)

c)

d)
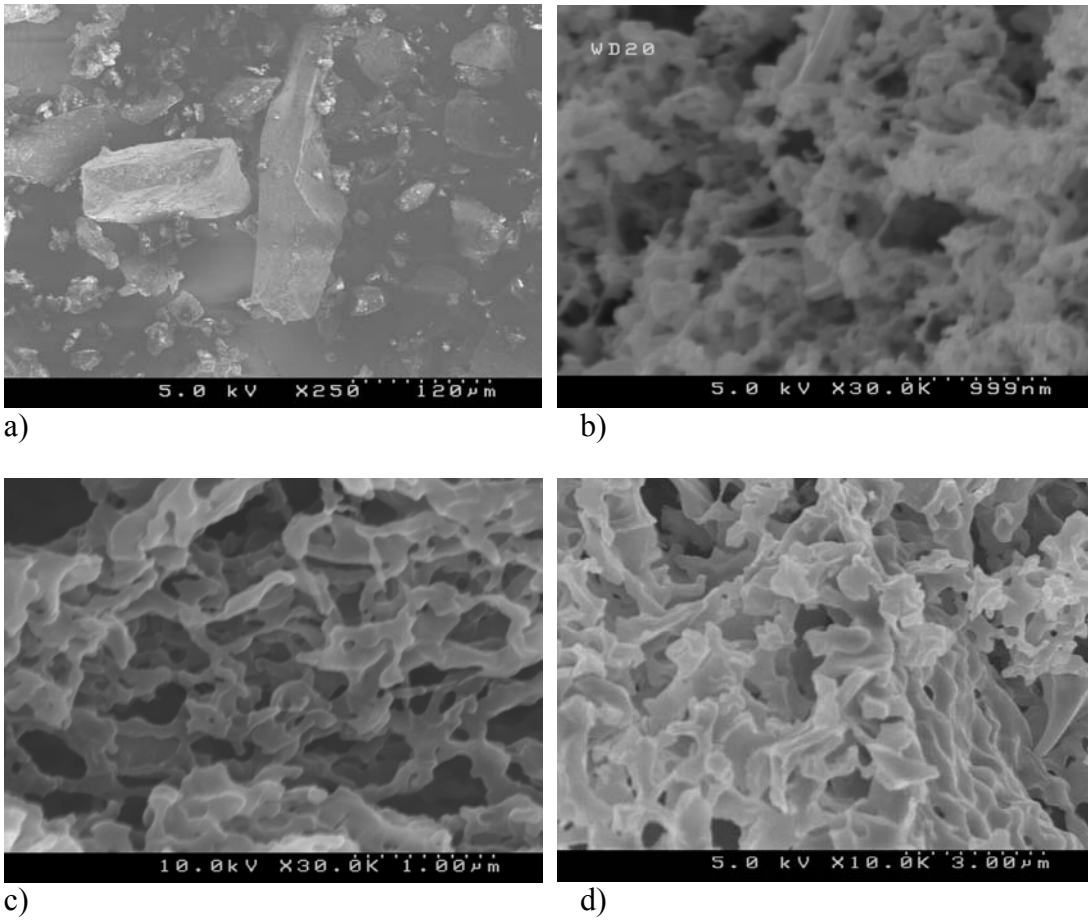
Figure 4.1: SEM micrographs of Bulk TAC (a), URF-SDS (b), URF-PVA:P407 (c), URF-P407 (d)
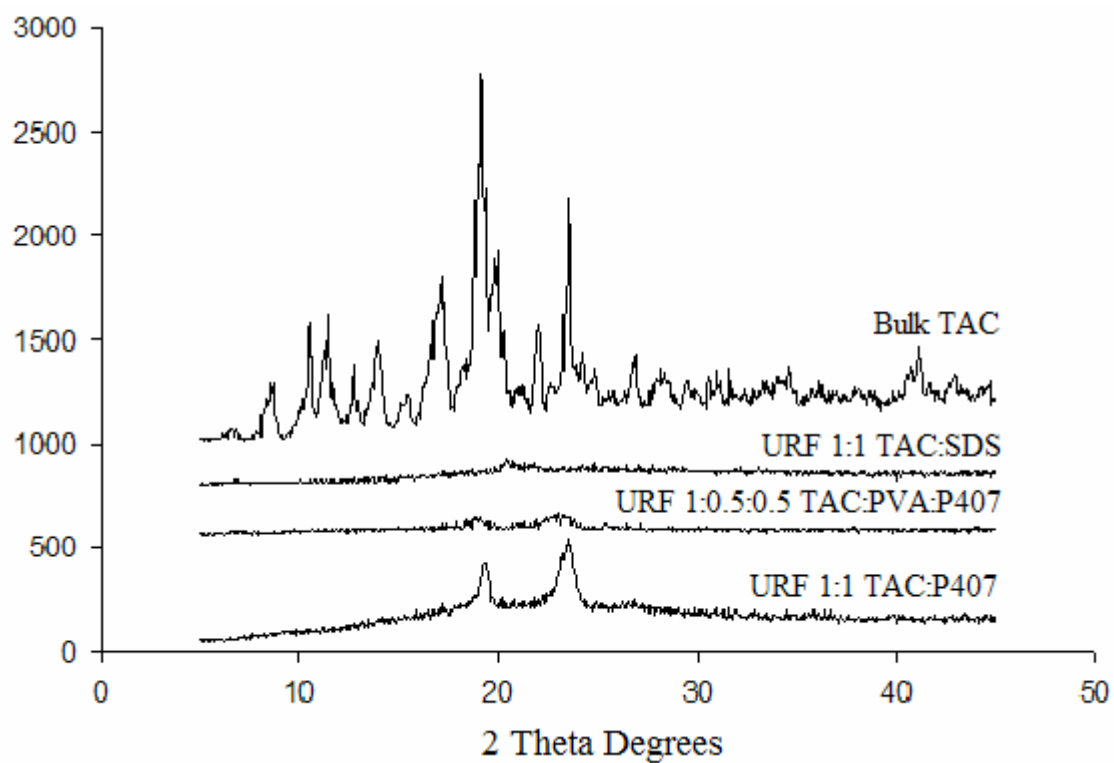
Figure 4.2: X-ray powder diffraction of amorphous TAC compositions prepared using the URF freezing process
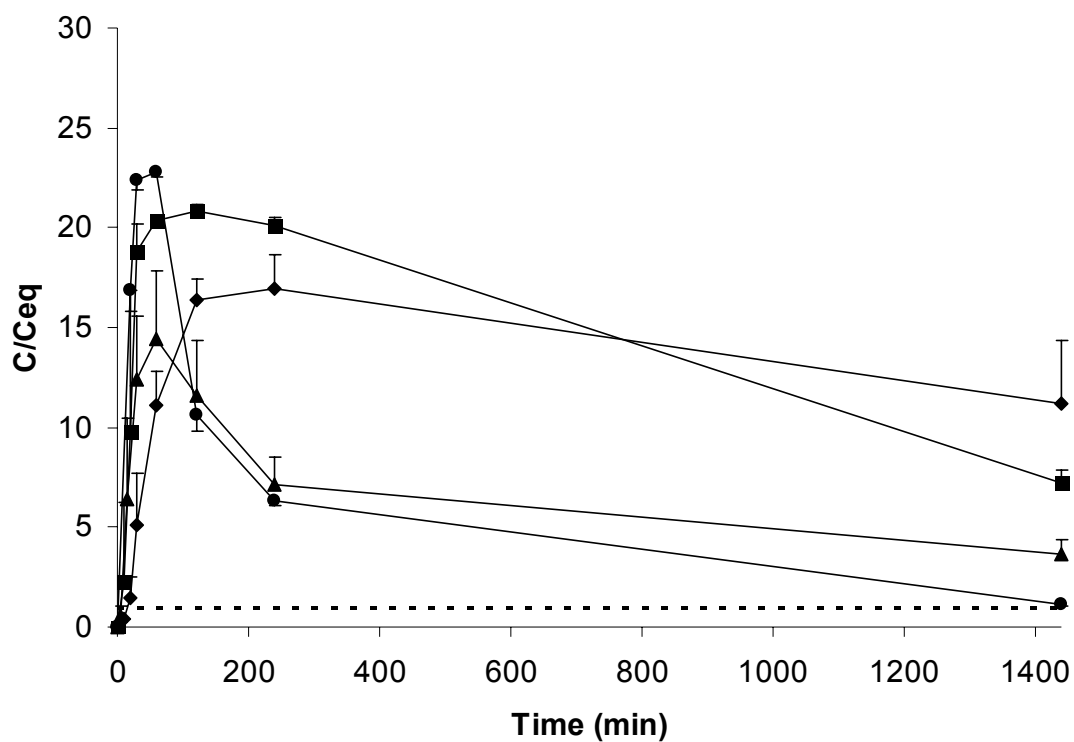
Figure 4.3: Supersaturated dissolution of tacrolimus in acidic dissolution medium: URF-SDS (■), URF-PVA:P407 (▲), URF-P407 (●), PRO capsule powder (♦), tacrolimus equilibrium solubility (---)
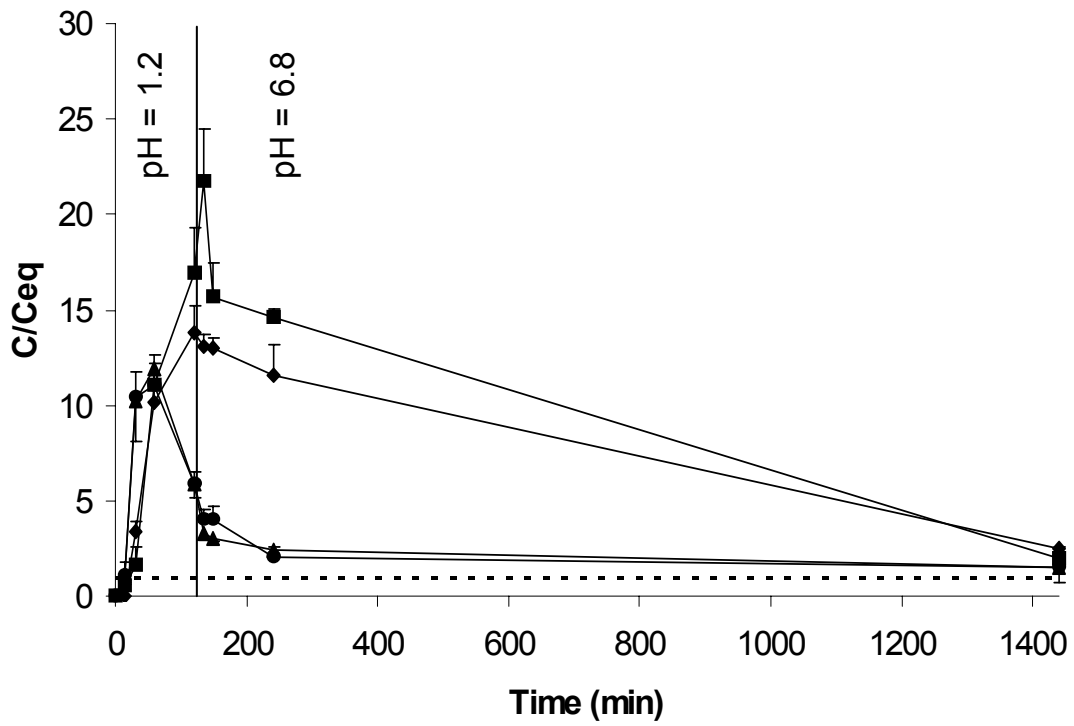
Figure 4.4: Supersaturated dissolution of tacrolimus under enteric conditions: URF-SDS (■), URF-PVA:P407 (▲), URF-P407 (●), PRO capsule powder (♦), tacrolimus equilibrium solubility (---)
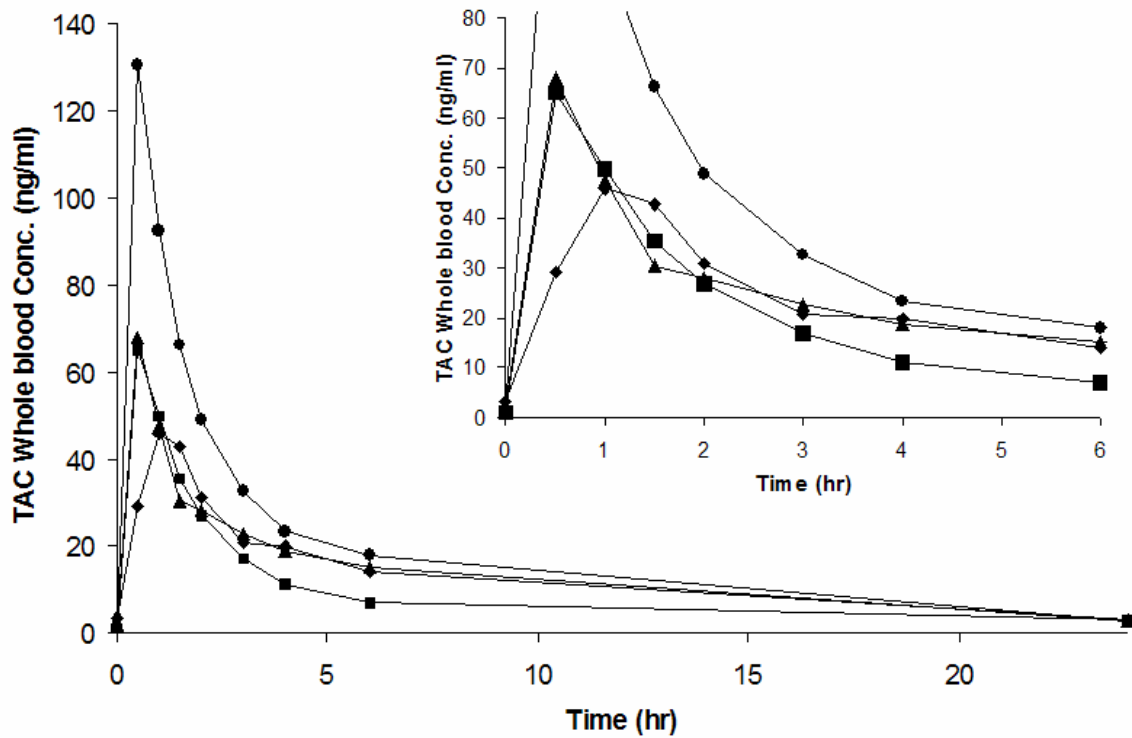
Figure 4.5: Mean whole blood absorption levels of TAC compositions produced using the URF process compared to the commercially available tacrolimus product. Powders were given an gelatin capsule containing 1.5 mg equivalent TAC (5 mg/kg) dosed via oral gavage to a rat model: URF-SDS (■), URF-PVA:P407 (▲), URF-P407 (●), PRO (♦)
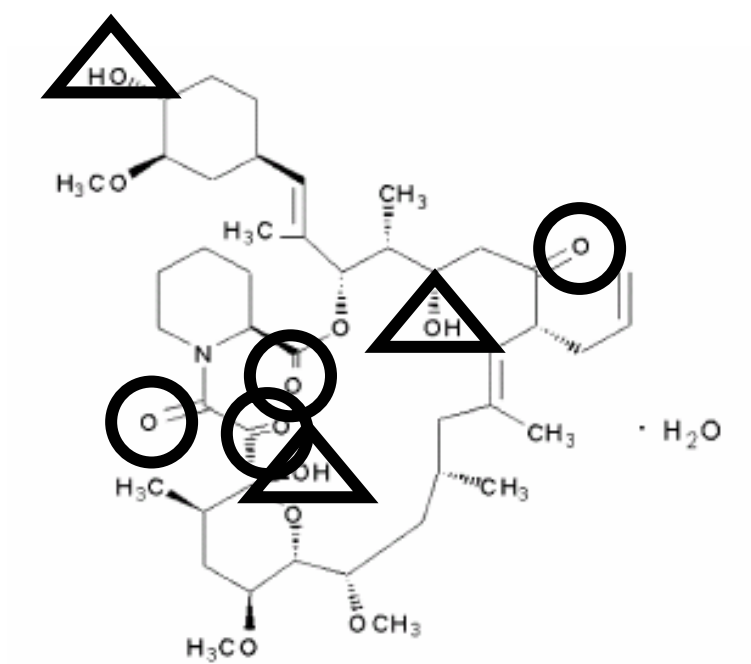
Figure 4.6: Possible hydrogen-bonding sites for tacrolimus: hydrogen-bond donor (Δ), hydrogen-bond acceptor (O)
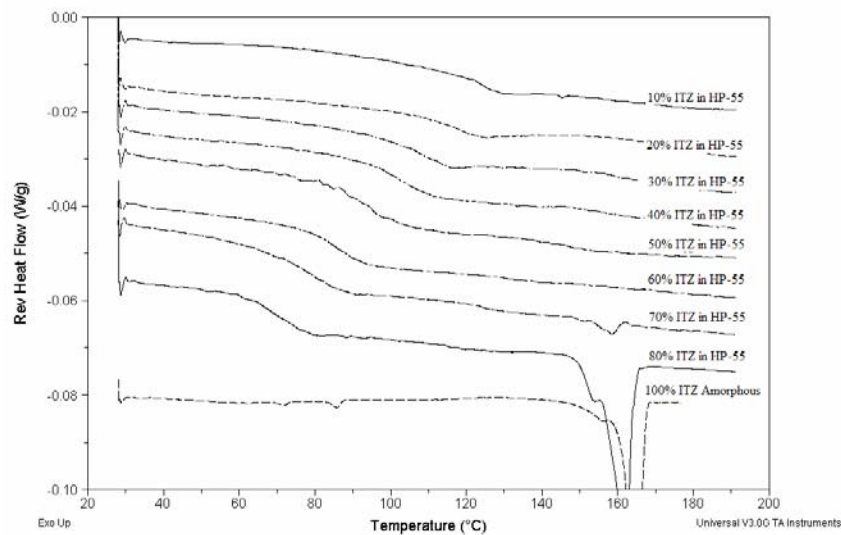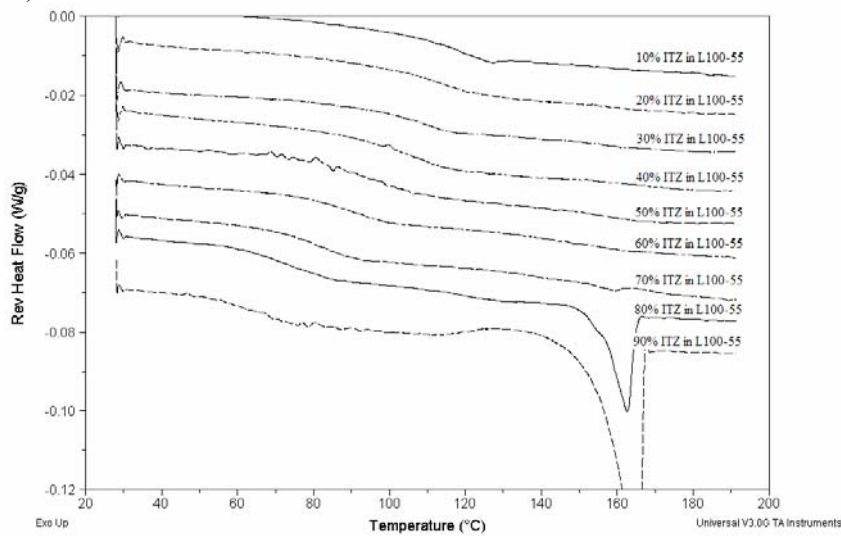
Figure 5.1: Reverse heat MDSC profile for increasing potencies of URF micronized compositions containing a.) ITZ:HP-55 manufactured from 2.0% total solids feed b.) ITZ:L100-55 manufactured from 0.2% total solids feed. Heat flow values are relative for comparison purposes.
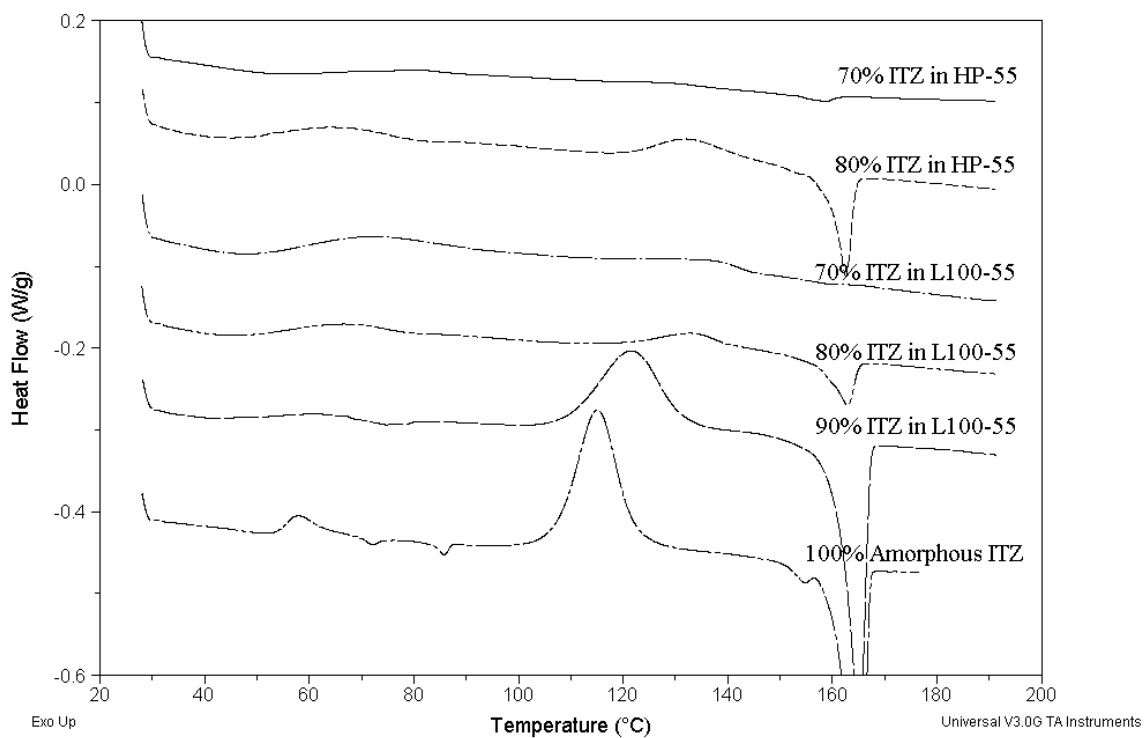
Figure 5.2: Total heat flow MDSC for high potency URF micronized ITZ:HP-55 (2%) and ITZ:L100-55 (0.2%) powders. Heat flow values are relative for comparison purposes.

Slight transition
observed
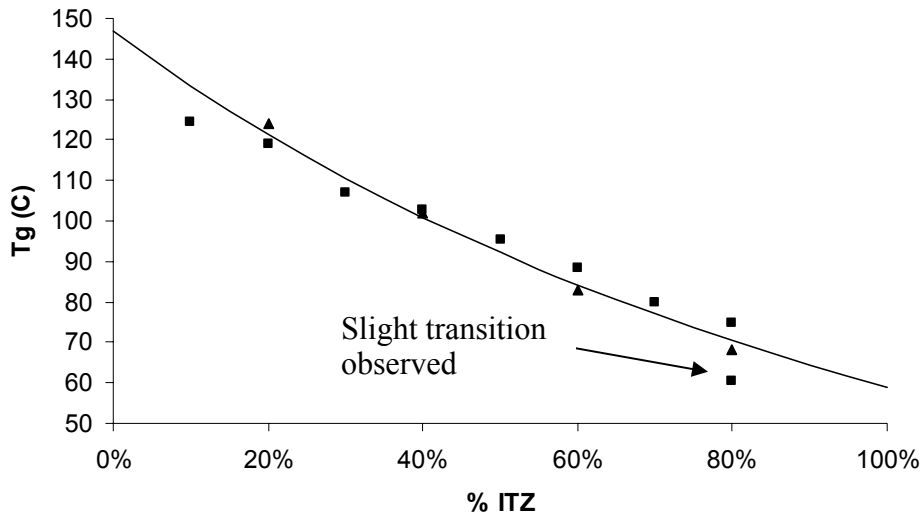
a.)
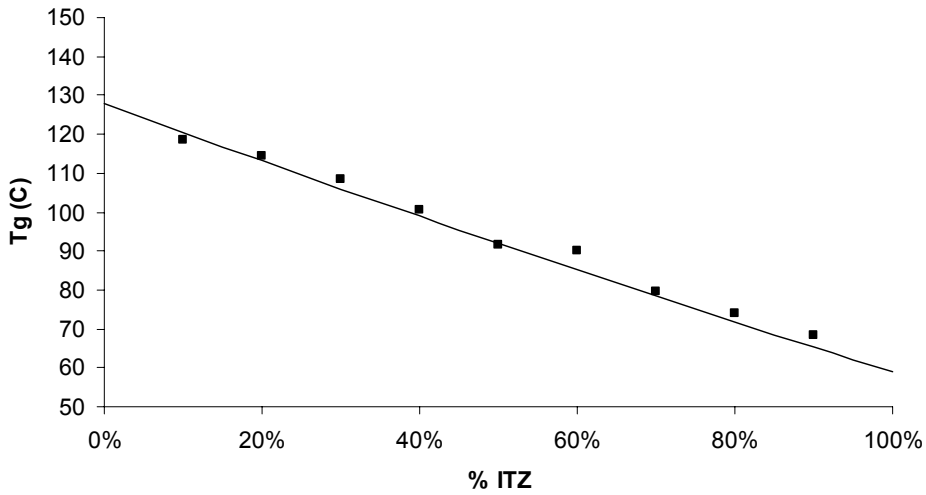
b.)

Figure 5.3: Measured glass transition (T_g) temperatures for increasing potencies of URF

micronized compositions plotted vs. theoretical T_g calculated from Gordon

Taylor equation, a.) ITZ:HP-55 from 2.0% feed (■); 0.2% feed (▲);

theoretical (-) b.) ITZ:L100-55 from 0.2% feed (■); theoretical (-)
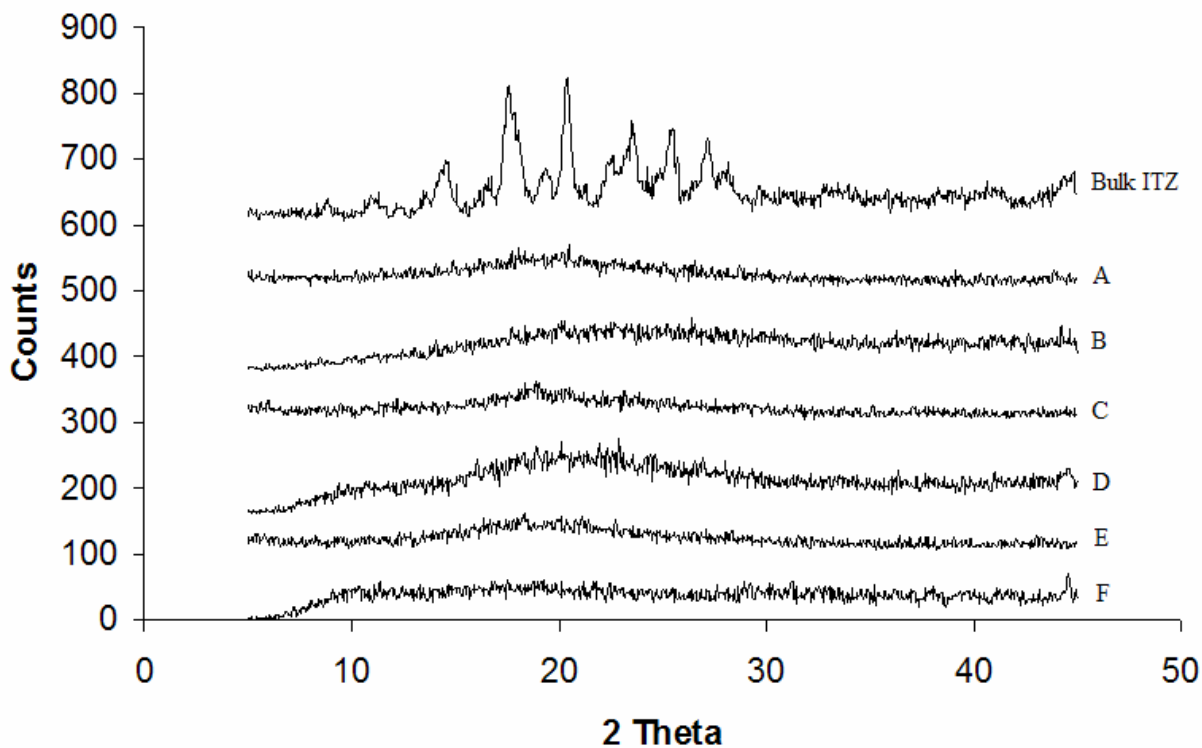
Figure 5.4: X-ray diffraction profiles for URF micronized powders containing binary
mixtures of ITZ and a enteric polymer (% total solids in feed): (Bulk ITZ)
bulk ITZ, (A) 4:1HP55(2%), (B) 1:4HP55(2%), (C) 4:1HP55(0.2%), (D)
1:4HP55(0.2%), (E) 4:1L100-55(0.2%), (F) 1:4L100-55(0.2%)

a.)

b.)

c.)

d.)

e.)

f.)
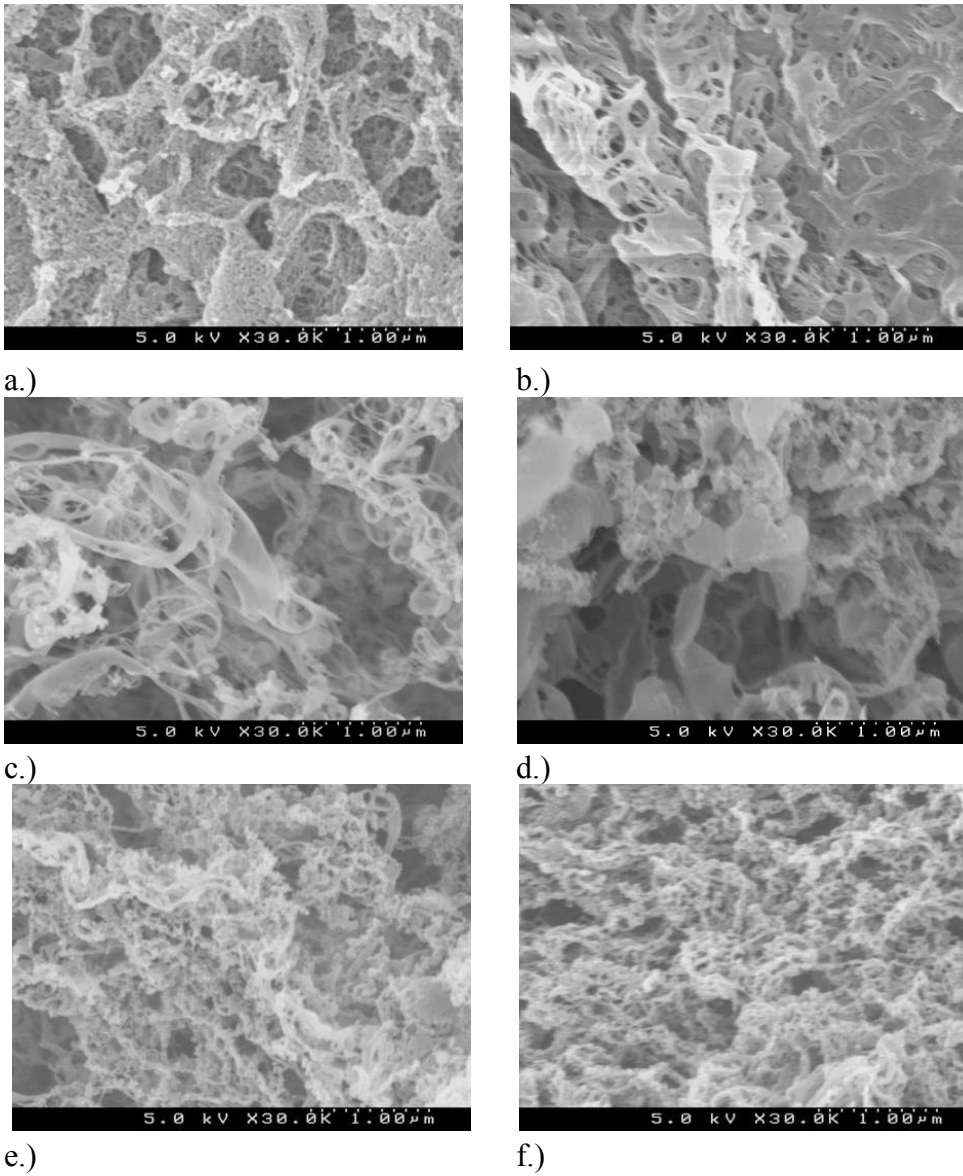
Figure 5.5: Scanning Electron Micrographs of URF micronized powders containing

binary mixtures of ITZ and a enteric polymer: (a) 4:1HP55(2%), (b)

1:4HP55(2%), (c) 4:1HP55(0.2%), (d) 1:4HP55(0.2%), (e) 4:1L100-

55(0.2%), (f) 1:4L100-55(0.2%)

a.)

b.)

213
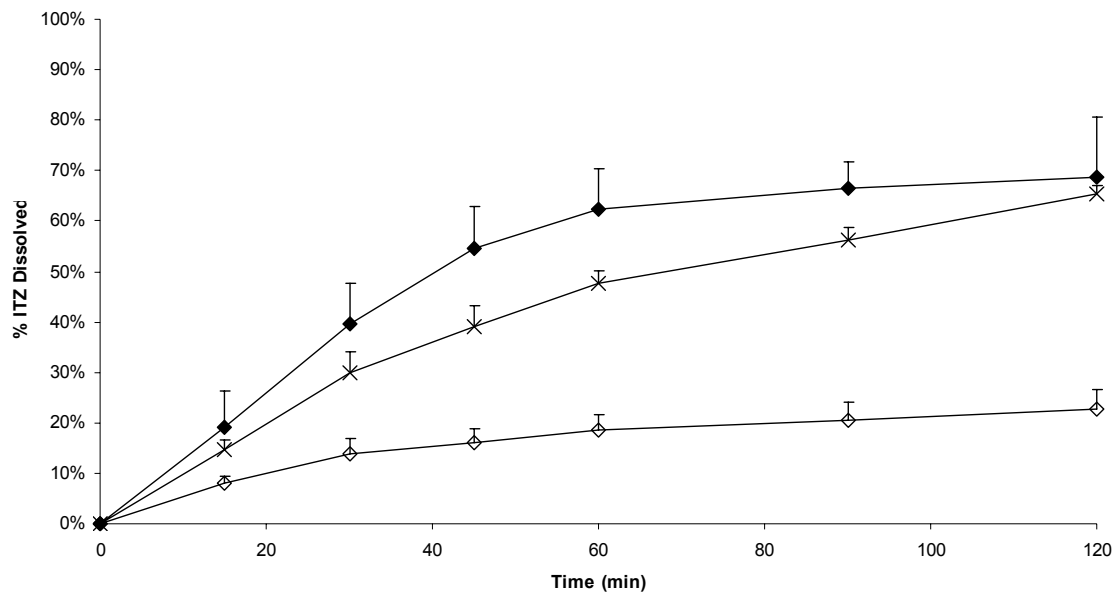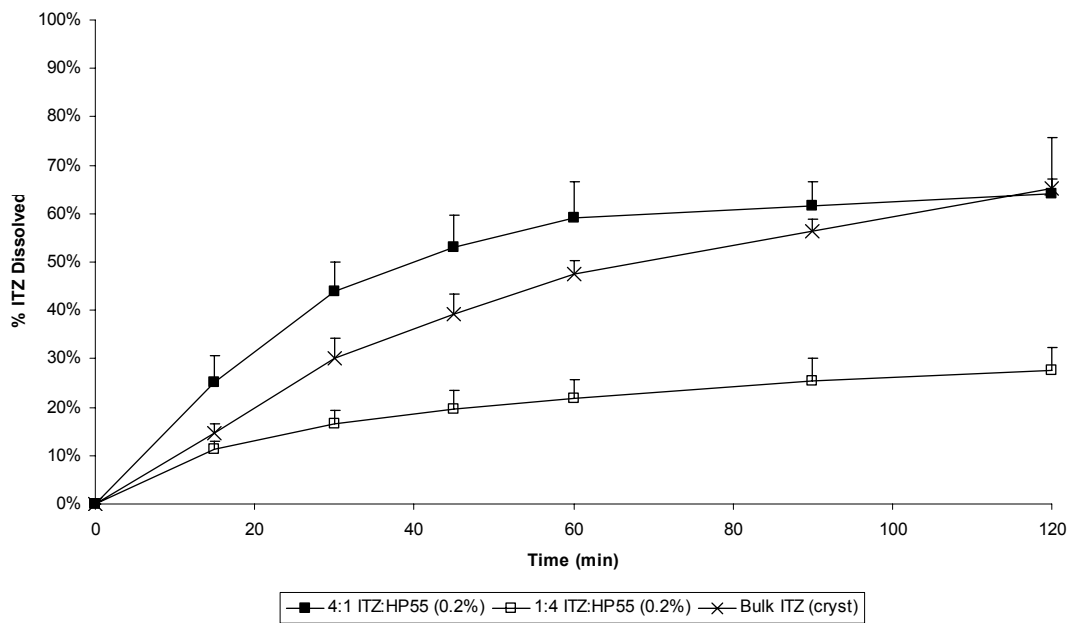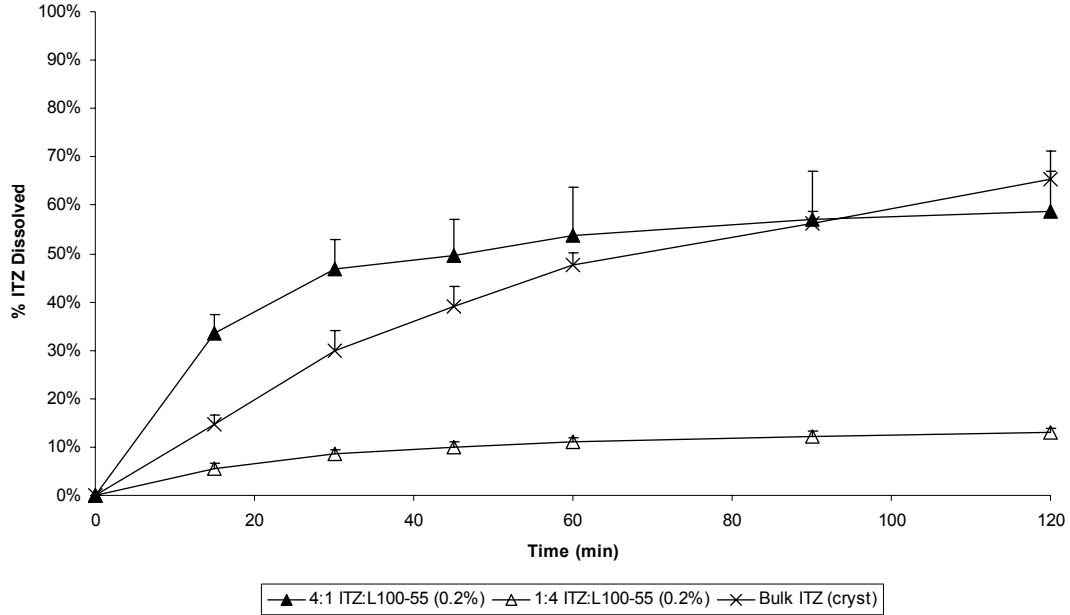
c.)

Figure 5.6: Sink dissolution profiles of URF micronized powders containing binary

mixtures of ITZ and enteric polymer conducted in 0.1N HCl: a.)

4:1HP55(2%) (♦), 1:4HP55(2%) (◊), bulk crystalline ITZ (X) b.)

4:1HP55(0.2%) (■), 1:4HP55(0.2%) (□), bulk crystalline ITZ (X) c.)

4:1L100-55(0.2%) (▲), 1:4L100-55(0.2%) (Δ), bulk crystalline ITZ (X)

a.)

b.)
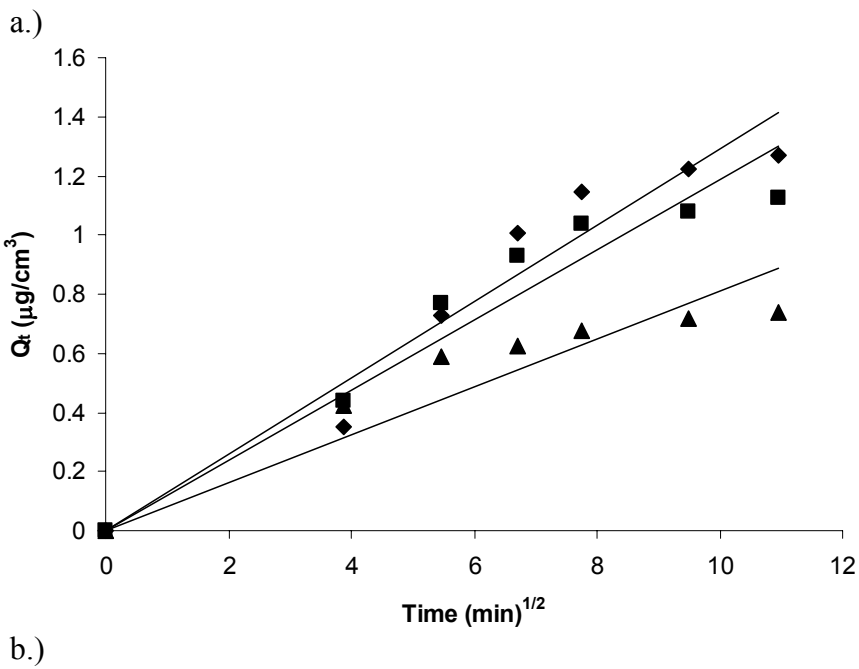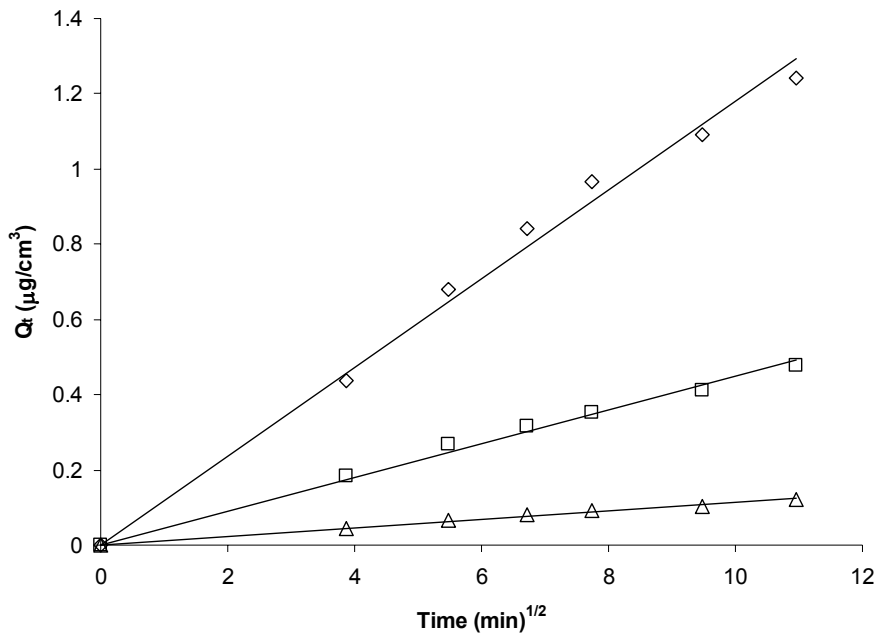
Figure 5.7: Higuchi square root diffusion model fitting of URF micronized powders a.)

1:4HP55(2%) (◊), 1:4HP55(0.2%) (□), 1:4L100-55(0.2%) (Δ); b.)

4:1HP55(2%) (♦), 4:1HP55(0.2%) (■), 4:1L100-55(0.2%) (▲)

215

a.)

b.)
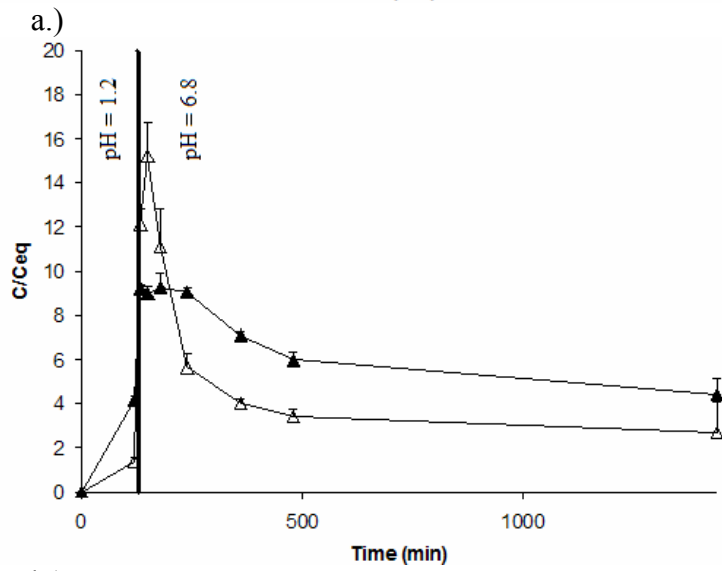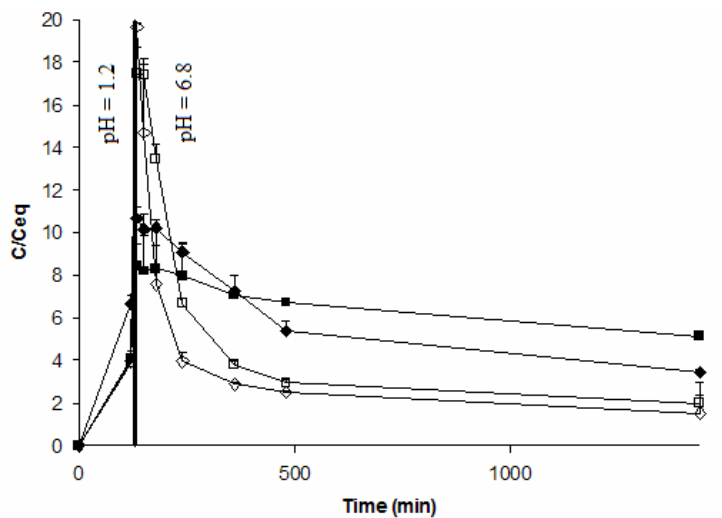
Figure 5.8: Supersaturation dissolution profiles of URF micronized powders containing binary mixtures of ITZ and enteric polymer conducted in 0.1N HCl for two hours and addition of 0.2M Na_3PO_4 with SDS (final SDS Conc. = 0.07%; USP enteric test method A): a.) 4:1HP55(2%) (♦), 1:4HP55(2%) (◊), 4:1HP55(0.2%) (■), 1:4HP55(0.2%) (□) b.) 4:1L100-55(0.2%) (▲), 1:4L100-55(0.2%) (∆)
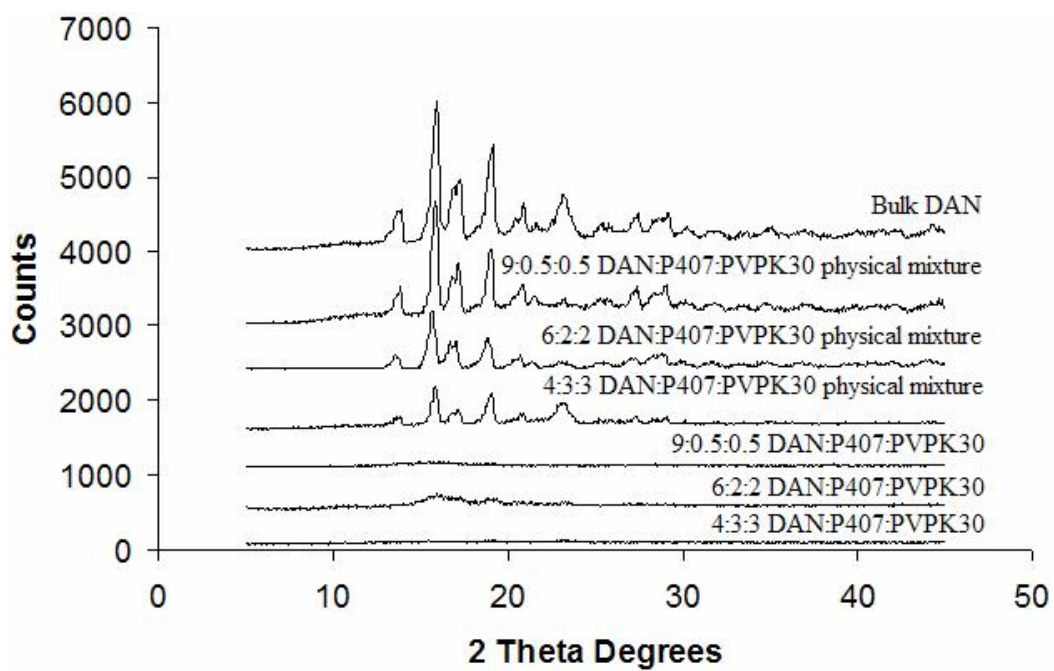
Figure A.1: X-ray diffraction patterns of processed DAN:P:407:PVP compositions compared to bulk DAN and the physical mixtures
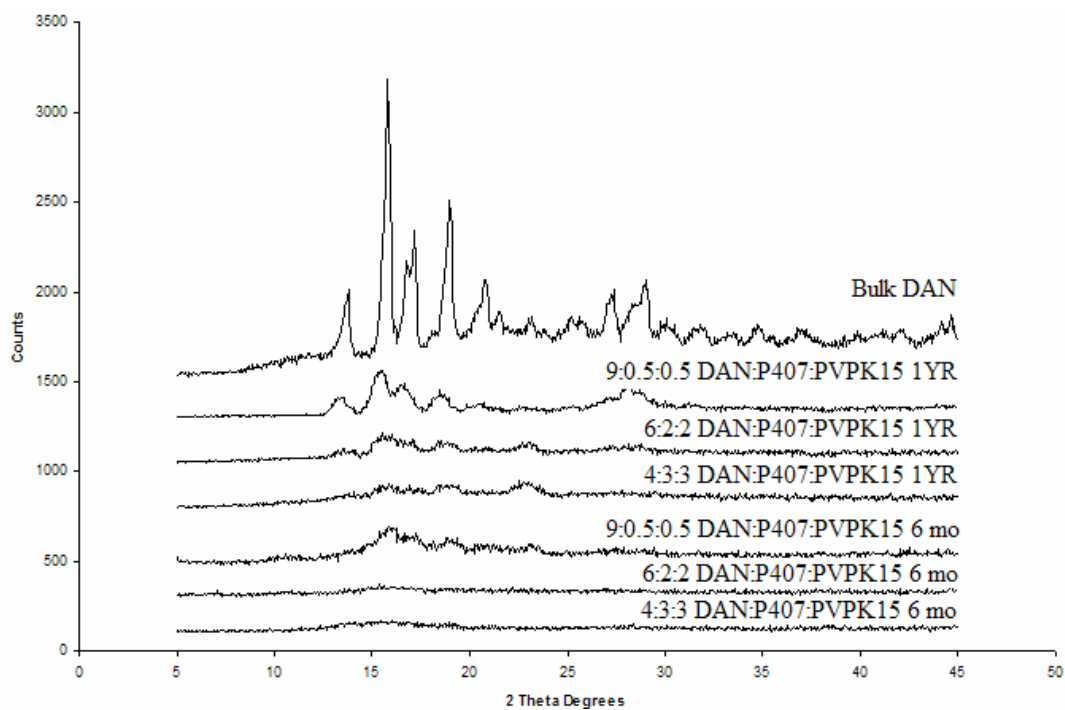
Figure A.2: Stability of processed DAN:P:407:PVP compositions after 6 months and 1 year at 25C/60%RH in open containers
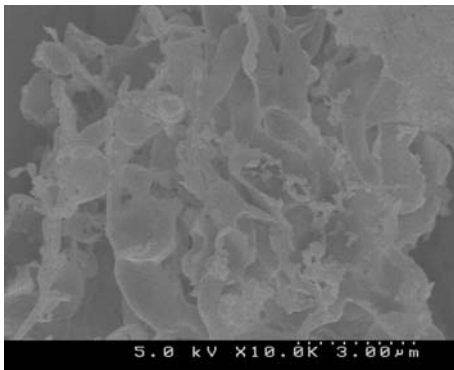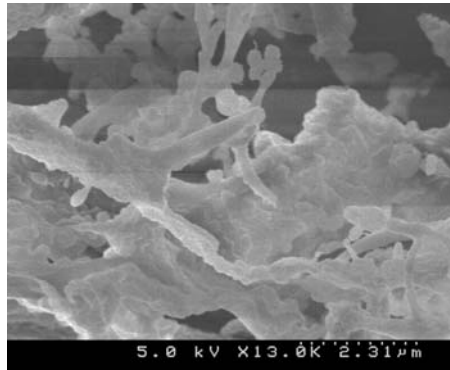
a.)   b.)
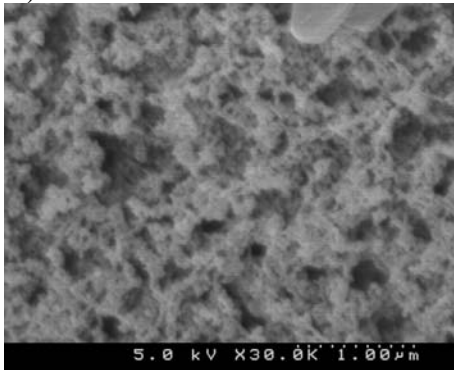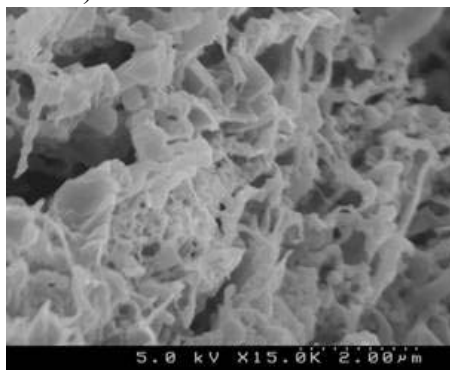
c.)   d.)
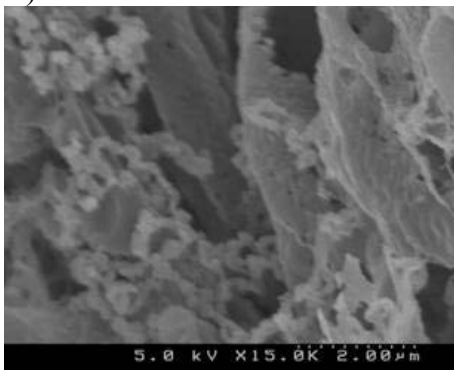
e.)

Figure A.3: SEM micrographs of URF processed powders from 2.0% total solids in feed:

4:3:3 DAN:P407:PVPK30 (a), 6:2:2 DAN:P407:PVPK30 (b), 9:0.5:0.5

DAN:P407:PVPK30 (c); SEM micrographs of URF processed powders

from 0.5% total solids in feed: 4:3:3 DAN:P407:PVPK30 (d), 6:2:2

DAN:P407:PVPK30 (e)

219
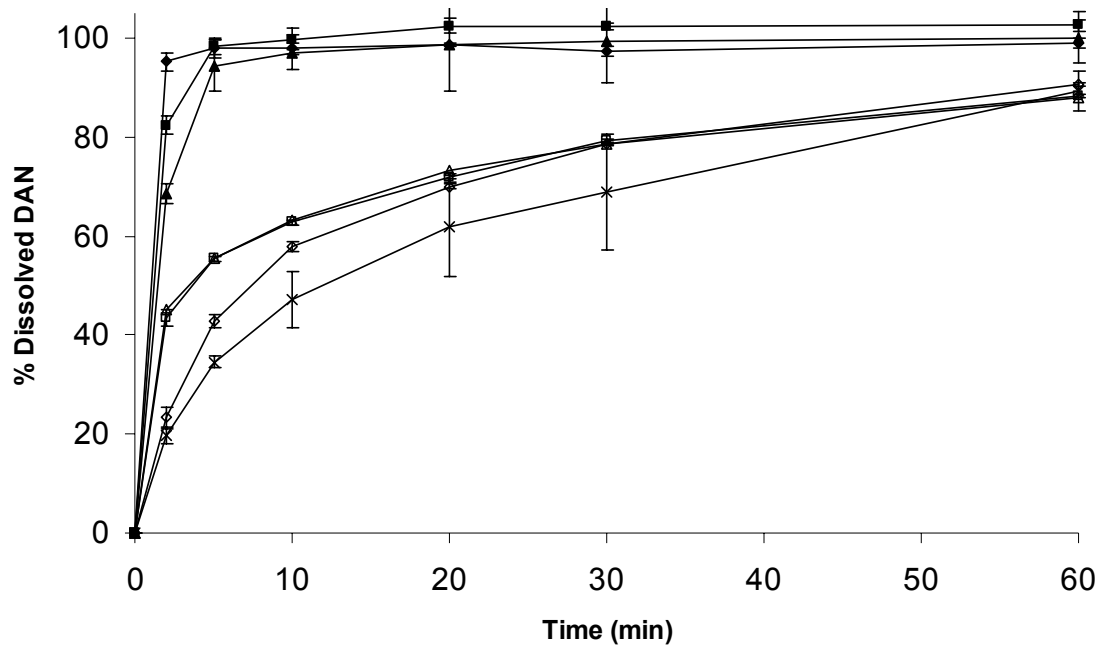
Figure A.4: Dissolution profile for URF processed 9:0.5:0.5 DAN:P407:PVPK30 (●), URF processed 6:2:2 DAN:P407:PVPK30 (■), URF processed 4:3:3 DAN:P407:PVPK30 (▲),9:0.5:0.5 DAN:P407:PVPK30 physical mixture (○),6:2:2 DAN:P407:PVPK30 physical mixture (□),4:3:3 DAN:P407:PVPK30 physical mixture (Δ), Bulk DAN (x)
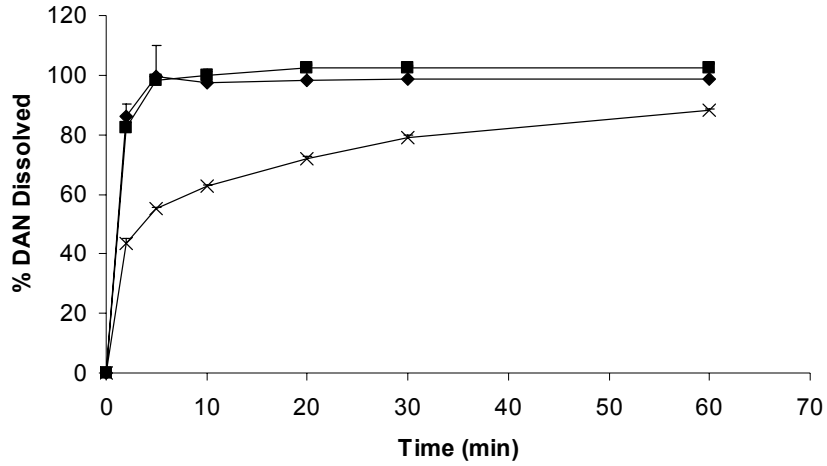
a.)
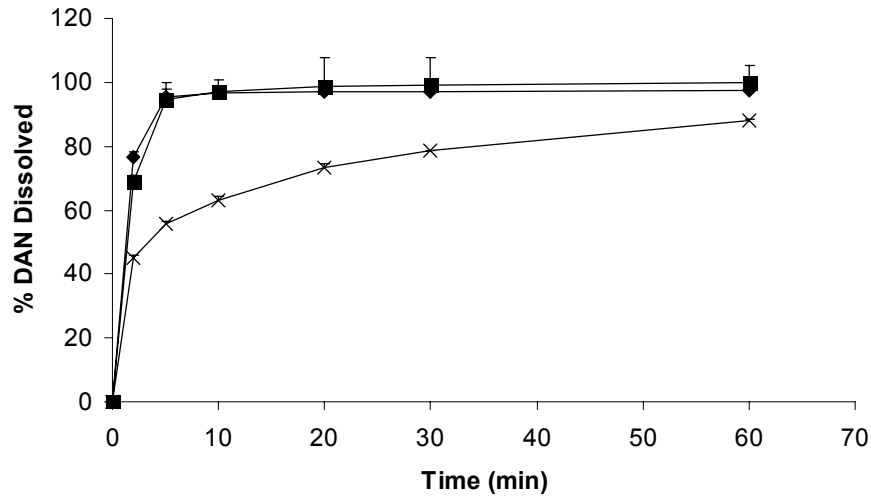
b.)

Figure A.5 - Dissolution profile for URF micronized powders: a.) 4:3:3

DAN:P407:PVPK30: Powder from 0.5% total solids loading in t-butanol

(♦), Powder from 2.0% total solids loading in t-butanol (■), Physical blend

(X). b.) 6:2:2 DAN:P407:PVPK30: Powder from 0.5% total solids loading

in t-butanol (♦), Powder from 2.0% total solids loading in t-butanol (■),

Physical blend (X)

221
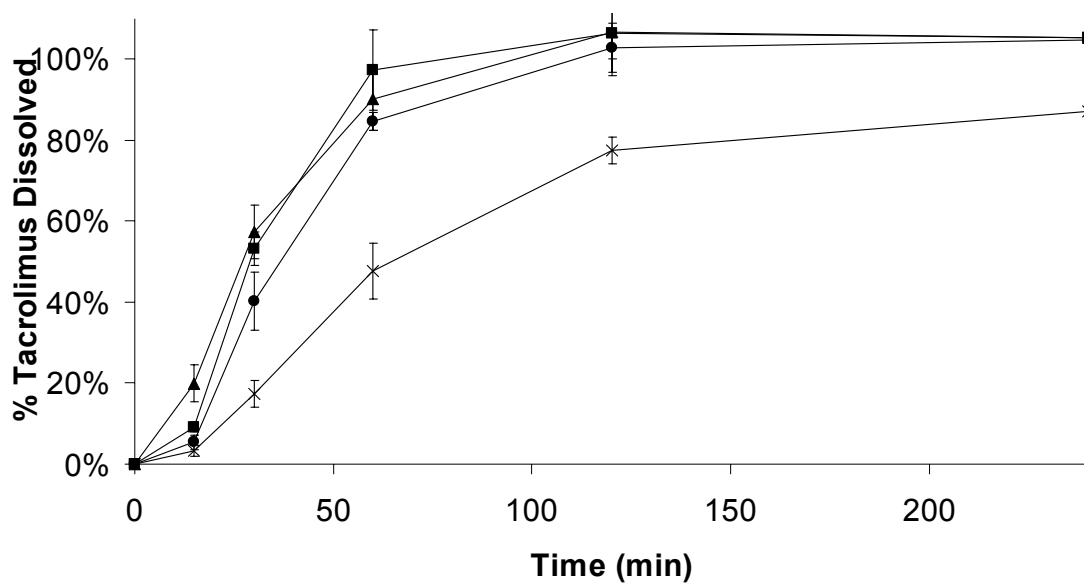
Figure B.1: Dissolution profiles for enhanced URF micronized powders compared to Prograf® having 2 mg TAC equivalent in 900 mL JP1 medium: 1:0.75:0.75 TAC:PVP:poloxamer 407 (■), 1:0.5:0.5 TAC:PVA:P407 (▲), 1:0.5:0.5 TAC:LAC:SDS (●), Prograf® 5 mg powder (X)

Dissolution Profiles of CryoURF Samples Containing SDS

a.)

Dissolution Profile of Cryo-URF Samples Containing PVA

b.)

223
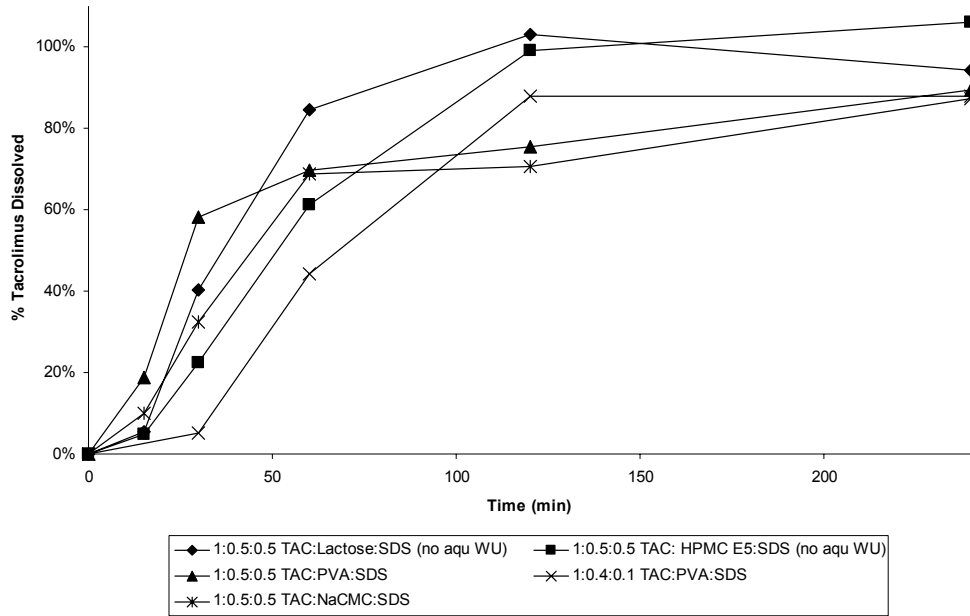
Dissolution Profile of Cryo-URF Samples Containing NaCMC
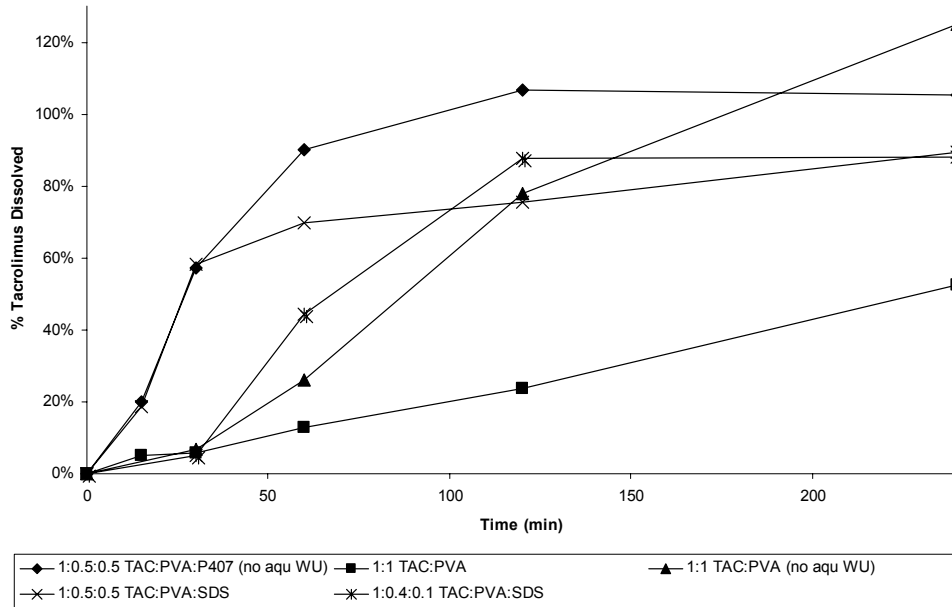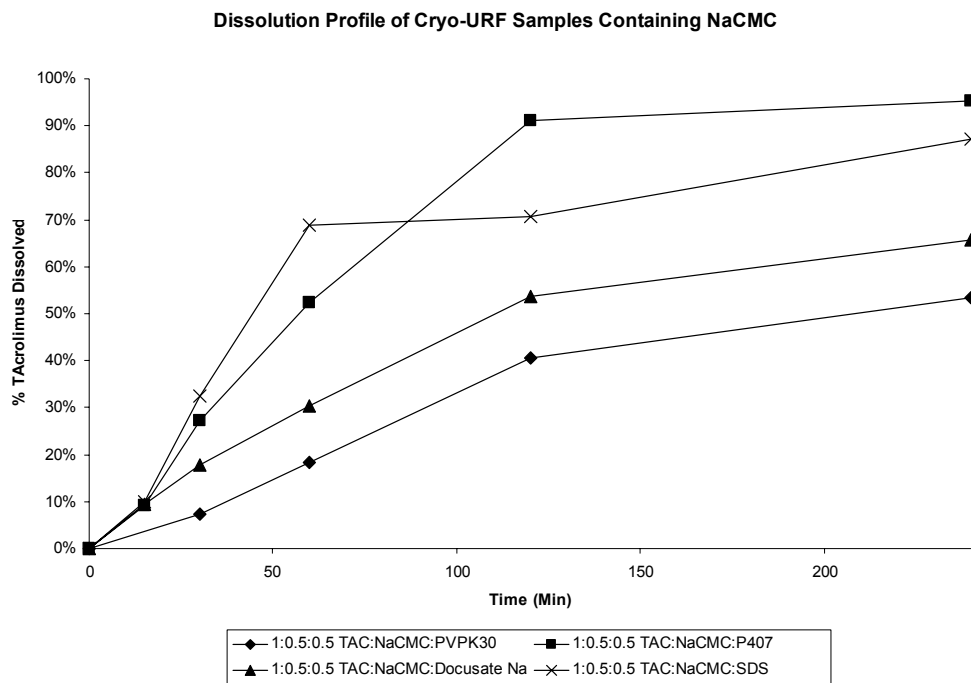
c.)

Figure C.1: Dissolution studies conducted at non-supersaturated conditions organized by compositions containing (a) SDS, (b) PVA, and (c) Na CMC. n=2
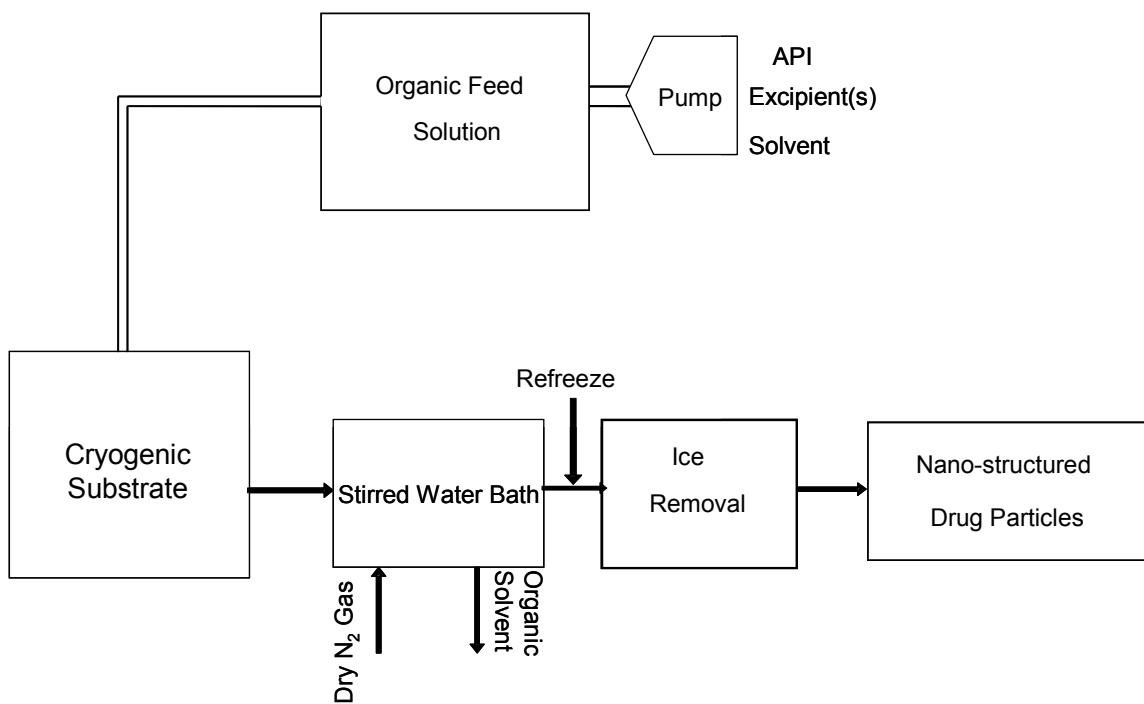
Figure C.2: Schematic of URF process with aqueous work-up post process

Appendix A: Investigation of Increasing Potency Danazol Compositions Prepared by Ultra-rapid Freezing

A.1 PURPOSE

The purpose of this study was to investigate the effects of increasing danazol (DAN) potency on the physico-chemical properties and stability of URF micronized powders. Compositions contained increasing API:polymer ratios while maintaining equal weight ratios of polyvinylpyrrolidone (PVP):poloxamer 407 (P407).

A.2 MATERIALS AND METHODS

A.2.1 Materials

Micronized danazol (DAN), sodium lauryl sulfate (SLS), poloxamer 407 (P407) and polyvinylpyrrolidone (PVP) K-15 were purchased from Spectrum Chemicals (Gardena, CA). High performance liquid chromatography (HPLC) grade acetonitrile (ACN) was obtained from EM Science (Gibbstown, NJ), and tert-butanol (T-BUT) was purchased from Fisher Scientific (Fair Lawn, NJ).

A.2.2 Preparation of URF Micronized Powders

The method for preparation of the URF micronized powders was outlined in section 3.3.2.

A.2.3 Scanning Electron Microscopy (SEM)

The method for scanning electron microscopy was outlined in section 3.3.5.

A.2.4 Dissolution Studies

The method for dissolution testing was outlined in section 3.3.6.

A.2.5 X-Ray Diffraction (XRD)

The method for X-ray diffraction was outlined in section 3.3.7.

A.2.6 Surface Area Analysis (BET)

The method for surface area analysis was outlined in section 3.3.8.

A.2.7 Contact Angle Measurement

The method for contact angle measurement was outlined in section 3.3.9.

A.3 RESULTS

Sample compositions included the non-ionic surfactant polymer P407 which has been shown to increase wetting of poorly water soluble APIs as well as PVPK30 to maintain physical stability of the samples. Because of the high solubility of DAN in T-BUT, the total solids content was increased to 2.0%. The composition parameters can be seen in Table A.1. Samples processed using the URF technology did not show any characteristic crystalline peaks for DAN indicating amorphous DAN present throughout

the sample as seen in Fig. A.1. These compositions were compared to the crystalline bulk DAN as well as physical mixtures of each of the compositions. Peak intensities of the physical mixtures were reduced as each composition was diluted with the hydrophilic excipients. As with the DAN:PVP compositions, sufficiently rapid freezing rates occurred, preventing crystallization of the API during the particle formation process. Long term stability was performed on the powders to determine the effectiveness of the polymers on preventing recrystallization of the DAN. Samples were stored at 25°C/60%RH and XRD was performed at 6 months and 12 months. The 9:0.5:0.5 DAN:P407:PVPK30 showed revealed crystalline DAN within 6 months while the 4:3:3 and 6:2:2 DAN:P407:PVPK30 powders maintained their physical stability for at least 6 months before crystalline DAN was observed after 1 year stability.

Surface areas for all the URF processed powders are summarized in Table A.2 and were considerably higher compared to the physical blends and the bulk DAN. Surface areas for the processed powders ranged from 22.94 m^2/g to 30.25 m^2/g and SSA improved 18 to 24 fold, respectively, compared to the physical mixture counterpart. However, the lower SSA for the higher potency samples was attributed to an increase in DAN loading in the feed solution leading to faster growth rates. This is reasonable since a clear trend can be seen as SSA decreases as DAN loading increases. Since all potencies of the URF processed powders maintained a 2.0% total solids loading, a substantial decrease in SSA was not seen as DAN potencies increased.

While the SSA was high for all potencies, differences were seen in the surface morphology for all DAN:P407:PVP compositions. For both the 40 and 60% DAN potency URF compositions (Fig. A.3a and A.3b, respectively), the surface morphology

228

consists of interconnected particles forming a larger highly porous aggregate. However, for the 6:2:2 DAN:P407:PVPK30 composition, more necking and discrete particle formation was observed. The micrograph of the 9:0.5:0.5 DAN:P407:PVPK30 processed powder (Fig. A.3c) revealed less necking but included substantially more areas were discrete nanoparticles were formed.

Dissolution studies of the URF processed powders revealed enhanced dissolution rates, even for the 90% DAN potency composition as seen in Fig A.4. While the 9:0.5:0.5 DAN:P407:PVPK30 composition had rapid wetting with nearly 95% of the powder dissolved after 2 minutes, all compositions were statistically similar after 5 minutes with 100% DAN dissolved. Physical mixture compositions revealed a slight increase in wetting compared to the bulk DAN. The close proximity of hydrophilic polymers, P407 and PVP were able to further decrease the surface tension of the dissolution medium allowing for better solid-liquid interface between the medium and the hydrophobic regions of DAN. Comparison of dissolution profiles of compositions manufactured from 0.5% and 2.0% total solids loading are seen in Figs. A.5a and A.5b for 4:3:3 and 6:2:2 DAN:P407:PVPK30, respectively. Differences were observed in surface areas and surface morphologies for the compositions manufactured from the different solids loadings. However, there were no differences observed in the dissolution profiles for these compositions.

Contact angles for the DAN:P407:PVPK30 compositions are shown in Table A.3. The 40% and 60% DAN potency URF processed powders showed slight improvement in wetting compared to their respective physical mixtures with contact angles of 24.0° and 24.0°, respectively. However, the 90% potency DAN composition showed a reduction in

contact angle from 39.5° for the physical mixture to 27.0° for the URF processed powder compared to the physical mixture. This is a statistically significant improvement (p<0.05) and helps support the improvement in dissolution rate for the high potency composition.

Appendix B: Development of Solid Phase Extraction (SPE) Method for Analysis of Tacrolimus using High Performance Liquid Chromatography (HPLC-UV)

B.1 PURPOSE

The purpose of this study was to develop a technique for the analysis of dissolution rates of enhanced compositions of TAC at concentrations below the limit of quantitation (LOQ) such as under sink conditions using traditional analytical techniques such as UV spectrophotometry. Dissolution studies performed under sink conditions are defined as addition of total amount of analyte to a given volume of medium is between 10-33% of the equilibrium solubility of the analyte within the medium[1]. Performance under sink conditions is important for Biopharmaceutics Classification System (BCS) class II compounds to maintain a driving force for dissolution which is concentration independent. Unfortunately, at sink conditions, the total concentration of TAC is below the LOQ for UV spectrophotometry due to the lack of chromophores in the TAC molecule. Therefore, a concentration step must be incorporated to analyze TAC at lower concentrations. In addition, transfer losses must be kept to a minimum to ensure accuracy. Two concentration steps were developed, a lyophilization/concentration step and a solid phase extraction (SPE) step. Spiked samples at low (0.22 μg/mL) and high (2.2 μg/mL) concentrations were prepared. Optimization of the lyophilization/concentration step included investigating various extraction solvents, as

well as mixing techniques. Optimization of the SPE step included investigation of various SPE cartridges and extraction solvents.

B.3 Materials and Methods

B.3.1 Materials

Bulk crystalline tacrolimus and Prograf® (1 mg and 5 mg capsules, Fujisawa, Japan) were kindly provided by the Dow Chemical Company (Midland, MI, USA). Concentrated hydrochloric acid (HCl) and sodium chloride (NaCl) was purchased from Fisher Scientific Chemicals (Hampton, NH, USA). Methanol (MeOH), acetone, dichloromethane (DCM), chloroform, and acetonitrile (ACN) were purchased from EM Industries Inc. (Gibbstown, NJ, USA). 200 proof ethanol, USP grade (EtOH) was purchased from Sigma-Aldrich (Milwaukee, WI, USA). All other solvents were of HPLC grade.

B.3.2 Spiking of TAC

A known amount of TAC was dissolved in acetonitrile and a known volume was added to Japanese First Media, 0.2% NaCl in 0.1N HCl (JP1). Final spiked sample concentrations were between 0.22 μg/mL and 2.2 μg/mL (the estimated equilibrium solubility of tacrolimus) in JP1 medium[2].

B.3.3 Lyophilization/concentration Procedure

Spiked solution at a concentration of 2.2 µg/mL TAC in 5 mL JP1 medium at 37°C was filtered using 0.45 µm filter GHP Acrodisc syringe filter (Pall, East Hills, NY, USA) into a 15 mL scintillation vial. Samples were rapidly frozen by submersion into liquid nitrogen and lyophilized at -20°C for 24 hours, ramping to 25°C over 12 hours and held at 25°C for 12 hours at 100 mTorr. After lyophilization, an extraction solvent was added to dissolve the TAC and transferred to 1.5 mL conical vial where the solvent was evaporated to dryness using pure nitrogen heated to 25°C. Investigated extraction solvents were acetone, chloroform, 75/25 acetonitrile/water, and 50/50 ethanol/dichloromethane (EtOH/DCM). In addition, an extraction mixing method was investigated to determine an optimum extraction procedure based on percent total theoretical recovered. These methods included single washing or three washing aliquots of 5 mL EtOH/DCM, vortexing a single washing aliquot of EtOH/DCM, or sonicating 15 mL EtOH/DCM for 5 minutes.

B.3.4 SPE procedure

Spiked or dissolution samples were heated to 37°C and added to a pre-conditioned SPE cartridge (Supleco, Bellefonte, PA, USA; (DSC); JT Baker, Phillipsburg, NJ, USA; (JT)). Preconditioning was performed on new SPE cartridges by pulling and vacuum on the cartridge, adding 1 mL HPLC grade MeOH, allowing the liquid to drain, and repeated with 1 mL de-ionized water. Without letting the cartridge come to complete dryness, the spiked sample was added to the cartridge. The sample

was partially drawn through the substrate, allowed to sit for five minutes in order to allow the analyte to bind to the substrate, and then the solution was then collected under vacuum. Two x 0.5 mL aliquots of ACN were added to the cartridge and drawn through at a rate of approximately one drop/second and collected in a 1.5 mL centrifuge vial (repeated twice). Collected samples were evaporated to dryness under pure nitrogen at room temperature (TAC degrades at high temperatures) and reconstituted with 150 μL filtered 70:30 ACN:water. The reconstituted samples were vortexed for 30 seconds and transferred to a HPLC 200 μL vial insert and analyzed according the method described in 4.3.4.

B.3.5 Sink dissolution testing

Dissolution testing was performed on the TAC compositions, both Prograf® and URF micronized powders using a USP 24 Type II paddle apparatus model VK7000 (Varian Inc., Cary, NC, USA). An equivalent of 2 mg ITZ was added to 900 ml of 0.1N HCl containing 0.2% NaCl (JP1) dissolution media and stirred at 100 rpm. The dissolution media was maintained at $37.0 \pm 0.2°C$. Samples (5ml) were withdrawn at 30, 60, 120 and 240 minute time points, filtered using a 0.45μm GHP Acrodisc filter, concentrated using the lyophilization/concentration step and the TAC was extracted with three washings of EtOH/DCM each vortexed for one minute. These aliquots were transferred to a 1.5 mL conical vial and dried using nitrogen gas. The residue was reconstituted with mobile phase and analyzed according the method described in 4.3.4.

B.4 RESULTS

B.4.1 Optimization of Lyophilization/concentration step

The lyophilization/concentration step was developed as a simple and reproducible method for investigating dissolution profiles of TAC in which TAC was dissolved at concentrations below the LOQ of HPLC-UV. Table B.1 shows differences in total TAC recovery of spiked samples of different extraction solvents. It was shown that EtOH/DCM had sufficient TAC recoveries (>90%) while 75/25 ACN/water was very close with 89.20% TAC recovered. TAC solubilities are higher in acetone (561 mg/mL) and chloroform (573 mg/mL) compared to EtOH (355 mg/mL) [3]; however, recoveries from acetone where lower because of poor peak resolution (absorbance of residual acetone at low wavelengths) and chloroform is a known carcinogen. EtOH/DCM was chosen as the extraction solvent because of its higher recovery and its ability to dissolve a wider range of excipients used in URF processed solid dispersions, although, 75/25 ACN/water could also be used when excipients are water soluble.

The extraction mixing method was also investigated to optimize the time for TAC recovery when many samples need to be analyzed; results are shown in Table B.2. It is clear that multiple washings lead to higher recoveries; however, this method of extraction can be time consuming when many samples need to be analyzed. Sonication can also lead to very high TAC recovery, but sonication also loosens the NaCl around the walls. High amounts of NaCl can lead to phase separation of ACN and water after reconstitution and was observed in the sonicated samples and proven experimentally. Only the ACN

phase was collected via pipette and analyzed on HPLC. In addition, 15 mL of EtOH/DCM were required to completely cover the lyophilized residue in the scintillation vials. However, sonication is advantageous since many samples can be sonicated at one time and sonication only needs to be performed once in order to obtain high TAC recoveries. Therefore, it was determined that vortexing multiple washings was preferred when few samples (> 20 samples) were analyzed while sonication is preferred when many samples (>20 samples) require analysis.

B.4.2 Optimization of SPE concentration step

SPE is a useful step for concentration and purification of liquid samples which need to be analyzed either qualitatively or quantitatively. In this study, C18 and C8 were selected as the SPE cartridge packing because of their effectiveness at binding to poorly water soluble compounds. From Table B.3, it can be seen that both C18 and C8 are effective packing substrates since all samples have high average total TAC recovered (>90%). Allowing for maximum binding of the TAC to the hydrophobic packing and slow addition of the extraction solvent allowed for high recoveries of TAC for all samples. However, greater recoveries of TAC within the first mL of extraction solvent were seen from extraction using 100 mg packing cartridges. It is unknown if these differences were attributed to the amount of packing or the packing substrate since cartridges containing 100 mg of C8 were not available for analysis. Elution solvent (ACN) was not investigated since this solvent was recommended by the SPE cartridge manufacturers as an acceptable elution solvent for TAC. However, recovery of both high and low concentration spiked samples were investigated to determine reproducibility of

the method at low concentrations to simulate early dissolution time points. Aliquots of 5 mL of 1.1 μg/ml spiked samples (total TAC = 5.5 μg) were recovered fully from the SPE cartridge while lower concentration spiked samples (0.22 μg/ml) were not fully recovered. This is most likely due to the small fraction which could not fully be extracted from the cartridge before evaporation of the elution solvent occurred thereby trapping the residual TAC in the SPE cartridge. Since this fraction is larger in the low concentration sample, lower percent recoveries are observed. Future SPE studies should examine higher loadings of sample solution (10 mL to 15 mL) in order to reduce the fraction of TAC remaining in the SPE cartridge.

B.4.3 Dissolution of Prograf[®] and URF micronized powders at low TAC loadings

An example of dissolution profiles for Prograf® and URF micronized powders can be seen in Fig. B.1. Enhanced dissolution rates were observed for the URF micronized powders while Prograf® powder had a slower dissolution rate. While not at sink conditions (2 mg TAC in 900 mL = 2.2 μg/mL = equilibrium TAC solubility), these dissolution profiles represent the ability to reproducibly analyze dissolution samples at concentrations below the LOQ for UV analysis.

B.5 Acknowledgements

237

B.6 References

[1]   Brown, C.K., *Dissolution Method Development: An Industry Perspective*, in *Pharmaceutical Dissolution Testing*, J.B. Dressman and J. Kramer, Editors. 2005, Taylor & Francis: Boca Raton, FL. p. 351-372.

[2]   Yamashita, K., et al., *Establishment of new preparation method for solid dispersion formulation of tacrolimus.* International Journal of Pharmaceutics, 2003. **267**(1-2): p. 79-91.

[3]   Tanaka, H., et al., *Physicochemical Properties of Fk-506, a Novel Immunosuppressant Isolated from Streptomyces-Tsukubaensis.* Transplantation Proceedings, 1987. **19**(5): p. 11-16.

Appendix C: Performance of URF micronized powders containing a variety of stabilizers/surfactants for the dissolution enhancement of tacrolimus

C.1 PURPOSE

The purpose of this study was to asses the performance of URF micronized powders using various stabilizers/surfactants to enhance the physico-chemical properties of compositions containing tacrolimus. URF screen compositions were assessed based on dissolution profiles compared to Prograf® and to be selected for further analysis.

C.2 MATERIALS AND METHODS

C.2.1 Materials

Bulk crystalline tacrolimus, Prograf® (1 mg and 5 mg capsules, Fujisawa, Japan) and HPMC E5 LV were kindly provided by the Dow Chemical Company (Midland, MI, USA). Polyvinylpyrrolidone (PVP), poloxamer 407 (P407), sodium carboxymethylcellulose (NaCMC), docusate sodium (DOC), lactose (LAC), and mannitol (MAN) were purchased from Spectrum chemical (Gardena, CA). Poly(vinyl) alcohol (PVA, Mw 13,000-23,000, 87-89% hydrolyzed), hydroxypropyl cellulose (MW 100,000; HPC) and sodium dodecyl sulfate (SDS) were purchased from Sigma-Aldrich (St. Louis, MO, USA).

C.2.2 Preparation of URF Micronized Powders

The process for manufacturing the URF micronized powders is outlined in section 4.3.2. Compositions which were manufactured are listed in Table C.1. Briefly, TAC and the stabilizers (polymers) were dissolved in the solvent at the listed TAC:polymer ratio and % total solids loading. The feed solutions were applied to a cryogenic solid substrate cooled to a temperature of -155°C, collected, and lyophilized using a VirTis Advantage benchtop tray lyophilizer (The VirTis Company, Inc. Gardiner, NY). Compositions which underwent the aqueous-work-up method were applied to the solid substrate cooled to -155°C. The frozen matter was added to a stirred water bath cooled to 2°C. If a polymer was added to the cooled water bath, it was listed under the aqueous work-up column in Table C.1. After addition of the frozen matter, the bath continued to stir while a dry nitrogen stream facilitated evaporation of the organic solvent. After 30 minutes, the aqueous slurry was rapidly frozen in liquid nitrogen and lyophilized.

C.2.3 Dissolution Testing

The dissolution studies were performed according to Japanese Pharmacopoeia (JPXIII) method 2 (paddle) for dissolution testing using a dissolution paddle apparatus model VK7000 (Varian Inc., Cary, NC, USA). An equivalent of 5 mg TAC was added to 900 mL of 0.005% HPC aqueous dissolution medium pH adjusted to 4.5 using H_3PO_4. The dissolution media was maintained at 37.0 ± 0.2°C and the paddle speed was maintained at 50 rpm throughout the testing period.

240

Samples (5 mL) were withdrawn at 30, 60, 90, 120 and 240 minute time points, filtered using a 0.20 μm Whatman nylon filter (Clifton, NJ, USA). Subsequent concentration was performed using solid phase extraction according to section B.3.4 and analyzed using the HPLC method described in section 4.3.4.

C.3 Results

A complete search was conducted in order to determine optimum stabilizers which could enhance the dissolution profile for TAC while preventing the compositions from reading on any existing patents. Possible stabilizers are listed in Table C.2 along with their advantages and disadvantages for dissolution enhancement. Screen compositions containing various ratios and combinations of the stabilizers with tacrolimus were manufactured using the URF process with or without the aqueous work-up method and are listed in Table C.2. Dissolution studies were performed to assess the effect of the stabilizer combination on dissolution enhancement. Dissolution profiles in Fig. C.1a contain compositions with SDS and all exhibit rapid dissolution except for 1:0.4:0.1 TAC:PVA:SDS which has the lowest ratio of SDS of all the compositions. Fig. C.1b contains dissolution profiles for URF compositions containing PVA. Compositions with surfactants such as the block-copolymer P407 displayed rapid dissolution while compositions without surfactants showed poor wetting and slower dissolution profiles. In addition, the effect of the aqueous work-up method was investigated using 1:1 TAC:PVA composition. PVA was added either in the feed solution or in the cooled water bath and will be referred to TAC:PVA (no aq-wu) and TAC:PVA (aq-wu), respectively. The dissolution rate for TAC:PVA (no aq-wu) was faster than TAC:PVA (aq-wu) as seen in Fig. C.1b. PVA is widely known to be a stabilizing polymer having poor wetting

properties. By incorporating the PVA into the aqueous work-up method, the PVA was added to the surface of the TAC domains. This led to overall decreased wetting of the composition. Fig. C.1c displays the dissolution profiles for URF compositions containing NaCMC. Only compositions containing hydrophilic surfactants P407 or SDS had enhanced dissolution profiles while those containing DOC and PVP had slower dissolution rates.

References

Terwogt, J.M.M., B. Nuijen, W.W.T. Huinink, and J.H. Beijnen, Alternative formulations of paclitaxel. Cancer Treat. Rev., 1997, 23(2): p. 87-95.

Cross, L.J., J. Bagg, and T.C. Aitchison, Efficacy of the cyclodextrin liquid preparation of itraconazole in treatment of denture stomatitis: Comparison with itraconazole capsules. Antimicrob. Agents Chemother., 2000, 44(2): p. 425-427.

Lee, V.H.L., Enzymatic Barriers to Peptide and Protein-Absorption. Critical Rev. in Therapeut. Drug Carrier Sys., 1988, 5(2): p. 69-97.

Delie, F. and M.J. Blanco-Prieto, Polymeric particulates to improve oral bioavailability of peptide drugs. Molecules, 2005, 10(1): p. 65-80.

Fu, L., L.C. Cao, Y.Q. Liu, and D.B. Zhu, Molecular and nanoscale materials and devices in electronics. Adv. Colloid Interface Sci., 2004, 111(3): p. 133-157.

Soppimath, K.S., T.M. Aminabhavi, A.R. Kulkarni, and W.E. Rudzinski, Biodegradable polymeric nanoparticles as drug delivery devices. J. Control. Release, 2001, 70(1-2): p. 1-20.

Vaughn, J.M., X.X. Gao, M.J. Yacaman, K.P. Johnston, and R.O. Williams, Comparison of powder produced by evaporative precipitation into aqueous solution (EPAS) and spray freezing into liquid (SFL) technologies using novel Z-contrast STEM and complimentary techniques. Eur. J. Pharm. Biopharm., 2005, 60(1): p. 81-89.

Dalgleish, D.G. and F.R. Hallett, Dynamic Light-Scattering - Applications to Food Systems. Food Res. Int., 1995, 28(3): p. 181-193.

Liversidge, G.G. and K.C. Cundy, Particle-Size Reduction for Improvement of Oral Bioavailability of Hydrophobic Drugs .1. Absolute Oral Bioavailability of Nanocrystalline Danazol in Beagle Dogs. Int. J. Pharm., 1995, 125(1): p. 91-97.

Muller, R.H., C. Jacobs, and O. Kayser, Nanosuspensions as particulate drug formulations in therapy Rationale for development and what we can expect for the future. Adv. Drug Deliv. Rev., 2001, 47(1): p. 3-19.

Rogers, T.L., K.P. Johnston, and R.O. Williams, Solution-based particle formation of pharmaceutical powders by supercritical or compressed fluid CO_2 and cryogenic spray-freezing technologies. Drug Dev. Ind. Pharm., 2001, 27(10): p. 1003-1015.

Hu, J.H., K.P. Johnston, and R.O. Williams, Nanoparticle engineering processes for enhancing the dissolution rates of poorly water soluble drugs - a review. Drug Dev. Ind. Pharm., 2004, 30(3): p. 247-258.

Hutchenson, K.W. and N.R. Foster, Innovations in supercritical fluid science and technology, in Innovations in Supercritical Fluids. 1995, ACS Press: Washington. p. 1-31.

Weber, M., L.M. Russell, and P.G. Debenedetti, Mathematical modeling of nucleation and growth of particles formed by the rapid expansion of a supercritical solution under subsonic conditions. J. Supercrit. Fluids, 2002, 23(1): p. 65-80.

Gander, B., P. Johansen, H. NamTran, and H.P. Merkle, Thermodynamic approach to protein microencapsulation into poly(D,L-lactide) by spray drying. Int. J. Pharm., 1996, 129(1-2): p. 51-61.

Raula, J., H. Eerikainen, and E.I. Kauppinen, Influence of the solvent composition on the aerosol synthesis of pharmaceutical polymer nanoparticles. Int. J. Pharm., 2004, 284(1-2): p. 13-21.

Eerikainen, H., W. Watanabe, E.I. Kauppinen, and P.P. Ahonen, Aerosol flow reactor method for synthesis of drug nanoparticles. Eur. J. Pharm. Biopharm., 2003, 55(3): p. 357-360.

Eerikainen, H., E.I. Kauppinen, and J. Kansikas, Polymeric drug nanoparticles prepared by an aerosol flow reactor method. Pharm. Res., 2004, 21(1): p. 136-143.

Vaughn, J.M., J.T. McConville, R.O. Williams III, and K.P. Johnston, Supersaturation Produces High Bioavailability of Amorphous Danazol Particles Formed by Evaporative Precipitation into Aqueous Solution (EPAS) and Spray Freezing into Liquid(SFL) Technologies. Drug Dev. Ind. Pharm., 2005, In Press.

Sinswat, P., X. Gao, M.J. Yacaman, R.O. Williams III, and K.P. Johnston, Stabilizer choice for rapid dissolving high potency itraconazole particles formed by evaporative precipitation into aqueous solution. Int. J. Pharm., 2005, 302(1-2): p. 113-124.

Chen, X., J.M. Vaughn, M.J. Yacaman, R.O. Williams III, and K.P. Johnston, Rapid dissolution of high-potency danazol particles produced by evaporative precipitation into aqueous solution. J. Pharm. Sci., 2004, 93(7): p. 1867-1878.

Chen, X., Z. Benhayoune, R.O. Williams III, and K.P. Johnston, Rapid dissolution of high potency itraconazole particles produced by evaporative precipitation into aqueous solution. J. Drug Deliv. Sci. Technol., 2004, 14(4): p. 299-304.

Chen, X., T.J. Young, M. Sarkari, R.O. Williams III, and K.P. Johnston, Preparation of cyclosporine A nanoparticles by evaporative precipitation into aqueous solution. Int. J. Pharm., 2002, 242(1-2): p. 3-14.

Sarkari, M., J. Brown, X. Chen, S. Swinnea, R.O. Williams III, and K.P. Johnston, Enhanced drug dissolution using evaporative precipitation into aqueous solution. Int. J. Pharm., 2002, 243(1-2): p. 17-31.

245

Kawasaki, E.S. and A. Player, Nanotechnology, nanomedicine, and the development of new, effective therapies for cancer. Nanomedicine, 2005, 1(2): p. 101-109.

Agnihotri, S.A., N.N. Mallikarjuna, and T.M. Aminabhavi, Recent advances on chitosan-based micro- and nanoparticles in drug delivery. J. Control. Release, 2004, 100(1): p. 5-28.

Pandey, R., A. Sharma, A. Zahoor, S. Sharma, G.K. Khuller, and B. Prasad, Poly (DL-lactide-co-glycolide) nanoparticle-based inhalable sustained drug delivery system for experimental tuberculosis. J. Antimicrob. Chemother., 2003, 52(6): p. 981-986.

Rosca, I.D., F. Watari, and M. Uo, Microparticle formation and its mechanism in single and double emulsion solvent evaporation. J. Control. Release, 2004, 99(2): p. 271-280.

Schwarz, C., W. Mehnert, J.S. Lucks, and R.H. Muller, Solid Lipid Nanoparticles (Sln) for Controlled Drug-Delivery .1. Production, Characterization and Sterilization. J. Control. Release, 1994, 30(1): p. 83-96.

Muller, R.H., S. Maassen, C. Schwarz, and W. Mehnert, Solid lipid nanoparticles (SLN) as potential carrier for human use: Interaction with human granulocytes. J. Control. Release, 1997, 47(3): p. 261-269.

Wissing, S.A., O. Kayser, and R.H. Muller, Solid lipid nanoparticles for parenteral drug delivery. Adv. Drug Deliv. Rev., 2004, 56(9): p. 1257-1272.

Muller, R.H., K. Mader, and S. Gohla, Solid lipid nanoparticles (SLN) for controlled drug delivery - a review of the state of the art. Eur. J. Pharm. Biopharm., 2000, 50(1): p. 161-177.

Mehnert, W. and K. Mader, Solid lipid nanoparticles - Production, characterization and applications. Adv. Drug Deliv. Rev., 2001, 47(2-3): p. 165-196.

Gasco, M.R., Method for producing solid lipid microspheres having a narrow size distribution, US Patent #5,250,236. 1993

Moghimi, S.M. and J. Szebeni, Stealth liposomes and long circulating nanoparticles: critical issues in pharmacokinetics, opsonization and protein-binding properties. Prog. Lipid Res., 2003, 42(6): p. 463-478.

Gref, R., M. Luck, P. Quellec, M. Marchand, E. Dellacherie, S. Harnisch, T. Blunk, and R.H. Muller, 'Stealth' corona-core nanoparticles surface modified by polyethylene glycol (PEG): influences of the corona (PEG chain length and surface density) and of the core composition on phagocytic uptake and plasma protein adsorption. Colloid Surf. B-Biointerfaces, 2000, 18(3-4): p. 301-313.

Oyler, J., Liquid substances freeze-drying systems and methods, US Patent #5,208,998. 1993

Williams, R.O., K.P. Johnston, T.L. Rogers, M.K. Barron, T.J. Young, Z. Yu, and J. Hu, Process for production of nanoparticles and microparticles by spray freezing into liquid, US Patent #6,862,890. 2003

Overhoff, K., B. Scherzer, E. Elder, K.P. Johnston, and R.O. Williams III. Ultra-rapid Freezing to Micronize Water Insoluble Drugs - A Comparison to Spray Freezing into Liquid. in The Proceedings of the American Association of Pharmaceutical Sciences. 2004. Salt lake city, UT.

Purvis, T., R.O. Williams III, and K.P. Johnston. Rapid Dissolving Repaglinide Powders Produced by Ultra-Rapid Freezing Process. in The Proceedings of the American Association of Pharmaceutical Scientists. 2005. Memphis, TN.

Hu, J.H., K.P. Johnston, and R.O. Williams, Stable amorphous danazol nanostructured powders with rapid dissolution rates produced by spray freezing into liquid. Drug Dev. Ind. Pharm., 2004, 30(7): p. 695-704.

Rogers, T.L., K.P. Johnston, and R.O. Williams, Physical stability of micronized powders produced by spray-freezing into liquid (SFL) to enhance the dissolution of an insoluble drug. Pharm. Dev. Technol., 2003, 8(2): p. 187-197.

Rogers, T.L., K.A. Overhoff, P. Shah, P. Santiago, M.J. Yacaman, K.P. Johnston, and R.O. Williams, Micronized powders of a poorly water soluble drug produced by a spray-freezing into liquid-emulsion process. Eur. J. Pharm. Biopharm., 2003, 55(2): p. 161-172.

Hu, J., K.P. Johnston, and R.O. Williams III, Spray freezing into liquid (SFL) particle engineering technology to enhance dissolution of poorly water soluble drugs: organic solvent versus organic/aqueous co-solvent systems. Eur. J. Pharm. Sci., 2003, 20(3): p. 295-303.

Hu, J.H., T.L. Rogers, J. Brown, T. Young, K.P. Johnston, and R.O. Williams III, Improvement of dissolution rates of poorly water soluble APIs using novel spray freezing into liquid technology. Pharm. Res., 2002, 19(9): p. 1278-1284.

Yu, Z.S., K.P. Johnston, and R.O. Williams, Spray freezing into liquid versus spray-freeze drying: Influence of atomization on protein aggregation and biological activity. Eur. J. Pharm. Sci., 2006, 27(1): p. 9-18.

Rogers, T.L., A.C. Nelsen, M. Sarkari, T.J. Young, K.P. Johnston, and R.O. Williams III, Enhanced aqueous dissolution of a poorly water soluble drug by novel particle engineering technology: Spray-freezing into liquid with atmospheric freeze-drying. Pharm. Res., 2003, 20(3): p. 485-493.

Rogers, T.L., A.C. Nelsen, J. Hu, J.N. Brown, M. Sarkari, T.J. Young, K.P. Johnston, and R.O. Williams III, A novel particle engineering technology to enhance dissolution of poorly water soluble drugs: spray-freezing into liquid. Eur. J. Pharm. Biopharm., 2002, 54(3): p. 271-280.

248

Hu, J., K.P. Johnston, and R.O. Williams III, Rapid dissolving high potency danazol powders produced by spray freezing into liquid process. Int. J. Pharm., 2004, 271(1-2): p. 145-154.

York, P., Strategies for particle design using supercritical fluid technologies. Pharm. Sci. Tech. Today, 1999, 2(11): p. 430-440.

Debenedetti, P.G., J.W. Tom, X. Kwauk, and S.D. Yeo, Rapid Expansion of Supercritical Solutions (Ress) - Fundamentals and Applications. Fluid Phase Equilib., 1993, 82: p. 311-321.

Dixon, D.J., G. Lunabarcenas, and K.P. Johnston, Microcellular Microspheres and Microballoons by Precipitation with a Vapor-Liquid Compressed Fluid Antisolvent. Polymer, 1994, 35(18): p. 3998-4005.

Yeo, S.D., G.B. Lim, P.G. Debenedetti, and H. Bernstein, Formation of Microparticulate Protein Powders Using a Supercritical Fluid Antisolvent. Biotechnol. Bioeng., 1993, 41(3): p. 341-346.

Wang, Y.L., R.N. Dave, and R. Pfeffer, Polymer coating/encapsulation of nanoparticles using a supercritical anti-solvent process. J. Supercrit. Fluids, 2004, 28(1): p. 85-99.

Tsutsumi, A., S. Nakamoto, T. Mineo, and K. Yoshida, A Novel Fluidized-Bed Coating of Fine Particles by Rapid Expansion of Supercritical-Fluid Solutions. Powder Technol., 1995, 85(3): p. 275-278.

Rasenack, N. and B.W. Muller, Dissolution rate enhancement by in situ micronization of poorly water-soluble drugs. Pharm. Res., 2002, 19(12): p. 1894-1900.

Steckel, H., N. Rasenack, P. Villax, and B.W. Muller, In vitro characterization of jet-milled and in-situ-micronized fluticasone-17-propionate. Int. J. Pharm., 2003, 258(1-2): p. 65-75.

Steckel, H., N. Rasenack, and B.W. Muller, In-situ-micronization of disodium cromoglycate for pulmonary delivery. Eur. J. Pharm. Biopharm., 2003, 55(2): p. 173-180.

Crooks, R., M. Joanicot, R.K. Prud'Homme;, and J. Coret, Aqueous suspension of nanoparticles comprising an agrochemical active ingredient, US Patent #6,638,994. 2003

Johnson, B.K. and R.K. Prud'homme, Flash NanoPrecipitation of organic actives and block copolymers using a confined impinging jets mixer. Aust. J. Chem., 2003, 56(10): p. 1021-1024.

Johnson, B.K. and R.K. Prud'homme, Mechanism for rapid self-assembly of block copolymer nanoparticles. Phys. Rev. Lett., 2003, 91(11).

Johnson, B.K. and R.K. Prud'homme, Chemical processing and micromixing in confined impinging jets. Aiche J., 2003, 49(9): p. 2264-2282.

Johnson, B.K., Flash NanoPrecipitation of Organic Actives via Confined Micromixing and Block Copolymer Stabilization, in Chemical Engineering. 2003, Princeton University: Princeton, NJ. p. 363.

Rogers, T.L., I.B. Gillespie, J.E. Hitt, K.L. Fransen, C.A. Crowl, C.J. Tucker, G.B. Kupperblatt, J.N. Becker, D.L. Wilson, C. Todd, and E.J. Elder, Development and characterization of a scalable controlled precipitation process to enhance the dissolution of poorly water-soluble drugs. Pharm. Res., 2004, 21(11): p. 2048-2057.

Schork, F.J., G.W. Poehlein, S. Wang, J. Reimers, J. Rodrigues, and C. Samer, Miniemulsion polymerization. Colloid Surf. A-Physicochem. Eng. Asp., 1999, 153(1-3): p. 39-45.

Antonietti, M. and K. Landfester, Polyreactions in miniemulsions. Prog. Poly. Sci., 2002, 27(4): p. 689-757.

Oyewumi, M.O. and R.J. Mumper, Engineering tumor-targeted gadolinium hexanedione nanoparticles for potential application in neutron capture therapy. Bioconjugate Chem., 2002, 13(6): p. 1328-1335.

Oyewumi, M.O. and R.J. Mumper, Gadolinium-loaded nanoparticles engineered from microemulsion templates. Drug Dev. Ind. Pharm., 2002, 28(3): p. 317-328.

Lockman, P.R., J.M. Koziara, R.J. Mumper, and D.D. Allen, Nanoparticle surface charges alter blood-brain barrier integrity and permeability. J. Drug Target., 2004, 12(9-10): p. 635-641.

Amidon, G.L., H. Lennernas, V.P. Shah, and J.R. Crison, A Theoretical Basis for a Biopharmaceutic Drug Classification - the Correlation of in-Vitro Drug Product Dissolution and in-Vivo Bioavailability. Pharm. Res., 1995, 12(3): p. 413-420.

Brown, C.K., Dissolution Method Development: An Industry Perspective, in Pharmaceutical Dissolution Testing, J.B. Dressman and J. Kramer, Editors. 2005, Taylor & Francis: Boca Raton, FL. p. 351-372.

Hecq, J., M. Deleers, D. Fanara, H. Vranckx, and K. Amighi, Preparation and characterization of nanocrystals for solubility and dissolution rate enhancement of nifedipine. Int. J. Pharm., 2005, 299(1-2): p. 167-177.

Kipp, J.E., The role of solid nanoparticle technology in the parenteral delivery of poorly water-soluble drugs. Int. J. Pharm., 2004, 284(1-2): p. 109-122.

Yoshihashi, Y., H. Kitano, E. Yonemochi, and K. Terada, Quantitative correlation between initial dissolution rate and heat of fusion of drug substance. Int. J. Pharm., 2000, 204(1-2): p. 1-6.

Solans, C., P. Izquierdo, J. Nolla, N. Azemar, and M.J. Garcia-Celma, Nano-emulsions. Curr. Opin. Colloid In., 2005, 10(3-4): p. 102-110.

Tadros, T., R. Izquierdo, J. Esquena, and C. Solans, Formation and stability of nano-emulsions. Adv. Colloid Interface Sci., 2004, 108-09: p. 303-318.

Ponchel, G. and J.M. Irache, Specific and non-specific bioadhesive particulate systems for oral delivery to the gastrointestinal tract. Adv. Drug Deliv. Rev., 1998, 34(2-3): p. 191-219.

Pappo, J. and T.H. Ermak, Uptake and Translocation of Fluorescent Latex-Particles by Rabbit Peyers Patch Follicle Epithelium - a Quantitative Model for M Cell Uptake. Clin. Exp. Immunol., 1989, 76(1): p. 144-148.

Jani, P., G.W. Halbert, J. Langridge, and A.T. Florence, The Uptake and Translocation of Latex Nanospheres and Microspheres after Oral-Administration to Rats. J. Pharm. Pharmacol., 1989, 41(12): p. 809-&.

Loper, A. Poorly soluble compounds: vehicle selection and solubilization. in Land O'Lakes Conference: Drug Metabolism and Pharmacokinetics. 1999.

Merisko-Liversidge, E., G.G. Liversidge, and E.R. Cooper, Nanosizing: a formulation approach for poorly-water-soluble compounds. Eur. J. Pharm. Sci., 2003, 18(2): p. 113-120.

Vaughn, J.M., J.T. McConville, R.O. Williams, and K.P. Johnston, Supersaturation Produces High Bioavailability of Amorphous Danazol Particles Formed by Evaporative Precipitation into Aqueous Solution (EPAS) and Spray Freezing into Liquid(SFL) Technologies. Drug Dev. Ind. Pharm., 2005, In Press.

Hickey, A.J., Delivery of Drugs by the Pulmonary Route, in Modern Pharmaceutics, G.S. Banker and C.T. Rhodes, Editors. 2002, Marcel Dekker, Inc.: New York, NY. p. 479-500.

Dailey, L.A., T. Schmehl, T. Gessler, M. Wittmar, F. Grimminger, W. Seeger, and T. Kissel, Nebulization of biodegradable nanoparticles: impact of nebulizer technology and nanoparticle characteristics on aerosol features. J. Control. Release, 2003, 86(1): p. 131-144.

Sham, J.O.H., Y. Zhang, W.H. Finlay, W.H. Roa, and R. Lobenberg, Formulation and characterization of spray-dried powders containing nanoparticles for aerosol delivery to the lung. Int. J. Pharm., 2004, 269(2): p. 457-467.

Dickinson, P.A., S.W. Howells, and I.W. Kellaway, Novel nanoparticles for pulmonary drug administration. J. Drug. Target., 2001, 9(4): p. 295-302.

Borm, P.J.A. and W. Kreyling, Toxicological hazards of inhaled nanoparticles - Potential implications for drug delivery. J. Nanosci. Nanotechnol., 2004, 4(5): p. 521-531.

McConville, J.T., R.O. Williams, T.C. Carvalho, A.N. Iberg, K.P. Johnston, R.L. Talbert, D. Burgess, and J.I. Peters, Design and evaluation of a restraint-free small animal inhalation dosing chamber. Drug Dev. Ind. Pharm., 2005, 31(1): p. 35-42.

Vaughn, J.M., J.T. McConville, D. Burgess, R.L. Talbert, J.I. Peters, R.O. Williams III, and K.P. Johnston, Single Dose and Multiple Dose studies of Aerosolized Itraconazole Nanoparticles. Eur. J. Pharm. Biopharm., 2005, 63(2): p. 95-102.

Koziara, J.M., P.R. Lockman, D.D. Allen, and R.J. Mumper, In situ blood-brain barrier transport of nanoparticles. Pharm. Res., 2003, 20(11): p. 1772-1778.

Lockman, P.R., M.O. Oyewumi, J.M. Koziara, K.E. Roder, R.J. Mumper, and D.D. Allen, Brain uptake of thiamine-coated nanoparticles. J. Control. Release, 2003, 93(3): p. 271-282.

Weiss, R.B., R.C. Donehower, P.H. Wiernik, T. Ohnuma, R.J. Gralla, D.L. Trump, J.R. Baker, D.A. Vanecho, D.D. Vonhoff, and B. Leylandjones, Hypersensitivity Reactions from Taxol. J. Clin. Oncol., 1990, 8(7): p. 1263-1268.

Evora, C., I. Soriano, R.A. Rogers, K.M. Shakesheff, J. Hanes, and R. Langer, Relating the phagocytosis of microparticles by alveolar macrophages to surface chemistry: the effect of 1,2-dipalmitoylphosphatidylcholine. J. Control. Release, 1998, 51(2-3): p. 143-152.

Hobbs, S.K., W.L. Monsky, F. Yuan, W.G. Roberts, L. Griffith, V.P. Torchilin, and R.K. Jain, Regulation of transport pathways in tumor vessels: Role of tumor type and microenvironment. Proc. Natl. Acad. Sci. U. S. A., 1998, 95(8): p. 4607-4612.

Yuan, F., M. Dellian, D. Fukumura, M. Leunig, D.A. Berk, V.P. Torchilin, and R.K. Jain, Vascular-Permeability in a Human Tumor Xenograft - Molecular-Size Dependence and Cutoff Size. Cancer Res., 1995, 55(17): p. 3752-3756.

Yoo, H.S., K.H. Lee, J.E. Oh, and T.G. Park, In vitro and in vivo anti-tumor activities of nanoparticles based on doxorubicin-PLGA conjugates. J. Control. Release, 2000, 68(3): p. 419-431.

Chen, D.B., T.Z. Yang, W.L. Lu, and Q. Zhang, In vitro and in vivo study of two types of long-circulating solid lipid nanoparticles containing paclitaxel. Chem. Pharm. Bull., 2001, 49(11): p. 1444-1447.

Fundaro, A., R. Cavalli, A. Bargoni, D. Vighetto, G.P. Zara, and M.R. Gasco, Non-stealth and stealth solid lipid nanoparticles (SLN) carrying doxorubicin: Pharmacokinetics and tissue distribution after i.v. administration to rats. Pharmacol. Res., 2000, 42(4): p. 337-343.

Feng, S.S. and S. Chien, Chemotherapeutic engineering: Application and further development of chemical engineering principles for chemotherapy of cancer and other diseases. Chem. Eng. Sci., 2003, 58(18): p. 4087-4114.

Brannon-Peppas, L. and J.O. Blanchette, Nanoparticle and targeted systems for cancer therapy. Adv. Drug Deliv. Rev., 2004, 56(11): p. 1649-1659.

254

Kohler, G. and C. Milstein, Continuous Cultures of Fused Cells Secreting Antibody of Predefined Specificity. Nature, 1975, 256(5517): p. 495-497.

Cortez-Retamozo, V., N. Backmann, P.D. Senter, U. Wernery, P. De Baetselier, S. Muyldermans, and H. Revets, Efficient cancer therapy with a nanobody-based conjugate. Cancer Res., 2004, 64(8): p. 2853-2857.

Xu, Z.H., W.W. Gu, J. Huang, H. Sui, Z.H. Zhou, Y.X. Yang, Z. Yan, and Y.P. Li, In vitro and in vivo evaluation of actively targetable nanoparticles for paclitaxel delivery. Int. J. Pharm., 2005, 288(2): p. 361-368.

Schiffelers, R.M., A. Ansari, J. Xu, Q. Zhou, Q.Q. Tang, G. Storm, G. Molema, P.Y. Lu, P.V. Scaria, and M.C. Woodle, Cancer siRNA therapy by tumor selective delivery with ligand-targeted sterically stabilized nanoparticle. Nucleic Acids Res., 2004, 32(19).

Chellat, F., Y. Merhi, A. Moreau, and L. Yahia, Therapeutic potential of nanoparticulate systems for macrophage targeting. Biomaterials, 2005, 26(35): p. 7260-7275.

Pinto-Alphandary, H., A. Andremont, and P. Couvreur, Targeted delivery of antibiotics using liposomes and nanoparticles: research and applications. Int. J. Antimicrob. Agents, 2000, 13(3): p. 155-168.

Makino, K., N. Yamamoto, K. Higuchi, N. Harada, H. Ohshima, and H. Terada, Phagocytic uptake of polystyrene microspheres by alveolar macrophages: effects of the size and surface properties of the microspheres. Colloid Surf. B-Biointerfaces, 2003, 27(1): p. 33-39.

Bocca, C., O. Caputo, R.B. Cavalli, L. Gabriel, A. Miglietta, and M.R. Gasco, Phagocytic uptake of fluorescent stealth and non-stealth solid lipid nanoparticles. Int. J. Pharm., 1998, 175(2): p. 185-193.

Salamat-Miller, N., M. Chittchang, and T.P. Johnston, The use of mucoadhesive polymers in buccal drug delivery. Adv. Drug Deliv. Rev., 2005, 57(11): p. 1666-1691.

Takeuchi, H., H. Yamamoto, and Y. Kawashima, Mucoadhesive nanoparticulate systems for peptide drug delivery. Adv. Drug Deliv. Rev., 2001, 47(1): p. 39-54.

Takeuchi, H., Y. Matsui, H. Sugihara, H. Yamamoto, and Y. Kawashima, Effectiveness of submicron-sized, chitosan-coated liposomes in oral administration of peptide drugs. Int. J. Pharm., 2005, 303(1-2): p. 160-170.

Ponchel, G., M.J. Montisci, A. Dembri, C. Durrer, and D. Duchene, Mucoadhesion of colloidal particulate systems in the gastro-intestinal tract. Eur. J. Pharm. Biopharm., 1997, 44(1): p. 25-31.

Maertens, J. and M. Boogaerts, The place for itraconazole in treatment. J. Antimicrob. Chemother., 2005, 56: p. 33-38.

Chiller, T.M. and D.A. Stevens, Treatment strategies for Aspergillus infections. Drug Resist. Update, 2000, 3(2): p. 89-97.

Lin, S.J., J. Schranz, and S.M. Teutsch, Aspergillosis case - Fatality rate: Systematic review of the literature. Clin. Infect. Dis., 2001, 32(3): p. 358-366.

Denning, D.W., Therapeutic outcome in invasive aspergillosis. Clin. Infect. Dis., 1996, 23(3): p. 608-615.

Heeres, J. and L.J.J. Backx, Heterocyclic derivatives of (4-phenylpiperazin-1-yl-aryloxymethyl-1,3-dioxolan-2-yl)methyl-1H-imidaz oles and 1H-1,2,4-triazoles, US Patent #U.S. Patent 4,267,179. 1981

Peeters, J., P. Neeskens, J.P. Tollenaere, P.V. Remoortere, and M.E. Brewster, Characterization of the Interaction of 2-Hydroxypropyl-bcyclodextrin with Itraconazole at pH 2, 4, and 7. J. Pharm. Sci., 2002, 91(6): p. 1414-1422.

Rogers, T.L., K.A. Overhoff, P. Shah, P. Santiago, M.J. Yacaman, K.P. Johnston, and R.O. Williams, Micronized powders of a poorly water soluble drug produced by a spray-freezing into liquid-emulsion process. Eur. J. Pharm. Biopharm., 2003, 55(2): p. 161-172.

Vaughn, J.M., J.T. McConville, D. Burgess, R.L. Talbert, J.I. Peters, R.O. Williams III, and K.P. Johnston, Single Dose and Multiple Dose studies of Aerosolized Itraconazole Nanoparticles. Eur. J. Pharm. Biopharm., 2005, 63(2): p. 95-102.

Yoo, S.D., E. Kang, B.S. Shin, H. Jun, S.H. Lee, K.C. Lee, and K.H. Lee, Interspecies comparison of the oral absorption of itraconazole in laboratory animals. Arch. Pharm. Res., 2002, 25(3): p. 387-391.

Yoo, S.D., S.H. Lee, E.H. Kang, H. Jun, J.Y. Jung, J.W. Park, and K.H. Lee, Bioavailability of itraconazole in rats and rabbits after administration of tablets containing solid dispersion particles. Drug Dev. Ind. Pharm., 1999, 26(1): p. 27-34.

Terada, K., H. Kitano, Y. Yoshihashi, and E. Yonemochi, Quantitative correlation between initial dissolution rate and heat of solution of drug. Pharm. Res., 2000, 17(8): p. 920-924.

Hancock, B.C. and M. Parks, What is the true solubility advantage for amorphous pharmaceuticals? Pharm. Res., 2000, 17(4): p. 397-404.

Vaughn, J.M., J.T. McConville, M.T. Crisp, R.O. Williams III, and K.P. Johnston, Supersaturation Produces High Bioavailability of Amorphous Danazol Particles Formed by Evaporative Precipitation into Aqueous Solution (EPAS) and Spray Freezing into Liquid(SFL) Technologies. Drug Dev. Ind. Pharm., 2006, 32(5): p. 559-567.

Engstrom, J., D. Simpson, E. Lai, R.O. Williams, and K.P. Johnston, Morphology of Protein Particles Produced by Spray Freezing of Concentrated Solutions. Eur. J. Pharm. Biopharm., 2006, In Press.

Sinswat, P., X. Gao, M.J. Yacaman, R.O. Williams III, and K.P. Johnston, Stabilizer choice for rapid dissolving high potency itraconazole particles formed by evaporative precipitation into aqueous solution. Int. J. Pharm., 2005, 302(1-2): p. 113-124.

Chen, X., Z. Benhayoune, R.O. Williams III, and K.P. Johnston, Rapid dissolution of high potency itraconazole particles produced by evaporative precipitation into aqueous solution. J. Drug Deliv. Sci. Technol., 2004, 14(4): p. 299-304.

Hu, J.H., K.P. Johnston, and R.O. Williams, Stable amorphous danazol nanostructured powders with rapid dissolution rates produced by spray freezing into liquid. Drug Dev. Ind. Pharm., 2004, 30(7): p. 695-704.

Jung, J.-Y., S.D. Yoo, S.-H. Lee, K.-H. Kim, D.-S. Yoon, and K.-H. Lee, Enhanced solubility and dissolution rate of itraconazole by a solid dispersion technique. 1999, 187: p. 209-218.

Kapsi, S.G. and J.W. Ayres, Processing factors in development of solid solution formulation of itraconazole for enhancement of drug dissolution and bioavailability. Int. J. Pharm., 2001, 229(1-2): p. 193-203.

Verreck, G., K. Six, G. Van den Mooter, L. Baert, J. Peeters, and M.E. Brewster, Characterization of solid dispersions of itraconazole and hydroxypropylmethylcellulose prepared by melt extrusion--part I. 2003, 251(1-2): p. 165-174.

Lipinski, C., Poor aqueous solubility - an industry wide problem in drug discovery. Am. Pharm. Rev., 2002, 5: p. 82-85.

Date, A.A. and V.B. Patravale, Current strategies for engineering drug nanoparticles. Curr. Opin. Colloid Interface Sci., 2004, 9(3-4): p. 222-235.

Muller, R.H., K. Mader, and S. Gohla, Solid lipid nanoparticles (SLN) for controlled drug delivery - a review of the state of the art. Eur. J. Pharm. Biopharm., 2000, 50(1): p. 161-177.

Soppimath, K.S., T.M. Aminabhavi, A.R. Kulkarni, and W.E. Rudzinski, Biodegradable polymeric nanoparticles as drug delivery devices. J. Control. Release, 2001, 70(1-2): p. 1-20.

Vaughn, J.M. and R.O. Williams, Nanoparticle Engineering, in Encyclopedia of Pharmaceutical Technology, J. Swarbrick, Editor. In Press, Dekker.

Rasenack, N. and B.W. Muller, Micron-size drug particles: Common and novel micronization techniques. Pharm. Dev. Technol., 2004, 9(1): p. 1-13.

Hu, J.H., K.P. Johnston, and R.O. Williams III, Nanoparticle engineering processes for enhancing the dissolution rates of poorly water soluble drugs - a review. Drug Dev. Ind. Pharm., 2004, 30(3): p. 247-258.

Leuenberger, H., Spray freeze-drying - the process of choice for low water soluble drugs? J. Nanopart. Res., 2002, 4(1-2): p. 111-119.

Maa, Y.F., P.A. Nguyen, T. Sweeney, S.J. Shire, and C.C. Hsu, Protein inhalation powders: Spray drying vs spray freeze drying. Pharm. Res., 1999, 16(2): p. 249-254.

Rogers, T.L., K.P. Johnston, and R.O. Williams, Solution-based particle formation of pharmaceutical powders by supercritical or compressed fluid CO_2 and cryogenic spray-freezing technologies. Drug Dev. Ind. Pharm., 2001, 27(10): p. 1003-1015.

Vaughn, J.M., X.X. Gao, M.J. Yacaman, K.P. Johnston, and R.O. Williams, Comparison of powder produced by evaporative precipitation into aqueous solution (EPAS) and spray freezing into liquid (SFL) technologies using novel Z-contrast STEM and complimentary techniques. Eur. J. Pharm. Biopharm., 2005, 60(1): p. 81-89.

Hu, J., K.P. Johnston, and R.O. Williams III, Spray freezing into liquid (SFL) particle engineering technology to enhance dissolution of poorly water soluble drugs: organic solvent versus organic/aqueous co-solvent systems. Eur. J. Pharm. Sci., 2003, 20(3): p. 295-303.

Rogers, T.L., K.A. Overhoff, P. Shah, P. Santiago, M.J. Yacaman, K.P. Johnston, and R.O. Williams, Micronized powders of a poorly water soluble drug produced by a spray-freezing into liquid-emulsion process. Eur. J. Pharm. Biopharm., 2003, 55(2): p. 161-172.

Hu, J., K.P. Johnston, and R.O. Williams III, Rapid dissolving high potency danazol powders produced by spray freezing into liquid process. Int. J. Pharm., 2004, 271(1-2): p. 145-154.

Evans, J.C., B.D. Scherzer, C.D. Tocco, G.B. Kupperblatt, J.N. Becker, D.L. Wilson, S.A. Saghir, and E.J. Elder, Preparation of Nanostructured Particles of Poorly Water Soluble Drugs via a Novel Ultr-Rapid Freezing Technology, in Polymeric Drug Delivery Volume II - Polymeric Matrices and Drug Particle Engineering, S. Svenson, Editor. In Press, American Chemical Society: Washington D.C.

Ni, N., M. Tesconi, E.S. Tabibi, S. Gupta, and S.H. Yalkowsky, Use of pure t-butanol as a solvent for freeze-drying: a case study. Int. J. Pharm., 2001, 226(1-2): p. 39-46.

Tesconi, M.S., K. Sepassi, and S.H. Yalkowsky, Freeze-drying above room temperature. J. Pharm. Sci., 1999, 88(5): p. 501-506.

260

Brunauer, S., P.H. Emmett, and E. Teller, Adsorption of gases in multimolecular layers. J. Am. Chem. Soc., 1938, 60: p. 309-319.

Fukai, J., T. Ozaki, H. Asami, and O. Miyatake, Numerical simulation of liquid droplet solidification on substrates. J. Chem. Eng. Jpn., 2000, 33(4): p. 630-637.

Bennett, T. and D. Poulikakos, Splat-Quench Solidification - Estimating the Maximum Spreading of a Droplet Impacting a Solid-Surface. J. Mater. Sci., 1993, 28(4): p. 963-970.

Kang, B., Z. Zhao, and D. Poulikakos, Solidification of Liquid-Metal Droplets Impacting Sequentially on a Solid-Surface. J. Heat Transf.-Trans. ASME, 1994, 116(2): p. 436-445.

Madejski, J., Solidification of Droplets on a Cold Surface. Int. J. Heat Mass Transf., 1976, 19(9): p. 1009-1013.

Pasandideh-Fard, M., R. Bhola, S. Chandra, and J. Mostaghimi, Deposition of tin droplets on a steel plate : simulations and experiments. Int. J. Heat Mass Transfer, 1998, 41: p. 2929-2945.

Pasandideh-Fard, M., S. Chandra, and J. Mostaghimi, A three-dimensional model of droplet impact and solidification. Int. J. Heat Mass Transfer, 2002, 45: p. 2229-2242.

Sanmarchi, C., H. Liu, E.J. Lavernia, R.H. Rangel, A. Sickinger, and E. Muehlberger, Numerical-Analysis of the Deformation and Solidification of a Single Droplet Impinging onto a Flat Substrate. J. Mater. Sci., 1993, 28(12): p. 3313-3321.

Sivakumar, D. and H. Nishiyama, Numerical analysis on the impact behavior of molten metal droplets using a modified splat-quench solidification model. J. Heat Transf.-Trans. ASME, 2004, 126(6): p. 1014-1022.

Trapaga, G. and J. Szekely, Mathematical-Modeling of the Isothermal Impingement of Liquid Droplets in Spraying Processes. Metall. Trans. B, 1991, 22(6): p. 901-914.

Wang, G.X. and E.F. Matthys, Modeling of Heat-Transfer and Solidification During Splat Cooling - Effect of Splat Thickness and Splat Substrate Thermal Contact. Int. J. Rapid Solidif., 1991, 6(2): p. 141-174.

Wang, G.X. and E.F. Matthys, Numerical Modeling of Phase-Change and Heat-Transfer During Rapid Solidification Processes - Use of Control Volume Integrals with Element Subdivision. Int. J. Heat Mass Transf., 1992, 35(1): p. 141-153.

Zhang, H., X.Y. Wang, L.L. Zheng, and X.Y. Jiang, Studies of splat morphology and rapid solidification during thermal spraying. Int. J. Heat Mass Transf., 2001, 44(24): p. 4579-4592.

Zhao, Z., D. Poulikakos, and J. Fukai, Heat transfer and fluid dynamics during the collision of a liquid droplet on a substrate .2. Experiments. Int. J. Heat Mass Transf., 1996, 39(13): p. 2791-2802.

Zhao, Z., D. Poulikakos, and J. Fukai, Heat transfer and fluid dynamics during the collision of a liquid droplet on a substrate .1. Modeling. Int. J. Heat Mass Transf., 1996, 39(13): p. 2771-2789.

Carslaw, H.S. and J.C. Jaeger, Conduction of Heat in Solids. 1959, Oxford University Press: London.

Bennett, T. and D. Poulikakos, Heat-Transfer Aspects of Splat-Quench Solidification - Modeling and Experiment. J. Mater. Sci., 1994, 29(8): p. 2025-2039.

Hancock, B.C. and M. Parks, What is the true solubility advantage for amorphous pharmaceuticals? Pharm. Res., 2000, 17(4): p. 397-404.

Terada, K., H. Kitano, Y. Yoshihashi, and E. Yonemochi, Quantitative correlation between initial dissolution rate and heat of solution of drug. Pharm. Res., 2000, 17(8): p. 920-924.

Gao, C.Y., A. Li, L.X. Feng, X.S. Yi, and J.C. Shen, Factors controlling surface morphology of porous polystyrene membranes prepared by thermally induced phase separation. Polym. Int., 2000, 49(4): p. 323-328.

Nam, Y.S. and T.G. Park, Porous biodegradable polymeric scaffolds prepared by thermally induced phase separation. J. Biomed. Mater. Res., 1999, 47(1): p. 8-17.

Peters, D.H., A. Fitton, G.L. Plosker, and D. Faulds, Tacrolimus - a Review of Its Pharmacology, and Therapeutic Potential in Hepatic and Renal-Transplantation. Drugs, 1993, 46(4): p. 746-794.

Jusko, W.J., W. Piekoszewski, G.B. Klintmalm, M.S. Shaefer, M.F. Hebert, A.A. Piergies, C.C. Lee, P. Schechter, and Q.A. Mekki, Pharmacokinetics of Tacrolimus in Liver-Transplant Patients. Clin. Pharmacol. Ther., 1995, 57(3): p. 281-290.

Lampen, A., U. Christians, F.P. Guengerich, P.B. Watkins, J.C. Kolars, A. Bader, A.K. Gonschior, H. Dralle, I. Hackbarth, and K.F. Sewing, Metabolism of the immunosuppressant tacrolimus in the small intestine: Cytochrome P450, drug interactions, and interindividual variability. Drug Metab. Dispos., 1995, 23(12): p. 1315-1324.

Mancinelli, L.M., L. Frassetto, L.C. Floren, D. Dressler, S. Carrier, I. Bekersky, L.Z. Benet, and U. Christians, The pharmacokinetics and metabolic disposition of tacrolimus: A comparison across ethnic groups. Clin. Pharmacol. Ther., 2001, 69(1): p. 24-31.

Wallemacq, P.E. and R.K. Verbeeck, Comparative clinical pharmacokinetics of tacrolimus in paediatric and adult patients. Clin. Pharmacokinet., 2001, 40(4): p. 283-295.

Venkataramanan, R., A. Swaminathan, T. Prasad, A. Jain, S. Zuckerman, V. Warty, J. McMichael, J. Lever, G. Burckart, and T. Starzl, Clinical pharmacokinetics of tacrolimus. Clin. Pharmacokinet., 1995, 29(6): p. 404-430.

Jacobson, P.A., C.E. Johnson, N.J. West, and J.A. Foster, Stability of tacrolimus in an extemporaneously compounded oral liquid. Am. J. Health-Syst. Pharm., 1997, 54(2): p. 178-180.

Yamashita, K., T. Nakate, K. Okimoto, A. Ohike, Y. Tokunaga, R. Ibuki, K. Higaki, and T. Kimura, Establishment of new preparation method for solid dispersion formulation of tacrolimus. Int. J. Pharm., 2003, 267(1-2): p. 79-91.

Arima, H., K. Yunomae, F. Hirayama, and K. Uekama, Contribution of P-glycoprotein to the enhancing effects of dimethyl-beta-cyclodextrin on oral bioavailability of tacrolimus. J. Pharmacol. Exp. Ther., 2001, 297(2): p. 547-555.

Arima, H., K. Yunomae, K. Miyake, T. Irie, F. Hirayama, and K. Uekama, Comparative studies of the enhancing effects of cyclodextrins on the solubility and oral bioavailability of tacrolimus in rats. J. Pharm. Sci., 2001, 90(6): p. 690-701.

Lee, M.J., R.M. Straubinger, and W.J. Jusko, Physicochemical, Pharmacokinetic and Pharmacodynamic Evaluation of Liposomal Tacrolimus (Fk-506) in Rats. Pharm. Res., 1995, 12(7): p. 1055-1059.

Moffatt, S.D., V. McAlister, R.Y. Calne, and S.M. Metcalfe, Potential for improved therapeutic index of FK506 in liposomal formulation demonstrated in a mouse cardiac allograft model. Transplantation, 1999, 67(9): p. 1205-1208.

264

Canadas, O., R. Guerrero, R. Garcia-Canero, G. Orellana, M. Menendez, and C. Casals, Characterization of liposomal tacrolimus in lung surfactant-like phospholipids and evaluation of its immunosuppressive activity. Biochemistry, 2004, 43(30): p. 9926-9938.

Egawa, H., S. Maeda, E. Yonemochi, T. Oguchi, K. Yamamoto, and Y. Nakai, Solubility Parameter and Dissolution Behavior of Cefalexin Powders with Different Crystallinity. Chem. Pharm. Bull., 1992, 40(3): p. 819-820.

Sato, T., A. Okada, K. Sekiguchi, and Y. Tsuda, Difference in Physico-Pharmaceutical Properties between Crystalline and Noncrystalline 9,3"-Diacetylmidecamycin. Chem. Pharm. Bull., 1981, 29(9): p. 2675-2682.

Imaizumi, H., N. Nambu, and T. Nagai, Pharmaceutical Interaction in Dosage Forms and Processing .18. Stability and Several Physical-Properties of Amorphous and Crystalline Forms of Indomethacin. Chem. Pharm. Bull., 1980, 28(9): p. 2565-2569.

Gao, P., M.E. Guyton, T.H. Huang, J.M. Bauer, K.J. Stefanski, and Q. Lu, Enhanced oral bioavailability of a poorly water soluble drug PNU-91325 by supersaturatable formulations. Drug Dev. Ind. Pharm., 2004, 30(2): p. 221-229.

Raghavan, S.L., B. Kiepfer, A.F. Davis, S.G. Kazarian, and J. Hadgraft, Membrane transport of hydrocortisone acetate from supersaturated solutions; the role of polymers. Int. J. Pharm., 2001, 221(1-2): p. 95-105.

Raghavan, S.L., A. Trividic, A.F. Davis, and J. Hadgraft, Effect of cellulose polymers on supersaturation and in vitro membrane transport of hydrocortisone acetate. Int. J. Pharm., 2000, 193(2): p. 231-237.

Hu, J.H., K.P. Johnston, and R.O. Williams, Stable amorphous danazol nanostructured powders with rapid dissolution rates produced by spray freezing into liquid. Drug Dev. Ind. Pharm., 2004, 30(7): p. 695-704.

Vaughn, J.M., J.T. McConville, M.T. Crisp, R.O. Williams III, and K.P. Johnston, Supersaturation Produces High Bioavailability of Amorphous Danazol Particles Formed by Evaporative Precipitation into Aqueous Solution (EPAS) and Spray Freezing into Liquid(SFL) Technologies. Drug Dev. Ind. Pharm., 2006, 32(5): p. 559-567.

Overhoff, K.A., K.P. Johnston, and R.O. Williams, Improvement of Dissolution Rate of Poorly Water Soluble Drugs Using a New Particle Engineering Process: Spray Freezing into Liquid, in Polymeric Drug Delivery II: Polymeric Matrices and Drug Particle Engineering, S. Svenson, Editor. 2006, American Chemical Society: Washington D.C. p. 305-319.

Overhoff, K.A., J. Engstrom, B. Chen, B. Scherzer, T.E. Milner, K.P. Johnston, and R.O. Williams, Novel Ultra-rapid Freezing Particle Engineering Process for Enhancement of Dissolution Rates of Poorly Water Soluble Drugs. Eur. J. Pharm. Biopharm., 2006, In Press.

Rogers, T.L., J.H. Hu, Z.S. Yu, K.P. Johnston, and R.O. Williams III, A novel particle engineering technology: spray-freezing into liquid. Int. J. Pharm., 2002, 242(1-2): p. 93-100.

Vaughn, J.M., J.T. McConville, D. Burgess, R.L. Talbert, J.I. Peters, R.O. Williams III, and K.P. Johnston, Single Dose and Multiple Dose studies of Aerosolized Itraconazole Nanoparticles. Eur. J. Pharm. Biopharm., 2005, 63(2): p. 95-102.

Megrab, N.A., A.C. Williams, and B.W. Barry, Estradiol Permeation through Human Skin and Silastic Membrane - Effects of Propylene-Glycol and Supersaturation. J. Control. Release, 1995, 36(3): p. 277-294.

Sung, M.H., J.S. Kim, W.S. Kim, and I. Hirasawa, Modification of crystal growth mechanism of yttrium oxalate in metastable solution. J. Cryst. Growth, 2002, 235(1-4): p. 529-540.

Law, S.L. and J.B. Kayes, Adsorption of Non-Ionic Water-Soluble Cellulose Polymers at the Solid Water Interface and Their Effect on Suspension Stability. Int. J. Pharm., 1983, 15(3): p. 251-260.

Raghavan, S.L., A. Trividic, A.F. Davis, and J. Hadgraft, Crystallization of hydrocortisone acetate: influence of polymers. Int. J. Pharm., 2001, 212(2): p. 213-221.

Usui, F., K. Maeda, A. Kusai, K. Nishimura, and K. Yamamoto, Inhibitory effects of water-soluble polymers on precipitation of RS-8359. Int. J. Pharm., 1997, 154(1): p. 59-66.

Suzuki, H. and H. Sunada, Influence of water-soluble polymers on the dissolution of nifedipine solid dispersions with combined carriers. Chem. Pharm. Bull., 1998, 46(3): p. 482-487.

Mackellar, A.J., G. Buckton, J.M. Newton, and C.A. Orr, The Controlled Crystallization of a Model Powder .2. Investigation into the Mechanism of Action of Poloxamers in Changing Crystal Properties. Int. J. Pharm., 1994, 112(1): p. 79-85.

Ueda, K., K. Shimojo, T. Shimazaki, I. Kado, and K. Honbo, Solid Dispersion of FR-900506 substance, US Patent #US4,916,138. 1990

Nishikawa, T., H. Hasumi, S. Suzuki, H. Kubo, and H. Ohtani, Kinetic-Analysis of Molecular Interconversion of Immunosuppressant Fk506 by High-Performance Liquid-Chromatography. Pharm. Res., 1993, 10(12): p. 1785-1789.

Brunauer, S., P.H. Emmett, and E. Teller, Adsorption of gases in multimolecular layers. J. Am. Chem. Soc., 1938, 60: p. 309-319.

Dietemann, J., P. Berthoux, J.P. Gay-Montchamp, M. Batie, and F. Berthoux, Comparison of ELISA method versus MEIA method for daily practice in the therapeutic monitoring of tacrolimus. Nephrol. Dial. Transplant., 2001, 16(11): p. 2246-2249.

Chutimaworapan, S., G.C. Ritthidej, E. Yonemochi, T. Oguchi, and K. Yamamoto, Effect of water-soluble carriers on dissolution characteristics of nifedipine solid dispersions. Drug Dev. Ind. Pharm., 2000, 26(11): p. 1141-1150.

McConville, J.T., K.A. Overhoff, P. Sinswat, J.M. Vaughn, B.L. Frei, D.S. Burgess, R.L. Talbert, J.I. Peters, K.P. Johnston, and R.O. Williams, Targeted high lung concentrations of itraconazole using nebulized dispersions in a murine model. Pharm. Res., 2006, 23(5): p. 901-911.

Tamura, S., A. Ohike, R. Ibuki, G.L. Amidon, and S. Yamashita, Tacrolimus is a class II low-solubility high-permeability drug: The effect of P-glycoprotein efflux on regional permeability of tacrolimus in rats. J. Pharm. Sci., 2002, 91(3): p. 719-729.

Dutkiewicz, E. and A. Jakubowska, Effect of electrolytes on the physicochemical behaviour of sodium dodecyl sulphate micelles. Colloid Polym. Sci., 2002, 280(11): p. 1009-1014.

268

Khutoryanskiy, V.V., G.A. Mun, Z.S. Nurkeeva, and A.V. Dubolazov, pH and salt effects on interpolymer complexation via hydrogen bonding in aqueous solutions. Polym. Int., 2004, 53(9): p. 1382-1387.

Pandit, N., T. Trygstad, S. Croy, M. Bohorquez, and C. Koch, Effect of Salts on the Micellization, Clouding, and Solubilization Behavior of Pluronic F127 Solutions. J. Colloid Interface. Sci., 2000, 222(2): p. 213-220.

Benet, L.Z., T. Izumi, Y.C. Zhang, J.A. Silverman, and V.J. Wacher, Intestinal MDR transport proteins and P-450 enzymes as barriers to oral drug delivery. J. Control. Release, 1999, 62(1-2): p. 25-31.

Hashimoto, Y., H. Sasa, M. Shimomura, and K. Inui, Effects of intestinal and hepatic metabolism on the bioavailability of tacrolimus in rats. Pharm. Res., 1998, 15(10): p. 1609-1613.

Yokogawa, K., M. Takahashi, I. Tamai, H. Konishi, M. Nomura, S. Moritani, K. Miyamoto, and A. Tsuji, P-glycoprotein-dependent disposition kinetics of tacrolimus: Studies in mdr1a knockout mice. Pharm. Res., 1999, 16(8): p. 1213-1218.

Chiou, W.L., S.M. Chung, and T.C. Wu, Apparent lack of effect of P-glycoprotein on the gastrointestinal absorption of a substrate, tacrolimus, in normal mice. Pharm. Res., 2000, 17(2): p. 205-208.

Saitoh, H., Y. Saikachi, M. Kobayashi, M. Yamaguchi, M. Oda, Y. Yuhki, K. Achiwa, K. Tadano, Y. Takahashi, and B.J. Aungst, Limited interaction between tacrolimus and P-glycoprotein in the rat small intestine. Eur. J. Pharm. Sci., 2006, 28(1-2): p. 34-42.

Kagayama, A., S. Tanimoto, J. Fujisaki, A. Kaibara, K. Ohara, K. Iwasaki, Y. Hirano, and T. Hata, Oral Absorption of Fk506 in Rats. 1993, 10(10): p. 1446-1450.

269

Lin, J.H., Species Similarities and Differences in Pharmacokinetics. Drug Metab. Dispos., 1995, 23(10): p. 1008-1021.

Peeters, J., P. Neeskens, J.P. Tollenaere, P.V. Remoortere, and M.E. Brewster, Characterization of the Interaction of 2-Hydroxypropyl-bcyclodextrin with Itraconazole at pH 2, 4, and 7. J. Pharm. Sci., 2002, 91(6): p. 1414-1422.

Mayersohn, M., Principles of Drug Absorption, in Modern Pharmaceutics, G.S. Banker and C.T. Rhodes, Editors. 2002, Marcel Dekker, Inc.: New York, NY. p. 23-66.

Sherwood, L., Human Physiology: From Cells to Systems. Fifth ed. 2004, Belmont, CA: Thomson Learning

Yoshihashi, Y., H. Kitano, E. Yonemochi, and K. Terada, Quantitative correlation between initial dissolution rate and heat of fusion of drug substance. Int. J. Pharm., 2000, 204(1-2): p. 1-6.

Hancock, B.C. and M. Parks, What is the true solubility advantage for amorphous pharmaceuticals? Pharm. Res., 2000, 17(4): p. 397-404.

Yamashita, K., T. Nakate, K. Okimoto, A. Ohike, Y. Tokunaga, R. Ibuki, K. Higaki, and T. Kimura, Establishment of new preparation method for solid dispersion formulation of tacrolimus. Int. J. Pharm., 2003, 267(1-2): p. 79-91.

Sato, T., A. Okada, K. Sekiguchi, and Y. Tsuda, Difference in Physico-Pharmaceutical Properties between Crystalline and Noncrystalline 9,3"-Diacetylmidecamycin. Chem. Pharm. Bull., 1981, 29(9): p. 2675-2682.

Raghavan, S.L., B. Kiepfer, A.F. Davis, S.G. Kazarian, and J. Hadgraft, Membrane transport of hydrocortisone acetate from supersaturated solutions; the role of polymers. Int. J. Pharm., 2001, 221(1-2): p. 95-105.

Raghavan, S.L., A. Trividic, A.F. Davis, and J. Hadgraft, Crystallization of hydrocortisone acetate: influence of polymers. Int. J. Pharm., 2001, 212(2): p. 213-221.

Sung, M.H., J.S. Kim, W.S. Kim, and I. Hirasawa, Modification of crystal growth mechanism of yttrium oxalate in metastable solution. J. Cryst. Growth, 2002, 235(1-4): p. 529-540.

Mackellar, A.J., G. Buckton, J.M. Newton, and C.A. Orr, The Controlled Crystallization of a Model Powder .2. Investigation into the Mechanism of Action of Poloxamers in Changing Crystal Properties. Int. J. Pharm., 1994, 112(1): p. 79-85.

Suzuki, H. and H. Sunada, Influence of water-soluble polymers on the dissolution of nifedipine solid dispersions with combined carriers. Chem. Pharm. Bull., 1998, 46(3): p. 482-487.

Hasegawa, A., H. Nakagawa, and I. Sugimoto, Solid Dispersion Obtained from Nifedipine and Enteric Coating Agent .1. Dissolution Behavior. Yakugaku Zasshi-J. Pharm. Soc. Jpn., 1984, 104(5): p. 485-489.

Hasegawa, A., M. Taguchi, R. Suzuki, T. Miyata, H. Nakagawa, and I. Sugimoto, Supersaturation Mechanism of Drugs from Solid Dispersions with Enteric Coating Agents. Chem. Pharm. Bull., 1988, 36(12): p. 4941-4950.

Varshosaz, J., R.A. Kennedy, and E.M. Gipps, Use of enteric polymers for production of microspheres by extrusion-spheronization. 1997, 72(3): p. 145-152.

Nakamichi, K., T. Nakano, H. Yasuura, S. Izumi, and Y. Kawashima, The role of the kneading paddle and the effects of screw revolution speed and water content on the preparation of solid dispersions using a twin-screw extruder. Int. J. Pharm., 2002, 241(2): p. 203-211.

271

Sertsou, G., J. Butler, J. Hempenstall, and T. Rades, Physical stability and enthalpy relaxation of drug-hydroxypropyl methylcellulose phthalate solvent change co-precipitates. J. Pharm. Pharmacol., 2003, 55(1): p. 35-41.

Kohri, N., Y. Yamayoshi, H. Xin, K. Iseki, N. Sato, S. Todo, and K. Miyazaki, Improving the oral bioavailability of albendazole in rabbits by the solid dispersion technique. J. Pharm. Pharmacol., 1999, 51(2): p. 159-164.

Kondo, N., T. Iwao, K. Hirai, M. Fukuda, K. Yamanouchi, K. Yokoyama, M. Miyaji, Y. Ishihara, K. Kon, Y. Ogawa, and T. Mayumi, Improved Oral Absorption of Enteric Coprecipitates of a Poorly Soluble Drug. J. Pharm. Sci., 1994, 83(4): p. 566-570.

Takeuchi, H., T. Handa, and Y. Kawashima, Spherical Solid Dispersion Containing Amorphous Tolbutamide Embedded in Enteric Coating Polymers or Colloidal Silica Prepared by Spray-Drying Technique. Chem. Pharm. Bull., 1987, 35(9): p. 3800-3806.

Eerikainen, H., L. Peltonen, J. Raula, J. Hirvonen, and E.I. Kauppinen, Nanoparticles containing ketoprofen and acrylic polymers prepared by an aerosol flow reactor method. AAPS PharmSciTech, 2004, 5(4).

Kai, T., Y. Akiyama, S. Nomura, and M. Sato, Oral absorption improvement of poorly soluble drug using solid dispersion technique. Chem. Pharm. Bull., 1996, 44(3): p. 568-571.

Rowe, R.C., P.J. Sheskey, and P.J. Weller, eds. Handbook of pharmaceutical excipients. 4th ed. 2003, Pharmaceutical Press: London.

Craig, D.Q.M., The mechanisms of drug release from solid dispersions in water-soluble polymers. Int. J. Pharm., 2002, 231(2): p. 131-144.

272

Six, K., C. Leuner, J. Dressman, G. Verreck, J. Peeters, N. Blaton, P. Augustijns, R. Kinget, and G. Van den Mooter, Thermal properties of hot-stage extrudates of itraconazole and eudragit E100 - Phase separation and polymorphism. J. Therm. Anal., 2002, 68(2): p. 591-601.

Six, K., G. Verreck, J. Peeters, M. Brewster, and G. Van den Mooter, Increased physical stability and improved dissolution properties of itraconazole, a class II drug, by solid dispersions that combine fast- and slow-dissolving polymers. J. Pharm. Sci., 2004, 93(1): p. 124-131.

Rogers, T.L., K.A. Overhoff, P. Shah, P. Santiago, M.J. Yacaman, K.P. Johnston, and R.O. Williams, Micronized powders of a poorly water soluble drug produced by a spray-freezing into liquid-emulsion process. Eur. J. Pharm. Biopharm., 2003, 55(2): p. 161-172.

Six, K., J. Murphy, I. Weuts, D.Q.M. Craig, G. Verreck, J. Peeters, M. Brewster, and G. Van den Mooter, Identification of phase separation in solid dispersions of itraconazole and Eudragit (R) E100 using microthermal analysis. Pharm. Res., 2003, 20(1): p. 135-138.

Van den Mooter, G., M. Wuyts, N. Blaton, R. Busson, P. Grobet, P. Augustijns, and R. Kinget, Physical stabilisation of amorphous ketoconazole in solid dispersions with polyvinylpyrrolidone K25. Eur. J. Pharm. Sci., 2001, 12(3): p. 261-269.

Eerikainen, H., E.I. Kauppinen, and J. Kansikas, Polymeric drug nanoparticles prepared by an aerosol flow reactor method. Pharm. Res., 2004, 21(1): p. 136-143.

Costa, P., J. Manuel, and S. Lobo, Modeling and comparison of dissolution profiles. Eur. J. Pharm. Sci., 2001, 13(2): p. 123-133.

Higuchi, T., Mechanism of Sustained-Action Medication. J. Pharm. Sci., 1963, 52(12): p. 1145-1149.

273

Brown, C.K., Dissolution Method Development: An Industry Perspective, in Pharmaceutical Dissolution Testing, J.B. Dressman and J. Kramer, Editors. 2005, Taylor & Francis: Boca Raton, FL. p. 351-372.

Yamashita, K., et al., Establishment of new preparation method for solid dispersion formulation of tacrolimus. International Journal of Pharmaceutics, 2003. 267(1-2): p. 79-91.

Tanaka, H., et al., Physicochemical Properties of Fk-506, a Novel Immunosuppressant Isolated from Streptomyces-Tsukubaensis. Transplantation Proceedings, 1987. 19(5): p. 11-16.

Vita

Kirk Alan Overhoff was born in Houston, TX on January 21, 1979 to Dietrich and Courtnay Overhoff. He graduated from Stratford High School in 1997 and began his college career in the fall of 1997 at The University of Texas at Austin seeking a Bachelor of Science in Chemical Engineering. During his undergraduate education he worked in the laboratories of Dr. Robert O. Williams III and Dr. James W. McGinity while enrolled in an internship program funded by DPT laboratories of San Antonio, TX where he was able to present his findings at the American Association of Pharmaceutical Scientists (AAPS) annual international meeting in Denver, CO. Upon graduation, he began graduate school under the co-supervision of Dr. Robert O. Williams III in the College of Pharmacy and Dr. Keith P. Johnston in the College of Engineering. During his graduate career, he has published a manuscript in *the European Journal of Pharmaceutics and Biopharmaceutics*, published a review chapter on the Spray-Freezing into Liquid (SFL) technology in the American Chemical Society Symposium Series 924, submitted a review chapter on Advances in Drug Delivery Technologies for Nanoparticulates, and significantly contributed to many other published works in international pharmaceutical and medical journals. During his graduate education, Kirk has been a teaching assistant and head teaching assistant for the Pharmaceutical Compounding and Calculations Laboratory. In 2004, he was awarded the pre-doctoral fellowship by the American Foundation for Pharmaceutical Education and, in 2005, was awarded the University of Texas Continuing Fellowship. Many of the chapters in his dissertation will be submitted to high impact pharmaceutical and medical journals for publication.

Permanent address: 1310 Arbor Circle, New Braunfels, TX 78130

This dissertation was typed by the author.